ATMOSPHERIC BLOCKING

IN THE NORTHERN HEMISPHERE

by

JOHN LEWIS KNOX

B.A., University of Toronto, 1939
M.A., University of Toronto, 1948

A THESIS SUBMITTED IN PARTIAL FULFILMENT OF

THE REQUIREMENTS FOR THE DEGREE OF

DOCTOR OF PHILOSOPHY

in

THE FACULTY OF GRADUATE STUDIES

Department of Geography

We accept this thesis as conforming

to the required standard

THE UNIVERSITY OF BRITISH COLUMBIA

June, 1981

In presenting this thesis in partial fulfilment of the requirements for an advanced degree at the University of British Columbia, I agree that the Library shall make it freely available for reference and study. I further agree that permission for extensive copying of this thesis for scholarly purposes may be granted by the head of my department or by his or her representatives. It is understood that copying or publication of this thesis for financial gain shall not be allowed without my written permission.

Department of Geography

The University of British Columbia
2075 Wesbrook Place
Vancouver, Canada
V6T 1W5

Date June 29th, 1981

DE-6 (2/79)

ABSTRACT

Blocking is generally understood as the obstruction on a large scale of the normal west - to - east motion of mid-latitude pressure systems. It is a persistent phenomenon lasting from one to several weeks and the resulting prolonged weather regimes may have serious economic and social consequences. The recent Northern Hemisphere winters, starting with 1976-77, featured unusually large circulation anomalies, many of which can be directly related to prolonged episodes of large scale blocking.

The intent of this study is to investigate the statistics and certain diagnostics of blocking in the Northern Hemisphere. The first of the three primary objectives is to present and interpret the spatial and temporal distribution of blocking during the past 33 years. We develop objective identification criteria, adaptable to machine processing methods, by relating the blocking anticyclone to its associated positive anomaly of 5-day mean 500MB height. Anomalies meeting the criteria are called 'blocking signatures.' We present the seasonal frequency of occurrence of these signatures by longitude and by area. The results are in good agreement with published studies for the oceans, but they also reveal a high frequency of blocking signatures over the Northeastern Canadian Archipelago. This result, dubbed the 'Baffin Island Paradox' is further investigated and rationalized.

A catalogue has been prepared which identifies the date, centre location and magnitude of every blocking signature which occurred from January 1, 1946 to December 31, 1978. A supplementary Catalogue identifies sequences of these signatures corresponding to actual blocking episodes.

The second objective is to investigate whether regions with high incidence of blocking, in either the developing or the mature stage, feature non-Gaussian distributions of 5-day mean geopotential. During winter, fields of significantly low kurtosis are found in certain mid-latitude regions where the genesis and amplification of blocking ridges are frequently observed. Fields of significantly positive skewness are found in higher latitude regions where mature blocking episodes often interrupt the smaller fluctuations about the normal geopotential height.

The final objective is to examine the association between the first six harmonics of the long wave pattern and the temporal and spatial characteristics of concurrent blocking episodes. Harmonics are calculated from profiles of daily 500MB height around latitude zones centred at 40°N and 60°N. Results for the northern zone are emphasized. It is found that there are spectral signatures distinctive to the regions where blocking anticyclones occur. Our results for the oceans are in general agreement with those of Austin (1980).

During the strongly amplified meridional flow patterns associated with major blocking, we found that, at 60°N, more than 90% of the spatial variance of 500MB height is accounted for by wave components one to four. When the meridional regime gives way to predominantly zonal flow there is a marked reduction of spatial variance of 500MB height. During such regimes the higher harmonics (waves five and six) often make significant contributions (15 to 25%) to the total variance.

The 'Baffin Island Paradox' is also studied using harmonics. It is found that in the majority of cases Baffin blocks originate from retrograding North Atlantic blocks.

Finally, full latitude zonal harmonic analyses (15°N to pole, waves 1 to 4) are presented for three case studies of major blocking - (a) Greenland-North Atlantic, (b) Pacific Ocean-Alaska, and (c) Double Blocking. The harmonics often reveal two wave structures, one in the higher and other in the lower latitudes. The motion and growth characteristics of the two structures can be interpreted in terms of well-known features of total blocking systems.

TABLE OF CONTENTS

CHAPTER Page

LIST OF TABLES

LIST OF FIGURES

LIST OF SYMBOLS

Symbols are usually defined on first introduction in the text; for ease of reference they are summarized here. In a few cases the symbolism is not unique but it will be obvious from the context in which it is used.

Symbol	Meaning	Units Usually Used
A	Anomaly of geopotential height $(Z - \overline{Z})$	(dam)
$^{yy}A_k(I,J)$	Anomaly of Z for pentad (yy,k) at (I,J)	(dam)
$^{yy}A_k$	Magnitude of an Anomaly Centre for pentad (yy,k)	(dam)
A_n	Amplitude of nth Harmonic (Wn)	(dam)
c	Phase speed of a wave	(m s^{-1})
CS	Coefficient of Skewness $\equiv \mu_3/\sigma^3$	(-)
CK	Coefficient of Kurtosis $\equiv \mu_4/\sigma^4$	(-)
dam) dm)	Decametre (1 dam = 10 m)	(dam)
f	Coriolis parameter $\equiv 2\Omega\sin\phi$	(s^{-1})
g	Acceleration of gravity = 9.81 m s^{-1}	(m s^{-1})
gph	Geopotential height	(dam)
h	Scale height $\equiv 29.3\overline{T} \equiv$ height of an isothermal atmosphere with temperature = $\overline{T}$	(km)

Symbol	Meaning	Units Usually Used
I	Abscissa, NMC Octagonal Grid Fig. 4.1	(-)
J	Ordinate, NMC Octagonal Grid Fig 4.1	(-)
k	Wave number in zonal (x) direction	(-)
L	Wave length (linear)	(km)
m	Wave number in meridional (y) direction	(-)
PE	Pentad, one of the 73 5-day intervals specified in Fig. IV - 1	(-)
yy_{PE_k}	The Kth pentad in year (19)yy	(-)
n	Wave number	(-)
Q_H	Sensible heat flux	($W\ m^{-2}$)
R_d	Gas constant for dry air $\equiv 287 \times 10^2\ m^2\ s^{-2}\ K^{-1}$	($K^{-1}\ m^2\ s^{-2}$)
R_t	Ratio (U_t/V_t) of zonal to meridional average of wind at time t	(-)
S_n	% of total variance of $Z(\lambda)$ around a latitude contributed by Wn	(-)
SEQ	Sequence of Blocking Signatures	(-)
SIG	Blocking Signature	(-)
T	Temperature (K)	(-)
u	x-component of velocity eastward	($m\ s^{-1}$)

Symbol	Meaning	Units Usually Used
$\overline{U}$	Background zonal current	$(m\ s^{-1})$
U_t	Zonal average at time t of the algebraic x-component of velocity $\equiv [u_t]$	$(m\ s^{-1})$
v	y-component of velocity poleward	$(m\ s^{-1})$
$\vec{V}$	Horizontal velocity vector	(-)
V_t	Zonal average of the absolute y-component $\equiv [\lvert v_t \rvert]$	$(m\ s^{-1})$
Wn	n^{th} Harmonic (or wave number)	(-)
x,y	Eastward and poleward distance, respectively	(km)
z	Upward distance	(m)
Z	Height (above MSL) of a constant pressure surface	(dam)
${}^{yy}Z_{1,k}(I,J)$	5-day mean height for pentad (yy,k) of 1000MB surface at (I,J)	(dam)
${}^{yy}Z_{2,k}(I,J)$	5-day mean height of 500MB surface	(dam)
$\overline{Z}_k(I,J)$	Normal height at (I,J) for pentad k	(dam)
$\overline{Z}_{WN}(I,J)$	Normal height at (I,J) for WINTER	(dam)
β	Poleward variation of the Coriolis parameter $\equiv \frac{df}{dy}$	$(m^{-1}\ s^{-1})$
ζ	Vertical component of relative vorticity	(s^{-1})

Symbol	Meaning	Units Usually Used
θ	Potential temperature[1]	(K)
$\overline{\theta}$	Mean (zonal average of θ)	(K)
λ	Longitude. Positive eastward	(-)
μ_k	Phase speed of wave k (radians/day)	(s^{-1})
μ_3	Third moment about mean	(m^3)
μ_4	Fourth moment about mean	(m^4)
σ	Standard deviation	(m)
τ_m	Mean temperature of an air column 1000MB surface to MSL	(K)
Φ	Geopotential (energy)	($m^2\ s^{-2}$)
ϕ	Latitude	(-)
yy_{ϕ_k}	Latitude of an Anomaly Centre Pentad (yy,k)	(-)
ϕ_n	Phase angle of Wn	(-)
ϕ_n/n	Phase shift of Wn	(-)
ψ	Streamfunction	($m^2\ s^{-1}$)
ω_n	Angular frequency wave number n	(s^{-1})
Ω	Angular speed of rotation of the Earth	(s^{-1})

[1] Except in Chapter 7 where θ designates Latitude

ACKNOWLEDGEMENT

I wish to express my sincere appreciation for encouragement and assistance received from the University of British Columbia during the course of this work. I am particularly grateful to my supervisor, Professor J.E. Hay, for his continuing support, prompt review of draughts, and for ensuring that I remained focussed on the goals we set out to achieve. My thanks, also, to the other members of my Committee, Professors R.W. Burling, M. Church, T.R. Oke, and L. de Sobrino, for constructive reviews of the final draft.

Valuable data-processing assistance was provided by Dr. D.G. Steyn (graphics), Mike Patterson (centre searches) and Peter Madderom (Fourier decomposition). I am particularly indebted to Mark Roseberry who carried out the considerable computer programming required for Chapters 5, 6 and 7.

The accuracy of our data base has been enhanced in no small measure through the assistance of the Department of Atmospheric Sciences, University of Washington. Dr. Harry Edmon screened erroneous data from the original analyses (500MB, MSL) and provided 5-day means for the 33 year period. Our thanks, also, to Professors J.M. Wallace, J.R. Holton and D.L. Hartmann and to Dr. G.H. White for sharing their knowledge and insights on topics related to this thesis.

Some support has been received from the Atmospheric Environment Service of Canada. We thank Dr. R.A. Treidl and co-authors who made available a comprehensive set of recently completed data concerning Blocking in the Northern Hemisphere.

Financial assistance was received from the University of British Columbia through an H.R. MacMillan Family Fellowship.

I sincerely wish to thank Irene Hull for typing the final manuscript.

And thank you, Mary Knox, for typing the draft and for your patient support and encouragement throughout this protracted venture.

CHAPTER 1

1. INTRODUCTION

1.1 Nature and importance of blocking

There are patterns of fluid flow which evoke analogous connotations. One reflects, for example, on the sinuous bends and cut-offs of meandering rivers, the shedding of vortices by large-scale ocean currents, orographic lee waves and their rotors, and, much farther afield, the gigantic red spot on the planet Jupiter. These phenomena, generated by differing physical processes operating on widely different time and space scales, all exhibit regularity of form and temporal persistence. To our group of analogies we might have added the great deformations observed from time to time in the Earth-girdling jet streams. It is to certain characteristics of these phenomena that this thesis is addressed.

The structure of the normal horizontal motion of the Earth's atmosphere is now well known, at least over the Northern Hemisphere, thanks to a substantial record of upper air data. An inspection of the winter season normal chart at the 500 millibar level shows the circumpolar westerlies in a fairly regular 3-wave pattern around the mid-latitudes (Fig. 1.1a). The large departures from normal of day-to-day motion, particularly in the mid- and high latitudes, are synthesized by the field of standard deviation (Fig. 1.1b). Significant contributors to these departures are, of course, the short-wave ($\sim 10^3$km) troughs and ridges associated with the transient baroclinic systems in their developing stage but their totality accounts for a minor portion of the total variance. It turns out that the "restlessness" of the atmosphere extends to fluctuations of longer periods (> 10 days) and often of larger dimensions

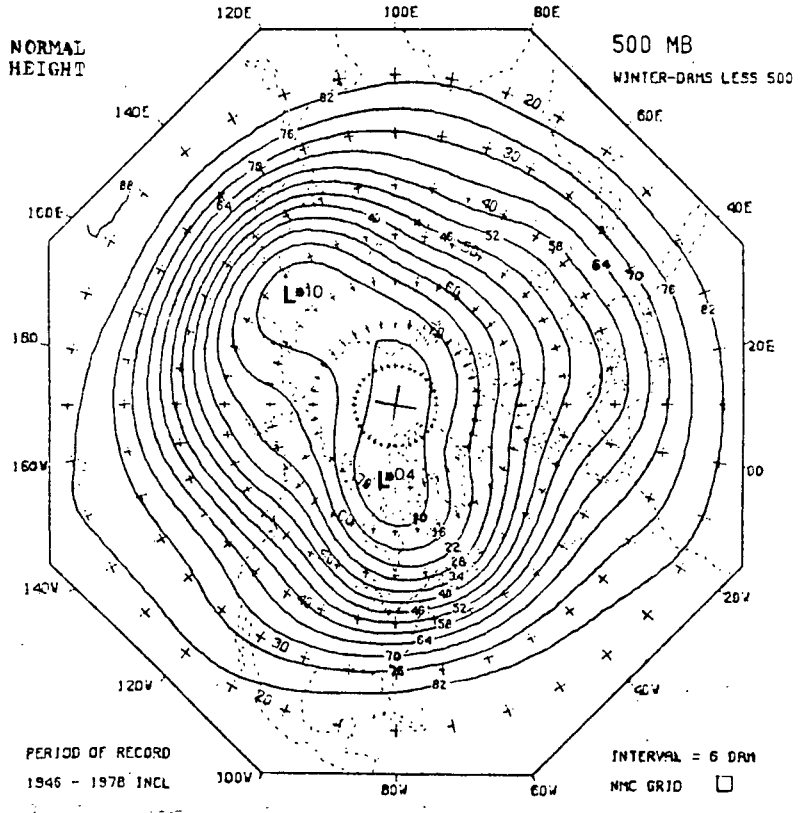

(a)

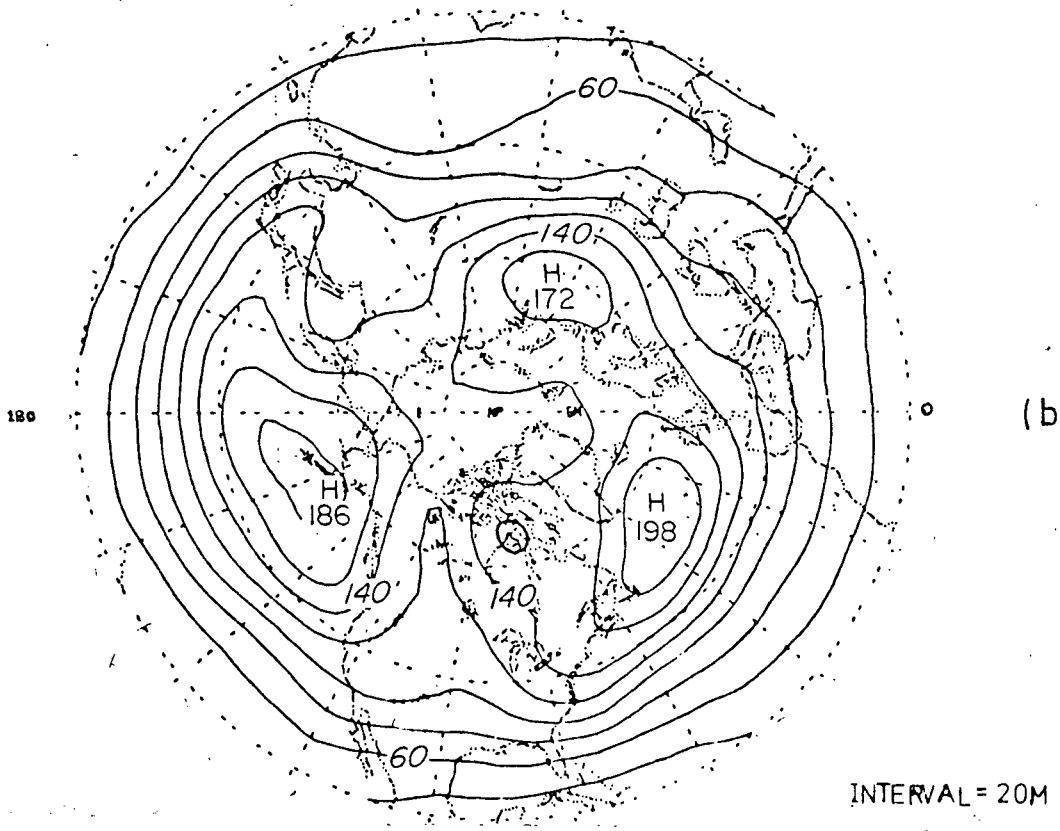

(b)

Fig. 1.1 500MB Winter Season
(a) Normal geopotential height contours (Knox)
(b) Standard deviation of twice-daily 500MB gph. (Lau, N-C from White, 1980).

($\sim 10^4$km). It is the mode, motion, growth and decay of these fluctuations that accounts for most of the variance (Blackmon et al., 1977).

It would be convenient if these wave categories could be treated in watertight divisions but the atmospheric fluid does not operate this way and there is constant interaction between them. For example, on daily 500MB analyses, we will sometimes notice parallel but separate short-wave systems with differing phase speeds. The constructive or destructive interference between members of these systems and, in turn, with long-wave components of the presiding circulation regime is a major determinant of the evolution of day-to-day weather.

We should recognize, however, that zonal flow often does persist over the greater part of the mid-latitudes, "steering" the families of baroclinic cyclones and anticyclones along the polar front in a sequence which may last for several days, or even weeks. In the upper troposphere (300MB) the kinetic energy of the flow is concentrated along the jet stream which, in this situation, exhibits gentle sinusoidal characteristics not far removed from the normal seasonal pattern. This is the typical "high index" scenario.

Then, in a manner to be described in more detail in Chapter 2, there is a striking change in jet structure over one or more regions of the mid-latitudes. Characteristically the jet splits into two branches, the northernmost curving sharply to the left and following the western flank of a ridge which is now amplifying in the downstream area occupied previously by the zonal current. The northern portion of this ridge usually develops into a closed anticyclone which, during major episodes, may grow to a diameter of about 2000km. The southern branch of the split jet usually bends to the right and can ultimately be found, with inter-

ruptions, along the southern flank of a succession of mid-troposphere low-latitude cold lows. A classic example of the mature stage of the foregoing evolution occurred over the eastern North Atlantic on February 20, 1948. It is shown in Fig. 1.2.

This process is called blocking and the term was coined to describe the obstruction of the normal west-to-east progress of migratory systems by that salient development in the mass field, the aforementioned anticyclone. This deep robust eddy is warm, almost thermally symmetric near the core, and capped by a high cold tropopause. It typically remains quasistationary or moves slowly eastward (progression) or westward (retrogression). Of course, transient systems continue to approach the blocked area from the west, and their subsequent history is not easy to generalize; some will be diverted to the north steered by the northern branch of the jet; others will move along the southern branch occasionally intensifying when they pass east of the pre-existing cold low.

The blocking process is important because it is the progenitor of spells of weather which, in more extreme cases, can have serious consequences for many sectors of the economy. The area dominated by the slow-moving anticyclone will be favoured by several days or even weeks of clear weather (interrupted on occasion when fog or stratus may persist below the shallow, surface-based inversion). The word "favoured" is used advisedly. Prolonged episodes during the growing season will drastically lower grain-crop yields, and invariably cause a high incidence of forest fires. The summer drought of 1976 over the United Kingdom was a direct result of blocking. During the winter, persistent anticyclonic conditions will cut off the normal accumulation of snow pack. A recent example was the extraordinarily dry winter of 1976-77 over the Western

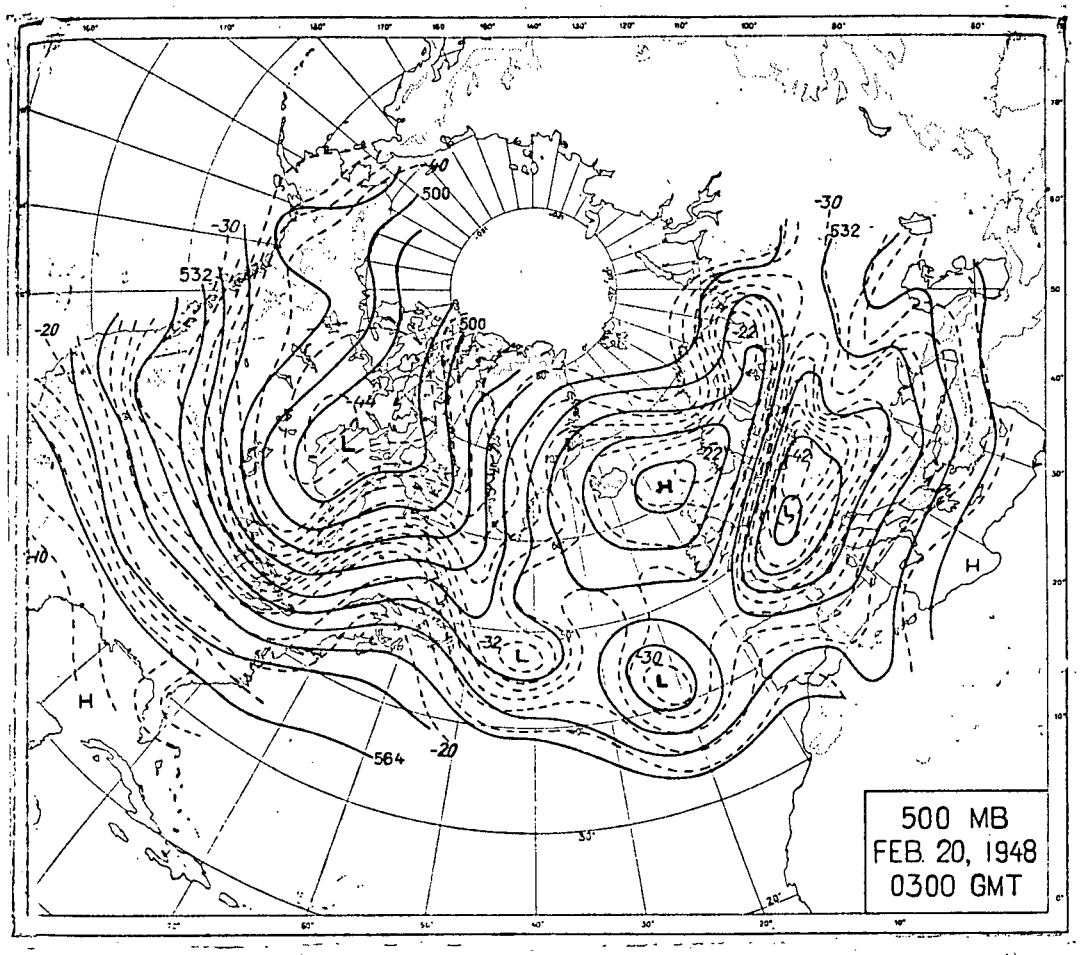

Fig. 1.2 Contours and isotherms on the 500MB surface 0300 GMT, February 20, 1948. (Berggren et al 1949)

Cordillera of North America, and the consequent depletion of usually abundant sources of hydropower. Boundary layer inversions are characteristically reinforced during blocking high episodes, and this in turn may increase the concentration of pollution over industrial areas to well above acceptable levels.

Problems of quite a different kind can arise in regions under the influence of the slow-moving troughs or cold lows flanking the anticyclone. The abundant precipitation from the cyclonically active sectors can produce a variety of impacts including blizzards in normally milder climates and serious local flooding. Events of this kind were experienced in southern Europe in February 1956. During that month an intensely active cyclonic complex, cradled by a blocking high to the north, persisted over southern Europe and the Mediterranean.

The persistent meridional flow associated with strong blocking invariably results in large temperature anomalies over vast regions. The most striking recent example was the winter of 1976-77 when a very large amplitude 500MB ridge persisted off the west coast of North America and an intense downstream trough extended along the 75°W meridian (Fig. 1.3). This configuration resulted in repeated and prolonged deployment of arctic air into central and eastern North America, where record-setting low temperatures and disastrous fuel shortages brought hardship to millions.

It is clear, therefore, that an understanding of the nature of blocking and of its causative processes should be one of the central goals of meteorology. It is a complex problem, so intimately wedded to the atmospheric system in its totality, that there are those who will argue that the only useful approach is exclusively by numerical modelling methods. We do not agree. There is still a good deal to be learned

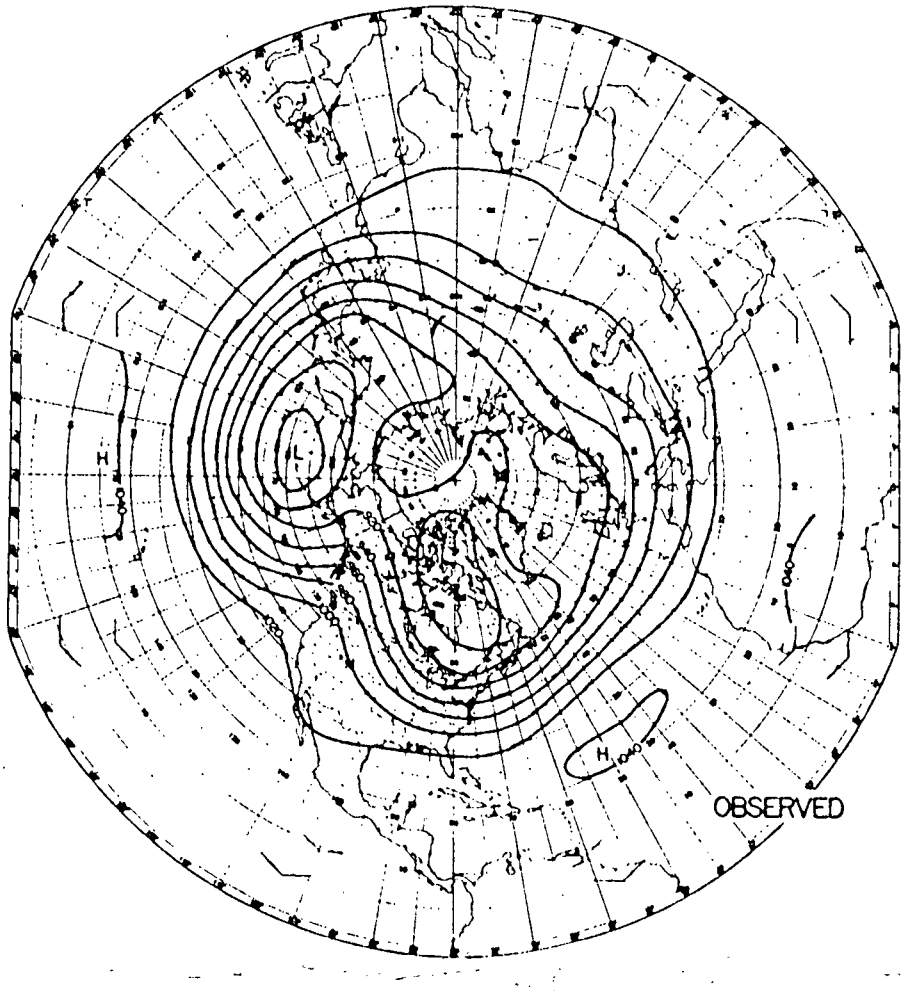

Fig. 1.3 Mean 700MB contours for winter 1976-77 (December, January and February) labeled in tens of feet. (Namias 1978)

about the climatology and diagnostics of blocking. The next section will outline the contribution in these areas that this thesis hopes to make.

1.2 Purpose and scope of this study

While atmospheric blocking, at least during major episodes, is easily recognized, and the importance of its relationship to macro-scale weather and short-term climate is beyond dispute, the phenomenon has been an awkward one for frequency of occurrence studies. There is, for example, the difficulty, well documented in the literature, of constructing an objective definition which would be generally acceptable. Moreover, some of the authors we shall refer to in Chapter 3 focussed their investigations on specific geographical regions and so there remains a need to synthesize their results.

A premise of this thesis, which was inferred during an initial pilot study (Knox, 1979) is that 5-day positive anomaly centres at appropriate levels of the troposphere (e.g., 700MB, 500MB) which meet certain criteria for location and intensity, have a close relationship with the actual location and intensity of a blocking anticyclone. These anomaly centres then serve as "blocking signatures" and so the first of our primary objectives will be to present and interpret the spatial and temporal distribution of 5-day positive anomaly centres over the Northern Hemisphere during the past 33 years. The results will then be compared with those of numerous studies of blocking frequency extant in the literature.

To test this premise relating positive anomaly centres to blocking anticyclones we needed sources listing specific details of the respective sets of events. In so far as blocking anticyclones were concerned, data

concerning their centres were obtainable from the literature (e.g., Treidl et al., 1980a and 1980b) or from synoptic weather maps. On the other hand, an archive providing time, location, and intensity of anomaly centres for the 33-year period of our study simply did not exist. Therefore, it was necessary to produce a catalogue providing this information. The preparation and use of this reference is explained in Chapter 4.

As indicated in section 1.1, a complete blocking system at its mature stage will feature not only a strongly anomalous mid- or high latitude warm ridge (or closed anticyclone) at 500MB but also anomalous cold troughs (or closed cyclones) at low or mid-latitudes. It turns out that the latter structures are often associated with 5-day negative 500MB anomaly centres. Therefore, it was decided that for future research, the locational histories of negative anomaly centres should be included in the catalogue and, moreover, that their frequency distributions should be described.

We also investigated whether regions with high incidence of blocking featured distributions of geopotential significantly different from Gaussian. For this purpose calculations of skewness and kurtosis fields at the 1000MB and 500MB levels were made for the Northern Hemisphere. The rationale, results and interpretation of this exercise will be found in Chapter 6.

Blocking is a manifestation of amplifying large scale waves, so we chose as the third primary objective of our study harmonic analysis of the daily atmospheric flow at 500MB during seven winters, each of which was notable for the occurrence of one or more major blocking episodes. (The feasibility and computational techniques were developed during a pilot study of 1977-78, 1978-79 data, Appendix VII). The results of

the 7-winter investigation are reported in Chapter 7.

Our data base is for two levels, 500MB and 1000MB. The record consists of once daily geopotential height values, January 1, 1946 to February 28, 1979, for each of 1977 points on a 381 km grid (true at 60°N). This data set (obtained from the National Centre for Atmospheric Research, U.S.A.) provides a sequence of over 12,000 grid-fields for each pressure level for the Northern Hemisphere from the pole to about 15°N (Jenne, 1975).

Those parts of the thesis (Chapters 4 and 5) which are concerned with identification and distribution of "blocking signatures" use a derived set of data consisting of contiguous 5-day means (i.e., 73 per annum) for the period of record. The skewness and kurtosis fields (Chapter 6) were also calculated from 5-day means. On the other hand, the harmonic components of the long waves (Chapter 7) were computed from daily values of 500MB gph.

Pilot-study material, background theory and mathematical techniques are contained in the Appendices.

In summary, the main purposes of this thesis are to investigate (a) the frequency distributions of "blocking signatures", (b) the connection between blocking and hemispheric fields of statistical moments of geopotential height at selected levels, and (c) the behaviour of the Northern Hemisphere long-wave components during the evolution of blocking episodes. It is hoped that certain by-products of the study, such as the catalogues, will prove to be useful for continuing research. Also, an attempt will be made in Chapter 2 to interpret and synthesize relevant literature. Some of the papers will not necessarily be germane to our

specific objectives, but it is intended that their review will provide useful perspectives on a complex and challenging subject.

CHAPTER 2

2. THE PHENOMENON OF BLOCKING

2.1 Introduction

A treatment of the blocking phenomenon in isolation from its antecedent processes would be somewhat analogous to investigating the incidence of occluded cyclones outside of the context of baroclinic waves. If the sole purpose were to prepare temporal and spatial distributions of the phenomenon of interest there would be no disadvantage in such a procedure. However, while this is one of our important objectives (Chapters 4 and 5) there will be a need to interpret the statistical results. Moreover, our second primary objective is to investigate blocking in the context of those planetary and synoptic scale processes from which it develops (Chapters 6 and 7).

This chapter, therefore, will present a number of results which we believe to be germane to those processes giving rise to the growth and decay of blocking, and to the motion of the associated wave-form. In addition, the respective roles of large scale topographic forcing and differential heating will be examined and an example of a successful simulation of blocking will be presented. The climatology of blocking will be treated in Chapters 3, 4 and 5.

Since a knowledge of the 3-dimensional structure of the atmosphere over a substantial portion of the hemisphere is necessary for an appreciation of the nature of a blocking system, it is not surprising that rather few papers on the subject were written prior to 1946. It is also evident that interest in the subject has waxed and waned down through the years. For example, from the Meteorological and Geophysical Abstracts (AMS(a))

and other sources, we have located a total of 61 papers for the fifteen year period 1945-1959, compared with 30 papers for the subsequent fifteen years 1960-1974.

The initial spate of interest was not accidental. The 1940's featured the introduction and development of long-wave theory pioneered by C.G. Rossby. The blocking phenomenon was a natural candidate for the extension of his ideas. Moreover, many of the pronounced departures from normal weather during the 1940's and 1950's (e.g., the winters of 1946-47 and 1955-56) were engendered by large-scale blocking.

The reduction in output from 1960-1974, particularly of papers concerning phenomenological aspects of blocking, is perhaps partially attributable to the remarkable development during that era of numerical methods in large-scale prediction and simulation. The progress along these lines probably generated an attitude that the onset of blocking episodes would soon be successfully predicted. Also, there appears to have been a modest decrease in blocking frequency during that period (Chapter 5) although 1962-63 was a notable exception.

Since 1975, however, there has been a resurgence of interest on both sides of the Atlantic. In Great Britain this was stimulated by events such as the west European drought during the summer of 1976, and in North America by the persistent cold over the eastern half of the continent during the winter of 1976-77. Both of these climate anomalies were a direct result of a protracted diversion of the mid-latitude westerlies from their normal position by large amplitude quasi-stationary long waves. Also, there is a growing consensus that numerical models, in spite of their remarkable development, have not really been successful beyond 4 or 5 days, in regard to their ability to simulate and predict

the rather abrupt way in which the real atmosphere switches from one long-wave mode to another (Somerville, 1980). In any event, the resurgence of interest in blocking, either in the areas of synoptic diagnostics and statistics or in numerical simulation has produced over 20 papers in U.S., Canadian and British journals alone, since 1975.

2.2 What is blocking?

The blocking phenomenon, in the sense in which it is understood for the purposes of this paper, is the obstruction, on a large scale, of the normal west-to-east progress of the migratory cyclones and anti-cyclones. It is attended by pronounced meridional flow in the upper levels, and, for a significant period of its evolution, there is usually a closed anticyclonic circulation in the mid-troposphere ($\simeq$ 500MB) at high latitudes (mainly north of 50°N). This is frequently referred to as a "warm cut-off high". It is not unusual for the complete blocking system to include cold cyclonic circulations at lower latitudes (south of 50°N), the so-called "cut-off cold lows". This anomalous circulation pattern ("the block") typically moves very slowly ($\lesssim$ 400km per day) and persists for one week or longer. Frequently the warm anticyclone to the north will move in a direction opposite to that of the cyclonic systems to the south.

There are atmospheric structures which possess some but not all of the attributes of blocking systems. The sub-tropical anticyclones - deep, warm, persistent and slow-moving - do not qualify as blocking highs. They are quasi-permanent features of the circulation and, in their normal position, do not interrupt the westerlies. Nevertheless we should note that a block is often characterized, in its initial stages, by the north-

ward amplification of a sub-tropical ridge, accompanied by a shifting of the polar jet stream to more northerly latitudes. The blocking system does not usually materialize, under our definition, until the formation of the higher latitude cut-off warm high. However, because of the continuous nature of the process, it will be appreciated that there must perforce be grey areas, and subjective judgment must be evoked to decide when and where the block has occurred.

Although the winter season anticyclones over the continents (e.g., the Siberian high) are persistent and slow-moving, they also do not qualify as blocking highs. Their rotational configuration at 1000MB, Fig. 2.1, gives way on average to zonal flow at 500MB, Fig. 2.2. This is a direct consequence of baroclinicity and of the hydrostatic balance equation. These anticyclones are shallow structures, rarely extending to more than 4km at their deepest point. The main contribution to the high pressure at MSL (or high gph at 1000MB) is from the density of the cold air mass.

Again, we must note a qualification. The mean winter Siberian anticyclone covers a vast area stretching from the Caspian Sea to Korea (almost 90° long) and from the 30th to the 60th parallel of latitude. The 500MB daily flow patterns show marked deviations from the regular westerly current shown on Fig. 2.2 and occasionally one will observe, particularly above the western portions of the 1000MB anticyclone, closed highs which clearly block the normal mid-tropospheric flow. Usually there is no ambiguity regarding what is the block and where it is located.

2.3 A typical major blocking episode

In a classic paper, Berggren et al. (1949) presented an aerological analysis of a remarkable break-down in zonal flow which occurred

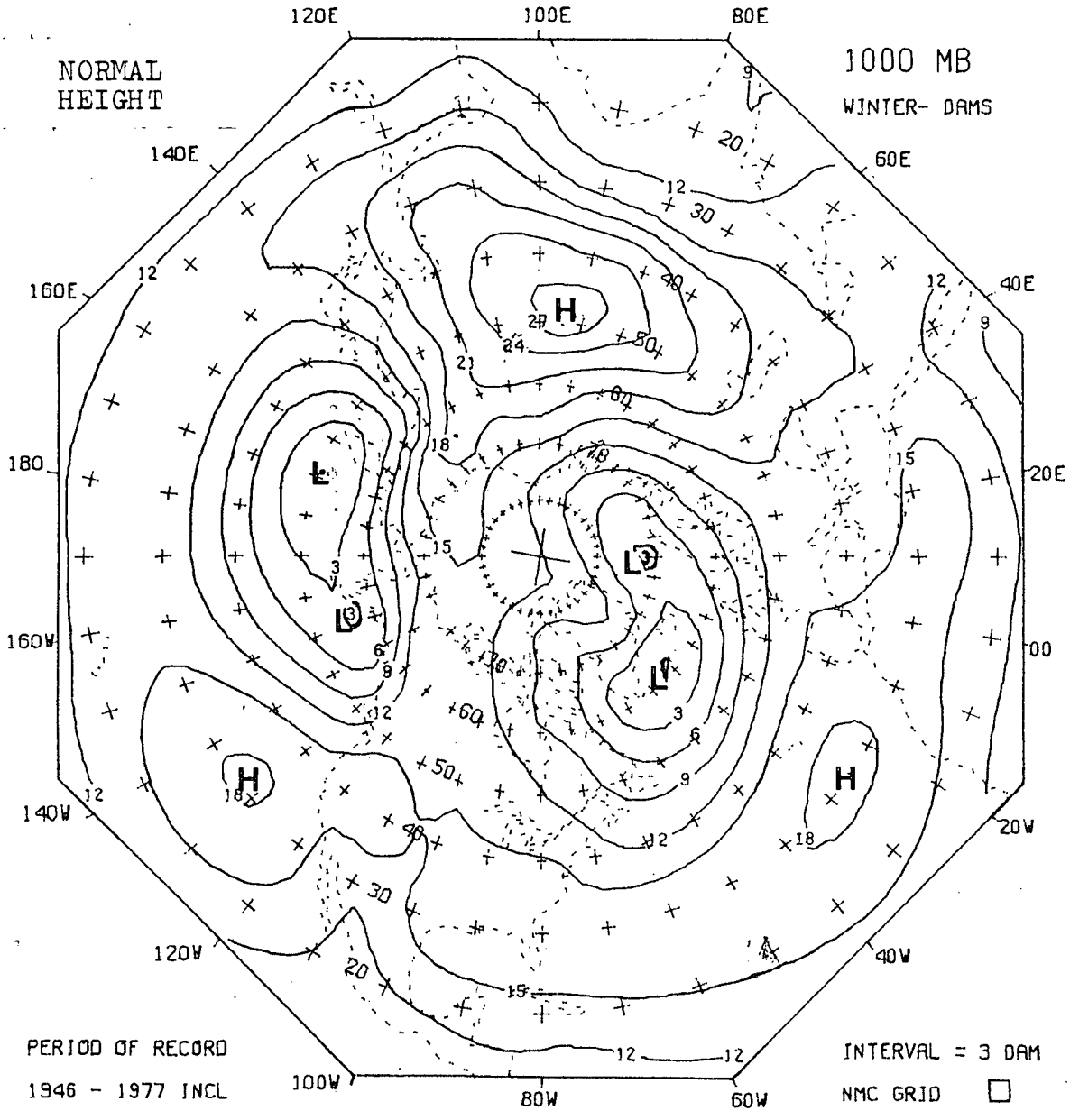

Fig. 2.1 Normal height of the 1000MB surface for WINTER (December 1 to February 28). Contours labelled in decametres (dams). Interval = 3 dams.

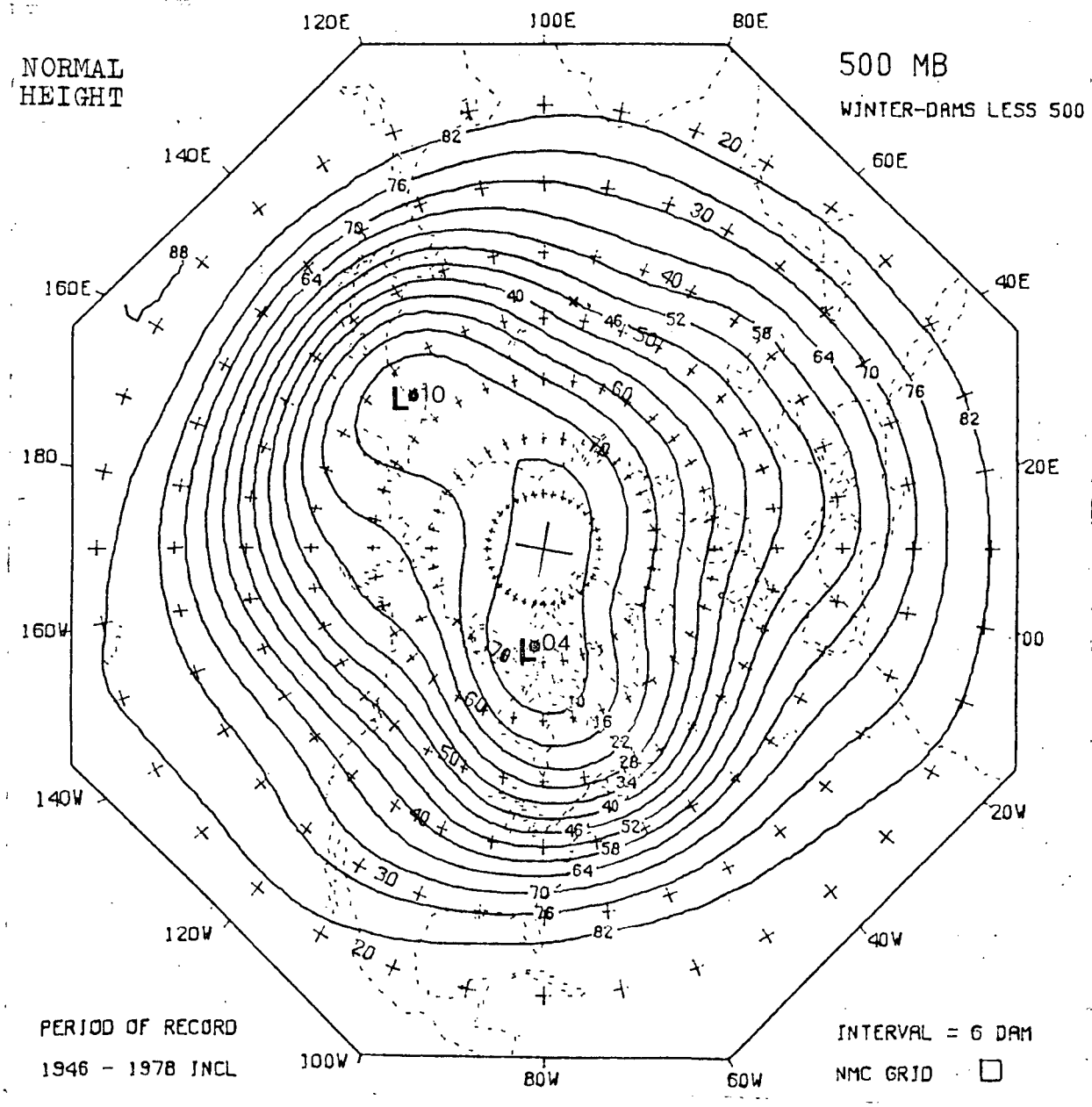

Fig. 2.2 Normal height of the 500MB surface for WINTER (December 1 to February 28). Contours labelled in decametres less 500. Interval = 6 dams.

over the North Atlantic and Western Europe, February 8th to 20th, 1948. Fig. 2.3(a) and (b) show the evolution at the 500MB level, from zonal flow (February 8th and 12th) to a mature blocking system (February 18th and 20th). The striking effect of this transformation of mid-troposphere flow on the motion of frontal systems (located at sea level) is shown in Fig. 2.4. Panel (i) shows the positions (once a day) of the fronts at sea level before the cut-off high began to develop, while Panel (ii) shows the positions during the 10-day period after the blocking high had formed.

The characteristic vertical structure of a blocking system is illustrated in Fig. 2.5 which shows the cross-section XY (Fig. 2.4a) Greenland to the Black Sea, February 18, 1948. The warm deep anticyclone over the U.K. and Scandinavia, capped by a cold and elevated (250MB) tropopause, contrasts markedly with the cold trough over the USSR, capped by a warm and depressed (400MB) tropopause.

2.4 The motion of blocking anticyclones

The blocking phenomenon can be investigated in terms of:

(a) Boundary conditions which may be initiating factors (e.g., large scale orography, longitudinally dependent differential heating, etc.)

(b) Internal dynamics of the atmosphere

(c) Motion of blocking components

(d) Factors which maintain the anticyclone

While this thesis does not intend to examine the theory of blocking in any depth, we shall discuss, from time to time, the above processes though not necessarily in the order in which they have been listed. We

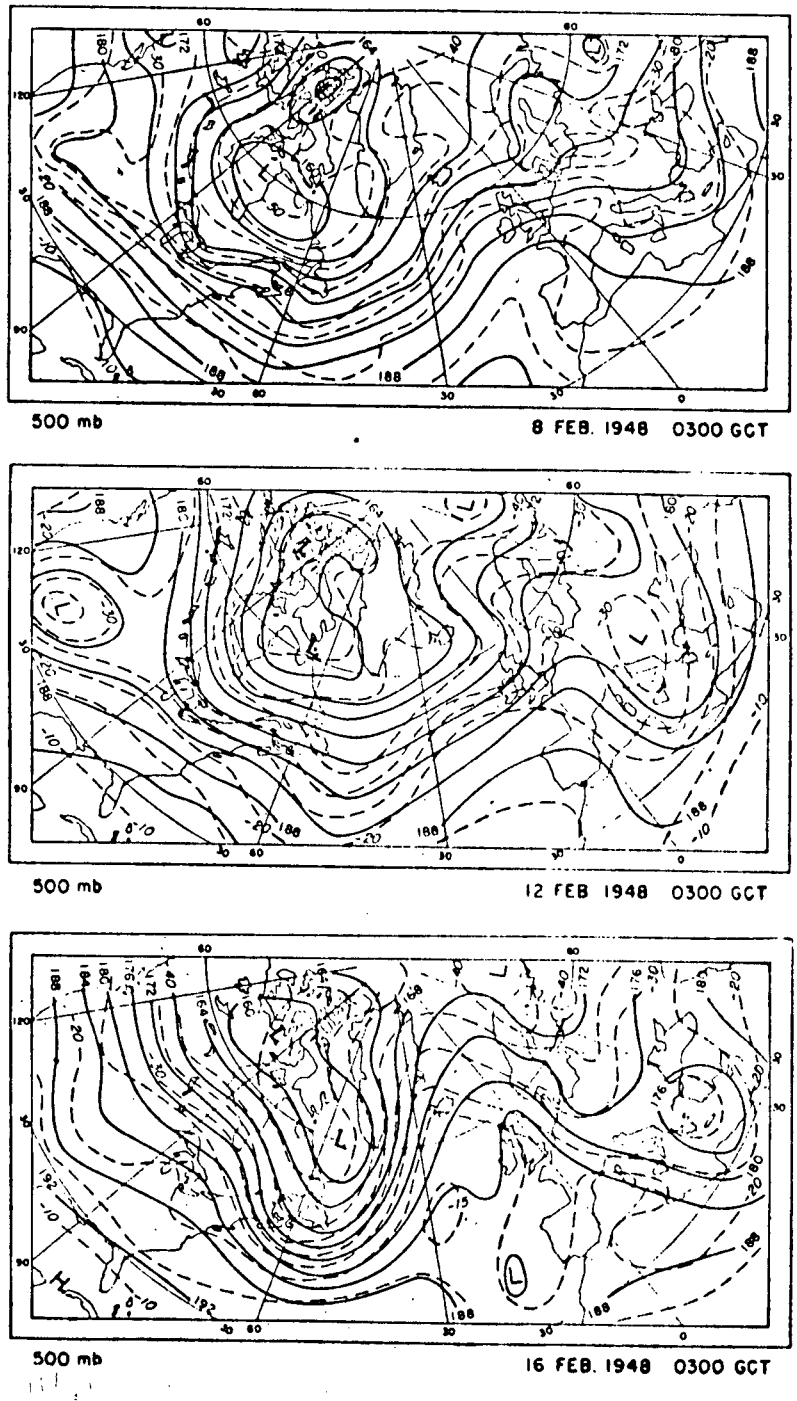

Fig. 2.3(a) Evolution from zonal flow February 8 through February 12 to amplifying wave on February 16. (Berggren et al 1949)

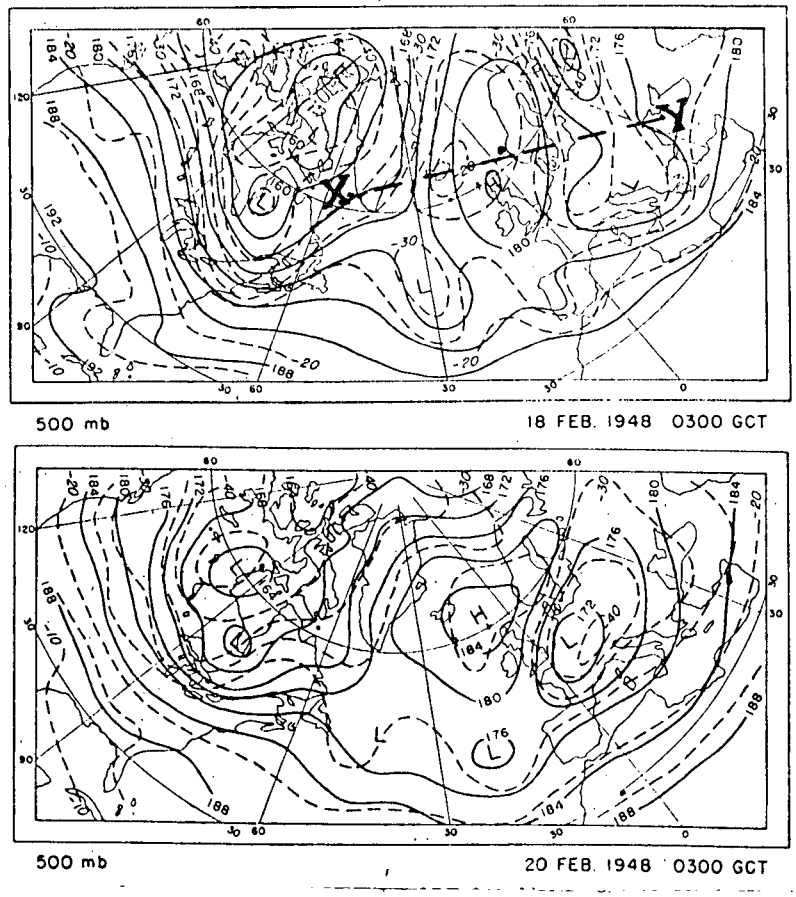

Fig. 2.3(b) Mature blocking anticyclone centred northern Scotland February 18 has retrograded toward Iceland February 20. Deep cold low centred over Germany now dominates Western Europe. X-----Y is projection of vertical cross-section shown in Fig. 2.5. (Berggren et al 1949)

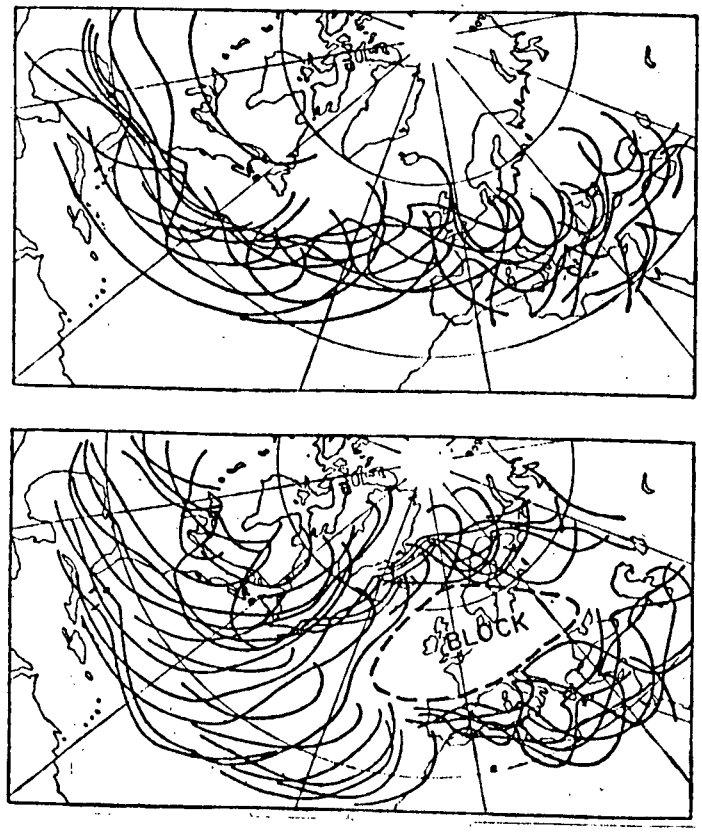

Fig. 2.4 Positions of fronts during two ten-day periods: 1. preceding the formation; 2. following the establishment of the cut-off high shown in Fig. 2.3(b).

(Berggen et al 1949)

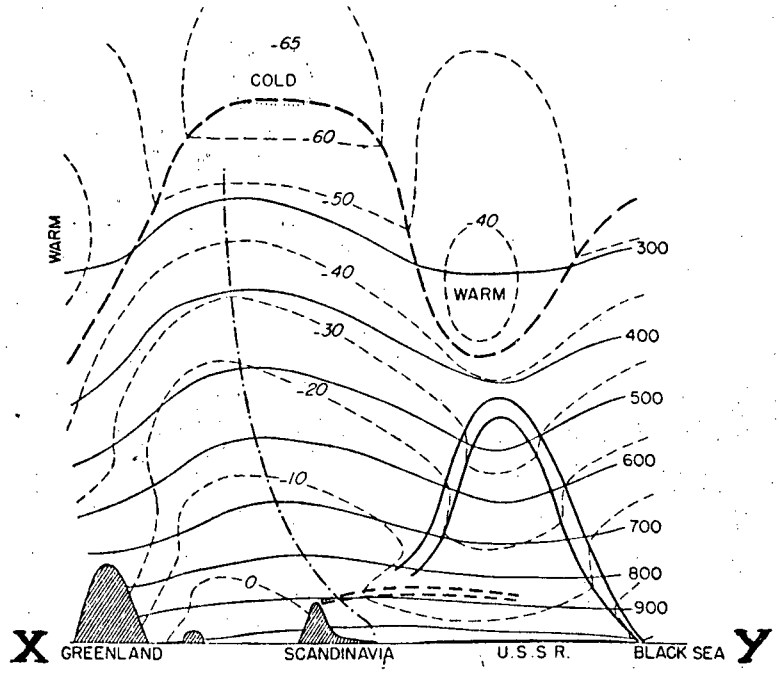

Fig. 2.5 Schematic representation of the vertical structure of a high-level anti-cyclone adapted to the case shown in Fig. 2.3(b) (February 18). The cold dome is indicated by heavy double lines. The tropopause is indicated by a heavy broken line, and the axis of the high by a dash-dot line. The slope of the isobaric surfaces has been exaggerated. (Berggren et al 1949).

shall begin with an interesting feature of the motion of certain types of blocking - retrogression.

Namias and Clapp (1944) used case studies to illustrate westward moving blocking waves which they described as a "retardation of the zonal circulation which appears first over western Europe and the eastern Atlantic and subsequently retrogresses further westward affecting particularly North America".

Why do blocking waves sometimes retrograde? Some insight into the mechanisms can be obtained from the theory of planetary waves and from the tendency equation for change of geopotential at the level of non-divergence. The results are developed in Appendix II and may be summarized as follows:

Rossby (1939) assumed a homogeneous incompressible fluid on an approximation to the rotating Earth (the β-plane) and a uniform non-divergent flow. From these conditions he deduced the principle of conservation of vorticity: $\zeta + f = \text{constant}$

Where ζ = the relative vorticity (due to the configuration of the relative flow field)

and f = the planetary vorticity (due to the spin of the earth).

For a uniform background zonal current $\overline{U}$ on which is superimposed a sinusoidal transverse velocity perturbation of wave length L he derived the well-known formula:

$$c = \overline{U} - \beta\left(\frac{L}{2\pi}\right)^2 \qquad (2.1)$$

Where c = phase speed

$\beta = df/dy = (2\Omega\cos\phi)a^{-1}$

L = wave length

Ω = angular speed of rotation of the earth ($\simeq 7.29\times10^{-5}$rad.S^{-1})

ϕ = latitude.

It turns out that for typical observed values of $\overline{U}$ and c the computed values of L are of the same order of magnitude as the long waves observed in the atmosphere. Also the formula indicates that Rossby waves propagate westward relative to the mean zonal flow with a speed which increases with the wave length. There will be a critical wave length L_c which, for a given $\overline{U}$ and ϕ, will make c = 0. If $L > L_c$ the wave will retrograde relative to the earth. In Chapter 7 we shall note numerous occasions when this happened during seven winters selected for analysis.

Equation (2.1) assumes that the wave structure is independent of latitude which, of course, is never the case. If we postulate the variation of the flow with ϕ is also sinusoidal, it can be shown, Haurwitz (1940a) that the phase speed toward the east is

$$c = \overline{U} - \frac{\beta}{k^2 + m^2} \qquad (2.2)$$

Where k = the wave number in the zonal direction

m = the wave number in the meridional direction.

The expressions for c in equations (2.1) and (2.2) were developed for an extremely simplified model, and the success with which they can be applied to the real atmosphere will depend on a number of factors. For example, best results are obtained at levels of small divergence (e.g., 600MB, 500MB) and for latitude zones within which the maximum wind is located (Petterssen, 1956). The formula tends to give excessive (westward) values of c for small k (1,2,3), i.e., large L, and works best for wave

numbers 4 to 8.

As demonstrated by equation (8) Appendix II, relative vorticity advection tends to move the vorticity pattern and hence the wave-form downstream. On the other hand advection of planetary vorticity tends to move the wave-form upwind. The resultant motion will be determined by the size of these opposing factors. Blocking anticyclones occur in high latitudes and, at 60°N, β is decreased to half its value at the Equator. However, as we shall note in Chapter 7, the main wave components of blocks have small wave numbers. The factor β/k^2 on balance, tends to increase with latitude for very long waves (k small) and this may decrease c to a stage where its sign becomes negative unless the ζ advection can compensate.

Blocking anticyclones, at least over the oceans, are quasi-barotropic near the core and the relative vorticity advection is very small there. Consequently the planetary vorticity advection will dominate. This accounts for their very slow movement and not infrequent retrogression.

Sometimes the retrograde motion of blocking waves is "discontinuous". By this we mean that while the initial anticyclone may be quasi-stationary (or moving slowly eastward) and weakening, there is anticyclogenesis immediately upstream and the newly formed anticyclone to the west of the original becomes the new blocking centre. This process may be repeated several times so that the resultant effect is equivalent to a westward propagating blocking wave.

A physical process which may contribute to this phenomenon, upstream energy dispersion, was discussed by Yeh (1949). His work was based on the fact that, because the phase speed of synoptic and planetary waves is wave length dependent, they must be dispersive (unlike sound waves) and over a spectrum of such waves there will be interference, which, it turns out,

creates a pattern of wave groups. These groups move with a velocity G, quite different from that of an individual wave:

$$G = c - L\frac{dc}{dL}$$

2.4.1 Progression

Now in the case of Rossby Waves in a non-divergent barotropic atmosphere the group velocity is (assuming m = 0)

$$G = \overline{U} + \beta\left(\frac{L}{2\pi}\right)^2$$

G therefore exceeds not only the individual wave speed

$$c = \overline{U} - \beta\left(\frac{L}{2\pi}\right)^2$$

but also the basic current $\overline{U}$, and so energy dispersion sweeps rapidly downstream. This effect is observed from time to time in the real atmosphere, where, following some point of energy intensification (e.g., west Pacific cyclogenesis) the amplification influence moves rapidly eastward (30^0 longitude per day is not uncommon) and acts successively on downwind waves, Haltiner and Martin (1957). It is conceivable that amplification of some downstream ridges, ultimately resulting in blocking anticyclones, is a result in part of this progressive energy dispersion mechanism.

2.4.2 Retrogression

Returning now to Yeh's paper, he introduced a temperature differential into the model (unlike the Rossby model of uniform density). He examined energy propagation through dispersive waves in an "incompressible atmosphere with a uniform north-south density gradient and with finite depth". He found that the group velocity depended on a critical

wave length L_c such that if the predominating wave length $L < L_c$ then $G > c > 0$. This does not differ from the uniform density case. On the other hand, if L is slightly $> L_c$ then $c > 0$ and $G < 0$. This corresponds to upstream propagation of energy opposite to wave velocity. Moreover, by examining the subsequent dispersion of a solitary wave (whose wave length $L > L_c$) at, respectively, 0°, 40^oN, 70^oN it turned out that only the wave at 70^oN maintained its amplitude for a time interval comparable to that for blocks in the real atmosphere.

We have devoted considerable space to the consideration of two of the mechanisms (advection of vorticity, energy dispersion) which appear to be factors in the motion (and, in the case of dispersion, growth) of blocking anticyclones. In Chapter 7 we shall examine characteristics of the motion and growth of wave components of actual blocking cases. It is hoped that the background theory just reviewed will be useful for interpretation.

2.5 Conservation of potential vorticity. A heuristic discussion of its relationship to blocking

Since warm blocking anticyclones are deep structures compared with the cold anticyclones confined to the lower troposphere, it may be useful to consider the reasons for changes in depth of air masses during meridional displacement. In reality, of course, the processes are very complicated, but, as always, it is best to proceed at first with the simpler concepts.

We shall assume the principle of the conservation of potential vorticity defined by the relationship (Rossby, 1940)

$$\frac{\zeta + f}{\Delta p} = \text{constant}$$

Where ζ = relative vorticity and Δp is the pressure depth of a small air column.

Consider now the case of three air columns A, B and C embedded in an air current initially uniform at, say, 60°N and being displaced equatorward, Fig. 2.6(a). The subsequent stream flow with an anticyclonic branch to the right of the flow and a cyclonic branch to the left is postulated such that when the columns arrive at their primed positions they have acquired vorticities typical of those found in the real atmosphere.

Column B whose relative vorticity ζ remains zero, must shrink because f decreases. Column A whose ζ decreases will shrink even more markedly. The change in column C will depend on the extent to which increasing ζ counters decreasing f, and in the real atmosphere, ζ is usually dominant and there is stretching.

Cold low level anticyclones will most frequently be characterized by shrinking air columns depicted ideally by the current AA'. The trajectory CC' corresponds to what is observed with cold lows.

Now consider an initially uniform poleward-bound current starting at, say, 30°N with a configuration shown in Fig. 2.6(b). Here the situation is reversed. An air column E experiences strong stretching as it curves cyclonically and column G experiences shrinking.

Warm, deep anticyclones are typically characterized, on their western and northern flanks by air columns conserving their absolute vorticity $\zeta + f$. On the western periphery the air columns may stretch

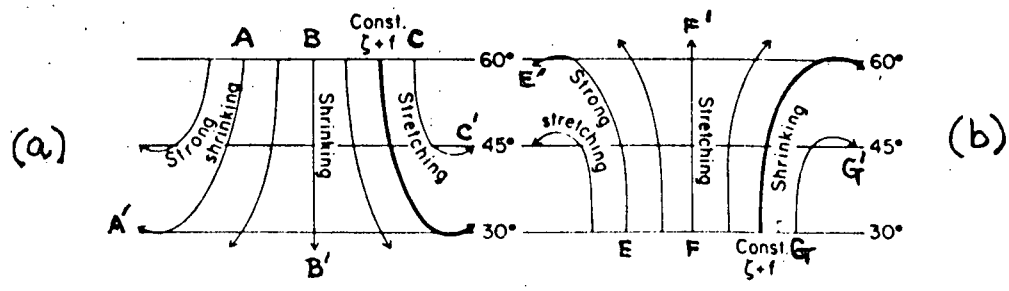

Fig 2.6 Meridional motion with with anticyclonic and cyclonic branches and the implied vertical stretching or shrinking. Along heavy streamlines, absolute vorticity is conserved, the change of coriolis parameter beingcompensated by an opposite change in relative vorticity by curvature. (After Petterssen, 1956)

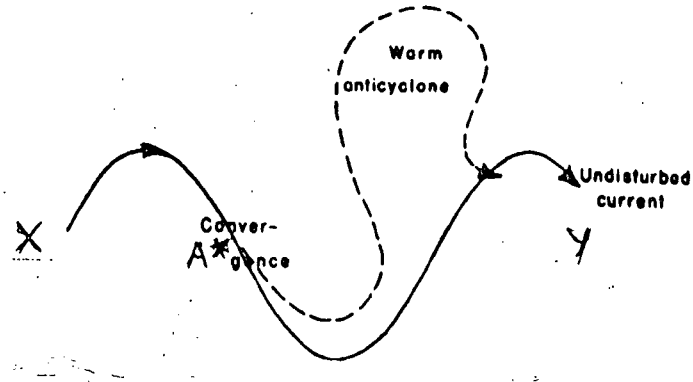

Fig. 2.7 Schematic diagram showing the changes from the normal "sinusoidal" air movement in the upper troposphere, resulting from convergence above a sinking cold-air mass in the trough. (After Palmén and Nagler, 1949)

slightly, but to conserve $\frac{\zeta + f}{\Delta p}$ as f increases it is necessary for ζ to decrease through most of this region.

These heuristic considerations suggest how a sinusoidal configuration in the upper troposphere may amplify in the manner sometimes observed during the formation of blocking systems. Consider an initial relatively undisturbed current XY in the upper troposphere, Fig. 2.7. If an intense cold outbreak takes place in the lower troposphere (say an anticyclone centred at A*), then its strong low level divergence and subsidence, and southward displacement, will be dynamically associated with strong convergence and stretching in the upper tropospheric trough. This will increase the vorticity in the trough and deform the current from its initial sinusoidal shape. The resulting more meridional orientation of the current east of the trough will be consistent with an accentuated downstream ridge. Moreover, the air stream, in its progress to higher latitudes, bends anticyclonically in order to conserve absolute vorticity. Continuation of this process may ultimately culminate in a closed anticyclone.

2.6 The index cycle

Namias (1950) showed that blocking over the Atlantic between 50°N and 70°N, appeared to be a necessary (though not sufficient) condition for the southward shift of the zonal wind maximum into the sub-tropics. This is the culminating stage of the "index cycle", a cycle through which the polar vortex, initially confined to high latitude, expands, strengthens and becomes unstable. This results in the formation of large amplitude ridges and troughs and, ultimately, cut-off warm highs in higher latitudes and cold lows in lower latitudes, Fig. 2.8. When the processes which generate these eddies terminate, the warm highs gradually weaken

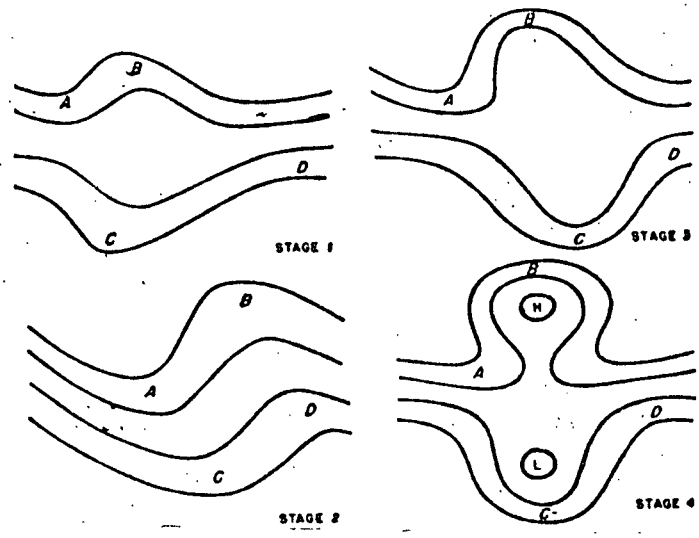

Fig. 2.8 Schematic representation of successive circulation patterns aloft during an index cycle. (After Namias and Clapp, 1951).

by radiative cooling and the cold lows weaken by low latitude low level heat exchanges. These cells eventually dissipate marking the end of the cycle, which on average takes about six weeks.

2.7 Baroclinic instability

Why does the expanding circumpolar vortex ultimately become unstable, to form large amplitude troughs and ridges? The answer lies in the process of baroclinic instability which is the major mechanism for energy transformation in the extra-tropical latitudes. The key to the process was developed by Charney (1947) and Eady (1949). Charney, using a 2-level baroclinic model of a compressible atmosphere, showed how baroclinic instability is dependent on vertical wind shear, lapse rate, latitude and wave length.

Both writers agreed that given the observed mean state of the atmosphere in the mid-latitudes, the wave lengths most likely to be associated with development were in the synoptic scale range ($\sim 10^3$km). If the wave length was in the planetary range ($\sim 10^4$km) its development was, other factors being equal, less likely because in that portion of the wave spectrum the β-effect $\left(\beta = \frac{df}{dy}\right)$ became significant as a stabilizing factor. In essence their results defined 2 wave length thresholds L_{c_1} and L_{c_2} for development to take place,

$$l < L_{c_1} \quad \text{stable}$$

$$L_{c_2} > l > L_{c_1} \quad \text{unstable}$$

$$l > L_{c_2} \quad \text{stable}$$

Here l = the actual wave length and L_{c_1} is at the shorter end of the spectrum.

Fig. 2.9 shows how the respective wave length cut-offs are dependent on the mean vertical stability $\frac{\partial\overline{\theta}}{\partial z}$, on the mean vertical wind shear (which arises from the mean N-S temperature gradient $\frac{\partial\overline{\theta}}{\partial y}$), and on latitude (implicit in the f and β terms).

Now, blocking waves do appear to be generated, at least in part, by the growth of planetary waves, so it is of interest to enquire of those circumstances which govern the value of L_{c_2}. It turns out (Haltiner, 1967) that if certain non-uniform lower boundary conditions are introduced into the two-level baroclinic model (e.g., Haltiner introduced a sensible heat source to the lower boundary), the resulting wave length stability criteria L_{c_1} and L_{c_2} are significantly changed. In fact, there are combinations of prescribed non-uniform boundary conditions which can increase L_{c_2} to $\simeq 7\times10^3$km which corresponds to k = 4 at 45° latitude and k = 3 near 60^oN.

White and Clark (1975) investigated blocking over the North Pacific Ocean to determine if the real atmosphere supported Haltiner's theoretical results. They calculated height anomalies from 700MB charts averaged by month over the period 1950-1970 (240 charts). From these patterns they prepared "composite" charts of predominately blocking and non-blocking months, respectively. They found that in autumn and winter the blocking ridge had a distinct modal position at about 170^oW and that it was quasi-stationary, with a modal wave length $\simeq$ 7000km which they noted was the width of the mid-latitude ocean. In spring and summer the modal location was unidentifiable and therefore they hypothesized that a critical factor was sensible heat transfer Q_H from ocean to atmosphere. For autumns and winters in which blocking predominated they found Q_H anomalously large under the trough in the western Pacific and anomalously small under the ridge.

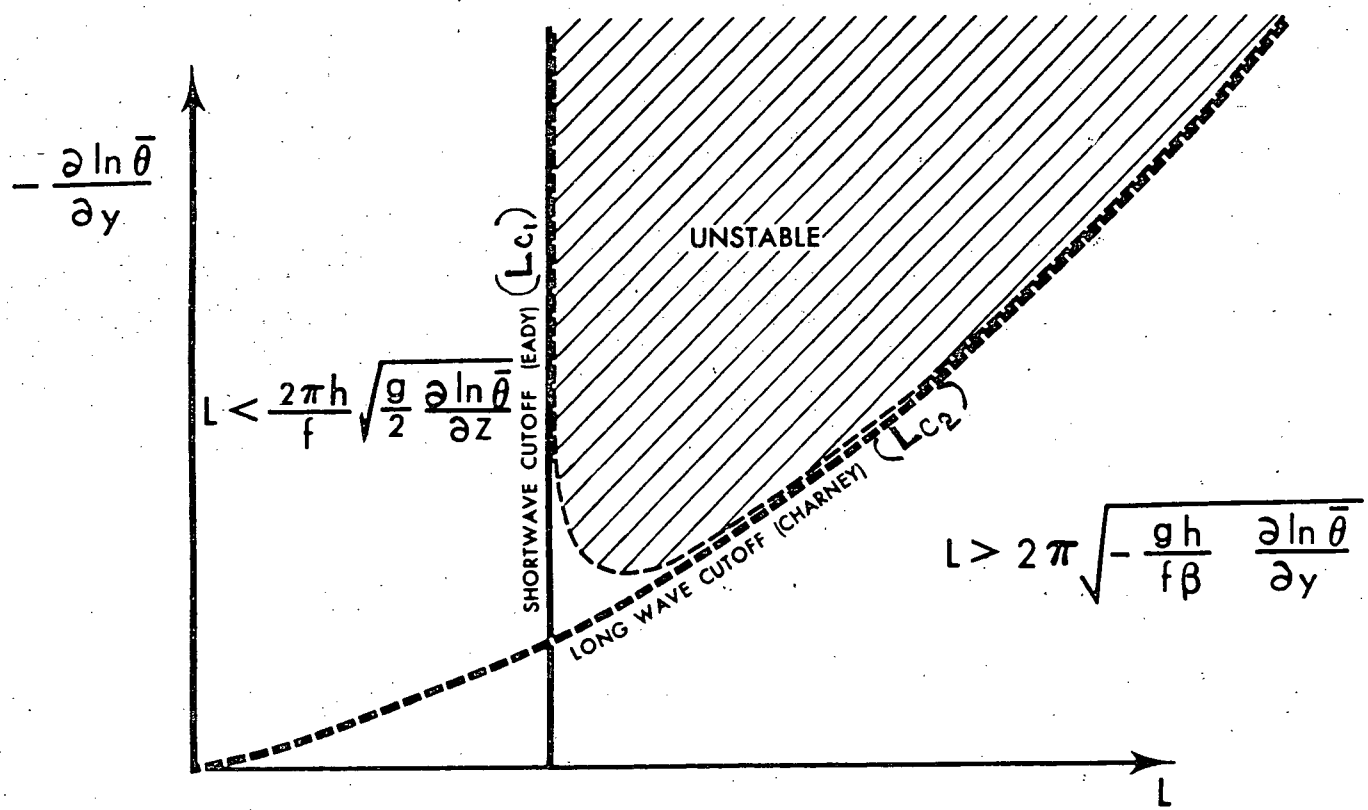

Fig. 2.9 Baroclinic stability criterion. L is the zonal perturbation wavelength, h is the vertical scale height, g is the acceleration of gravity, f is the Coriolis parameter and $\beta = df/dy$; the dashed curved line is the combined theory (see for example Phillips, 1954).

$h = \frac{R\bar{T}}{g}$ where $\bar{T}$ = layer mean temperature between p_1 and p_2

from Smagorinsky (1972)

In the absence of sensible heat transfer (or some other non-uniform lower boundary condition such as orography or friction), baroclinically unstable long-waves are not possible in 2-level models except at unrealistically high values of the thermal wind (Charney's and Eady's results indicated that mobile synoptic scale waves $L \cong 3 \times 10^3$km were more likely to be unstable under normal thermal wind values). However, White and Clark noted that Haltiner had found that for these normal winter values of the background mid-tropospheric thermal wind, the otherwise stable stationary long wave became unstable when a sensible heat transfer source was introduced into his model. Moreover, the wave length was 7000-8000km with a growth time of about two weeks and it could be either quasi-stationary or retrogressive. They therefore concluded that their statistical results on blocking (which also included seasonal and year-to-year variability) are all in agreement with Haltiner's theory.

Diehl (1977) also hypothesized that blocking-ridge formation originates from the realization of baroclinic instability operating in the long wave length part of the macro-wave spectrum (7000-9000km). Using a 2-level baroclinic model with an initial steady state current characteristic of the real troposphere, he tested its response to a simple perturbation:

(i) for adiabatic frictionless flow,

(ii) for flow subject to surface heat exchange,

(iii) for flow subject to surface friction only, and

(iv) for flow subject to both surface heat exchange and friction.

In (i) his results agreed with those of the aforementioned classical papers and, in (ii), with those of Haltiner. In (iv) he found that the inclusion of both friction and sensible heating from the surface, still

further cut off the shortwave end of the spectrum and made baroclinic instability realizable further into the long-wave portion. Moreover, these unstable long waves could be stationary, progressive or retrogressive depending on the zonal current. They had growth times and wave lengths comparable to the dimensions of North Pacific blocks reported by White and Clark. Diehl therefore concluded that blocking ridges could develop from the realization of a baroclinically unstable long wave. He also emphasized the limitations of his study. Linear perturbation theory (used by all the foregoing investigators) cannot explain the sustenance without further amplification of blocking highs. Moreover, his model did not include latent heat release, orographic effects or large-scale differential surface heating.

2.8 Topographic forcing

In Chapter 5 we shall examine histograms of blocking frequency vs longitude around the Northern Hemisphere. The results quoted in the following discussion of topographic forcing should provide a context within which to judge the importance of this factor in the formation of blocking anticyclones.

Using the principle of the conservation of potential vorticity $\frac{\zeta + f}{\Delta p}$ for a small air column embedded in a westerly current flowing across a mountain barrier with a N-S orientation, it can readily be demonstrated that the air column will be deflected southward with anticyclonic curvature at first, and subsequently execute a series of dampened downstream oscillations. If we visualize this process operating across mountain barriers on the scale of, say, the Rocky Mountain Cordillera it is reasonable to expect that within the complex of oscillations so generated, some will be found on the long-wave scale.

An easterly current flowing over a mountain barrier (e.g., the Greenland massif) will turn southward with cyclonic curvature prior to reaching the barrier, recurve anticyclonically as it passes the crest and resume its previous undisturbed flow without executing further oscillations.

Thus north-south oriented mountain barriers generate anticyclonic vorticity within uniform westerly and easterly currents but the downstream response is periodic in the former case and zero in the latter.

Clearly the orientation and shape of the large scale topography must be considered for determining the resultant flow. The Himalayan plateau for example, with less of a N-S extent than the Rockies, and more circular in areal aspect, will constrain westerly (and easterly) air streams to flow around as well as over the barrier, while the generally E-W oriented Alpine-Caucasian chain will have a significant influence on meridional air stream components.

To further add to the complexity of orographic effects, the Rocky Mountain Cordillera and the Himalayan - NE Siberia Mountains act as containment barriers to the vast low level winter air masses generated primarily by boundary layer radiative processes.

Some evidence of the impact of large-scale topography on global air currents can be obtained by a comparison of mean 500MB flow for the two hemispheres for corresponding seasons. The normal charts for the Southern Hemisphere winter, Fig. 2.10, and summer, Fig. 2.11, show a fairly uniform circumpolar flow between latitudes 40°S and 60°S, a zone of prevailing westerlies almost entirely uninterrupted by significant mountain barriers. These charts support the not unreasonable assumption that if the earth's surface were frictionally uniform, and thermally uniform by

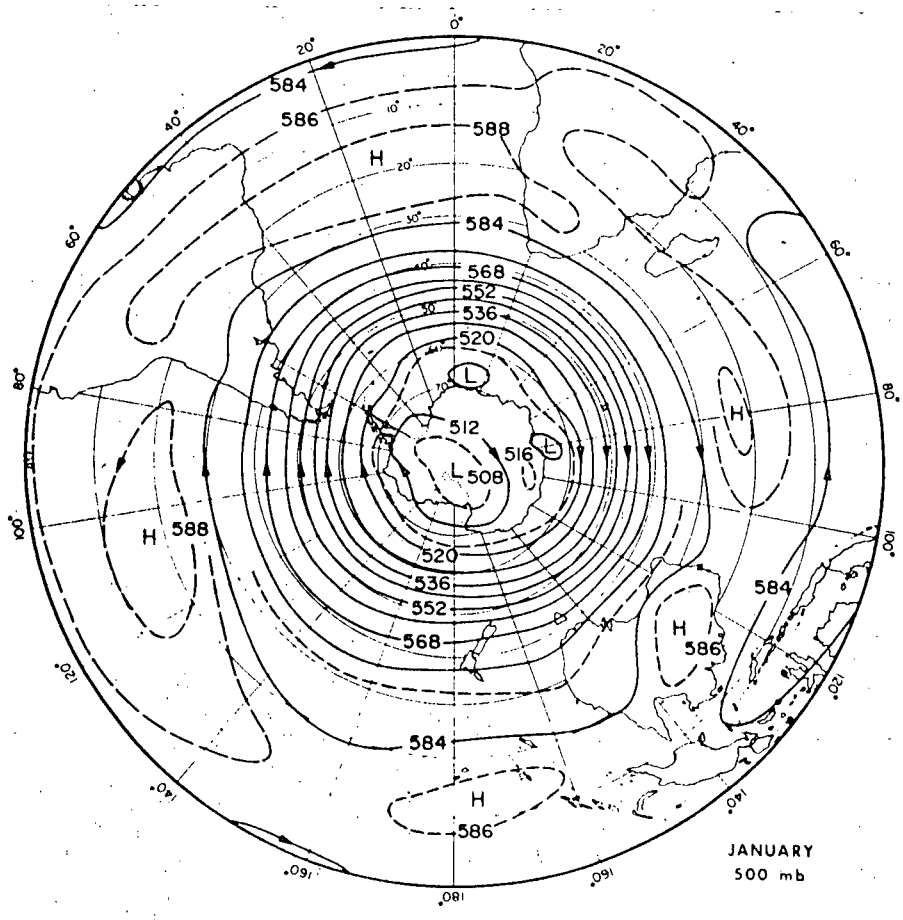

Fig. 2.10 Mean 500MB contours (80-m interval) in January (summer), Southern Hemisphere. (After Taljaard et al., 1969).

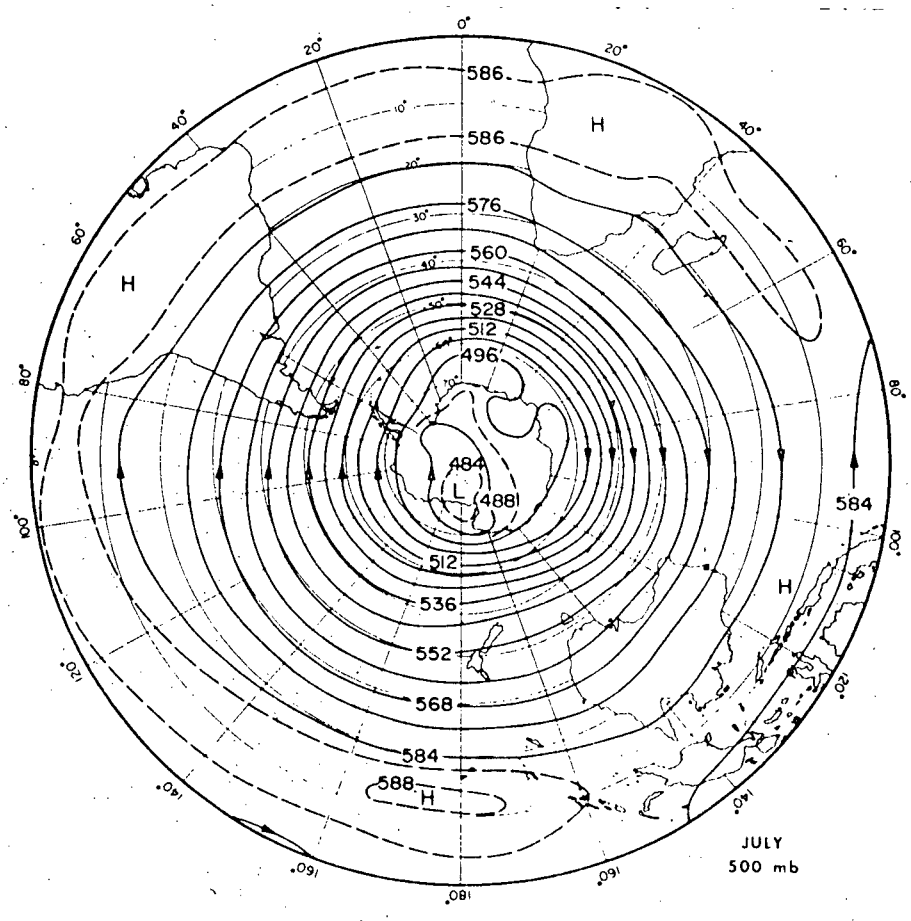

Fig. 2.11 Mean 500MB contours in July (winter), Southern Hemisphere. (After Taljaard et al., 1969).

longitude, the long period mean flow would have no meridional component.

On the other hand, normal charts of 500MB flow for the corresponding seasons in the Northern Hemisphere, Fig. 2.12 and Fig. 2.13, show substantial longitudinal variation. This is particularly noticeable for the winter when a strong 3-wave component is evident, with pronounced mean troughs located near 140°E and 80°W and a third of diminished amplitude near 40°E. These departures from purely zonal flow are caused by the extent to which large-scale topography and longitudinally dependent heating are distributed over the Northern Hemisphere.

The question is how to assess the respective influences of these major factors. For this purpose investigators have turned to general circulation models (GCMs) of the atmosphere. In a recent experiment with the GCM at the Geophysical Fluid Dynamics Laboratory (GFDL), Princeton, N.J., Lau (1980) clearly demonstrated the climatological influence of the earth's major mountain complexes during the winter season. The model used is one of the most successful simulators of the real atmosphere in existence.

It was run for 10 successive winters (December, January, February)

(a) with Mountains (M)

(b) without Mountains (NM)

and the mean flows were calculated for the 1000MB and 300MB levels, respectively (not shown). The NM flow was then subtracted from the M flow and the difference patterns (M-NM) are shown by Figs. 2.14 and 2.15. At 300MB a weak pattern of anticyclonicity is evident just east of the Himalayas, and much stronger patterns are located immediately upstream of the Rocky Mountains (the centre is over B.C.) and east of Greenland (centred near Iceland). It is also of interest to note the downstream

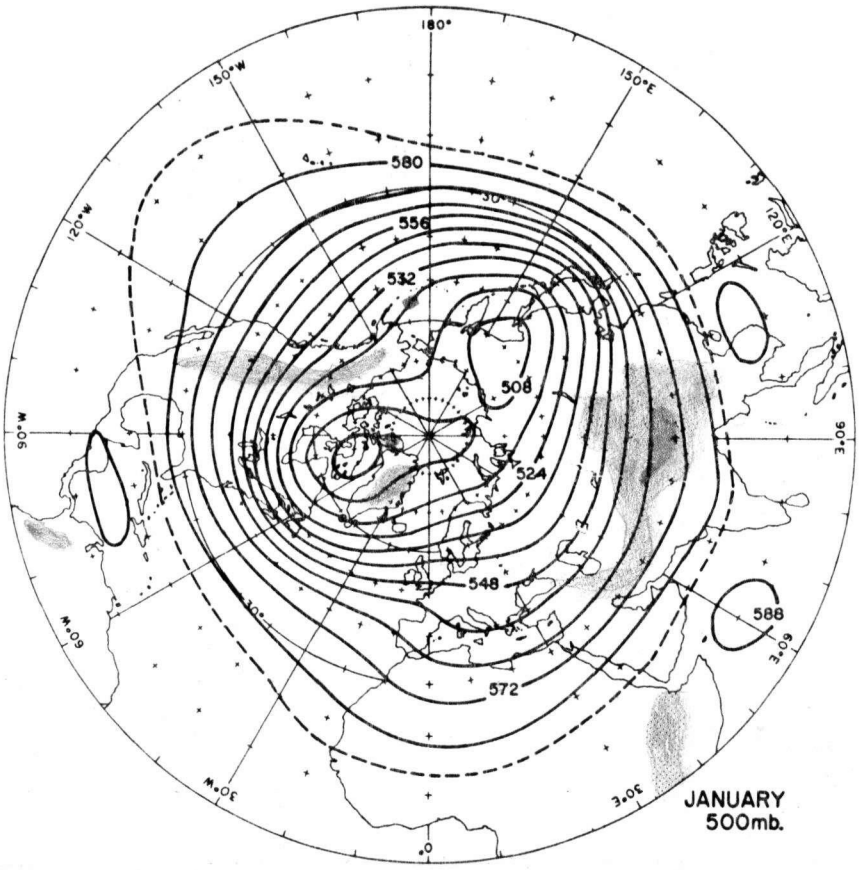

Fig. 2.12 Mean 500MB contours in January (winter), Northern Hemisphere. Redrawn at 80-m intervals from I. Jacobs (1958). Light and heavier stippling show regions where elevations are above 1.5 km and 5 km (smoothed over 5° latitude-longitude tessera), from Berkofsky and Bertoni (1955).

(Palmén and Newton, 1969)

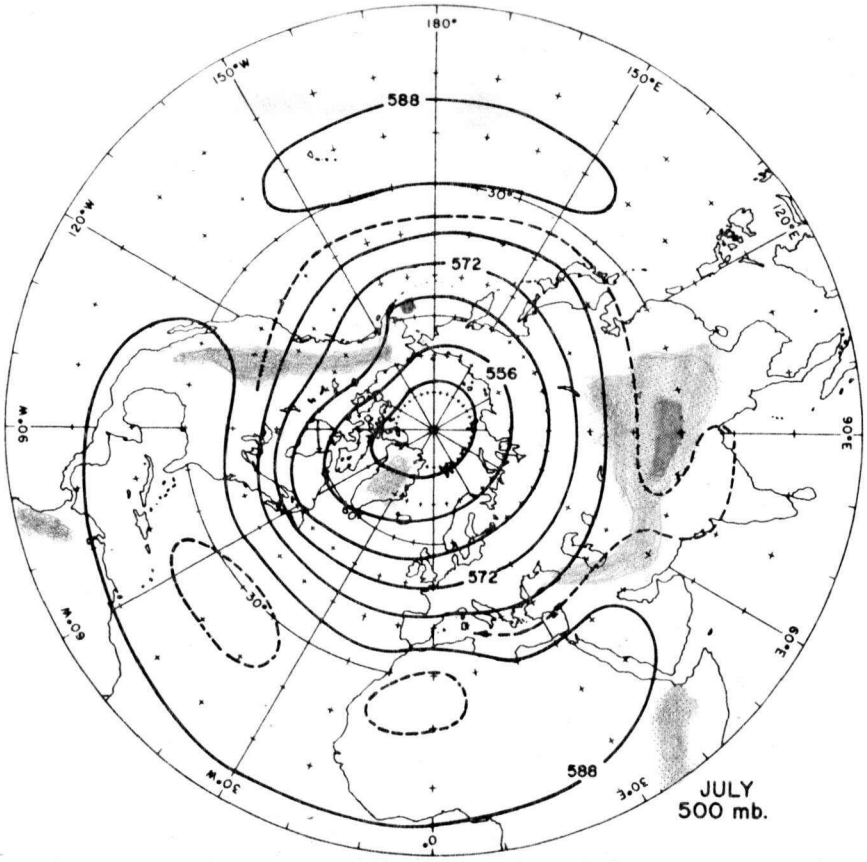

Fig. 2.13 Mean 500MB contours in July (summer), Northern Hemisphere. (Redrawn from I. Jacobs, 1958).

(Palmén and Newton, 1969)

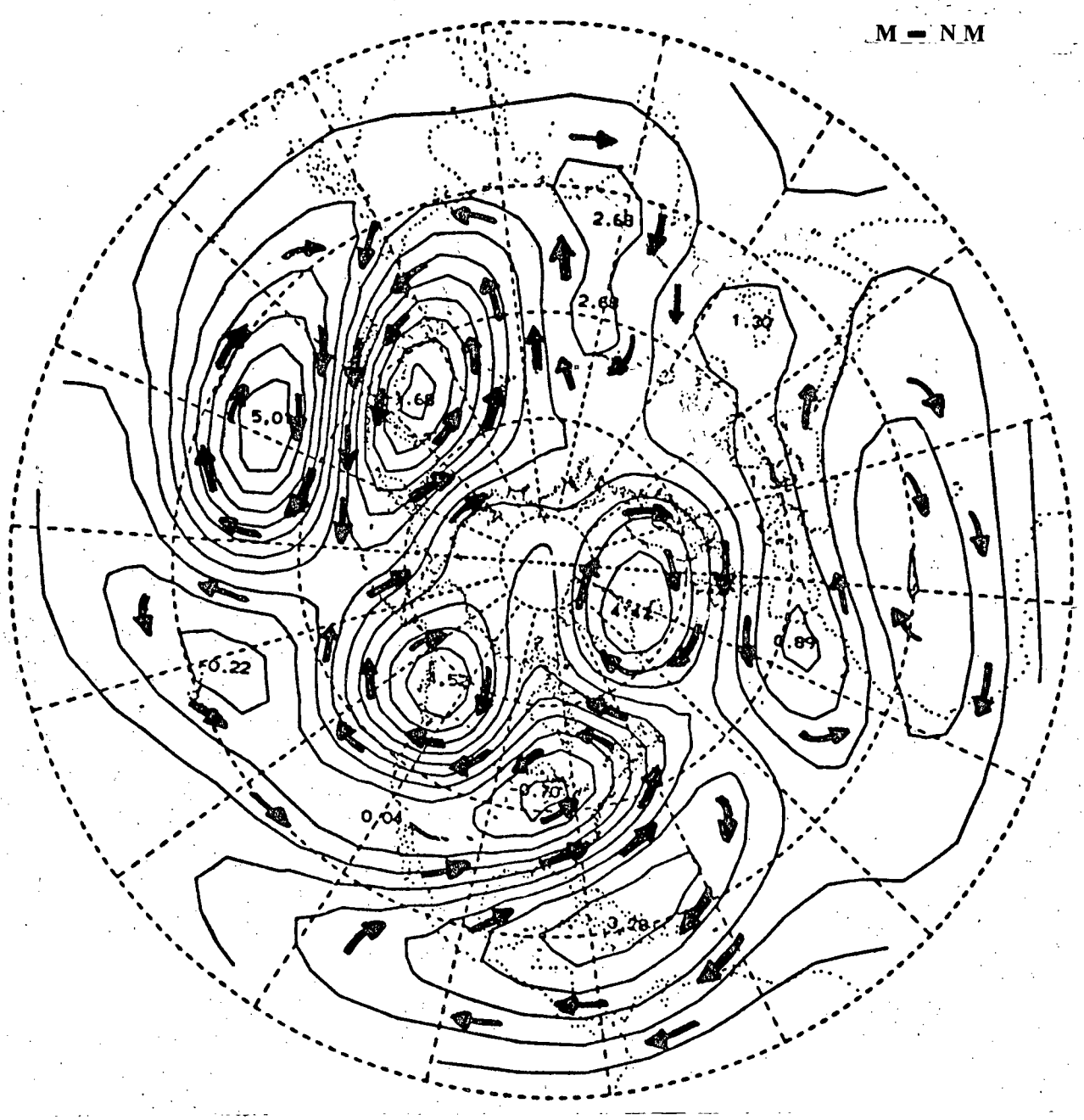

Fig. 2.14 Illustrating effect of Northern Hemisphere major mountain systems on stream flow at 300MB using GFDL General Circulation Model for 10 winter seasons. ψ equals difference between "with mountain" (M) and "without mountain" (NM) runs. Lau (1980).

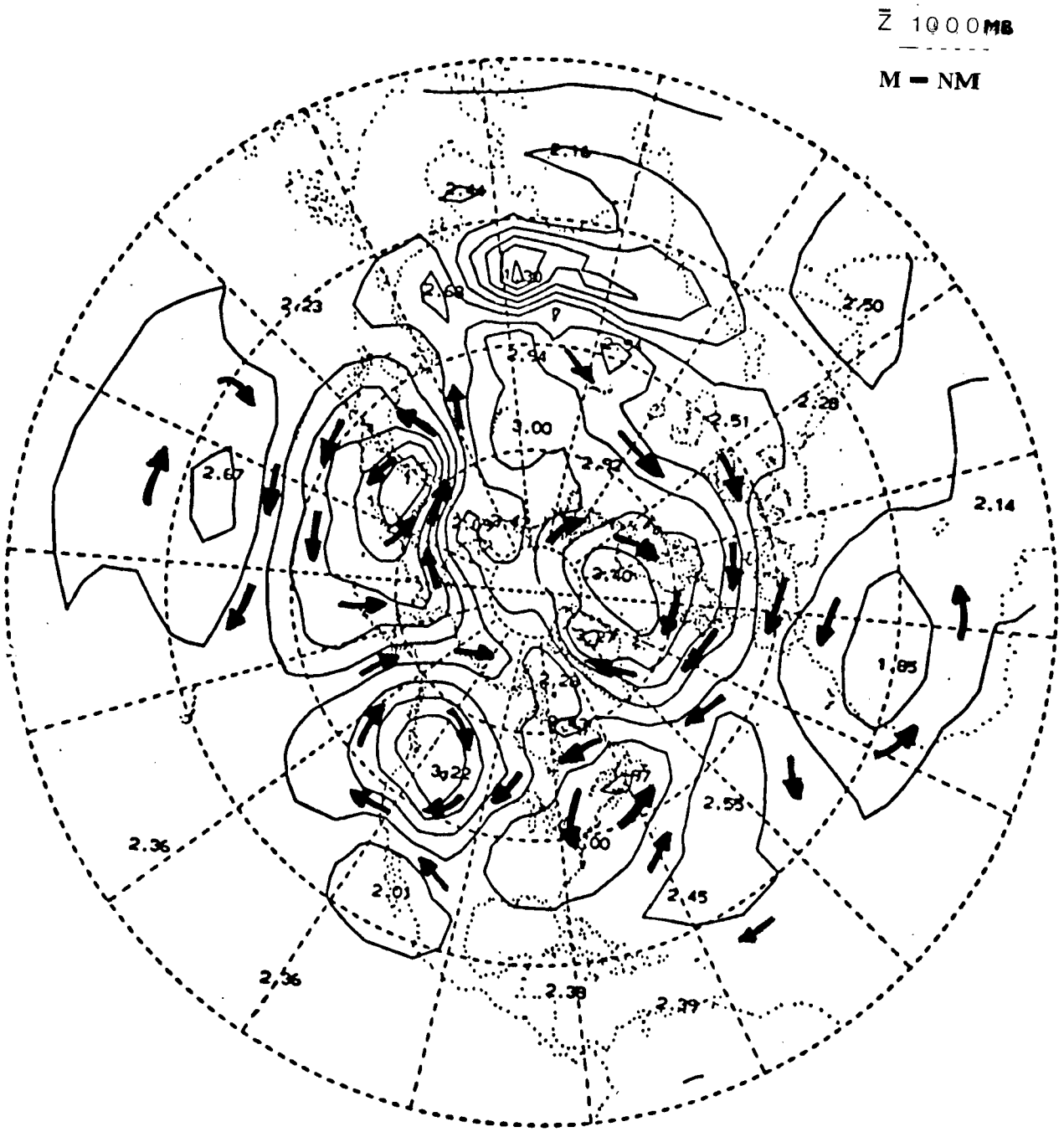

Fig. 2.15 As in Fig. 2.14 except at 1000MB. Geopotential Height $\bar{Z}$ used instead of stream function. (Lau, 1980).

resonant effects of orography on the quasi-permanent centres of action. The western lobes of both the Atlantic and Pacific sub-tropical anti-cyclones are strengthened, and the cyclonic vorticity of the E. Asiatic and E. North America troughs is increased. The Himalayan plateau with its rounded configuration appears to exercise a somewhat different influence both in its vicinity and downstream, from barriers with a predominant N-S component.

Since the longitudinally dependent large scale differential surface heating remained the same during both experiments (M) and (NM), the conclusion is that large scale orography exercises a major influence on the mean flow of the GCM and, by implication, the real atmosphere.

We would like to be able to report on a similar experiment with regard to the effect of longitudinally dependent differential heating but to our knowledge it has yet to be carried out on the latest GCM. Therefore, the comparative effects of the two major factors on the mean atmospheric flow are yet to be assessed. Also we should be aware that strong non-linear interaction is to be expected between oscillations produced by orographic forcing and differential heating, respectively. This will greatly add to the complexity of the problem.

It is interesting to note a point remarked upon by several writers, e.g., Bolin (1950), that the mid- and upper tropospheric flow shows a significant relationship between wave location and topography <u>in summer</u> as well as in winter (Fig. 2.16). This lends weight to the existing consensus (Smagorinsky, 1972) that the dynamic forcing of the large mountain systems rather than the thermodynamic influence of the surface temperature distribution is the ultimate determinant of the wave characteristics of the mean flow in the <u>upper</u> troposphere.

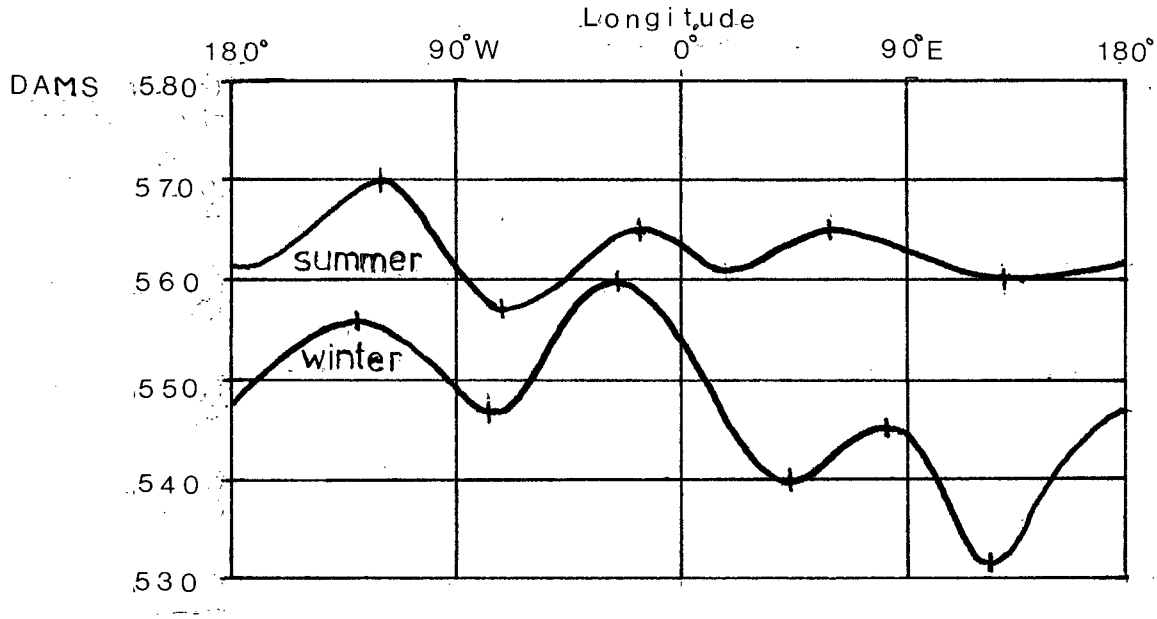

Fig. 2.16 The mean height of the 500MB surface as a function of longitude . In summer the figure represents conditions in the latitude belt 45°N - 50°N, in winter 35°N - 40°N. The profiles have been computed from the hemispherical mean charts published by Sherhag (1948).

2.9 Simulation of a "real-time" blocking episode

The results of running a GCM (of the type described in the last section) are not continuously examined at GFDL in terms of their day-to-day output. However, it is important that the model behave like the real atmosphere in developing systems with magnitudes and characteristics of the synoptic and long waves. Hence, the output for specific sequences of days is looked at from time to time.

Apparently one of the failings of GCMs is their inability to simulate blocking with the frequency, persistence and intensity characteristics that are in fact observed. However, a few successful cases have been reported and Mahlman (1979) presented the results of a simulation (by the 1967 GFDL 11-level model) of an east Atlantic blocking anticyclone. Fig. 2.17 ('Jan. 22') shows the stream flow when the block was first initiated. Note that the overall structure includes a robust anticyclone at 35°N, 30°W, the typical up-stream split jet, and a low latitude cyclone at 25°N, 40°W. This system drifted slowly eastward at a speed of about 5m s^{-1} ($\simeq$ 10kts) and persisted for about nine days. Note, however, that the latitude of the "blocking anticyclone" was well south of what is normally observed. Hopefully the more recent models are showing greater success but, unfortunately, the phenomenological characteristics of the day-to-day GFDL simulations are not being reported in the literature.

2.10 The effect of blocking on the circulation of the stratosphere

Fig. 2.18(a) shows the summer mean stratospheric circulation at 30MB, a remarkably uniform (almost circular) slack easterly circulation which is thermally consistent with the temperature field between the warm pole and cold equator.

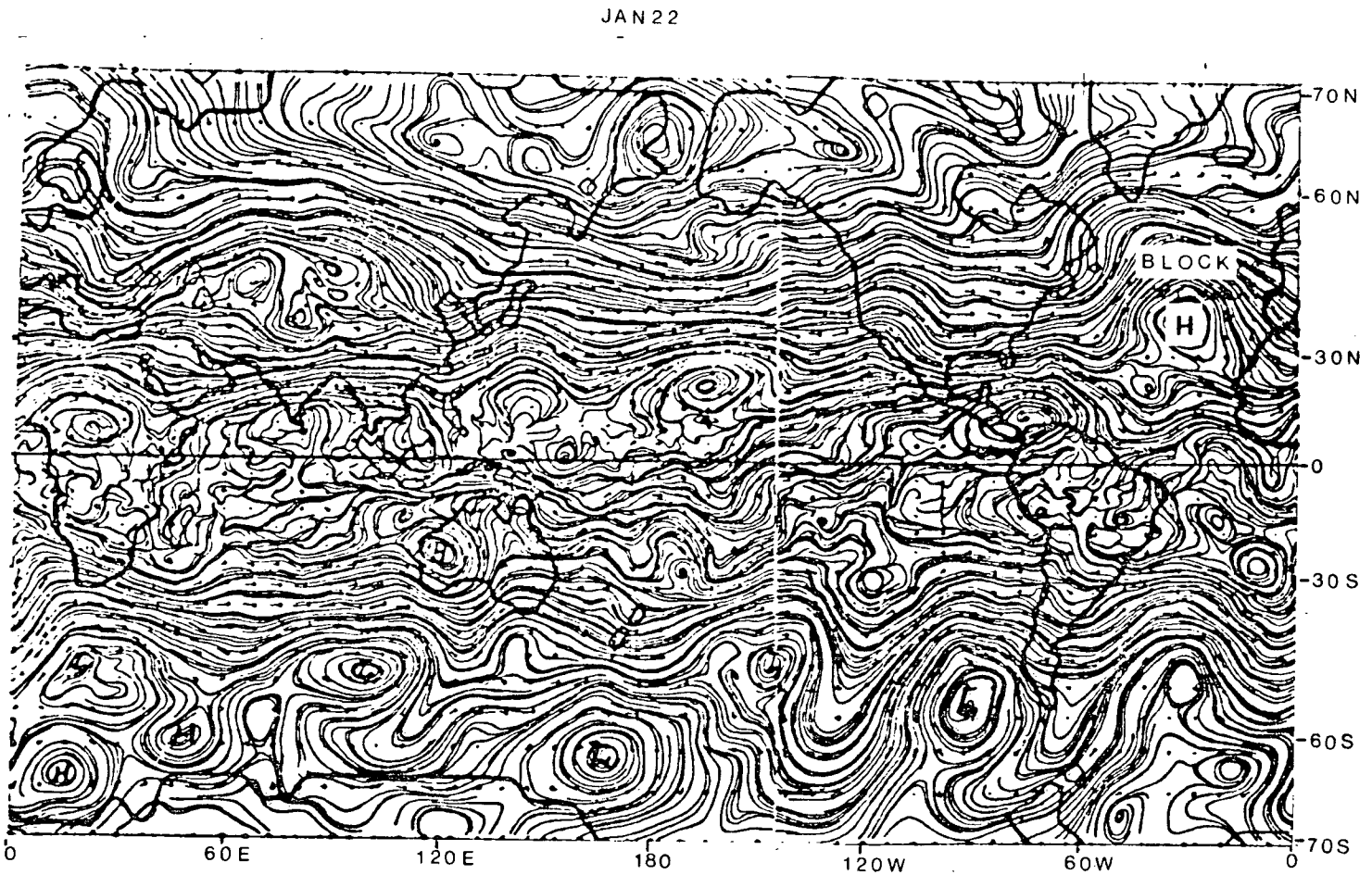

Fig. 2.17 Illustrating simulation at 500MB of a blocking episode using 1967 11-level GFDL GCM. Note blocking anticyclone at 35°N 30°W, cyclone at 25°N 40°W and upstream split jet. Lau(1980).

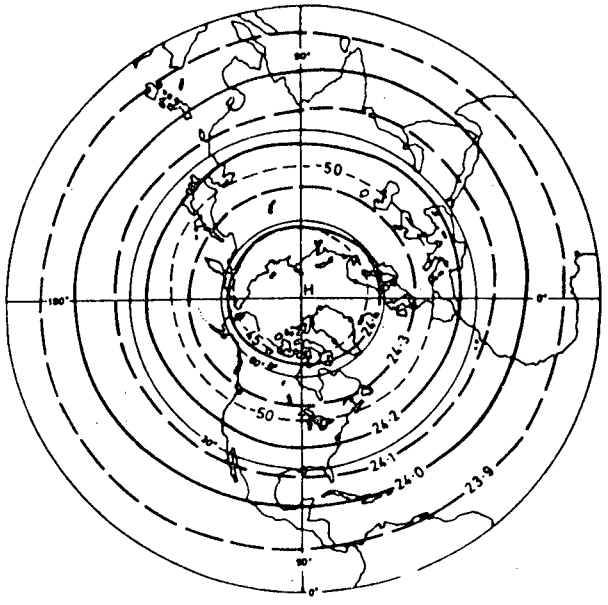

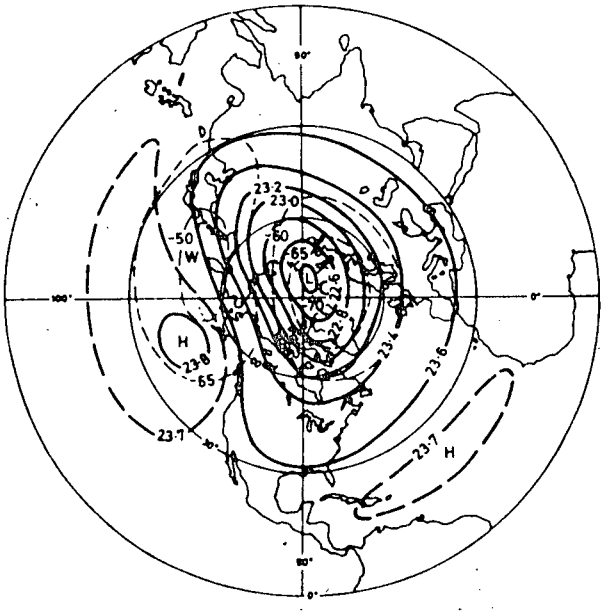

Fig. 2.18 Seasonal mean 30MB geopotential height (solid lines, km) and temperatures (dashed lines, °C) fields for summer (top) and winter (bottom) Northern Hemisphere seasons (After Hare, 1968).

Fig. 2.18(b) shows a dramatic reversal in the motion and temperature fields for the winter season. The mean flow in the mid- and high latitudes is characterized by fast "polar night" westerlies in a pattern made strongly asymmetric by the prevailing Aleutian anticyclone.

This asymmetric feature in winter and its absence in summer is explained by the manner in which the primary long waves in the stratosphere are generated. They do not develop 'in situ' but "appear to be produced by the vertical propagation of planetary waves forced in the troposphere by orography and land-sea contrasts. [These, in turn,] can only propagate vertically when the stratospheric winds are westerly" (Holton, 1979). Consequently, the summer mean vortex is almost completely undisturbed, but the winter vortex is highly distorted (often anticyclonically over the Aleutian area) by upward propagating waves.

Every two or three years (e.g., 1976-77, 1978-79) tropospheric planetary zonal wave numbers 1 or 2 become anomalously large and their upward propagation into the stratosphere results in a deceleration of the mean zonal winds. The subsequent sequence of events culminates in a rapid breakdown of the polar night jet, a sudden large scale warming (as much as $40^{o}C$ in a few days has been observed) and the creation of a circum-polar easterly current.

These stratospheric warmings have been investigated by Labitzke (1978), Johnson (1978) and Quiroz (1979) and theoretical treatments have been developed by Tung (1977) and Egger (1979). The consensus seems to be that strong blocking is a necessary but not sufficient condition for a major mid-winter warming. If the blocking event is initiated by constructive interference between wave numbers 1 and 2 then a subsequent

warming will result. If the dominant initiation wave components are ≥ 2 then a major warming will not occur.

2.11 Concluding remarks

In this Chapter we have attempted to explain what is meant by "blocking" and have described a typical major episode. The "conservation of absolute vorticity" principle was invoked to discuss inertial responses of an idealized atmosphere to an internal perturbation or external forcing. Some of these responses could be related to the motion and development of high latitude anticyclones.

Blocking is frequently observed during that part of the index cycle where meridional flow becomes strongly established in the mid-latitudes. Moreover, it is conceivable that the growth of a blocking anticyclone is the outcome of baroclinic instability at the long-wave part of the spectrum.

Numerical simulations using a general circulation model disclosed the effect of the Northern Hemisphere's topography on the low level and upper troposphere circulation. It was also noted that characteristics of blocking episodes as they occur from day-to-day in the real atmosphere are not being well simulated by the models.

Finally there was a brief discussion of the relationship between blocking and sudden warmings in the polar vortex of the winter stratosphere.

It is hoped that this chapter has provided a useful background from which to draw interpretations of data to be subsequently presented. We have deliberately avoided a literature review and will refer to relevant papers as the dissertation is further developed.

CHAPTER 3

3. ANOMALY FIELDS AND IMPLICATIONS FOR IDENTIFICATION OF BLOCKING

3.1 Introduction

The literature includes a number of comprehensive investigations into the climatology of blocking, and the identification criteria quite naturally reflect those aspects of the phenomenon considered important by the respective authors. Rex (1950a, 1950b), for example, perceived the splitting of the jet stream into two branches of comparable mass-transport characteristics to be essential to the blocking process and indeed recorded the location of the split as his "block position". He further stipulated that, for the process to qualify as a blocking episode, the observed double jet system must extend over at least 45 degrees of longitude and the pattern must maintain recognizable continuity for at least ten days.

Sumner (1954, 1959) was less restrictive in his criteria. His experience as a synoptician gave him an appreciation of the variety of configurations of the pressure field which can occur even within the context of a predominant atmospheric mode such as blocking. He described the essential characteristics of blocking as a "rather sharp diminution of zonal flow within the band occupied elsewhere and previously by the main concentration of westerlies". But to identify episodes he resorted to <u>pattern recognition at the 500MB level</u> using, for guidance, <u>six patterns</u> typical of the more frequent occurrences. Of the six, two examples appeared to predominate:

(a) The "split-jet", comparable to the Rex configuration

(b) The "meridional", known in North America as the "Ω-block"

These are illustrated schematically in Fig. 3.1. The other four patterns are variants from, or combinations of (a) and (b).

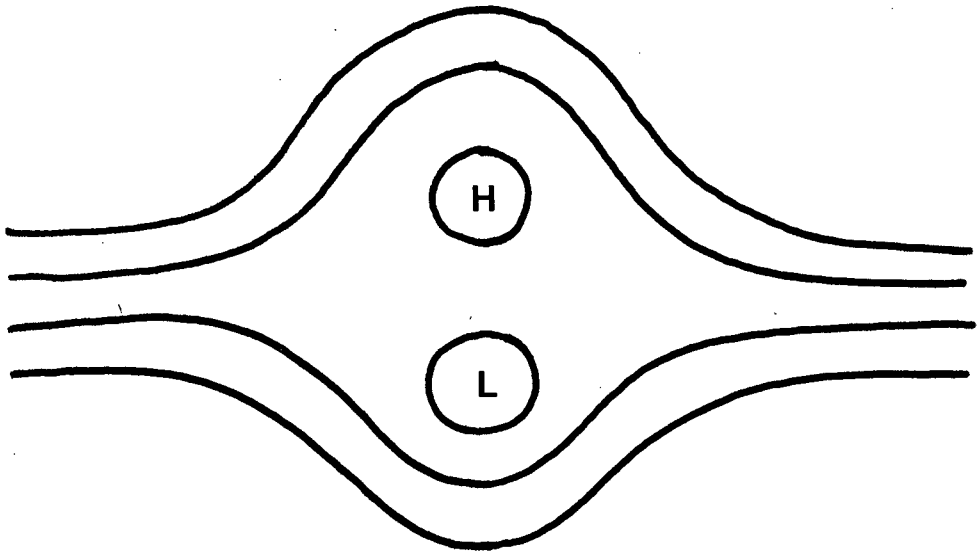

Fig. 3.1(a) Split-jet Block

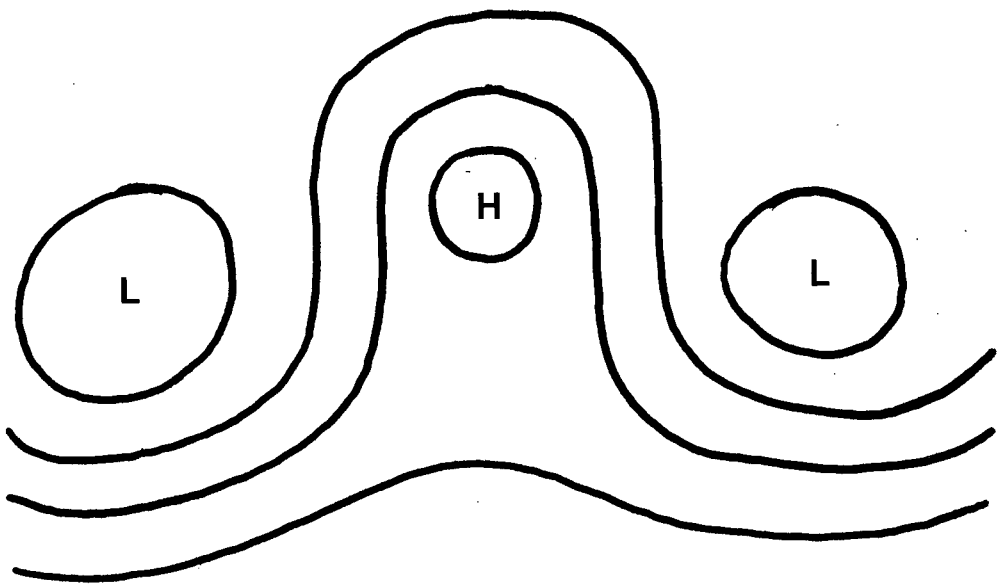

Fig. 3.1(b) Omega Block

Treidl et al. (1980a) stipulated that:

(a) Closed isopleths must be present simultaneously in the surface and 500MB charts.

(b) The westerly current must split into two branches.

(c) The minimum duration must be five days.

The last-named authors applied these criteria to the 33-year period 1945-1977, inclusive. Over 12,000 days of 500MB analyses of the Northern Hemisphere were individually examined and the corresponding MSL analyses were used for supplementary information. Adjuncts to this study have been made available by the senior author.

The criteria used in these three papers did not exclude the need for subjective judgment. Often cases were counted where, in principle if not to the letter, they appeared to qualify. Moreover, none of the methods was amenable to machine processing. Each required the extremely demanding procedure of inspecting hundreds, and in the case of Treidl et al., thousands, of synoptic weather maps and manually recording the relevant data. There was the ever-present possibility that cases would inadvertently be overlooked and, particularly over a long period of record, the accumulation of such omissions could become significant.

3.2 Anomaly fields

As indicated in Chapter 1, one of the goals of this thesis is to investigate the climatology of blocking by using objective criteria adaptable to machine processing large data sets. Since the block appears to be a strongly anomalous feature of the height field, it seemed natural to consider the relationship between the geometry of the anomaly field and those other fields from which it was derived.

We assume an infinite plane, on which simple, idealized patterns are described with reference to a rectangular coordinate system where:

x = longitude (+)ve to the East of the Greenwich meridian

y = latitude (+)ve to the North

Let the "normal" height field be $\bar{Z} = -a_1 y$ (3.1)

(which implies a uniform West to East flow)

and let the "instantaneous" height field be

$$Z = -a_2 y + a_3 \sin kx \sin my \tag{3.2}$$

By "instantaneous" we mean for a designated calendar day and time. Since we shall later use the 5-day interval (pentad) for a time unit, the term "instantaneous" will also be understood in the sense of "for a designated pentad".

The expression for Z in (3.2) describes a composite field which is the resultant of a uniform zonal W-E flow, and also a cellular structure defined by wave numbers k and m. One measure for assessing which of these two components (zonal or cellular) will predominate is

$$\left| \frac{a_2}{-ma_3} \right|$$

As explained in Appendix III, if the ratio > 1, no centres of maximum or minimum will appear, whereas, as the ratio decreases from 1 to 0 the cellular structure is increasingly amplified over the pattern domain.

The Anomaly field, by definition, is

$$Z - \bar{Z} = (a_1 - a_2)y + a_3 \sin kx \sin my$$

Now, a_1 and a_2 are both positive in the mid-latitudes and usually each is $> |a_1 - a_2|$ in the mid-troposphere

Therefore

$$\left| \frac{a_1 - a_2}{-ma_3} \right| < \left| \frac{a_2}{-ma_3} \right|$$

Consequently an anomaly field will usually have a larger number of maximum and minimum centres per given domain than either the "normal" or the "instantaneous" fields.

As an example, Fig. 3.2 shows the anomaly field $Z - \overline{Z}$ arising from subtracting a hypothetical "normal" field $\overline{Z} = -4y$ from an "instantaneous" field $Z = -4y + 2\sin 3x \sin y$

Note that for this case the ratio $\left| \frac{a_1 - a_2}{-ma_3} \right| = 0$

Hence the anomaly field has zero zonal component and is markedly cellular.

Although the example is highly idealized the principle is general and illustrated by a series of schematics (Figs. 3.3., 3.4 and 3.5). Figures 3.3 and 3.4 are structures typical of the amplifying stage of the meridional type of blocking which often evolve into an omega pattern. There is a significant difference in orientation of the respective trough - ridge patterns, NW - SW in the case of Fig. 3.3 and NW - SE in Fig. 3.4. A diffluent jet schematic is shown in Fig. 3.5. All three figures show how the anomalies (drawn by graphical subtraction) have a distinctive cellular structure with clearly identified centres.

Several studies (e.g., Treidl et al., 1980a) stipulate a closed anticyclonic Z - contour of the 500MB surface in the mid- and high latitude as one criterion to be met on an "instantaneous" chart to qualify as a possible blocking high. The analysis of constant pressure charts in the

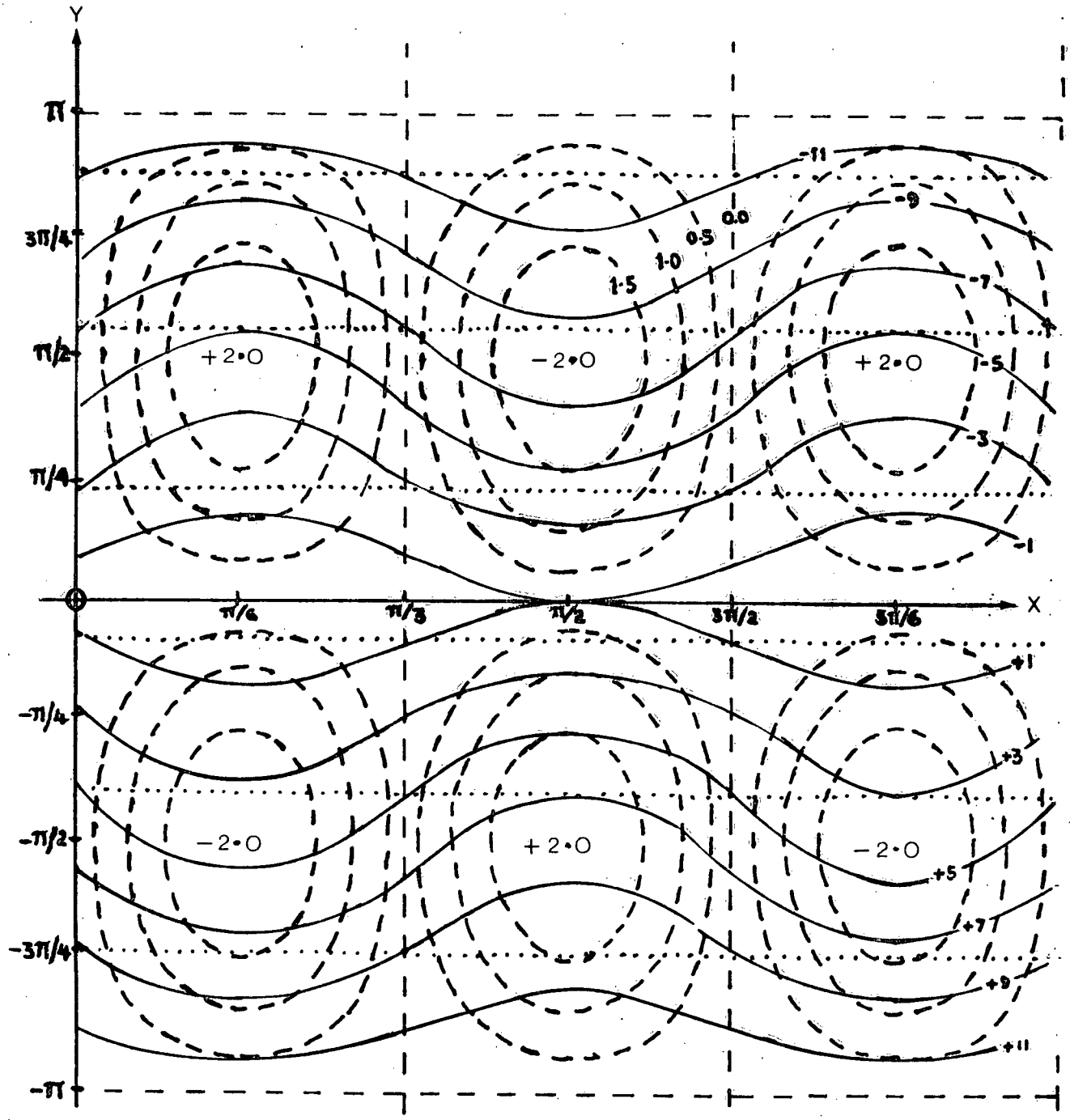

Fig. 3.2 Analytical example of Anomaly Field

Normal Field	$\bar{Z} = -4y$	.....
Instant Field	$\underline{Z} = -4y + 2\sin 3x \sin y$	————
Anomaly Field	$Z - \bar{Z} = 2\sin 3x \sin y$	— — — —

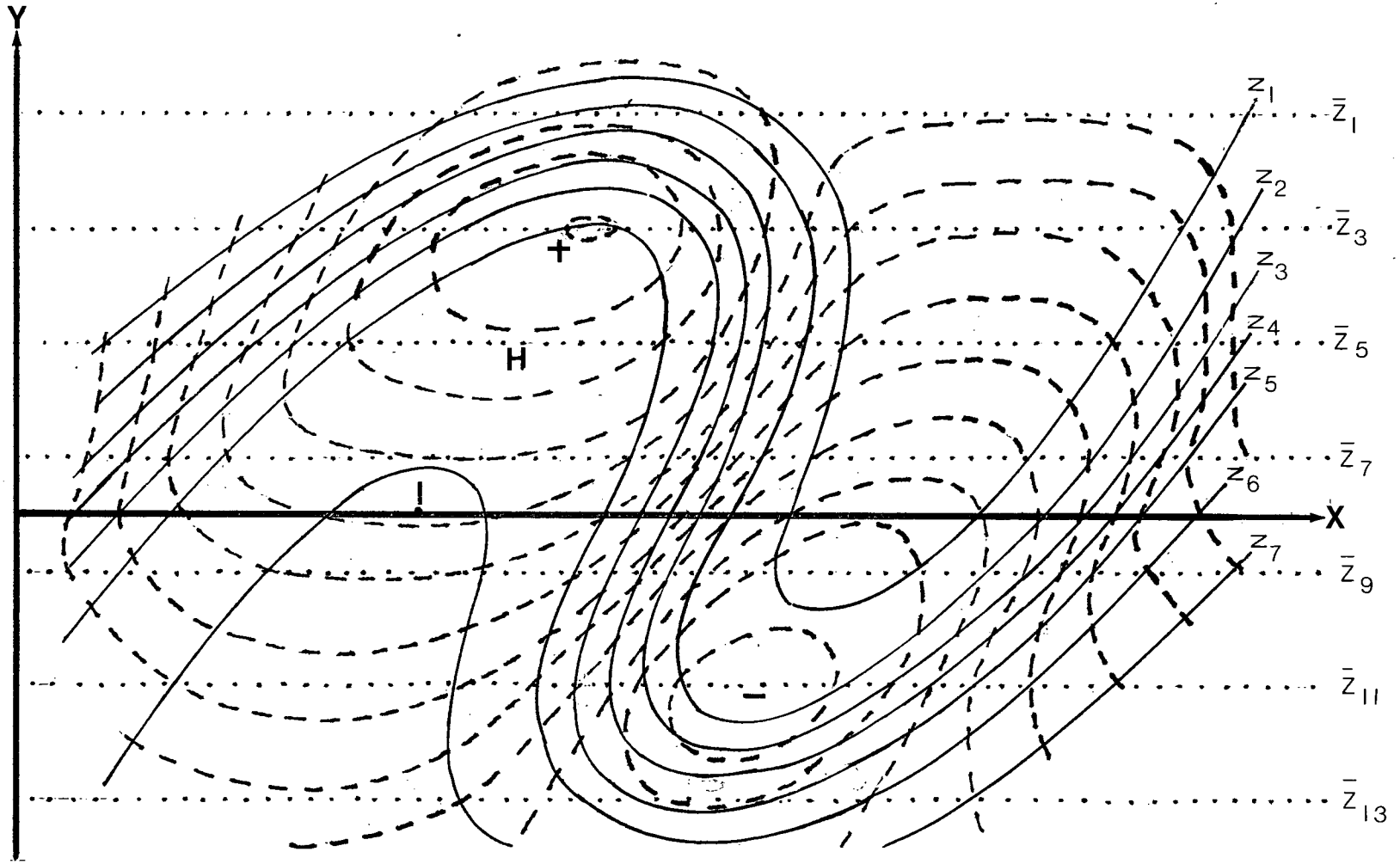

Fig. 3.3 Amplifying Wave, NE-SW tilt. "I" is the intersection of ridge line with x-axis. Probable location of incipient Blocking Anticyclone marked "H". Positive Anomaly Centre is NE of "I" and "H".
$\bar{Z}$ field ····· Z field ———— Z - $\bar{Z}$ — — — — —

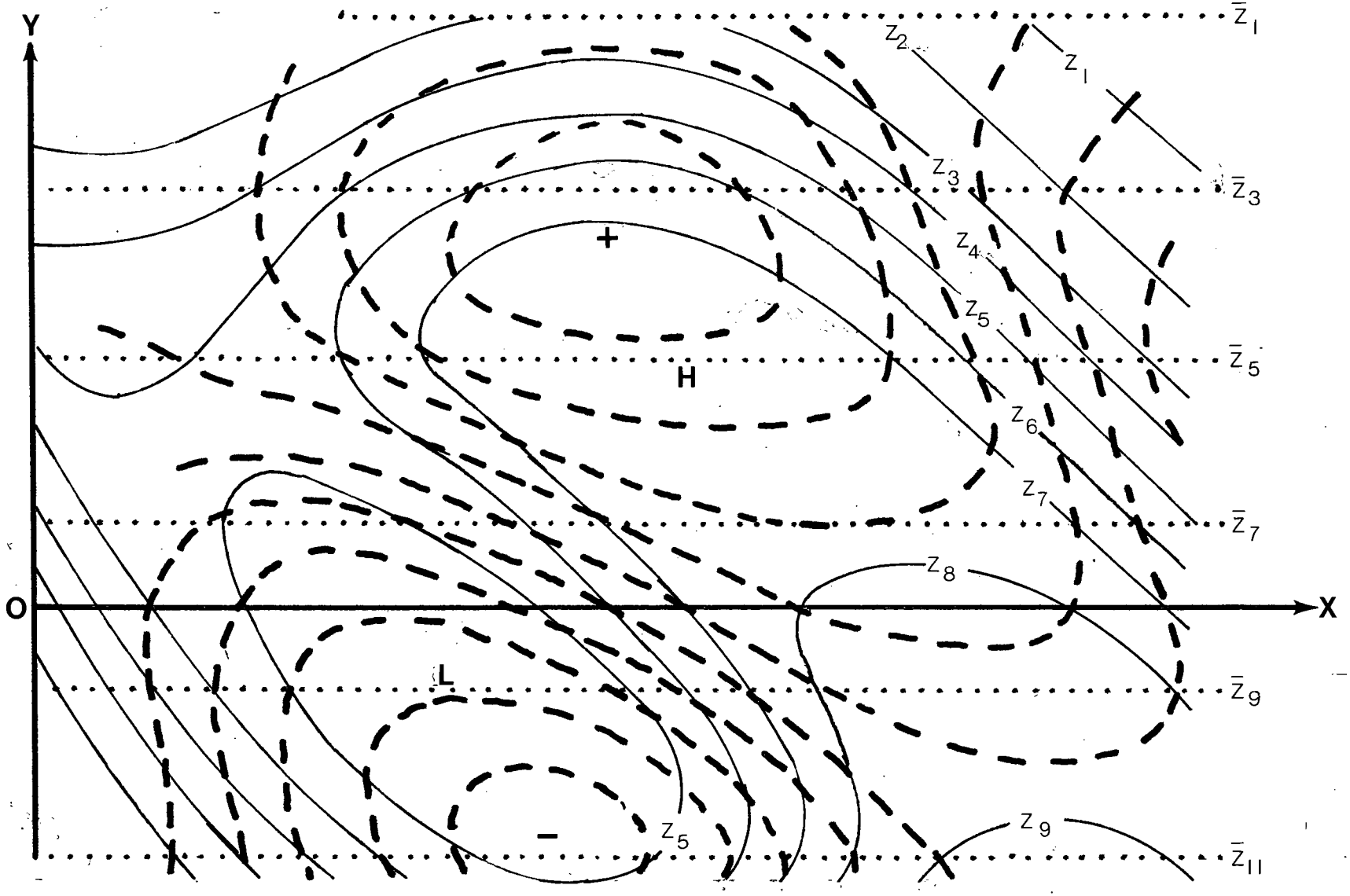

Fig. 3.4 Amplifying Wave, NW-SE tilt. Positive Anomaly Centre is NW of "H". Legend as in Fig. 3.3.

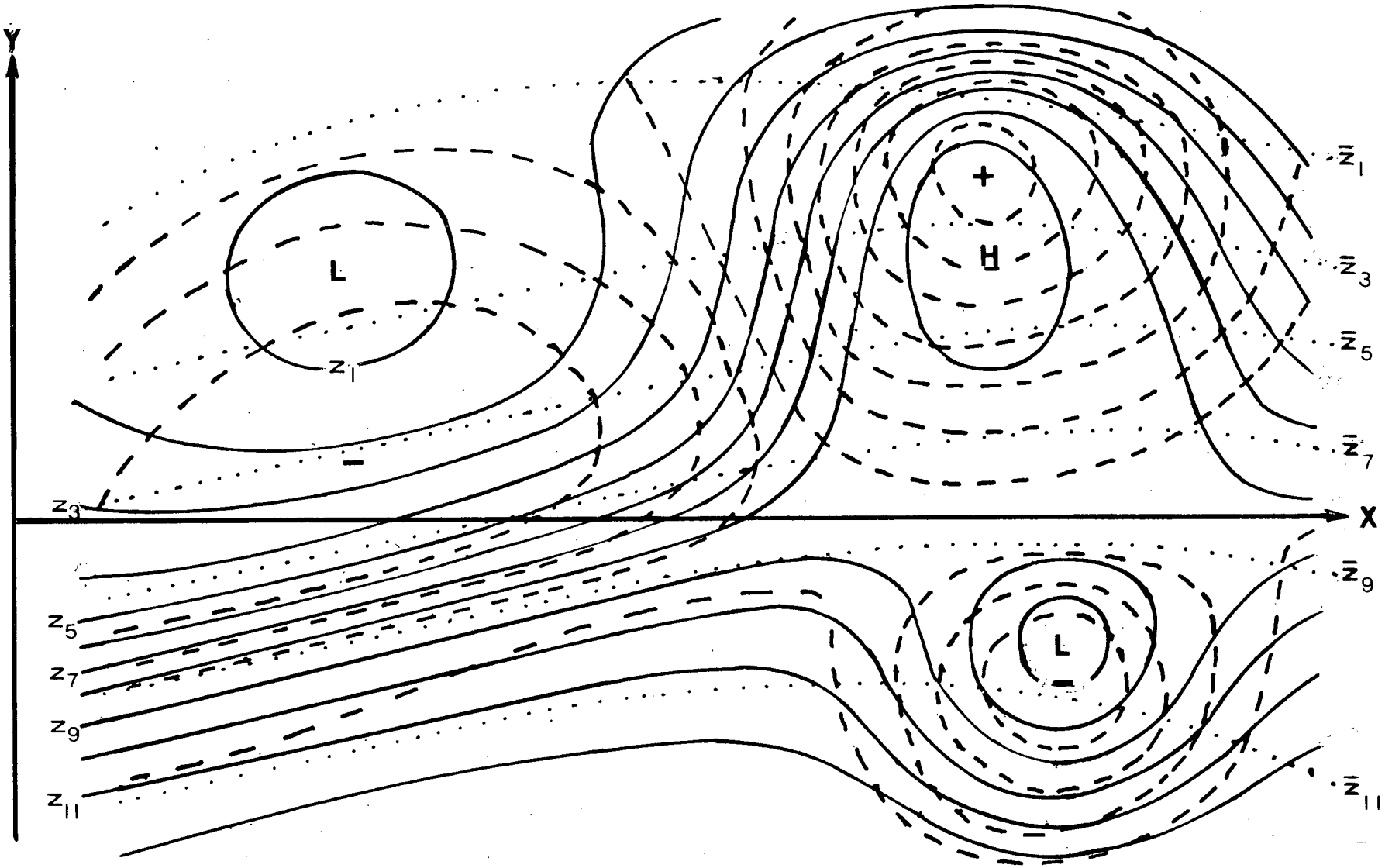

Fig. 3.5 Diffluent Jet. Legend as in Fig. 3.3

mid-troposphere is conventionally carried out by drawing contours at a 6 dam interval. It will be appreciated that the application of a "closed contour criterion" will be influenced by the arbitrary choice of isopleth interval. On the other hand the nature of the geometry of the associated anomaly pattern to a large extent eliminates this difficulty.

It is important to remind ourselves that anomaly centres do not exactly coincide with the centres of the associated lows and highs of the Z-field. Positive anomalies are displaced north of the high and negative anomalies south of the low. The amount of displacement will vary with the respective $\bar{Z}$ and Z fields. A robust closed blocking anticyclone with a centre, say, 30 dams above normal, will usually have an associated anomaly centre located within one or two degrees of latitude. On the other hand meridionally oriented ridges, e.g., Figs. 3.3 or 3.4, may feature an anomaly centre some five to ten degrees north of the reference latitude (x-axis) of the wave form. If the anomaly is large (criteria will be developed in the next chapter) it is very likely that the ridge is in an amplifying stage and that the subsequent instantaneous chart will reveal an eddy (i.e., the blocking anticyclone) at the northern extremity. If this does occur the anomaly centre will usually be within 1 to 5 degrees latitude of the anticyclone.

There may also be a longitudinal displacement of the anomaly relative to the location of the blocking anticyclone. The sign and amount of the shift will depend on the orientation of the axes of the respective Z and $\bar{Z}$ field wave forms. Fig. 3.3 shows that a positive (NE-SW) tilt will displace the anomaly centre east of the ridge intersection I with the x-axis, while Fig. 3.4 shows that a negative (NW-SE) tilt will result in a westward displacement.

Most of these displacements are greatest for daily fields at the amplification and decay stages of the episodes. This is one of the reasons why we chose to use 5-day averages of Z for basic data units in Chapters 4, 5 and 6.

3.3 A Case Study

The sequence of 700MB 5-day mean contours shown in Figs. 3.6 and 3.7 from Green (1968) illustrates the relationship between the position and strength of actual blocking episodes and the corresponding (+)ve anomaly. December 1968 was unusual in that it featured the development of three geographically separated areas of blocking activity within the Western Hemisphere:

(1) A progressive amplifying ridge over Western Canada December 10-14 (anomaly +8 dams) develops into a blocking high over Hudson Bay, December 17-21 (anomaly +23 dams), which by December 24-28 has progressed to 60°N, 25°W (anomaly +30 dams) southwest of Iceland.

(2) A split in the westerlies over the Pacific Ocean near 40°N, 180°W, December 17-21, is synchronous with amplification of the sub-tropical high centred at 25°N, 135°W, and the subsequent establishment of a moderately strong blocking anticyclone over Alaska December 24-28 (anomaly +21 dams).

(3) A blocking anticyclone centred near 55°N, 10°E (Denmark), December 10-14 (anomaly +14 dams), moves eastward and off the chart by December 17-21.

In cases (1) and (2) the distance between the blocking anticyclone centre and the associated positive anomaly centre ranges from a minimum of 100km (Hudson Bay and Alaska positions, respectively) to a maximum of 500km (Iceland-Greenland position on December 24-28).

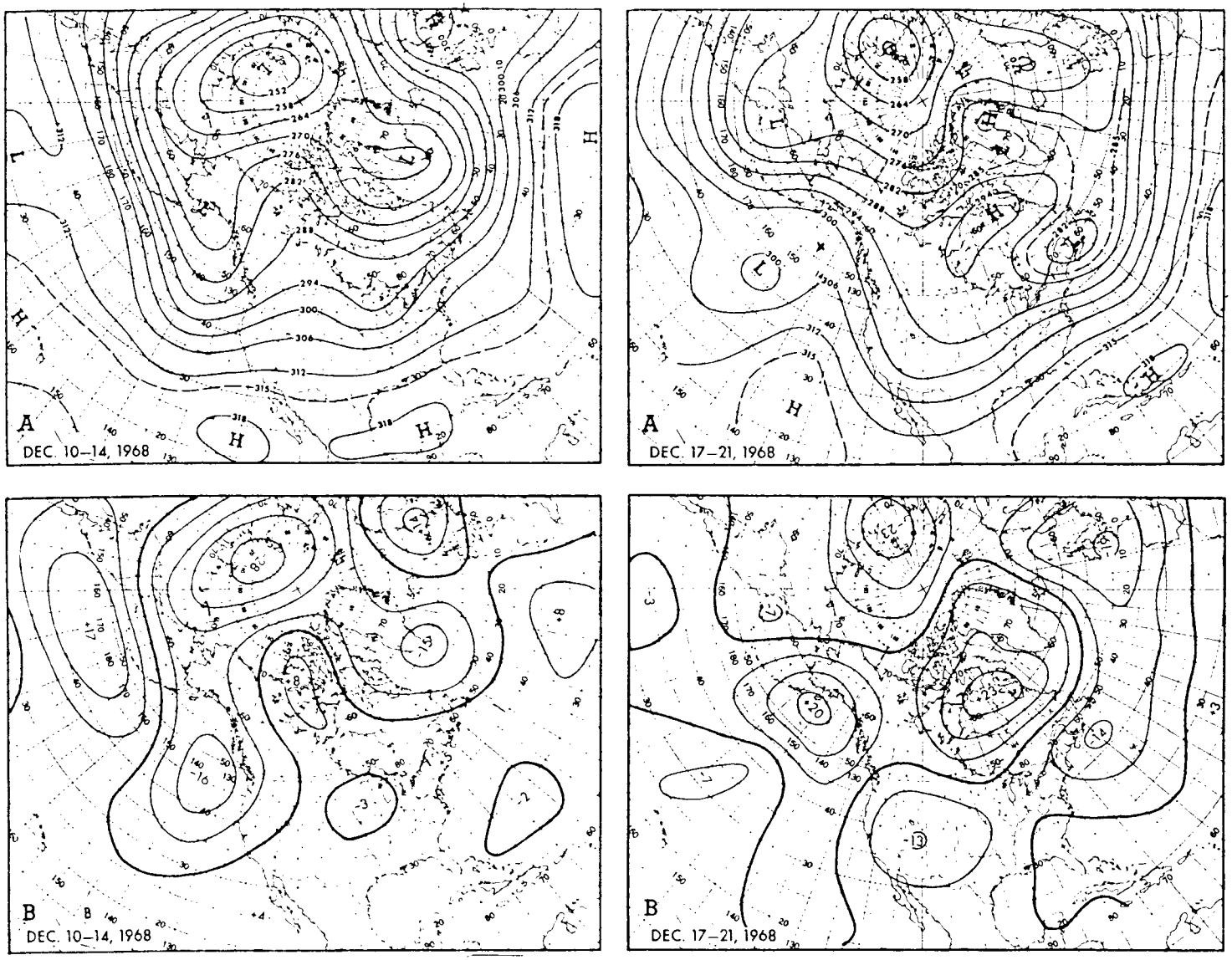

Fig. 3.6 (A) mean 700MB contours and (B) departure from normal of 700MB height (both in decametres) for December 10-14, 1968 and December 17-21, 1968 . (Green, 1968).

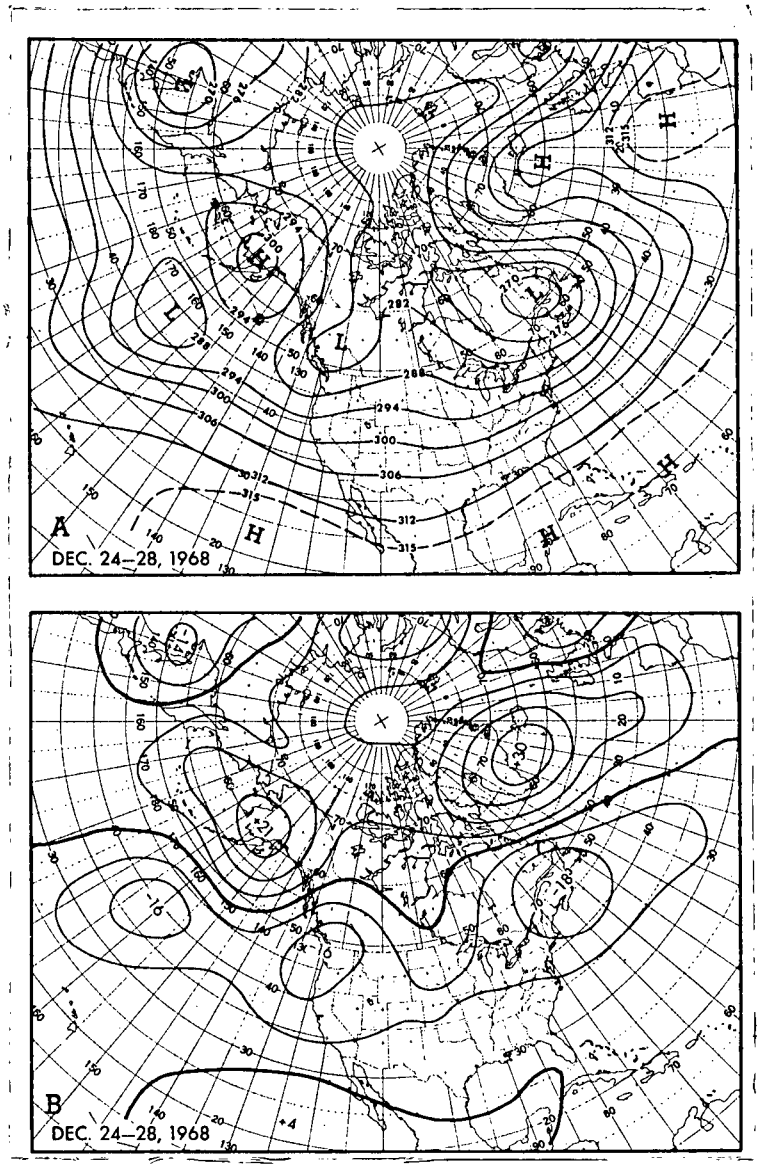

Fig. 3.7 Same as Fig. 3.6 except (A) and (B) for December 24-28, 1968. (Green, 1968).

3.4 Summary

A review of selected studies from the literature has revealed a considerable diversity in criteria by which to judge the occurrence or otherwise of a blocking episode. Moreover, the actual identification of an occurrence was carried out by subjective inspection of daily charts, a very time-consuming procedure for a large data set.

An investigation into the relationship between height anomalies and the Z-field configurations from which they arise, has disclosed a strong propensity for cellular structure of the $Z - \overline{Z}$ field which, in turn, implies centres of maxima and minima. The positive centres were closely identified with amplified anticyclones or ridges and the relative locations depended on the orientation of the original Z structure.

From examination of a case study, it was clear that centres of strong positive anomalies in the mid- and high latitudes corresponded unambiguously to blocking anticyclones, or, more generally, to the amplified feature (e.g., the wave crest) of the Z-field which has effectively become part of the blocking process.

In the next chapter we shall first present the rationale for application of an appropriate time filter to the data base. We shall then describe the results of empirical tests on positive anomalies. These will be designed to provide objective criteria for frequency studies of blocking using machine processing methods.

CHAPTER 4

4. THE BLOCKING SIGNATURE

4.1 Introduction

So far our attention has been primarily focussed on certain spatial properties of two-dimensional fields of geopotential and, in particular, on the use of the anomaly for the identification and measurement of significant features. However, before proceeding with the empirical tests referred to in Chapter 3, there is an important question to be addressed with regard to the data base. The data available consists of twice-daily values of geopotential at each point of a 381 km grid over the Northern Hemisphere for 33 years of record. For statistical investigations into blocking did we really need a series of observations with a time interval as small as 12 hours? For two reasons it seemed to be preferable to use a temporal resolution more related to the time scale of the phenomenon being studied. First, we did not want to include the high frequency short-wave transient features conventionally referred to as synoptic-scale systems. Second, a significant reduction in the size of the enormous data base, without loss of the features of interest would reduce the computation time and make the task of cataloguing results more tractable.

4.2 Considerations for a Time Filter

One of the primary characteristics of major blocking systems is their association with large amplitude slow moving long waves. Therefore we required a technique which, when applied to the available data, would pass these features and filter out the faster moving transients. Typical

of the latter category are the frontal waves of the lower troposphere. They are usually scaled (Holton, 1979) as:

$l \sim 10^6 m$ where l = length scale $\simeq 1/4\ L$

$c \sim 10\ m\ s^{-1}$ where c = speed scale

$T \sim 10^5 s$ where T = time scale $\simeq 1$ day

It would therefore take the order of four days for a complete wave ($L \sim 4 \times 10^6 m$) to pass a reference point. Clearly, then, a simple 5-day average filter will provide a derived set of data which will strongly suppress the features of transient synoptic-scale systems.

The slow moving long waves are conventionally regarded as having wave numbers in the range k = 1 to 5 and typically c ranges between -5 and +5 m s^{-1}. If, for example, k = 4 at 60^oN ($L = 5 \times 10^6 m$) and the speed is 2.5 m s^{-1}, then it will take the wave 23 days to pass a reference point. (If the amplitude is large and the wave is associated with a blocking anticyclone, we might regard the latter as the quarter wave length centred about the crest. It will pass a reference point in about six days.) The 5-day average will not likely result in a serious attenuation of the wave's features and therefore the blocking anticyclone will still be readily identifiable.

4.3 The Response to a Five-Day Average Filter

The above discussion is heuristic. In Appendix IV-1, we have developed an expression for the response of a longwave harmonic to a contiguous 5-day average following Barrett (1958). The filtering function, Figure 4.0, is:

$$\frac{\overline{A}_k{}^2}{A_k{}^2} = \frac{2(1 - \cos 5k\mu_k)}{(5k\mu_k)^2}$$

Where k = wave number

A_k = amplitude

$\overline{A}_k$ = amplitude of the time averaged wave

μ_k = phase speed (radians of longitude day^{-1})

ω_k = angular frequency (day^{-1}) = $k\mu_k$

We tested this filter on harmonics of characteristic large amplitude long waves associated with blocking (k = 1 to 4, μ_k = 0 to 5 degrees day^{-1}) and also on those associated with transient baroclinic waves in the mid-latitudes (k = 8 to 14, μ_k > 5 degree day^{-1}). The former group were passed with little loss of amplitude while the latter were completely attenuated. The suppressed daily fluctuations caused by the baroclinic motions are then regarded as 'noise', but only because of the choice of our time scale. We must remain aware of the <u>continuous</u> spectrum between the wave length thresholds for instability (Chapter 2) and also of the crucial role of the short-wave eddies during energy exchange processes with the larger systems.

Statistical studies of the kind we envisage must be founded on the creation of categories relevant to the physical system. The atmosphere can be categorized using devices such as scaling and pattern recognition but we would be naïve to expect these categories to bear a one-to-one relationship to individual large scale structures. For example, we have suggested that a blocking anticyclone, viewed as a component of an amplified long-wave structure, will have time and space characteristics

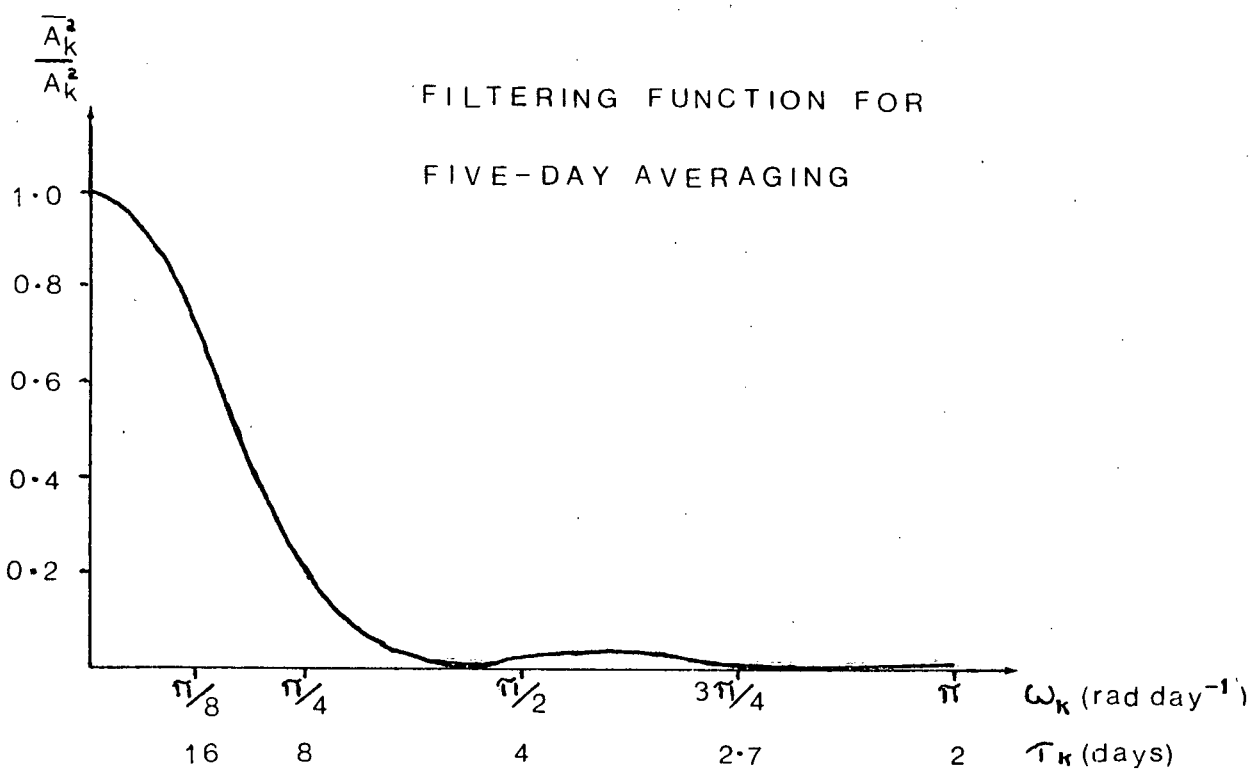

Fig. 4.0 Attenuation of squared amplitudes of harmonic waves resulting from five-day averaging, as a function of angular frequency (ω_k) in radians per day or period (τ_k) in days. For details see Appendix IV. (After Barrett, 1958).

of the same order of magnitude. In the case of major blocking episodes this is true. But an inspection of daily 500MB weather maps will disclose a surprising number of configurations (particularly over the continents) which have the characteristics of blocking highs (split upstream flow, barotropic core structure) but a wavelength closer in magnitude to that of a baroclinic system. They do move slowly but, because they have smaller dimensions than major blocks, the contiguous 5-day averages will sometimes attenuate these cases so that they fall below our threshold of recognition. We shall attempt to design criteria which will minimize the number of times this happens.

On balance we conclude that the 5-day average is an effective low pass filter and we shall therefore use it for the purpose of this Chapter and also 5 and 6.

4.4 Purpose

In Section 3.3 (Anomaly Fields) there is the implicit hypothesis that positive anomalies of the 5-day mean 700MB or 500MB height may turn out to be useful identifiers of blocking occurrence. This was tested for the 700MB level in a pilot study (Knox, 1979). We compared samples of positive anomalies of 5-day averaged 700MB height fields (of the kind illustrated in Figs. 3.6 and 3.7) with actual blocking episodes observed on day-to-day mid-troposphere analyses. The episodes were identified either by the author or from sources in the literature such as Rex (1950), Treidl et al. (1980a), etc. This approach sidestepped the issue of common criteria by which to judge the occurrence of a blocking episode, an issue we shall attempt to resolve later in this Chapter.

The reason we chose the 700MB level was because of the availability of a catalogue of 700MB 5-day average anomaly centres (O'Connor,

1966). This publication lists the date, position and magnitude of each positive and negative 700MB anomaly centre that has occurred in the Northern Hemisphere during the sixteen year period 1947-1963, inclusive. It was then possible by cross-comparison to develop a set of "associative" criteria against which a 700MB positive anomaly centre could be compared, to determine if, in fact, it was associated with an observed blocking episode. The criteria turned out to be functions of time of year, anomaly magnitude and latitude.

We coined the term BLOCKING SIGNATURE for a positive anomaly centre which met the criteria. This derived quantity has a central role in the results to be developed. The purpose of this Chapter is to develop criteria for the blocking signature using a much longer record of data at a more appropriate level in the troposphere.

4.4.1 Sequel to the Pilot Study

Although the results were encouraging, there were limitations to the pilot study which were important to overcome in the subsequent investigation:

(a) the data base needed to be updated from 1963 to the present.

(b) the resolution of centre locations in the O'Connor Catalogue (±5 degree latitude and ±5 degree longitude) was relatively coarse.

(c) the issue of "what is an actual observed blocking episode?" needed to be clarified.

(d) the somewhat "ad hoc" method we used to determine "blocking signature" needed to be replaced by a more objective systematic procedure.

(e) the 700MB level is too close to boundary layer processes, and is entirely inappropriate in the vicinity of the world's major mountain massifs.

(f) because of the enormous volume of information, it was essential for the technique to be amenable to automatic data processing.

We selected the 500MB level (≈5.5 km). It is generally removed from turbulent and convective boundary layer processes, and is more representative of the mid-troposphere. (We considered the 300MB level but were concerned with complications arising from the frequent winter season lowering of the tropopause below 300MB. Moreover, we preferred a longer data base than is available at that level.) A 33-year (1946-1978) set of analyses of the daily 500MB height field over the Northern Hemisphere was available on magnetic tape.

In the next sections we shall outline the procedures and present the results of the 500MB 'blocking signature' investigation.

4.5 Processing the Data Base

4.5.1 The Data Base

A 33-year record of 500MB grid point data for the Northern Hemisphere was obtained from the National Center for Atmospheric Research (NCAR), Boulder, Colorado. This record includes daily values (00GMT), of 500MB heights at each of 1,977 points on the NMC Octagonal Grid, which extends from 15°N to the pole (Jenne, 1970). The map projection is polar stereographic and the grid resolution is 381 km, true at 60°N (Fig. 4.1). The exact record is from January 1, 1946 to February 28, 1979 which ensures data for 33 complete winters. The entire data set consists of 24 x 10^{6} values of 500MB height expressed to the nearest tenth of a metre.

4.5.2 Pentad Averages

A pentad is a specified period of five consecutive days, and the pentad calendar we shall use will be found in Fig. IV - 1. The conventions

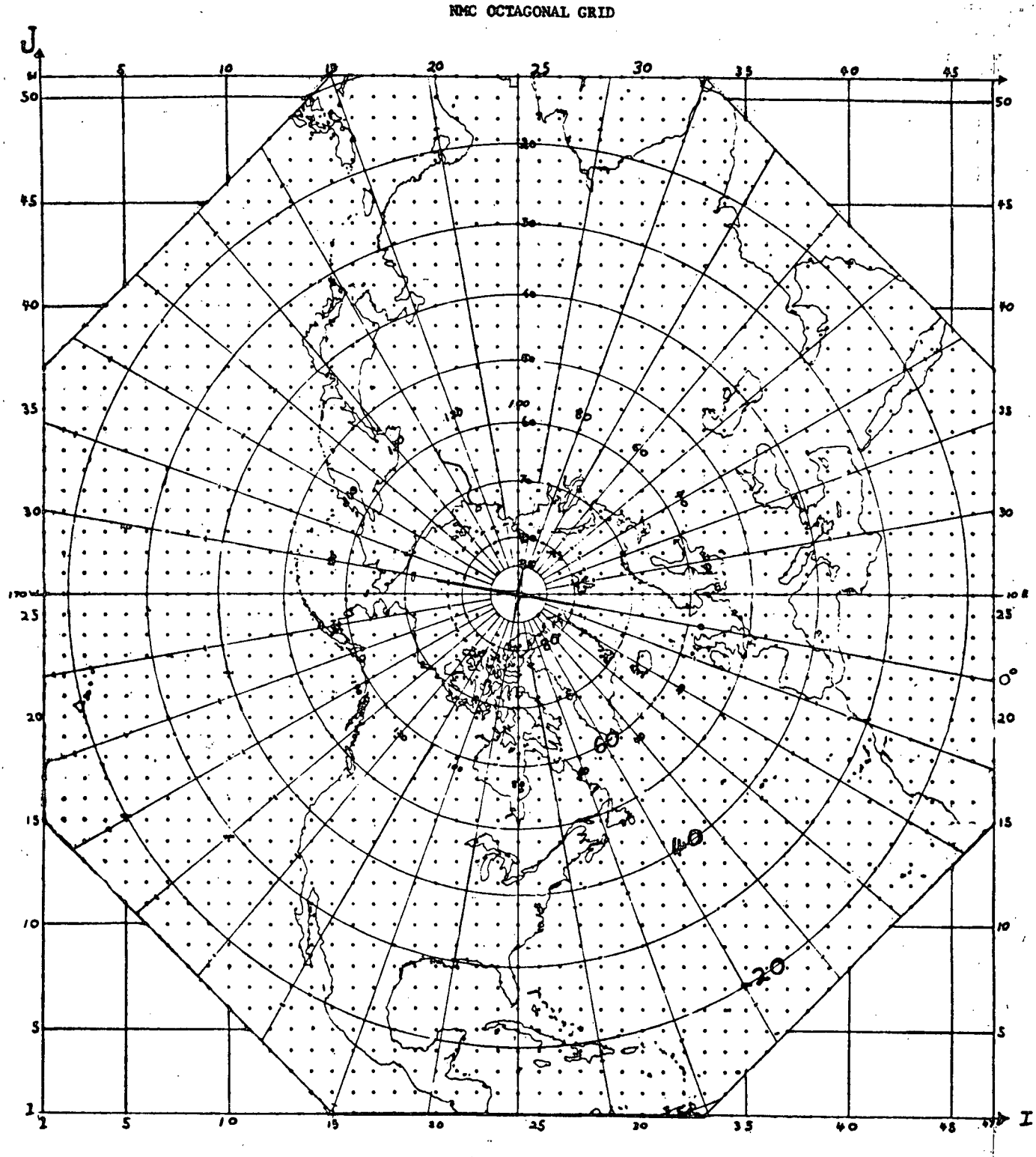

Fig. 4.1 NMC Octagonal Grid. There are 1977 data points in the octagon. The Pole point is I,J = 24,26. (Jenne, 1970).

adopted here are that Spring contains 19 pentads, while the other seasons have eighteen each, and that in the event of leap year, pentad number 12 (February 25 to March 1) will contain six days.

We shall designate a pentad as: yy_{PE_K}

Where yy = year

K = pentad number (1 to 73)

The <u>5-day average height</u> at grid point (I,J) for pentad K is

$$yy_{z_K}(I,J) = \frac{1}{5}\sum_{n=1}^{5} yy_{z_{K_{(n)}}}(I,J)$$

Where I = abscissa

J = ordinate

(see Fig. 4.1 for location of axes).

The data were converted to contiguous 5-day averages, thus reducing the data-sets from 365 to 73 grid-point fields per annum, or a total of approximately 2,400 fields of 500MB 5-day mean height for the period of record. For the purposes of this Chapter the five-day average is the basic unit.

4.5.3 Pentad Normals

Symbolically the <u>normal height</u> at (I,J) for pentad K is

$$\bar{z}_K(I,J) = \frac{1}{33}\sum_{yy=1}^{33} yy_{z_K}(I,J)$$

This operation was carried out to compute 73 sets of normal 500MB heights corresponding respectively to each pentad. Each set, in effect, consisted of the average of 33 x 5 = 165 daily height values at each grid point. These normals provide the baselines from which to calculate the anomalies.

4.5.4 Pentad Anomalies

The anomaly of the 5-day average 500MB height for year yy, pentad K, grid point I,J, is

$$^{yy}A_K(I,J) = {}^{yy}Z_K(I,J) - \overline{Z}_K(I,J)$$

and this operation was carried out to produce approximately 2,400 anomaly fields for the 33-year period of record.

4.6 Anomaly Centres

4.6.1 Location of centres

The anomaly fields, for reasons explained in Chapter 3, feature a cellular pattern of positive and negative isopleths, and the next step was to locate the centres of the cells. Each of the 2,400 fields of $^{yy}A_K(I,J)$ was searched for maxima and minima. (Negative anomaly centres were not required for this investigation, but they were located and listed for use in a future study of cold lows and troughs.) Trivial centres were excluded by the requirement that to qualify, the centre's anomaly value must be greater than 5 dams or less than -5 dams.

All centres were located to the nearest grid point (I,J) so that their positions are accurate to within $\pm 1.7^{o}$ latitude. This resolution was a decided improvement over the $\pm 5.0^{o}$ latitude of the data used for the pilot study.

4.6.2 Preparation of the Master Catalogue

Since our objective was to determine criteria for the "blocking signature" (section 4.2) we needed a convenient source of positive anomaly information. Therefore the anomaly centres were listed according to year, pentad of occurrence, location and value (dams). In effect, a Master Catalogue was created which provided, in compact format, salient information concerning the anomalous features of over 2,400 contiguous 500MB 5-day average height fields during the 33 years of record.

The (I,J) grid, though best for the centre search, and indeed for all our data processing programs, was inconvenient for geographical location. Hence all anomaly centre positions were converted to latitude and longitude for the Catalogue. A sample page is illustrated in Fig. 4.2.

For an "internal" consistency check we acquired a sequence of operational 500MB 5-day average height and anomaly analyses from the U.S. National Weather Service. The positive and negative anomaly centres were compared for position and magnitude with those of our catalogue and the mean differences were 150 km and 1.5 dams which are within our limits of resolution. We therefore concluded that the catalogue is an accurate source of 500MB anomaly data.

4.7 Blocking Signatures

4.7.1 Development of Signature Criteria

The earlier Pilot Study, Section 4.4, indicated the feasibility of developing criteria for the purpose of testing whether a single positive anomaly is likely associated with a concurrent blocking anticyclone. A positive anomaly which so qualified would be called a "blocking signature" and of course one would expect to find a sequence of blocking signatures

PENTAD 66 1968

MAXIMA			MINIMA		
LA	LO	DM	LA	LO	DM
38	91W	6	27	18W	-14
28	44W	9	57	31W	-26
31	132W	6	48	146W	-6
30	147W	6	70	102W	-29
43	2E	16	58	176W	-13
79	10E	11	44	177E	-14
75	176E	8	34	24E	-14
58	37E	14	60	86E	-27
47	135E	16			
41	125E	16			

PENTAD 67 1968

MAXIMA			MINIMA		
LA	LO	DM	LA	LO	DM
36	80W	12	30	107W	-16
45	80W	12	53	51W	-25
23	141W	7	64	88W	-16
66	17W	27	43	17W	-14
38	162W	11	65	170W	-24
54	16E	19	34	27E	-9
80	55E	8	61	100E	-33
33	60E	6	26	79E	-7
28	125E	6	20	76E	-6
26	115E	6			

PENTAD 68 1968

MAXIMA			MINIMA		
LA	LO	DM	LA	LO	DM
38	57W	10	44	93W	-16
21	133W	5	56	112W	-8
39	128W	11	48	32W	-28
61	10E	26	56	152W	-16
51	180	17	77	136W	-16
43	142E	17	31	26E	-7
			35	32E	-7
			29	168E	-5
			56	68E	-40

PENTAD 69 1968

MAXIMA			MINIMA		
LA	LO	DM	LA	LO	DM
37	107W	12	43	63W	-23
32	44W	9	49	139W	-25
75	156W	6	34	4W	-16
64	2E	22	78	62W	-14
43	142E	25	26	178E	-10
			72	137E	-30
			52	44E	-22
			58	81E	-16
			27	162E	-8

PENTAD 70 1968

MAXIMA			MINIMA		
LA	LO	DM	LA	LO	DM
25	117W	5	33	77W	-8
48	56W	17	45	138W	-25
33	30W	9	54	27W	-23
54	91W	13	56	152W	-15
70	102W	14	22	5E	-9
61	17E	12	39	14E	-13
45	167E	23	80	145E	-37
54	111E	12	66	73E	-25
25	40E	6	59	64E	-26
			45	42E	-15
			31	131E	-8

PENTAD 71 1968

MAXIMA			MINIMA		
LA	LO	DM	LA	LO	DM
26	135W	5	38	112W	-24
28	22W	7	42	59W	-13
61	73W	31	27	161W	-9
25	8W	10	53	7W	-28
53	153W	28	75	100E	-36
82	53W	12	30	37E	5
52	51E	14	31	159E	-6
39	38E	7			
24	37E	7			
43	142E	10			

PENTAD 72 1968

MAXIMA			MINIMA		
LA	LO	DM	LA	LO	DM
21	129W	5	36	45W	-20
28	22W	8	45	131W	-17
61	50W	18	28	15W	7
41	2W	19	68	89W	-6
60	156W	36	79	80W	-6
49	170E	19	33	163W	-11
57	51E	27	68	1E	-7
			58	4E	-9
			83	100E	-7
			31	26E	-16
			61	107E	-23
			28	75E	-10

PENTAD 73 1968

MAXIMA			MINIMA		
LA	LO	DM	LA	LO	DM
32	70W	5	51	53W	-16
30	53W	5	32	26W	-10
20	127W	5	50	118W	-26
71	69W	32	40	154W	-15
64	24W	38	48	15E	-25
60	176E	31	30	176W	-7
67	139E	26	27	162E	-9
70	78E	36	46	145E	-18
			47	91E	-23
			21	72E	-10

PENTAD 1 1969

MAXIMA			MINIMA		
LA	LO	DM	LA	LO	DM
37	120W	18	45	76W	-22
55	35W	28	32	26W	-18
70	58W	30	56	152W	-25
54	4E	14	27	167W	-13
57	177E	41	35	17E	-18
75	114E	30	45	68E	-21
62	60E	35	39	137E	-20
			24	67E	-10

PENTAD 2 1969

MAXIMA			MINIMA		
LA	LO	DM	LA	LO	DM
31	118W	11	44	89W	-17
19	134W	7	28	22W	-14
72	43W	35	52	136W	-16
51	170W	38	62	130W	-16
64	18E	18	48	14W	-25
77	156E	17	24	164W	-15
29	129E	6	29	32E	-10
			60	86E	-11
			44	153E	-6
			37	50E	-6
			45	68E	-13

PENTAD 3 1969

MAXIMA			MINIMA		
LA	LO	DM	LA	LO	DM
31	33W	11	38	72W	-19
68	89W	39	48	128W	-33
51	160W	24	31	154W	-11
85	145E	29	48	14W	-27
55	34E	7	72	10E	-9
54	153E	-7	55	166E	-11
			66	73E	-19
			48	142E	-14
			30	103E	-5

PENTAD 4 1969

MAXIMA			MINIMA		
LA	LO	DM	LA	LO	DM
45	76W	18	36	45W	-23
31	6W	12	33	142W	-22
56	152W	21	50	125W	-25
74	37E	34	54	1W	-17
34	176E	9	55	166E	-21
35	152E	10	34	24E	-12
			55	145E	-23
			56	118E	-24
			52	78E	-28

PENTAD 5 1969

MAXIMA			MINIMA		
LA	LO	DM	LA	LO	DM
22	111W	6	43	38W	-23
51	70W	25	46	125W	-22
53	153W	29	32	146W	-28
72	27W	23	78	28E	15
44	1E	21	80	145E	-17
75	55E	19	55	166E	-23
35	160E	10	22	29E	-22
35	143E	12	52	78E	-30
30	66E	7			

PENTAD 6 1969

MAXIMA			MINIMA		
LA	LO	DM	LA	LO	DM
53	51W	38	26	65W	-11
44	157W	29	31	37W	-12
75	125W	11	46	125W	-32
39	6E	12	67	8W	-5
37	163E	17	60	176E	-23
61	100E	-6	22	178W	-7
37	140E	19	71	111E	-15
			56	42E	-6
			41	35E	-13
			18	169E	-5
			16	30E	-21
			47	86E	-18
			20	97E	-6
			14	93E	-7

PENTAD 7 1969

MAXIMA			MINIMA		
LA	LO	DM	LA	LO	DM
27	89W	6	33	120W	-6
30	80W	6	33	40W	-15
52	46W	21	26	135W	-5
61	80W	6	35	28W	-16
70	102W	5	56	138W	-23
41	178W	37	77	24W	-18
80	145E	9	61	10E	-20
75	55E	8	64	178W	-14
33	31E	10	59	46E	-18
			64	134E	-16
			19	172E	-9
			65	100E	-21

Fig. 4.2 Sample page of Master Catalogue, indicating position and intensity of positive and negative Anomaly Centres of 5-day mean 500MB height.

associated with an amplified block of substantial duration (> 10 days).

The pilot study also indicated that the criteria would be functions of the time of the year, anomaly magnitude and latitude. These were the attributes selected from the Master Catalogue when testing for the anomaly's association with a blocking anticyclone.

4.7.1.1 Data Sources

To determine if, in fact, a block was in progress we used the following sources of information:

(a) Daily Series, Synoptic Weather Maps, Northern Hemisphere Sea Level and 500MB Charts (Air Weather Service, 1946-1948; U.S. Department of Commerce, 1949-1956).

(b) A Catalogue of Northern Hemisphere Blocking Situations for the Period 1945-1977 (Treidl et al., 1980b).

(c) Monthly Weather Review (U.S. Department of Commerce, 1954-1973; American Meteorological Society, 1974-1979).

The source for the positive anomaly attributes was, of course, the Master Catalogue (Knox, 1981).

4.7.1.2 Blocking Episode Guidelines

As indicated in Section 3.2, the literature discloses an extremely broad range of criteria which authors have used to judge the occurrence or otherwise of a blocking episode, and this has been reflected in the published frequency of occurrence results. The one area of agreement is on major blocking episodes. The objective of this study is, so far as is possible, to design a threshold such that the set of qualifying positive anomalies (signatures) will reflect the full spectrum of blocking episodes - minor, moderate or major.

The first step was to establish guidelines by which to judge the occurrence or otherwise of blocking on the daily analyses.

We decided that the Treidl guidelines (Appendix IV - 2B) used to prepare his Catalogue were sufficient for a block to be judged to have occurred. Therefore if the 5-day life of our Master Catalogue positive anomaly, selected for testing, occurred within the duration of a blocking episode listed in his Catalogue, it qualified as a blocking signature. However, it was not necessary for all the Treidl criteria to be met for a block to have occurred. For example, during an inspection of a large sample of daily 500MB analyses we found a significant number of relatively short-lived (3 to 7 days) occasions when the pre-existing zonal flow was interrupted by a blocking anticyclone, which were not listed. Therefore if, corresponding to the Master Catalogue-selective positive anomaly, the Treidl Catalogue did not list a block, we then went directly to the 5-day sequence of Daily 500MB analyses and, over the region concerned, applied the following guidelines: (see also Appendix IV - 2A).

(i) During the pentad of the positive anomaly being tested, an anticyclonic centre must be observed on at least 3 out of the 5 consecutive daily analyses.

(ii) The anticyclonic structure will clearly have disrupted the pre-existing zonal flow.

(iii) The anticyclone centre must be N of 45°N.

If these guidelines were met we decided a block was in progress.

For assistance with marginal cases there was frequent recourse to the Monthly Weather Review (1951-1979), which presents the four 5-day average 700MB height analyses most representative of the month under review.

In summary, the Treidl guidelines were considered sufficient, while ours were considered necessary and sufficient. In effect this means that the guidelines used in this investigation for judging the occurrence or otherwise of an actual blocking episode on daily 500MB analyses are essentially our own, as set out in full in Appendix IV - 2. It is important to keep this in mind when comparing the results of this thesis with other studies.

4.7.1.3 Procedure

We selected a large sample of positive anomalies from the Master Catalogue and plotted centre value (dams) against latitude. The plot also identified whether or not, during that pentad, a blocking episode was in progress in the region of the anomaly being tested by:

(i) Occurrence ●

(ii) Non-occurrence ○

(Further details of the procedure are provided in Appendix IV - 3).

The WINTER and SUMMER seasons were examined first and the number of anomalies were:

WINTER 318

SUMMER 384

4.7.1.4 Results

The results are presented in Figs. 4.3(a) and 4.3(b). Note that the separation curves are approximate hyperbolas.

Usually to analyze the relationship between two variates of the atmospheric continuum one uses formal statistical techniques. This analysis, however, is concerned, not with elements of the continuum, but with spatially isolated derivatives (anomaly maxima and centres of anti-

Fig. 4.3(a) Threshold for Blocking Signatures, WINTER. 318 positive anomaly centres are tested for association with a blocking episode. (For details see Appendix IV, Sections 2 and 3).

Legend ● Anomaly was found to be associated with a contemporaneous blocking episode.

○ No blocking episode observed.

Cases tested were from following years: 1947, 1948, 1951, 1953, 1954, 1955, 1956, 1958, 1961, 1965, 1966, 1968, 1970, 1971, 1972, 1973, 1974, 1975.

Not shown in Figure is one outlier at 57°N with a centre value of 55 dams. This occurred December 17 - 21 (PE 71) in 1955 and was associated with a strong 11 day blocking high over the mid-Pacific Ocean.

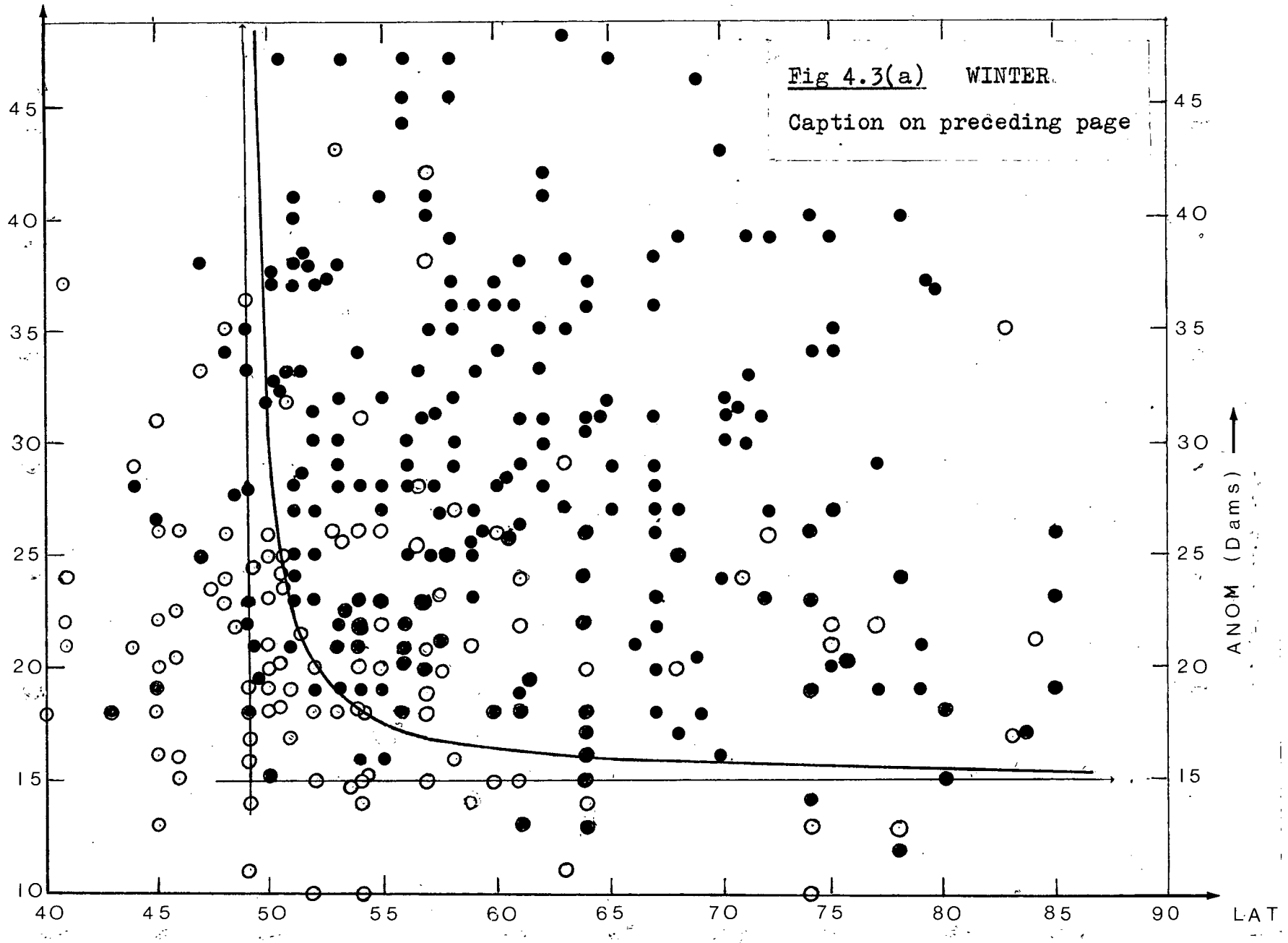

Fig 4.3(a) WINTER

Caption on preceding page

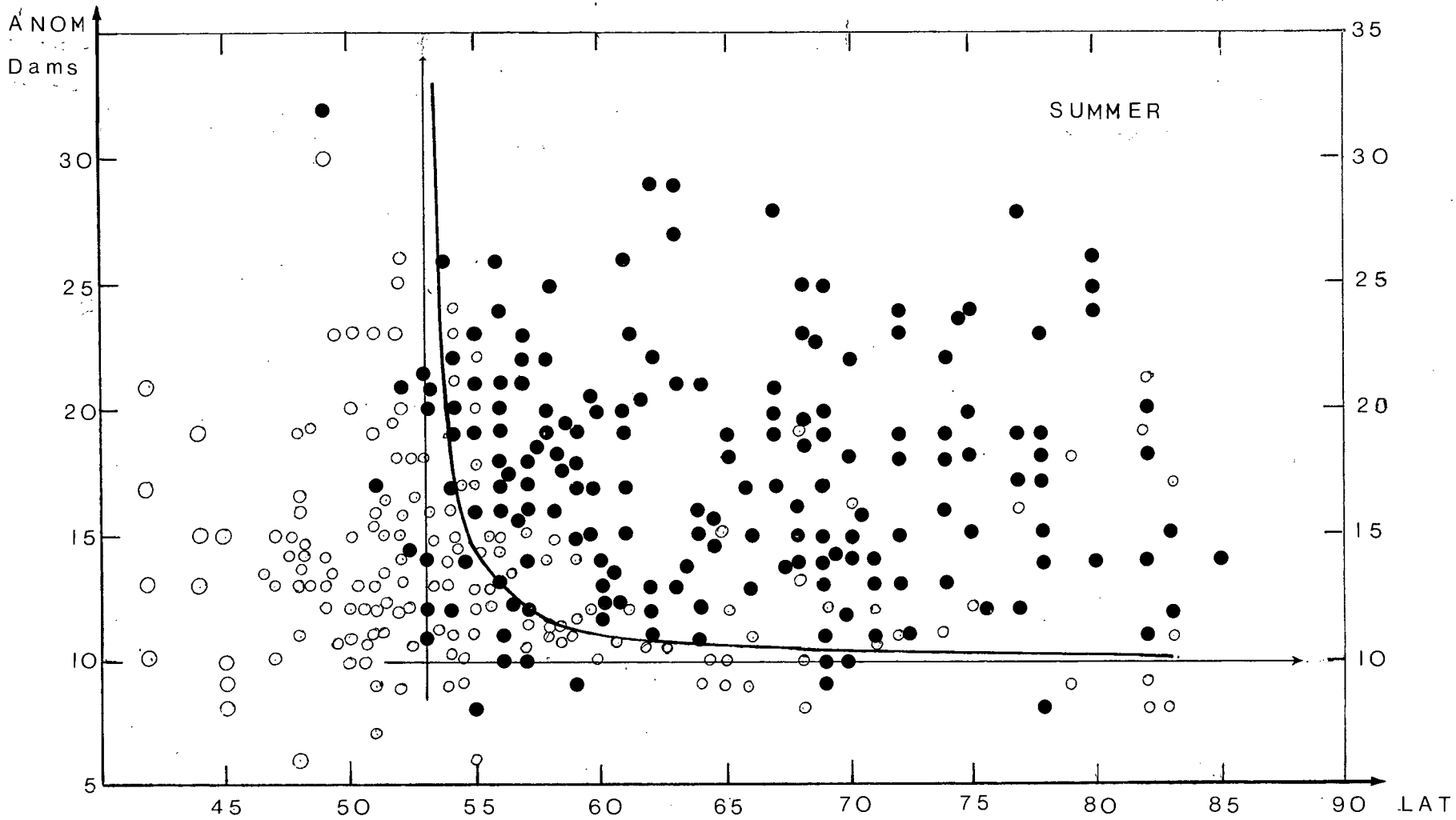

Fig 4.3 (b) As in Fig. 4.3(a) except for SUMMER. The plot is for 384 positive anomalies which occurred in June, July and August for the years 1949, 1950, 1951, 1964, 1965, 1969, 1970, 1971 and 1972.

cyclones). Moreover, we have used quasi-subjective guidelines to determine the dichotomous fields in Fig. 4.3. Under these circumstances we decided to estimate the separation curves by eye.

For the anomaly to qualify as a "blocking signature", the criteria were:

WINTER $({}^{yy}A_K - 15)({}^{yy}\phi_K - 49) > 16$ (1)

SUMMER $({}^{yy}A_K - 10)({}^{yy}\phi_K - 53) > 9$ (2)

Where yy = year, pentad number = K, anomaly magnitude = ${}^{yy}A_K$

and anomaly latitude = ${}^{yy}\phi_K$

It is noted that the anomaly magnitude threshold values of 15 dams (winter) and 10 dams (summer) are close to the <u>mid-latitude maxima</u> of the seasonal standard deviation at 60°N (Figs. 4.4 and 4.5). This is not surprising considering the amplification associated with blocking.

The anomaly latitude threshold values of 49°N (winter) and 53°N (summer) are consistent with the northward displacement of the E-W axis of the sub-tropical anticyclones (Figs. 4.6 and 4.7).

The values 16 and 9 on the R.H.S. of inequalities (1) and (2) have no obvious physical explanation, but we assumed that the difference was related to the annual cycle.

It was decided to generalize (1) and (2) into a single inequality which would take account of the nearly sinusoidal annual cycle. (To determine the phase angle parameter a sinusoid was fitted to a plot of 73 maximum standard deviations of 500MB 5-day mean height for the Northern Hemisphere.)

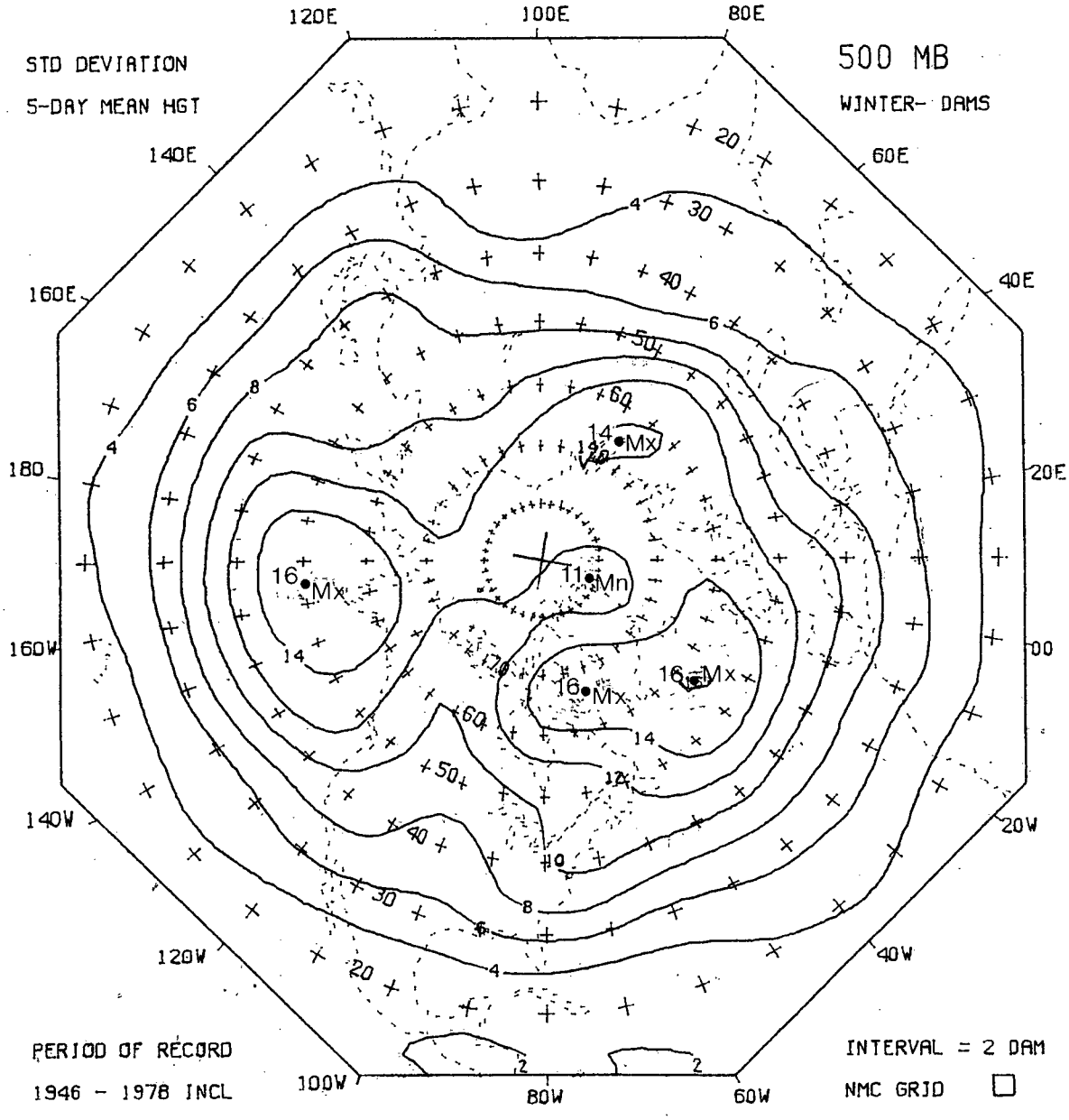

Fig. 4.4 Standard deviation of 5-day mean 500MB height for WINTER (December 1 to February 28). Contour interval = 2 dams.

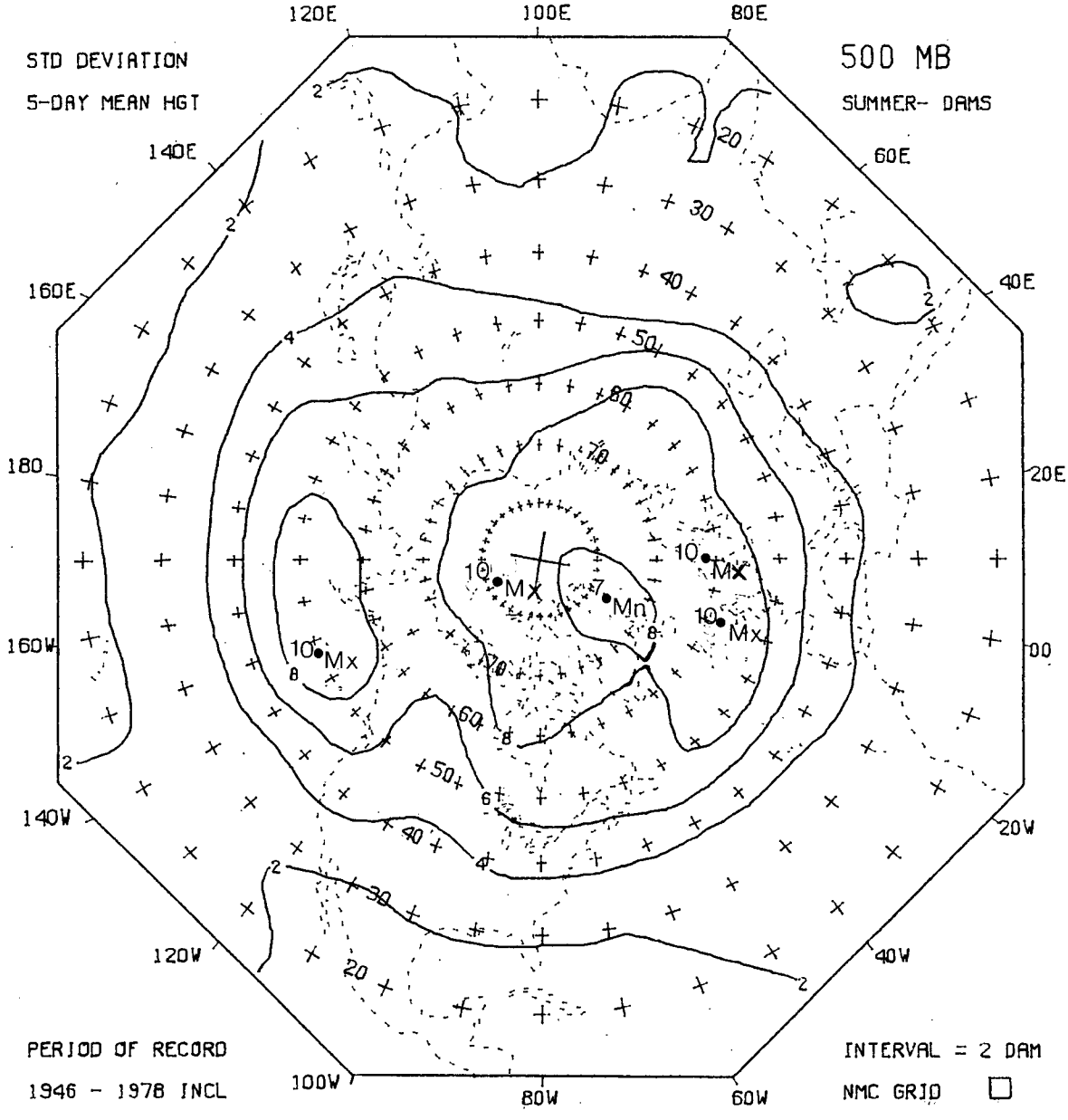

Fig. 4.5 Standard deviation of 5-day mean 500MB height for SUMMER (June 1 to August 31). Contour interval = 2 dams.

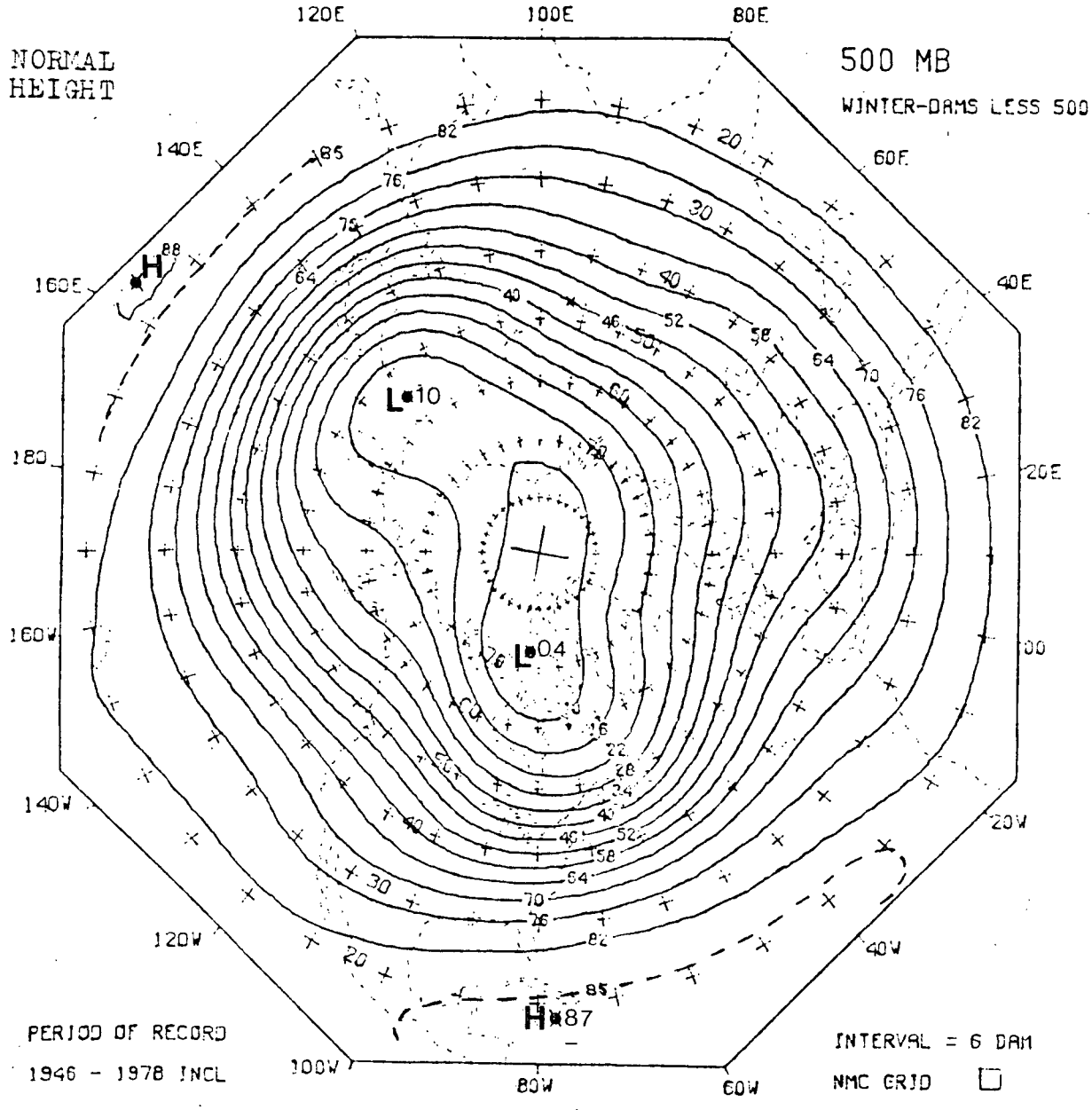

Fig. 4.6 Normal height of the 500MB surface for WINTER (December 1 to February 28). Contours labelled in decametres less 500. Interval = 6 dams.

---------- 585 dam contour

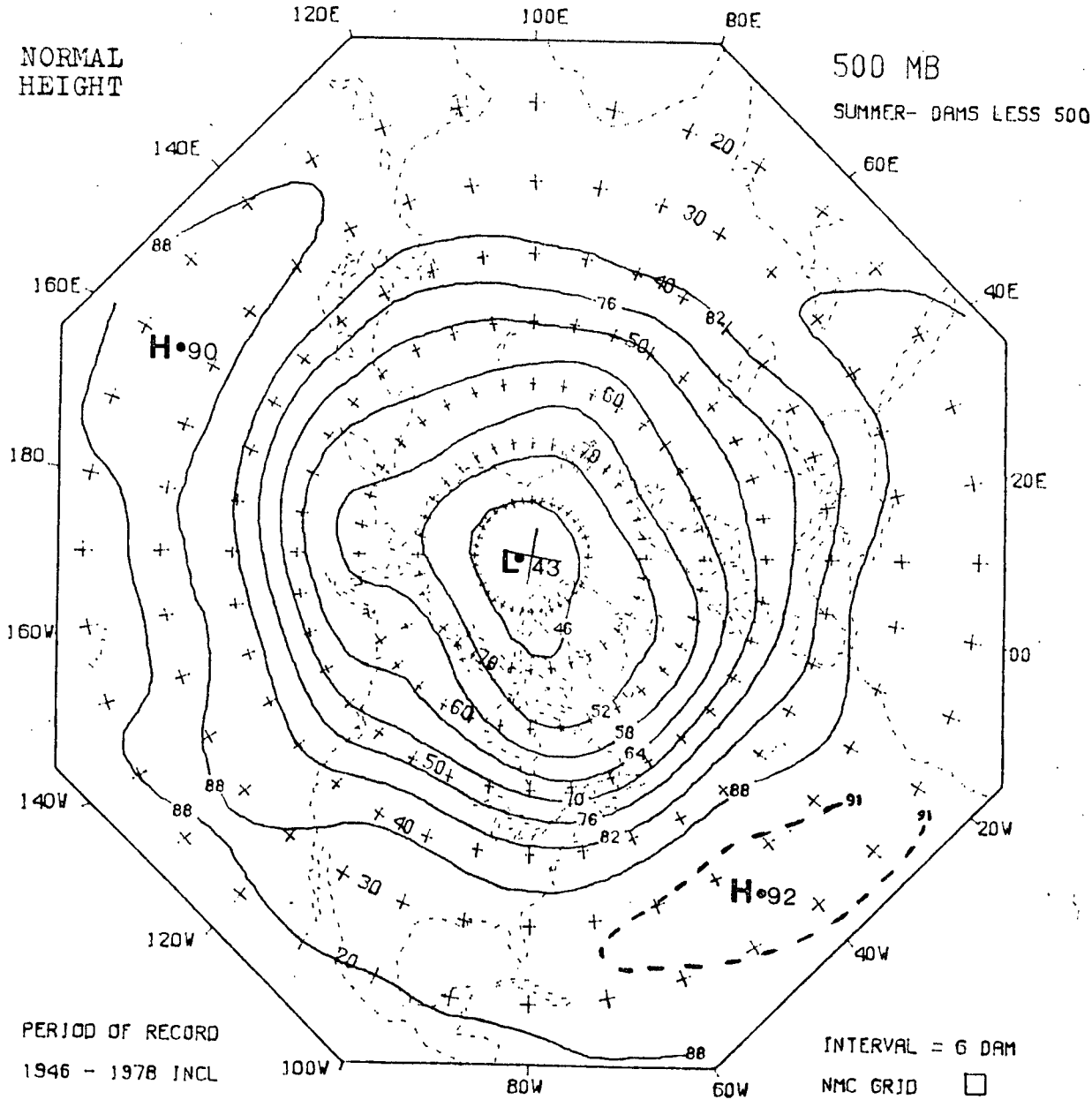

Fig. 4.7 Normal height of the 500MB surface for SUMMER (June 1 to August 31). Contours labelled in decametres less 500. Interval = 6 dams.

---------- 591 dam contour

The generalized criterion is:

$$({}^{yy}A_K - A_K)({}^{yy}\phi_K - \phi_K) > Q_K \qquad (3)$$

Where $A_K = 12.5 + 2.5 \cos (0.08607K - 0.2582)$

$\phi_K = 51.0 - 2.0 \cos (0.08607K - 0.2582)$

$Q_K = 12.5 + 3.5 \cos (0.08607K - 0.2582)$

K = Pentad number (1 to 73)

This expression provides for a <u>within season</u> change of anomaly magnitude and latitude threshold for a corresponding change to Q_K. The hyperbolic threshold changes in 73 discrete steps through the course of a year.

It was decided to test Criterion (3) on SPRING and FALL data. These are the seasons when the rate of change of all criterion factors are greatest. We proceeded as before and drew curves of separation for the respective seasons (not shown). Again they approximated hyperbolas which turned out to be reasonably close to the analytical curves in criterion (3) for mid-spring (K = 21) and mid-fall (K = 57), respectively. The results were sufficiently encouraging that we decided the Criterion could be used for the entire year.

4.7.2 Interpretation of Criterion

Criterion (3) tells us that blocking episodes, in the main, are associated with a signature threshold which is proportional to the product of the latitude and magnitude of the anomaly centre. Therefore, in order to qualify as a signature near the cut-off southern latitude (ϕ_K) the

anomaly magnitude ${}^{yy}A_K$ must be much larger than the cut-off value A_K. This has the desirable effect of screening out those positive anomalies, say, near 50°N, which are attributable either to amplification of the sub-tropical anticyclone, or to a temporary shift north of its normal position, or some combination of these two events.

4.7.3 Blocking Signature Catalogue

The Master Catalogue described in 4.6 identifies all 500MB pentad anomalies, positive and negative, that occurred from 1946 to 1978. Our next requirement was to prepare a catalogue listing only those positive anomalies which qualified as Blocking Signatures. This was done by application of Criterion (3) to each positive centre in the Master Catalogue. The resulting Blocking Signature Catalogue provides a compact inventory of all blocking signatures that occurred during the 33 years of record. A sample page is illustrated in Fig. 4.8.

By scanning across the pentads one can discern sequences of varying length which contain geographically proximate signatures and which therefore are probably with observed blocking episodes of corresponding duration. In Chapter V we shall describe a modification of this Catalogue designed to conveniently identify these sequences of blocking signatures.

5-DAY MEAN BLOCKING SIGNATURES 1971 ****- NONE RECORDED

PE 1 1971	PE 2 1971	PE 3 1971	PE 4 1971	PE 5 1971	PE 6 1971	PE 7 1971	PE 8 1971	PE 9 1971	PE 10 1971
LA LO DM	LA LO DM	LA LO DM	LA LO DM	LA LO DM	LA LO DM	LA LO DM	LA LO DM	LA LO DM	LA LO DM
64 80W 31	54 16E 23	61 170W 34	68 80W 25	****	61 40W 18	70 102W 16	56 138W 21	78 118E 33	81 73E 19
61 30W 16		57 23E 35			71 69W 19	56 22W 32	53 1W 31		
					56 172E 38	61 150E 32	70 122E 37		
					54 55E 26	58 73E 29			
					61 107E 19				

PE 11 1971	PE 12 1971	PE 13 1971	PE 14 1971	PE 15 1971	PE 16 1971	PE 17 1971	PE 18 1971	PE 19 1971	PE 20 1971
LA LO DM	LA LO DM	LA LO DM	LA LO DM	LA LO DM	LA LO DM	LA LO DM	LA LO DM	LA LO DM	LA LO DM
81 37E 28	71 10E 25	61 20W 26	67 71W 28	78 62W 21	81 107W 32	74 156W 34	78 172E 27	67 1E 15	79 145E 17
	74 86E 28	71 47E 27	56 22W 20	67 82E 29				71 153E 20	63 26E 18
		59 154E 25	61 130E 22						
			64 92E 22						

PE 21 1971	PE 22 1971	PE 23 1971	PE 24 1971	PE 25 1971	PE 26 1971	PE 27 1971	PE 28 1971	PE 29 1971	PE 30 1971
LA LO DM	LA LO DM	LA LO DM	LA LO DM	LA LO DM	LA LO DM	LA LO DM	LA LO DM	LA LO DM	LA LO DM
57 3W 24	53 51W 22	62 57W 19	67 89W 23	61 100E 16	61 17E 13	****	74 125W 12	78 28E 18	62 33E 17
90 100E 14	68 80W 21	74 94W 34	67 172E 28						61 140E 13
	81 53W 22								

PE 31 1971	PE 32 1971	PE 33 1971	PE 34 1971	PE 35 1971	PE 36 1971	PE 37 1971	PE 38 1971	PE 39 1971	PE 40 1971
LA LO DM	LA LO DM	LA LO DM	LA LO DM	LA LO DM	LA LO DM	LA LO DM	LA LO DM	LA LO DM	LA LO DM
67 19E 20	61 30W 29	62 57W 27	81 107W 18	76 136W 19	71 170W 22	84 125W 14	76 136W 16	56 22W 24	63 46W 21
59 136E 15	73 143W 18	75 170W 12	60 86E 13	81 37E 16		75 170W 15	54 164W 17	53 159W 23	70 122E 18
				64 92E 14		75 10E 11	57 10E 20	79 145E 24	
							76 134E 17		

PE 41 1971	PE 42 1971	PE 43 1971	PE 44 1971	PE 45 1971	PE 46 1971	PE 47 1971	PE 48 1971	PE 49 1971	PE 50 1971
LA LO DM	LA LO DM	LA LO DM	LA LO DM	LA LO DM	LA LO DM	LA LO DM	LA LO DM	LA LO DM	LA LO DM
73 143W 11	54 133W 17	57 23E 13	71 100E 14	56 152W 15	56 22W 13	60 4W 18	57 86W 14	74 145E 23	53 1W 19
81 53W 14	57 23E 16						71 153E 15		76 134E 14
64 145E 12									
57 59E 18									

PE 51 1971	PE 52 1971	PE 53 1971	PE 54 1971	PE 55 1971	PE 56 1971	PE 57 1971	PE 58 1971	PE 59 1971	PE 60 1971
LA LO DM	LA LO DM	LA LO DM	LA LO DM	LA LO DM	LA LO DM	LA LO DM	LA LO DM	LA LO DM	LA LO DM
65 53W 19	54 56W 15	53 141W 23	62 123E 13	61 73W 13	68 80W 14	****	****	****	60 4W 21
64 2E 25	59 11W 18			66 151E 17	56 8W 19				
59 55E 19	67 179W 14								
	56 68E 21								

PE 61 1971	PE 62 1971	PE 63 1971	PE 64 1971	PE 65 1971	PE 66 1971	PE 67 1971	PE 68 1971	PE 69 1971	PE 70 1971
LA LO DM	LA LO DM	LA LO DM	LA LO DM	LA LO DM	LA LO DM	LA LO DM	LA LO DM	LA LO DM	LA LO DM
57 10E 21	****	59 35W 31	57 80W 16	61 50W 17	63 96W 18	65 163E 25	57 4E 20	51 12W 37	****
		60 114E 18	51 24W 24	57 113E 26	54 27W 24	61 40E 23	69 145E 18		
					56 68E 22				

PE 71 1971	PE 72 1971	PE 73 1971
LA LO DM	LA LO DM	LA LO DM
51 165W 40	53 159W 34	62 13W 38
64 100E 23	81 73E 30	82 100E 17

Fig. 4.8 Sample page from Blocking Signature Catalogue. Qualifying positive Anomaly Centres listed by pentad, location and intensity (DM = dams).

CHAPTER 5

5. DISTRIBUTION OF SIGNATURES AND SEQUENCES

5.1 Introduction

We recall that a Blocking Signature is a positive anomaly of 500MB 5-day mean height which, for a specific year (yy) and pentad (K) meets Criterion (3), viz:

$$({}^{yy}A_K - A_K)({}^{yy}\phi_K - \phi_K) > Q_K$$

Where the signature magnitude = ${}^{yy}A_K$

the signature latitude = ${}^{yy}\phi_K$

and the threshold values A_K, ϕ_K, Q_K are sinusoidal functions of K (Section 4.4.3).

One purpose of this chapter will be to present and interpret the frequency distribution of Blocking Signatures for the Northern Hemisphere. Later (Section 5.3), it will be shown how the Signature Catalogue can be modified to reveal the beginning and ending of Sequences of Signatures. We shall then present and interpret the frequency distribution of these sequences.

5.2 Distribution of Blocking Signatures

5.2.1 Areal Distribution

All blocking signatures, having now been identified and recorded, were counted according to their (I,J) location. Isopleths of equal frequency were drawn over the two-dimensional grid and the resulting areal

distribution is presented by TOTAL, Fig. 5.1. (A slight smoothing routine was introduced as explained in Appendix V - 1.) An isopleth numbered 'n' means that it encloses an area within which a blocking signature centre occurred at least n times per 381 km grid per 33 years.

The TOTAL (Annual) Fig. 5.1, confirms the well-known propensity for blocking over

(i) the NE Pacific Ocean and SW Alaska, and

(ii) the NE Atlantic and NW Europe (Rex, 1950).

However, it also reveals areas of comparable blocking signature frequency over

(iii) NE Canada (including Baffin Island)

(iv) the portion of the high Arctic (N of 75°N) clockwise from 90°W to about 40°E

(v) a vast reach of the Soviet Union extending from 40°E to 100°E.

The intensity of the Baffin Island frequency maximum, located in the vicinity of the mean 500MB trough, would have been a surprise had we not already noted a similar pattern in the 700MB Pilot Study. What little comment we have seen concerning blocking in this region has been somewhat controversial. For example, Sumner (1959) stated that "well-developed blocks are almost non-existent over North America". On the other hand, Woffinden (1960) responded to the contrary, with convincing evidence from his own paper, and those of Namias and Clapp (1944) and others, that in this area "some form of blocking 'wave' or 'impulse' [often] proceeded upstream against the westerly current". We shall return to address the paradox in Section 5.3.6.

FREQ 5-DAY MEAN

BLOCKING SIGS

500 MB

TOTAL-SMOOTHED

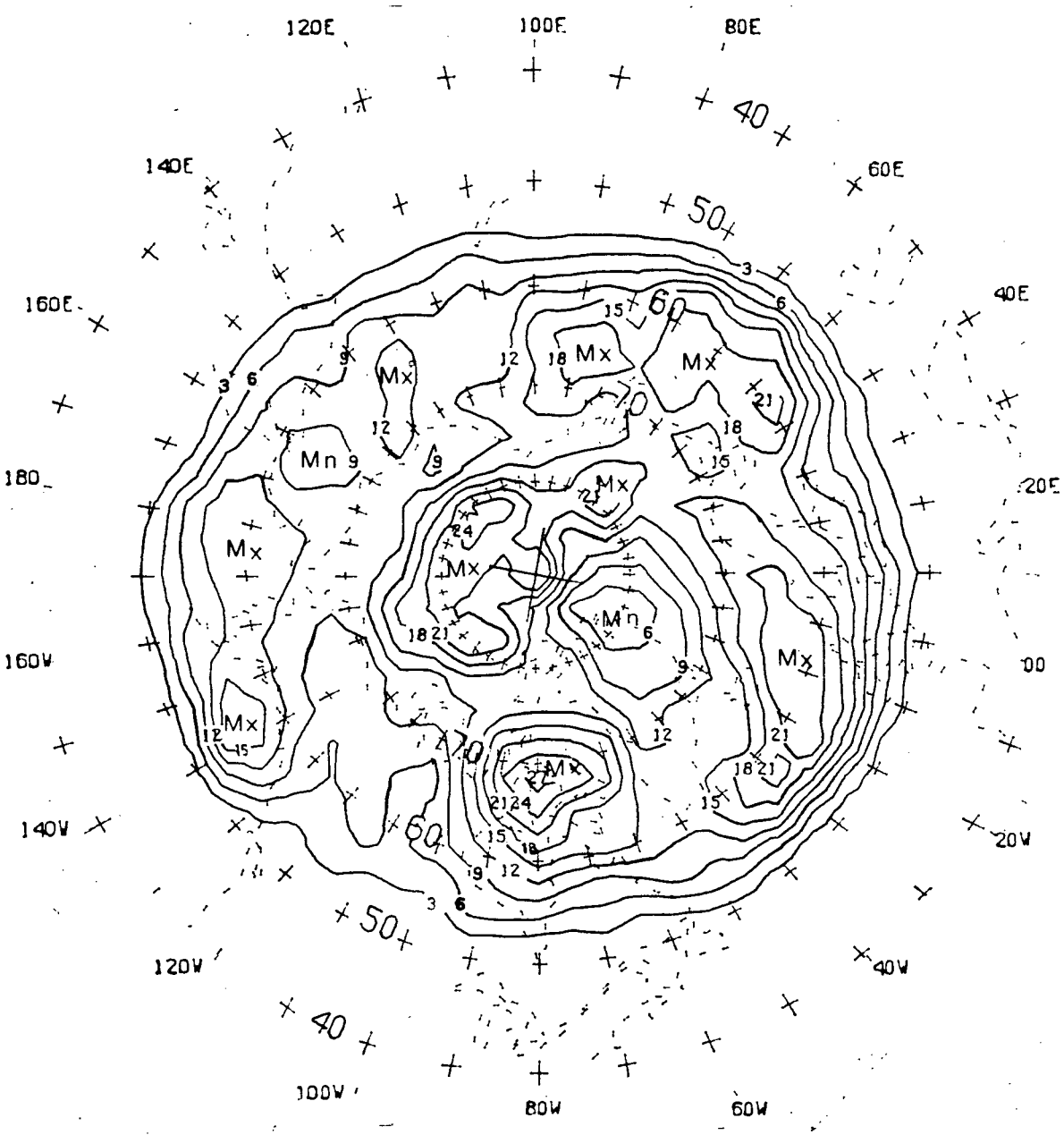

PERIOD OF RECORD

1946 - 1978 INCL

INTERVAL=3 WEIGHT=4

NMC GRID

Fig. 5.1 Frequency of occurrence of Blocking Signatures within squares of 381 km x 381 km (exact at 60°N) for all seasons (1946 to 1978).

Turning now to the high Arctic, let us examine the distribution of blocking signatures not only by YEAR (Fig. 5.1) but also by SEASON (Figs. 5.2 - 5.5). In all of these frequency distributions the closed isopleths in that region are explained, in part at least, by the not unusual observation (from daily 500MB analyses) of warm anticyclones, removed from the mainstream of the westerlies, drifting slowly around the Pole. They no longer block the zonal flow in the usual sense.

Namias (1958) has suggested that, "one of the more significant differences [between synoptic-scale phenomena of Arctic and Temperate latitudes] appears to be that the Polar Basin itself is either a sort of transit area or a sink for cyclones and anticyclones which develop elsewhere".

In the case of blocking anticyclones, Figs. 5.3 (SPRING) and 5.4 (SUMMER) suggest that the Basin acts as a sink. During these seasons we sometimes observe high pressure cells over extreme northern Greenland (80° - 85°N) which have evolved from the meridional extension of warm Atlantic ridges. It is also not unusual to find a second cell further west (120° - 180°W), either concurrently or subsequently, with a probable genesis over Yukon-Alaska, drifting into the 75° - 80°N zone. Now, because the normal 500MB circulation (Figs. 4.6 and 4.7) features a Pole-centred low, the signature centres corresponding to these cells will, for reasons explained in Chapter 3, be very close to the Pole. This accounts for the clustering of signatures at the Pole in Fig. 5.4.

For reasons discussed above we decided to do a frequency analysis on signatures north of 75°N, and found a striking seasonal variation from a minimum in WINTER to a maximum in SUMMER. The results are summarized as follows:

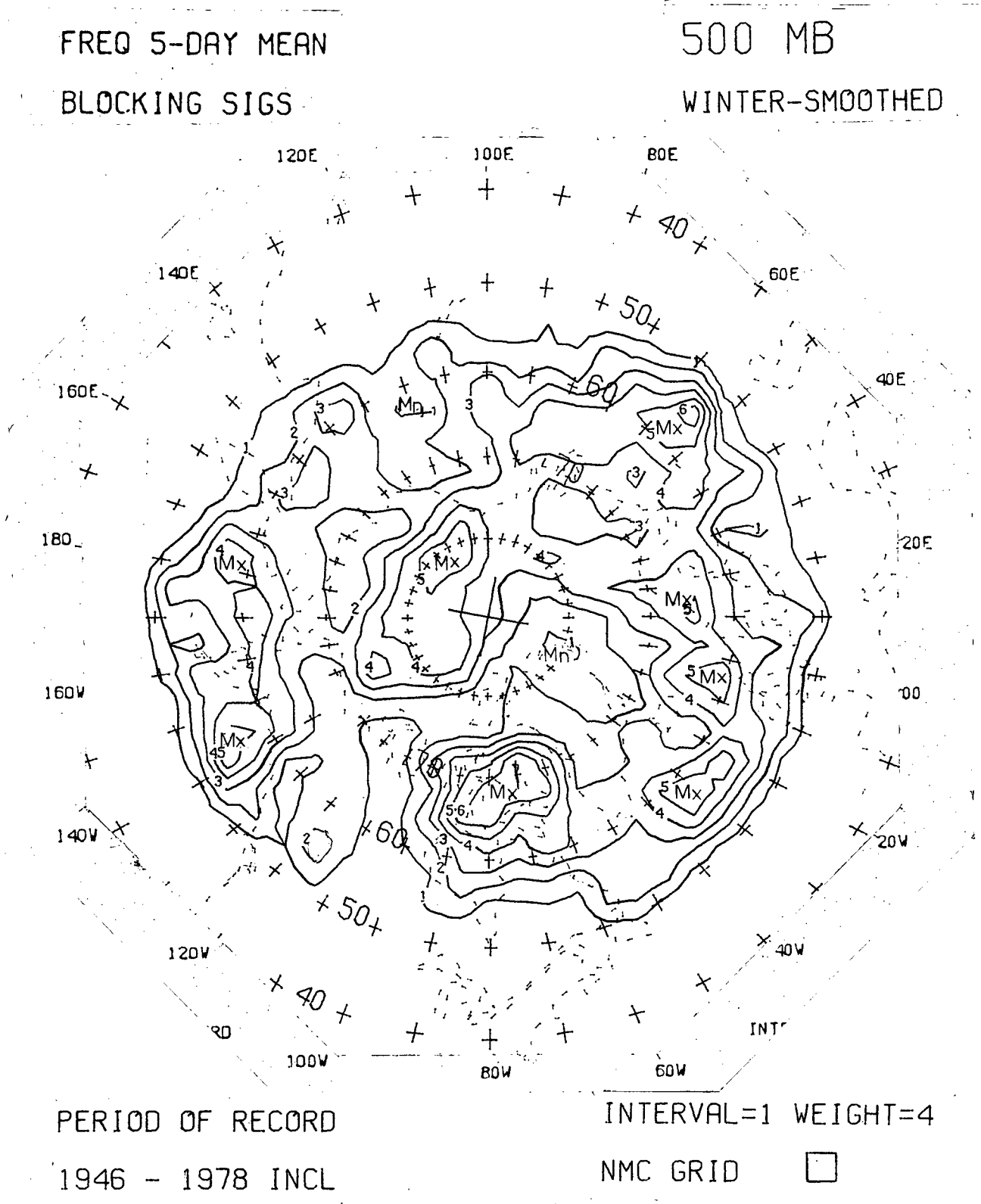

Fig. 5.2 As in Fig. 5.1 except for WINTER

FREQ 5-DAY MEAN

BLOCKING SIGS

500 MB

SPRING-SMOOTHED

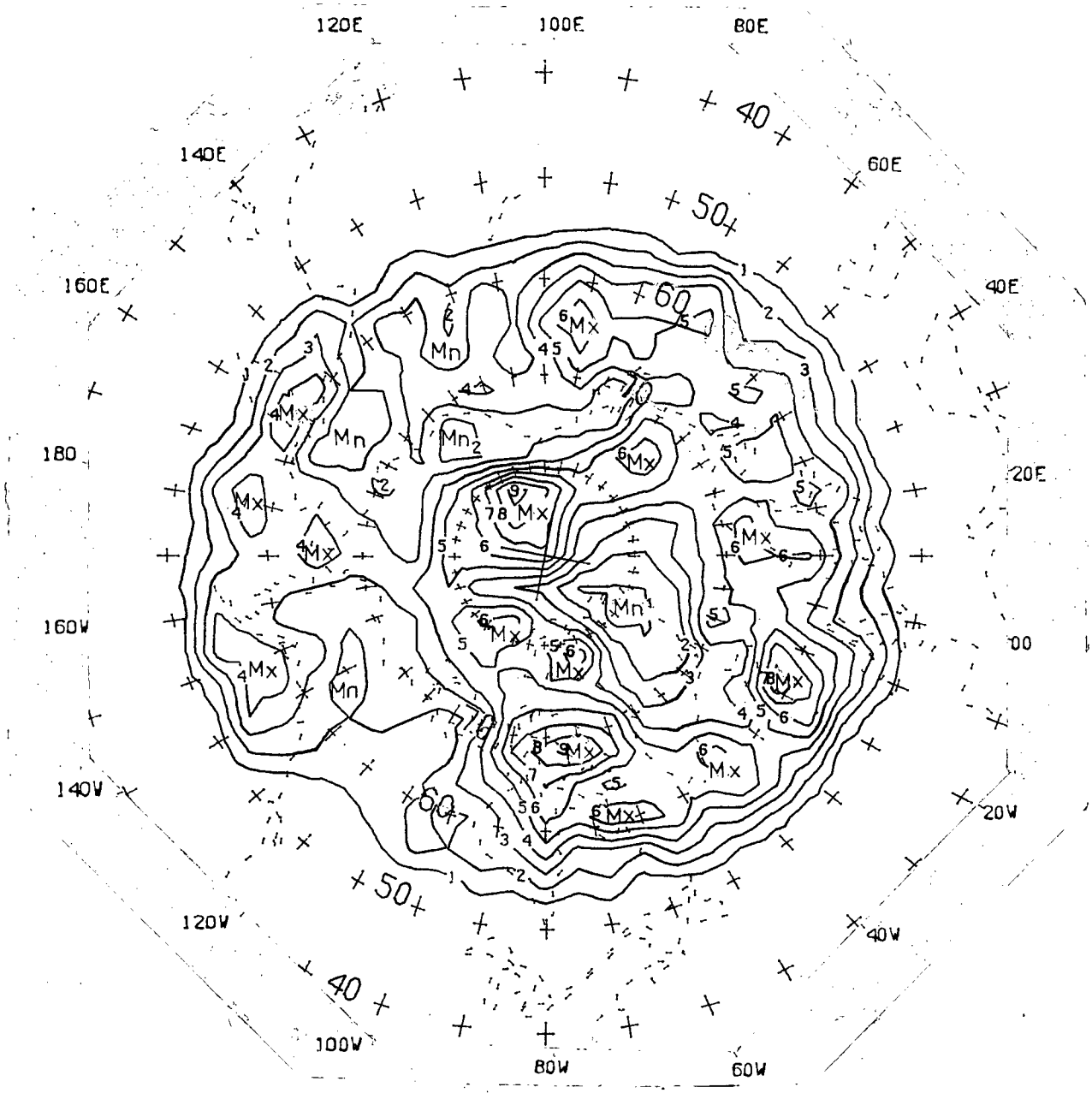

PERIOD OF RECORD

1946 - 1978 INCL

INTERVAL=1 WEIGHT=4

NMC GRID

Fig 5.3 As in Fig. 5.1 except for SPRING

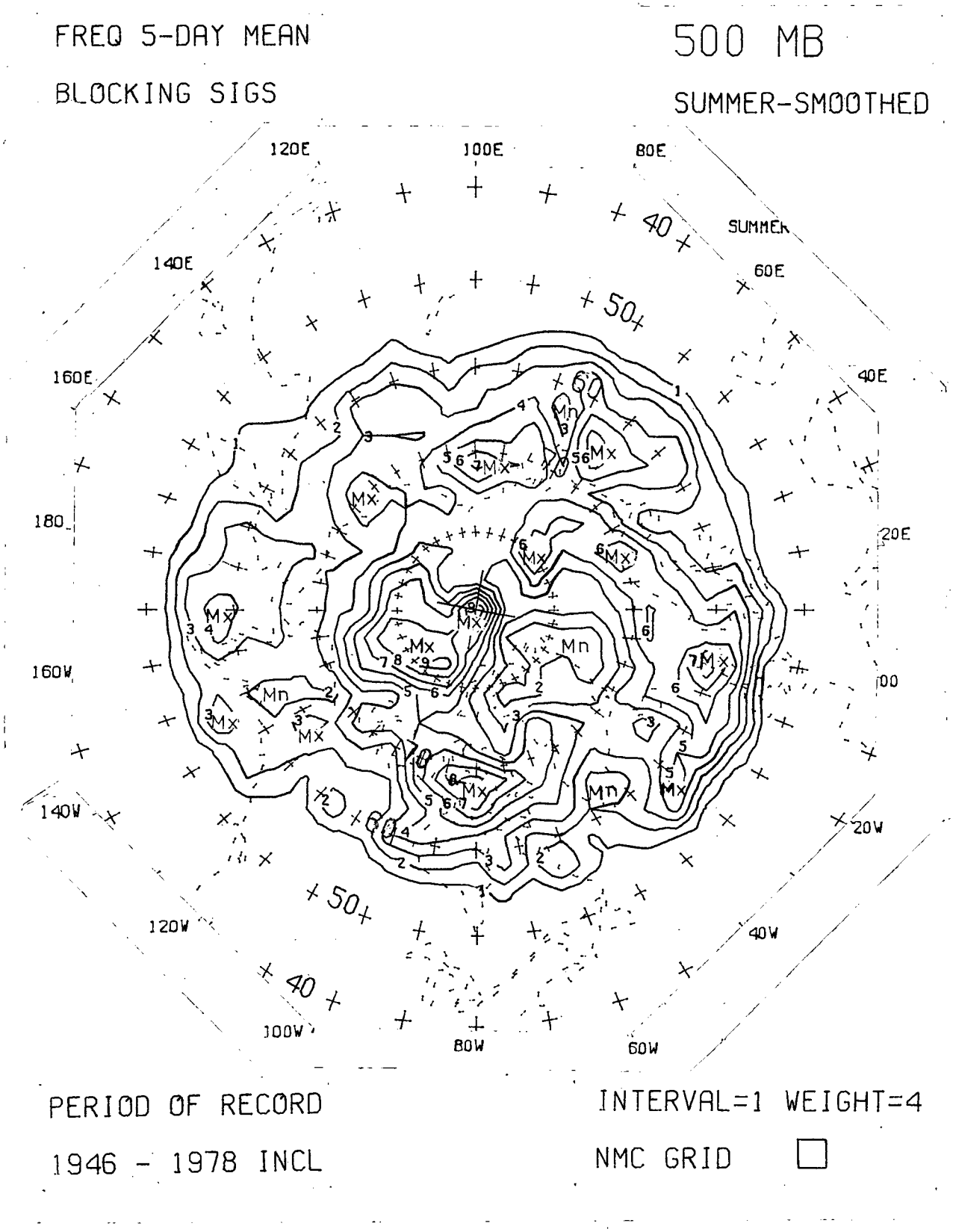

Fig. 5.4 As in Figure 5.1 except for SUMMER

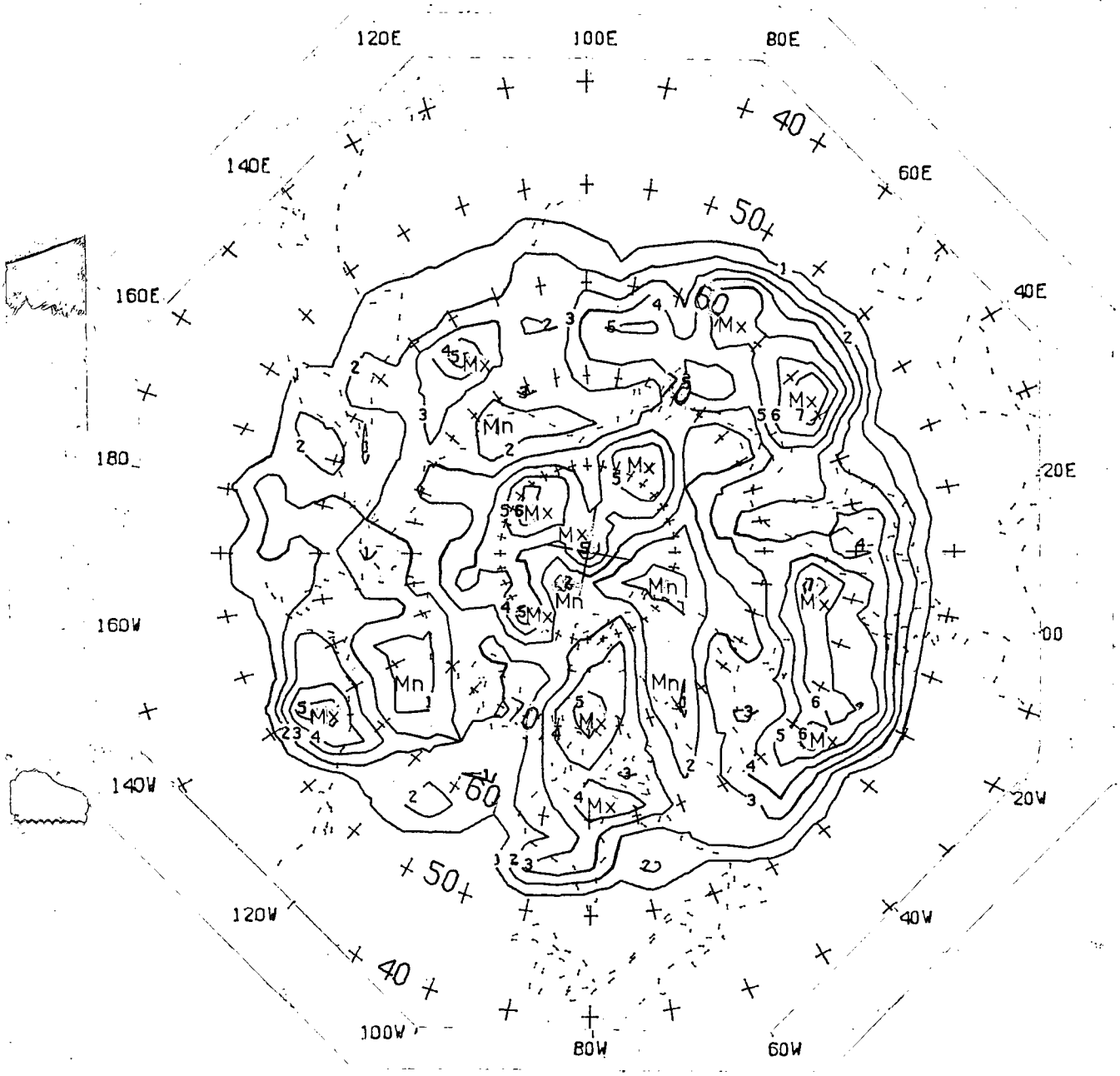

Fig. 5.5 As in Fig. 5.1 except for FALL

TABLE 5.1

Blocking Signatures North of 75°N 1946 - 1978

Winter	154
Spring	217
Summer	245
Fall	170
Total	786

Although the physical reasons for the increase in blocking frequency in the SPRING and SUMMER are not clear, we can speculate on a number of contributing factors. For example, by summer the westerlies have shifted at least 5 degrees north of their winter position, and we may therefore infer that blocking action will have a corresponding displacement. This will increase the possibility of anticyclones migrating into the Arctic. Moreover, the normal pressure around the Pole is higher and the circumpolar circulation less vigorous. Therefore, whatever the original cause of these high latitude warm anticyclones, once they do drift over the Polar Basin they are less likely to be displaced.

South of 75°N the increase in blocking signature frequency from WINTER to SPRING is immediately evident from Figs. 5.2 and 5.3, and the higher incidence of observed SPRING blocking episodes has been noted many times (Rex, 1950; Sumner, 1959). There are also longitudinal seasonal displacements of frequency maxima (and minima) but these are perhaps illustrated more clearly by histograms presented in the next sub-section.

5.2.2 Longitudinal Distributions

Blocking signatures were counted for every 10 degrees of longitude from the southernmost latitude of occurrence to 75°N.[1] The resulting histogram (TOTAL) is shown in Fig. 5.6 and the strong longitudinal dependence described in the previous section is strikingly evident.

The seasonal variations are shown in Figs. 5.7 to 5.10. In WINTER, Fig. 5.7, the low frequency of signatures in Zone 3 (E Siberia, W Pacific) is not surprising for that zone is centred near the axis of the normal 500MB east Asiatic trough (Fig. 4.6) and also in an area of relatively low standard deviation (Fig. 4.4).

Continuing eastward into Zone 4, we note the unmistakably higher frequency from 180°W to 140°W, a result which is consistent with Rex (1950) and Treidl et al. (1980a). From the discussion in Chapter 2 it seems reasonable to suggst that this high frequency area may be attributed to complex interaction between, on the one hand thermally-forced baroclinically unstable waves meeting the criteria of Fig. 2.8 and, on the other, topographically-forced planetary waves. The primary seat of the thermal forcing is located in the western half of the Pacific Ocean between 20° and 50°N, while the topographic forcing agency is the Rocky Mountain Cordillera.

Fig. 5.8, SPRING, and Fig. 5.9, SUMMER, indicate that, during the reversal of the ocean-continent thermal contrast, there is an eastward drift of the high frequency signatures in the northeast Atlantic which

---

[1] For all computations we retained our data on the I,J, grid system. However, for this exercise a problem arose concerning a bias introduced when counting grid point centres into the 10° poleward converging sectors. A computer algorithm for interpolation, which avoids repeated and expensive coordinate system transformations on very large data sets, will be found in Appendix V.

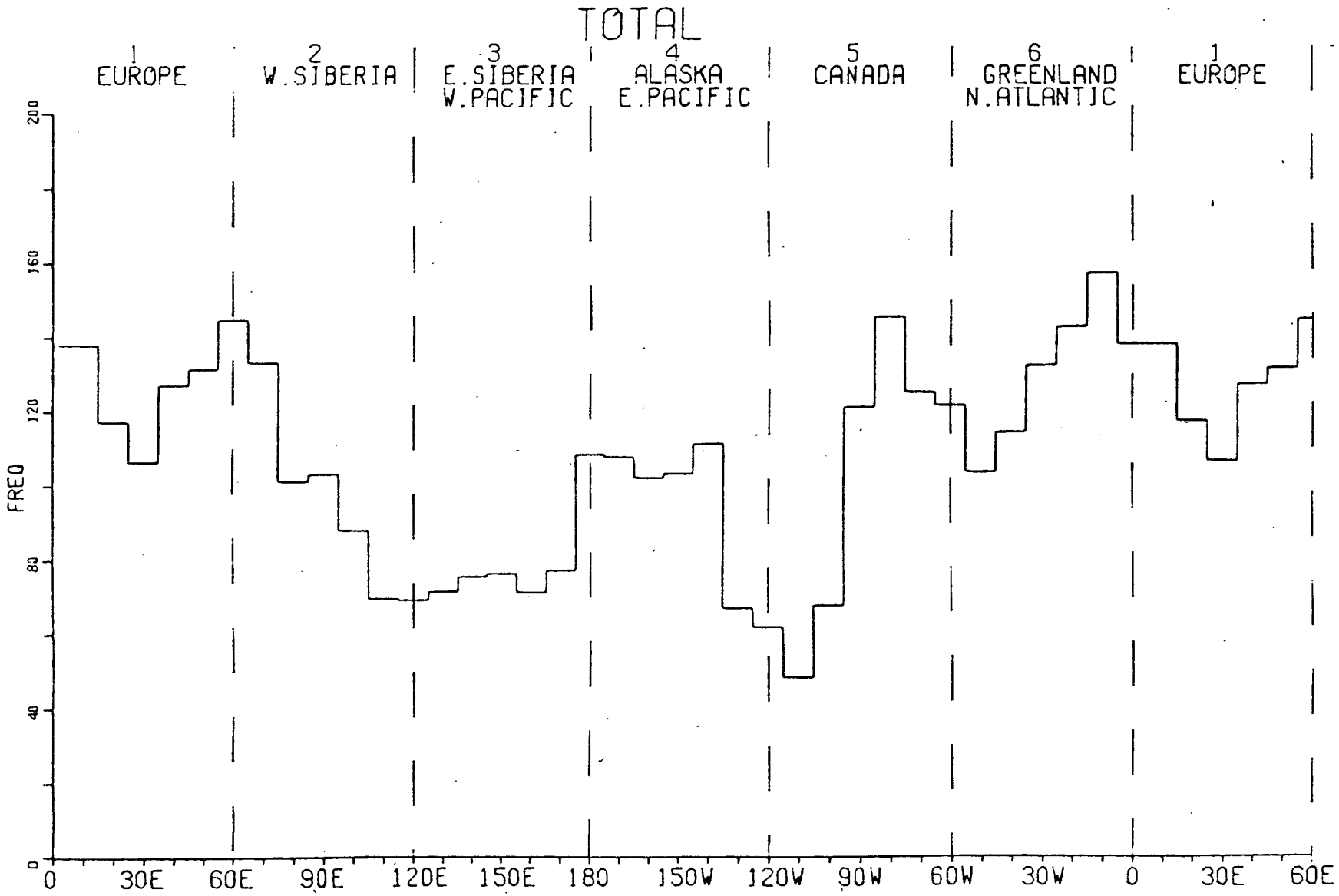

Fig. 5.6 Frequency of occurrence of Blocking Signatures for each 10 degrees of longitude counted from southernmost latitude of occurrence to 75°N. For ALL SEASONS (1946 to 1978).

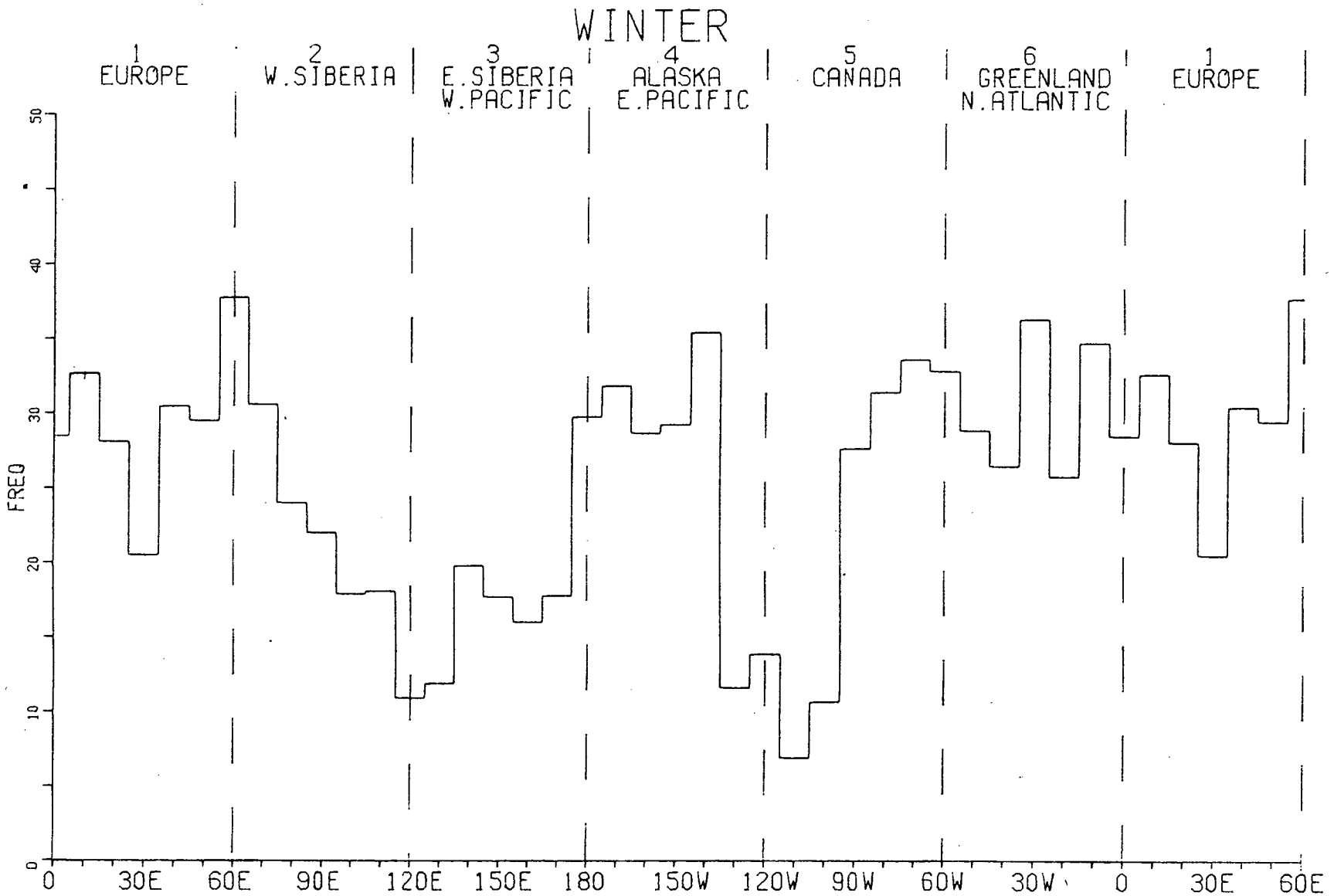

Fig. 5.7 As in Fig. 5.6 except for WINTER

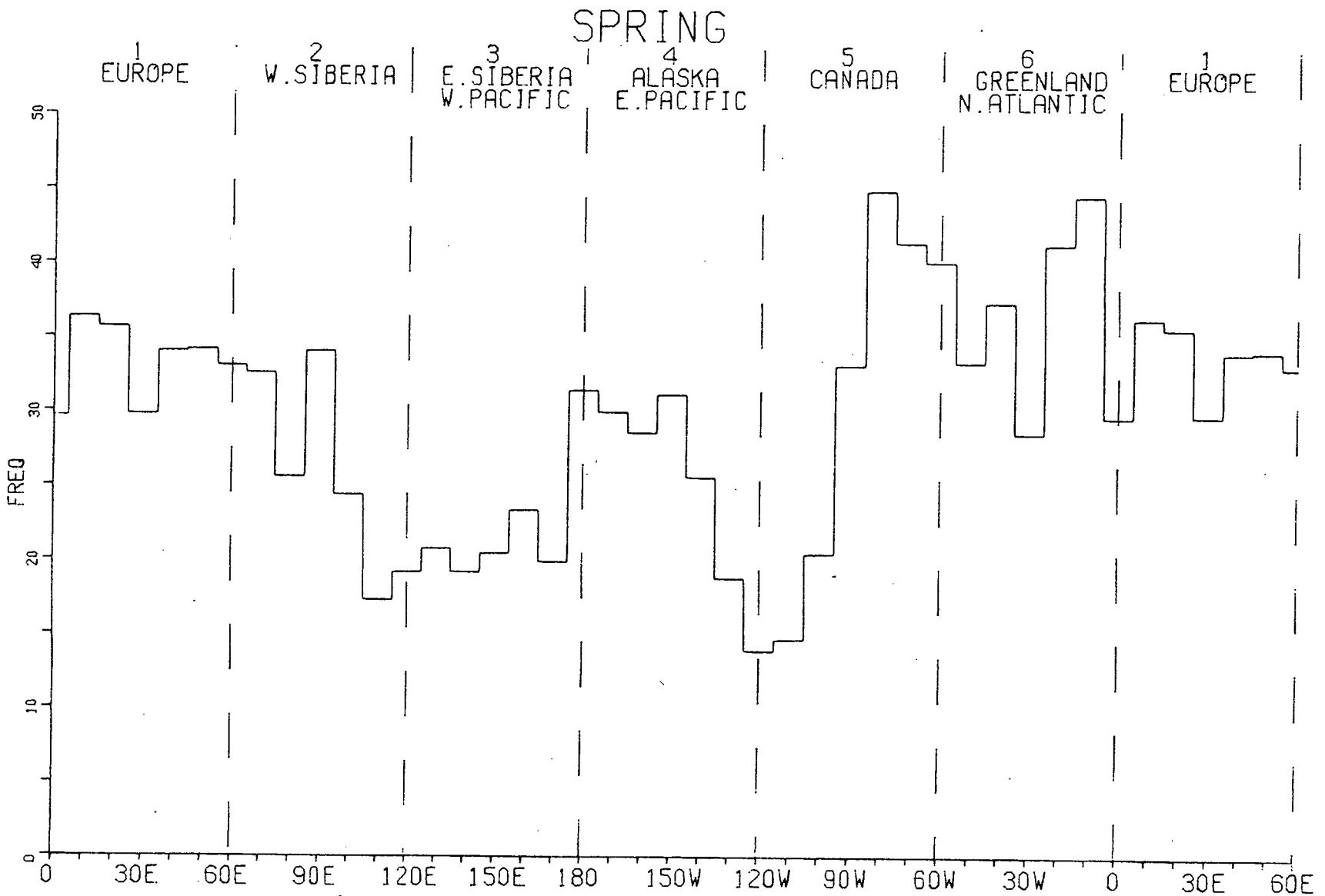

Fig. 5.8 As in Fig. 5.6 except for SPRING

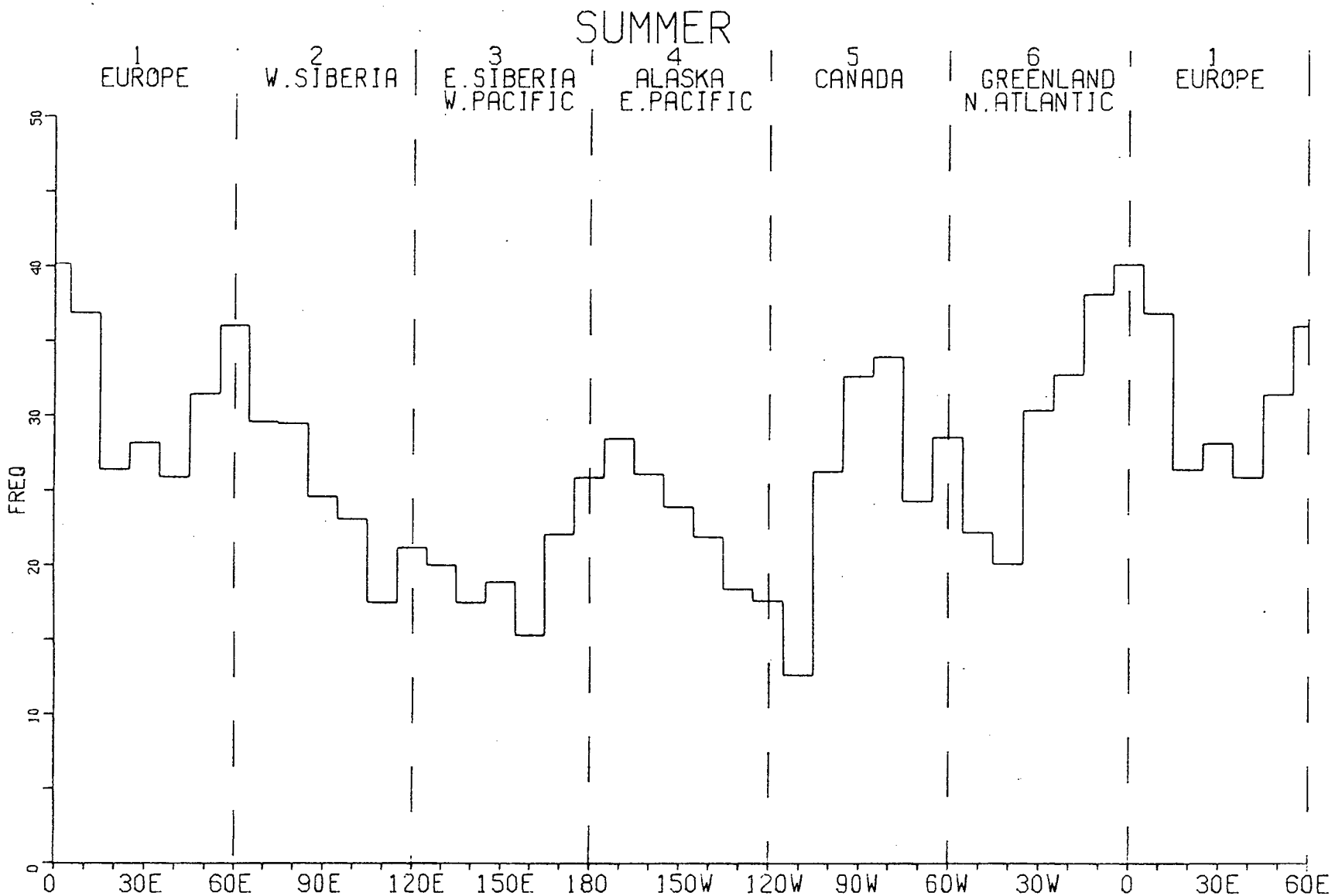

Fig. 5.9 As in Fig. 5.6 except for SUMMER

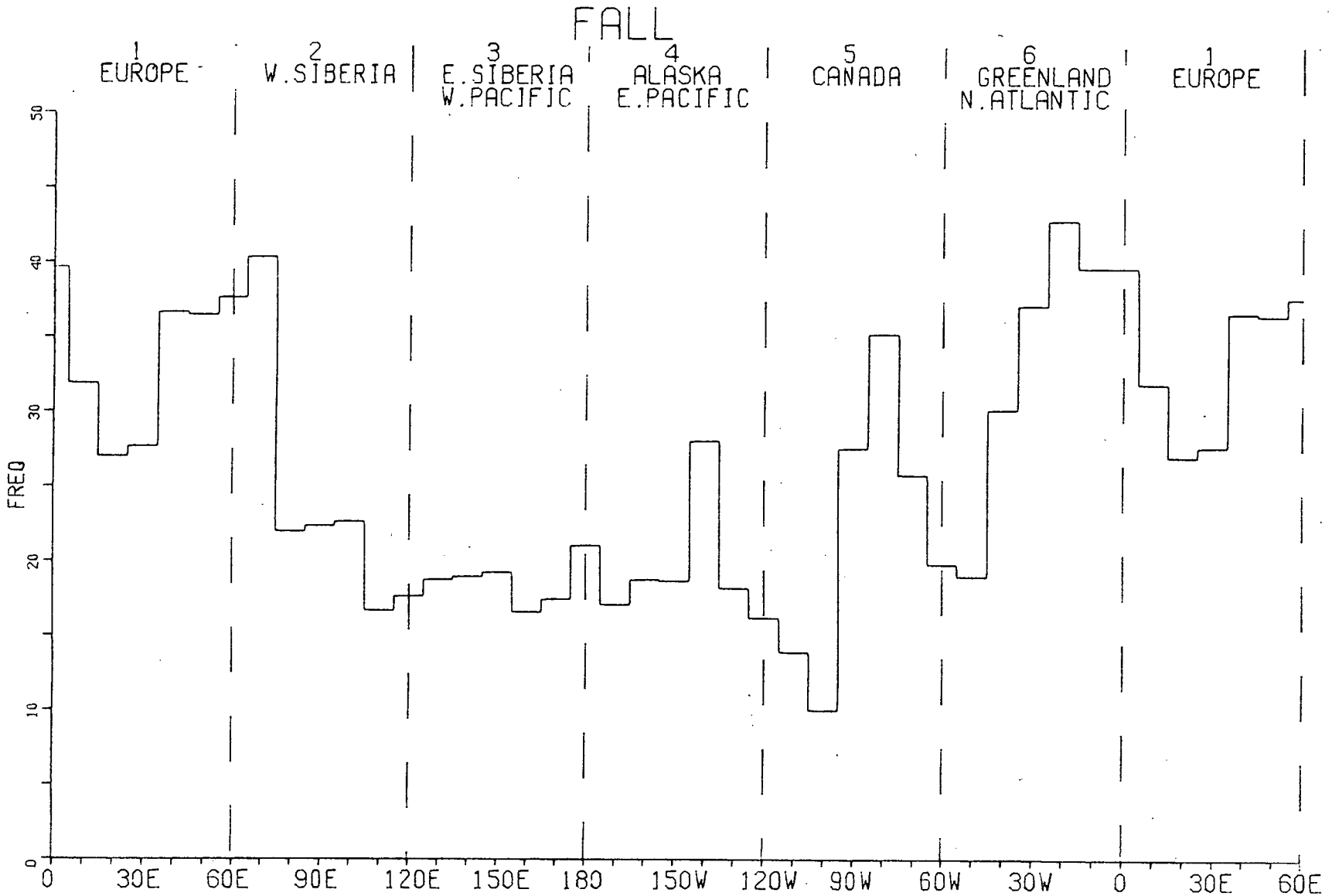

Fig. 5.10 As in Fig. 5.6 except for FALL

culminates by SUMMER, with a well-defined maximum centred on the Greenwich meridian. Over Canada, the phenomenon of persistent Hudson Bay highs in SPRING is well-known (Johnson, 1948) and this is reflected by the blocking signature maximum at 80°W. Over Zone 4 (Alaska and the E. Pacific) we observe, not an eastward drift as in the case of the Atlantic, but a westward drift from WINTER through SPRING to SUMMER by which time the maximum is located at 170°W. This motion is not inconsistent with the thermal contrast reversal theory when we consider the summer heating of the vast Alaskan land mass. If the disposition of the planetary waves favours anticyclonic conditions at the surface over Alaska, the substantial heating in the lower troposphere, greatly enhanced by the nature of the terrain, will (from hydrostatic considerations) increase the 500MB gph and therefore the positive anomaly. The blocking anticyclones centred over Alaska will usually have signature centres located between 70° and 75°N, and between 140° and 180°W. These contribute to the SUMMER distribution in Zone 4.

By FALL (Fig. 5.10) the blocking signatures in that area have declined, partly because the thermal effect over Alaska is in reverse. It now becomes a source region for cold air masses, hence signatures over the Alaska-Yukon area are rare (Fig. 5.5). Moreover, under appropriate synoptic conditions, cold air is deployed over the relatively warmer Gulf of Alaska, and the large diabatic heating contributes to vigorous cyclogenesis in that area during FALL and WINTER. Blocking can still occur (Fig. 5.10 shows a concentration of signatures 135° - 145°W between Latitude 50° and 60°N) provided there is a favourable long wave disposition, but there is no reinforcement from the thermal regime over the adjoining continent.

One feature common to all seasons is the maximum at 60°E in the vicinity of the Ural Mountains. This result is supported by Baur (1958), Serebreny et al. (1961) and Knox (1979). What is the reason for this maximum? The normal WINTER 500MB flow (Fig. 4.6) and the three centres of maximum Standard Deviation located downstream from the respective troughs (Fig. 4.4) indicate the dominance of Wave component 3 on the mean flow. As discussed in Chapter 2, the first two waves starting from the west Pacific trough are primarily the result of topographic forcing combined with longitudinally dependent heating. We cannot invoke these factors for the third wave. (The low profile of the Urals does not provide a significant orography and the thermal forcing does not exist.) Its presence was explained (Bolin, 1950) as a resonant response, required to produce a dynamically stable circumpolar system. The associated axis of maximum standard deviation is located, for each season, in the vicinity of 60°E and it is reasonable to assume that the Ural Mountain blocking anticyclones make a significant contribution, just as do their oceanic counterparts, to variance maxima at 160°W and 20°W, respectively.

Finally, to compare the seasonal frequency of blocking signatures south of 75°N, we present Table 5.2 (which complements Table 5.1).

TABLE 5.2

Blocking Signatures South of 75°N 1946 - 1978

Winter	1055
Spring	1278
Summer	1186
Fall	1089
TOTAL	4608

Adding to this total the 786 counted North of 75°N we have a grand total of 5,394 signatures, or an average of 2.24 per individual pentad. Baur (1958), in a study of Northern Hemisphere blocking from 1949 to 1957, found a comparable rate of 2.8 blocks. The higher incidence of blocking in SPRING (20 per cent greater than in WINTER or FALL) has already been noted (See 5.2.1).

It is well to re-emphasize the distinction between a blocking signature and the actual blocking episode observed on the daily 500MB analyses. We shall find that an episode, if a short one, say, 3 to 7 days, has a better than even chance of being matched by a single blocking signature. But episodes may be longer, with durations from 10 to ≃ 50 days, in which case they will correspond to a sequence of signatures. In Section 5.3 we shall describe a proposal to objectively identify these sequences, to catalogue their attributes and calculate their frequencies.

5.3 Blocking Signature Sequences

5.3.1 Rationale and Technique

The Blocking Signature Catalogue (Fig. 4.8) reveals sequences of positive anomaly centres whose trajectories could often be related to the ensemble behaviour of anticyclone centres on the daily 500MB analyses. (An example is discussed in Appendix V - 4, and illustrated by Fig. V - 2.) Exceptions understandably occurred during the initial and terminal stages of an episode but, especially for ≥ 10-day episodes, there was a very close correspondence. Moreover, in the event of concurrent blocking (the Catalogue indicates that anywhere from zero to four episodes may be in progress around the hemisphere during a specified pentad), the respective trajectories were geographically well separated.

The signatures moved with speeds characteristic of blocking anticyclones (1 to 5 m s^{-1}). Could we use this fact as a data processing criterion for grouping the signatures into their respective sequences? If so, it might then be possible to prepare a catalogue of these sequences which would enable a user to quickly identify where, when and with what intensity real blocking episodes likely occurred in the Northern Hemisphere during the 33-year period.

To determine the criterion threshold we made a large number of manual comparisons of signature motions during these episodes. The results indicated that the maximum displacement was $\approx$ 5 Grid Points (or 1905 km) per 5 days, which is equivalent to a speed of 4.4 m s^{-1} at 60°N.

If we designate a sequence of n successive signatures (σ_1, σ_2, σ_3, . . . σ_K . . . σ_n) as $S(\sigma_n)$ then the criterion for σ_{K+1} to be a member is that <u>the distance from σ_K to $\sigma_{K+1} \leq$ 5 grid lengths.</u> This will be referred to as Criterion (4). Therefore, to determine if a signature in pentad K had a successor, Criterion (4) was applied to the distance between σ_K and each signature listed in pentad K + 1. Either there was no successor, in which case the sequence was terminated, or one was determined and the process was repeated with the signatures in K + 2. Occasionally (usually with cases in the high Arctic), two signatures qualified, in which case the one providing the smaller displacement was selected.

5.3.2 Signature-Sequence Catalogue

A computer program was written for the purpose of identifying and listing all such sequences over the 33-year period. A sample page from the resulting Blocking Signature-Sequence Catalogue is shown in Fig. 5.11.

5-DAY MEAN BLOCKING SIGNATURE SEQUENCES 1955 ****-NO SIGNATURES RECORDED

PE 1 1955	PE 2 1955	PE 3 1955	PE 4 1955	PE 5 1955	PE 6 1955	PE 7 1955	PE 8 1955	PE 9 1955	PE 10 1955
LA LO DM	LA LO DM	LA LO DM	LA LO DM	LA LO DM	LA LO DM	LA LO DM	LA LO DM	LA LO DM	LA LO DM
67 8W 38*	*63 57W 41	63 57W 31	57 67W 23*		****	*61 80W 24*		*62 30W 42	59 44W 36
57 51E 19	*54 133W 23*	*75 94W 21*	*58 100E 27*			*79 100E 21	80 145E 18	79 100E 19*	
	57 113E 21	*55 76E 20	60 86E 26	56 82E 21*					

PE 11 1955	PE 12 1955	PE 13 1955	PE 14 1955	PE 15 1955	PE 16 1955	PE 17 1955	PE 18 1955	PE 19 1955	PE 20 1955
LA LO DM	LA LO DM	LA LO DM	LA LO DM	LA LO DM	LA LO DM	LA LO DM	LA LO DM	LA LO DM	LA LO DM
51 53W 37*	*58 170W 39*	*61 20W 21	58 17W 19	57 31W 32*	*70 58W 37	59 59W 19	64 24W 20*		*75 55E 19
	*78 82E 24	78 82E 26	78 82E 18*		*83 100E 28	86 100E 30	85 145E 20*		
		64 134E 24			*64 66E 20*	*72 117W 24*	*57 93W 18	58 86W 18*	

PE 21 1955	PE 22 1955	PE 23 1955	PE 24 1955	PE 25 1955	PE 26 1955	PE 27 1955	PE 28 1955	PE 29 1955	PE 30 1955
LA LO DM	LA LO DM	LA LO DM	LA LO DM	LA LO DM	LA LO DM	LA LO DM	LA LO DM	LA LO DM	LA LO DM
69 69E 15*		*75 80W 28	64 88W 17*	****	****	*58 53W 23	64 46W 13*	*59 136E 22*	*67 8W 17
*53 7W 21	63 13W 23*	*63 77E 28	69 69E 19*				*56 98W 16*		
							60 35W 13		
							*59 64E 16	69 69E 13	64 84E 30

PE 31 1955	PE 32 1955	PE 33 1955	PE 34 1955	PE 35 1955	PE 36 1955	PE 37 1955	PE 38 1955	PE 39 1955	PE 40 1955
LA LO DM	LA LO DM	LA LO DM	LA LO DM	LA LO DM	LA LO DM	LA LO DM	LA LO DM	LA LO DM	LA LO DM
68 1E 22*	*90 19*	*63 123E 13	66 127E 14	67 82E 18	75 100E 11	85 145E 17*	*60 4W 19	61 10E 22	56 8W 15
*58 80W 19	58 74W 30	59 101W 19*	*61 20W 12*	*61 80W 20*				*60 94W 13	56 98W 15*
		58 73E 14	*61 170W 12*	*59 116W 13	59 101W 13*				
58 73E 17*			*69 145E 14*						

PE 41 1955	PE 42 1955	PE 43 1955	PE 44 1955	PE 45 1955	PE 46 1955	PE 47 1955	PE 48 1955	PE 49 1955	PE 50 1955
LA LO DM	LA LO DM	LA LO DM	LA LO DM	LA LO DM	LA LO DM	LA LO DM	LA LO DM	LA LO DM	LA LO DM
60 4W 23	60 4W 22	55 14W 16	55 14W 20	65 10E 18	59 31E 15	56 28E 15	60 24E 17*	****	*64 134E 16*
69 139W 16					*61 130E 14*	*54 4E 17*			
*57 157W 15	67 172E 11	72 170W 15	71 179E 13*			*67 28E 16*			

PE 51 1955	PE 52 1955	PE 53 1955	PE 54 1955	PE 55 1955	PE 56 1955	PE 57 1955	PE 58 1955	PE 59 1955	PE 60 1955
LA LO DM	LA LO DM	LA LO DM	LA LO DM	LA LO DM	LA LO DM	LA LO DM	LA LO DM	LA LO DM	LA LO DM
*82 37E 17	80 55E 23*	*78 62W 21*			*68 89W 15	67 62W 23	60 66W 44	60 35W 15	64 46W 23
*56 28E 15	59 46E 18	60 55E 22	74 37E 22	69 69E 16	60 86E 17*	*58 37E 20*		*56 82E 16*	
					58 73E 17				

PE 61 1955	PE 62 1955	PE 63 1955	PE 64 1955	PE 65 1955	PE 66 1955	PE 67 1955	PE 68 1955	PE 69 1955	PE 70 1955
LA LO DM	LA LO DM	LA LO DM	LA LO DM	LA LO DM	LA LO DM	LA LO DM	LA LO DM	LA LO DM	LA LO DM
59 59W 37	58 53W 30	63 57W 19*	*59 11W 25	56 8W 31	59 26W 30*	****	*75 170W 20	86 80W 25	85 145E 19*
*61 177W 27	66 163E 30*			*54 179E 27*	*65 80W 19*			*64 72W 24*	*56 152W 33
58 73E 22									

PE 71 1955	PE 72 1955	PE 73 1955
LA LO DM	LA LO DM	LA LO DM
*74 53W 26	68 80W 27*	*64 66E 17
57 177E 55	51 175W 41*	*59 136E 26*

Fig. 5.11 Sample page from Blocking Signature Sequence Catalogue. * indicates beginning and end of a sequence. Component signatures remain on same row.

Note that the beginning and end of a sequence is indicated by an asterisk (*) and that its component signatures always occupy the same row.

Example 1. The entry listed for pentad 50 (September 3 to 7, 1955), a positive anomaly centred at 64°N 134°E, magnitude 16 dams, represents a single signature sequence. (An inspection of the daily 500MB analyses discloses a short-lived but well-defined blocking anticyclone over eastern Siberia.)

Example 2. The entry listed for pentad 64 (November 12 to 16, 1955) 59°N 11°W is the starting signature of a 3-member sequence which ends with pentad 66 (November 22 to 26) at 59°N 26°W. This corresponded to a well-defined 14-day block over the eastern Atlantic (Treidl et al., 1980b).

5.3.3 Test on Independent Data

Of course we did not expect that all signature sequences would identify blocks with the same precision as these two examples. The limitations of our basic unit, the 5-day average 500MB height anomaly, have already been discussed in Chapter 4 and these carry over into the signature-sequences. On the other hand, the trajectory tests suggested that, particularly in the case of the more protracted blocks, there would be a high rate of correspondence.

It is also important to remember that the "objective criteria" developed so far are the result of empirical analyses on what at best may be termed quasi-objective data. These were the data concerning blocking systems extracted by individuals from analyses of daily 500MB height fields. Any test of the criteria must inevitably be made on data obtained in a similar manner.

For the test we chose a sample of data which had not been used to calculate Criterion (3) (What determines a qualifying signature?) or Criterion (4) (What determines a qualifying sequence?). We carried out a tedious but, we believe, ultimately rewarding examination of twelve months of daily analyses of 500MB height for

January, February, December 1952

June to November 1955

March to June 1956.

The procedure (Appendix V - 3) was to compare each catalogued sequence which occurred during this period with the contemporaneous daily analyses and to determine the frequency with which a geographically related blocking episode occurred. What were the guidelines for judging the occurrence of an actual blocking episode during this test? They were those used during the development of Criterion (3) in the first place, that is to say, the necessary and sufficient conditions (Appendix IV - 2) which, in our judgment, must obtain for a block to occur.

The results are summarized in Table 5.3. It will be noted that, not only have we compared the number of times a sequence was related to one or more associated blocking episodes which occurred within its duration (column 3) but also the number of times its component signatures actually concurred with the blocking episode (Column 6). The rationale was that, particularly during long sequences, there would be interruptions of blocking occurrence, and a more appropriate measure of the success of the Catalogue would be the percentage of the component signatures which were concurrent with blocking.

TABLE 5.3

Results of the Test of Catalogue Sequences on the Independent Data Months of January, February and December 1952, June - November 1955, and March - June 1956.

Col.	1	2	3	4	5	6
	# of SEQ's tested (including those N of 75N)	# of SEQ's within which one or more blocking episodes occurred	% of SEQ's which were related to one or more associated blocking episodes. (Col. 2 ÷ Col. 1) x 100	# of SIG's contained in SEQ's listed in Col. 1	# of SIG's within the SEQ's of Col. 2 which <u>were concurrent</u> with blocking episode	% of SIG's which were concurrent with a related blocking episode (Col. 5 ÷ Col. 4) x 100
SEQ_1	21	13	62	21	13	62
SEQ_n	26	25	96	109	90	83
ALL	47	38	81	130	103	79

It will be noted that a total of 47 signature-sequences (SEQ's) were listed in the Catalogue for the test period. Of these, 21 were one-pentad duration (SEQ_1's) and the remaining 26 were two or more (SEQ_n's where $n \geq 1$).

The success ratio of the SEQ_1's was 62% and of the SEQ_n's 96%. The success ratio of SEQ_1 signatures was, of course, 62% while of SEQ_n signatures it was 83%. This difference is not surprising because the latter are associated with the more persistent blocking episodes, often with large equally persistent positive anomalies. The former are sometimes associated with transient ridges of sufficient amplitude to produce a single qualifying anomaly.

Of the total of 130 signatures listed, 103, or nearly 80% were concurrent with an ongoing related block. Now, since we have no reason to believe the test period was unrepresentative, we conclude that the Signature-Sequence Catalogue will provide a useful and convenient source of information for investigations into the nature of blocking. It is important for the user to be aware of the author's guidelines for identifying a blocking episode, and to have an understanding of the limitations of using 5-day averages for the specification of events in a continuum. Subject to those reservations, the Signature-Sequence Catalogue can be used to advantage

(a) for quick identification of probable periods of blocking

(b) for a wide variety of frequency studies, the results of which will be closely connected with corresponding frequency studies of blocking.

5.3.4 Signature-Sequence Frequency by Duration

The number of signature-sequences (all durations) which occurred during the 33 years of record is 1,868. Of these, 994 were 2 pentads or

longer, and the remaining 874 had a duration of only one pentad. The complete distribution is shown in Fig. 5.12(a). (SEQ's which were initiated north of 75°N were not counted.)

As a matter of interest the 16-pentad 'outlier' was initiated July 20th, 1976 at 56°N 22°W and terminated October 7th, 1976 at 72°N 10°E (PE 41 to PE 56, inclusive). This extraordinarily long sequence was immediately preceded by one which also resided in the E. Atlantic - N.W. Europe region. It began June 25th at 54°N 4°E and ended July 19th at 74°N 37°E, and was associated with the blocking episode which resulted in an exceptional heat wave over England and neighboring countries.

Figure 5.12(b) from Treidl et al. (1980a) represents the frequency distribution of durations of those blocks which they identified over the northern Hemisphere 1945 to 1977. Treidl does not ascribe any statistical significance to the 'spikes' at 12 and 19 days, respectively. The relative similarity between Figs. 5.12(a) and 5.12(b) does confirm, in a climatological sense, a strong relationship between Signature Sequence Duration and Observed Blocking Duration.

5.3.5 Signature-Sequence Frequencies by Longitude

In section 5.2 we presented areal and longitudinal distribution by season and year of the frequency of occurrence of Blocking Signatures. Although these diagrams clearly revealed areas of high and low blocking frequency, they could not be used to distinguish between areas where Signature-Sequences were initiated and those where they terminated. We now have the means to do so and a program was written to identify and count all sequences which

(a) started in a 10° longitude sector

(b) ended in a 10° longitude sector.

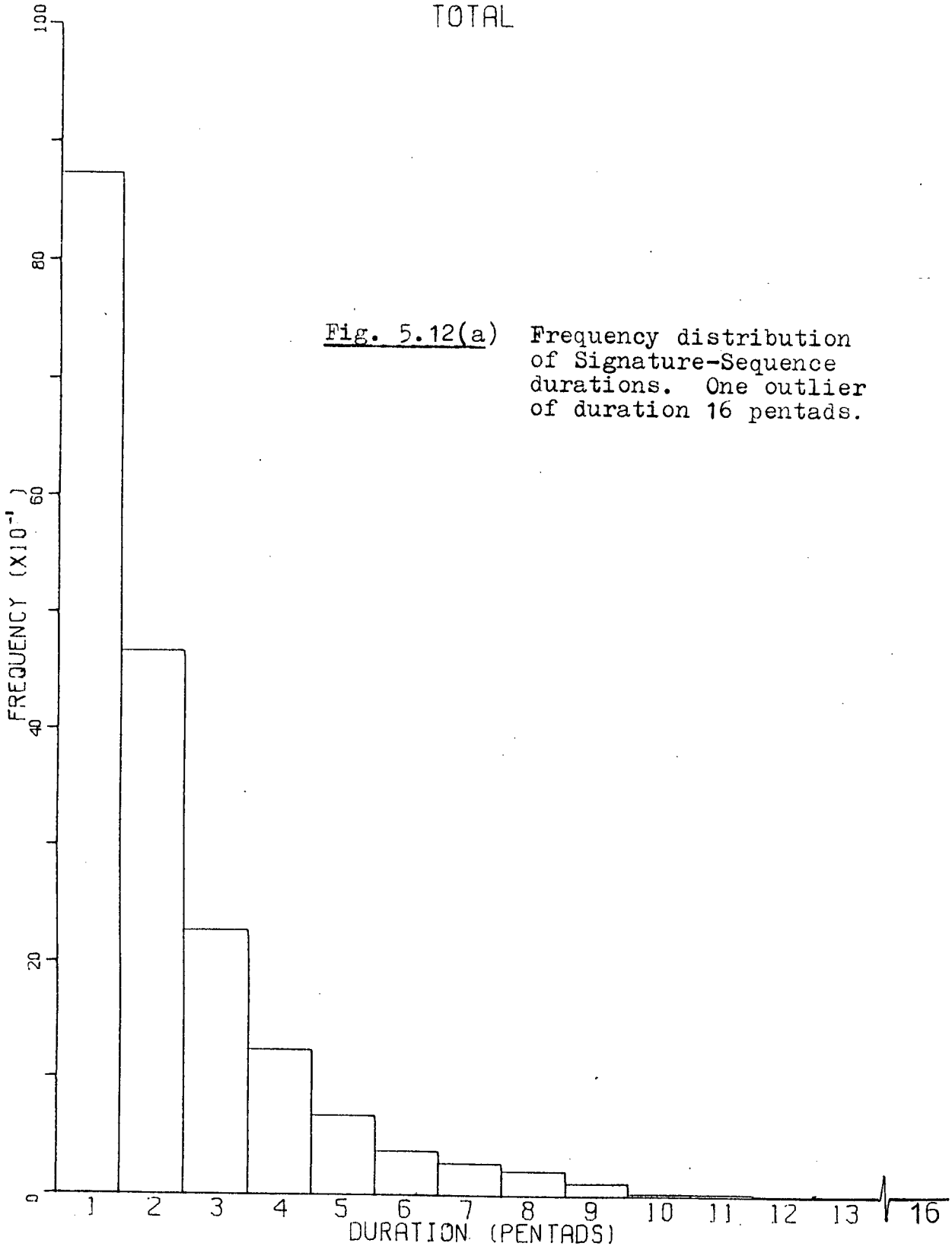

Fig. 5.12(a) Frequency distribution of Signature-Sequence durations. One outlier of duration 16 pentads.

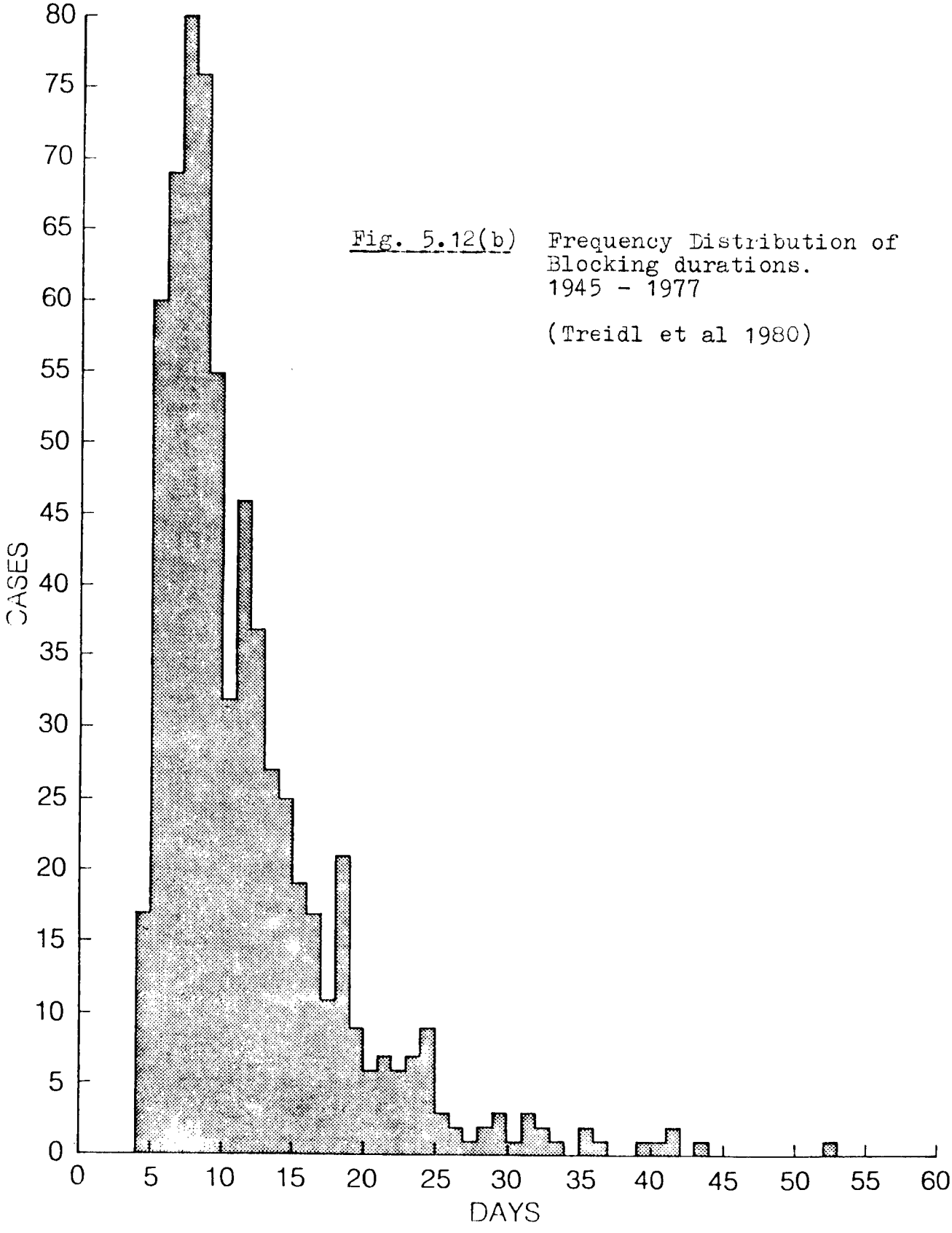

Fig. 5.12(b) Frequency Distribution of Blocking durations. 1945 - 1977

(Treidl et al 1980)

Fig. 5.13 presents the frequency distribution of the initial positions of all sequences which were started south of 75°N, while Fig. 5.14 presents the corresponding distribution of the final positions. (It should be noted that some signatures drifted north of 75°N in which case their final position was noted and they were included in the distribution of Fig. 5.14.)

It would appear (Fig. 5.13) that blocking sequences have a preferred longitudinal band of initiation in the East Atlantic and that subsequently (Fig. 5.14) they are more likely to retrograde or progress than to remain quasi-stationary. This is consistent with the results of Rex (1950) and Treidl et al. (1980a). In the 30 degree sector centred on the Urals (60°E) starting signatures outnumber ending ones, whereas the reverse is the case from 90°E to 110°E (central Siberia). Personal observation of a large number of 500MB Northern Hemisphere analyses confirms that this reflects a propensity for blocks identified in the Ural Mountain area to progress and terminate before reaching the east Asian coast. Proceeding still further east to 130° - 150°E the excess of ENDS over STARTS can only be surmised in the absence of a latitudinal distribution. The results of Namias (1958) suggest that many of these terminations over NE Siberia and the Arctic Ocean reflect warm anticyclones that retrograde from the Aleutians. A comparison of Figs. 5.13 and 5.14 indicates that some could have even have retrograded from mainland Alaska.

The most revealing of the comparisons by season is SPRING (Figs. 5.15 and 5.16). For example, western Russia (30°E to 40°E) appears to be a site of maximum initiation, and Central Siberia one of maximum termination. Again, this reflects the predominance of progressive motion for blocks over this part of the Eurasian continent. Moving to the Pacific

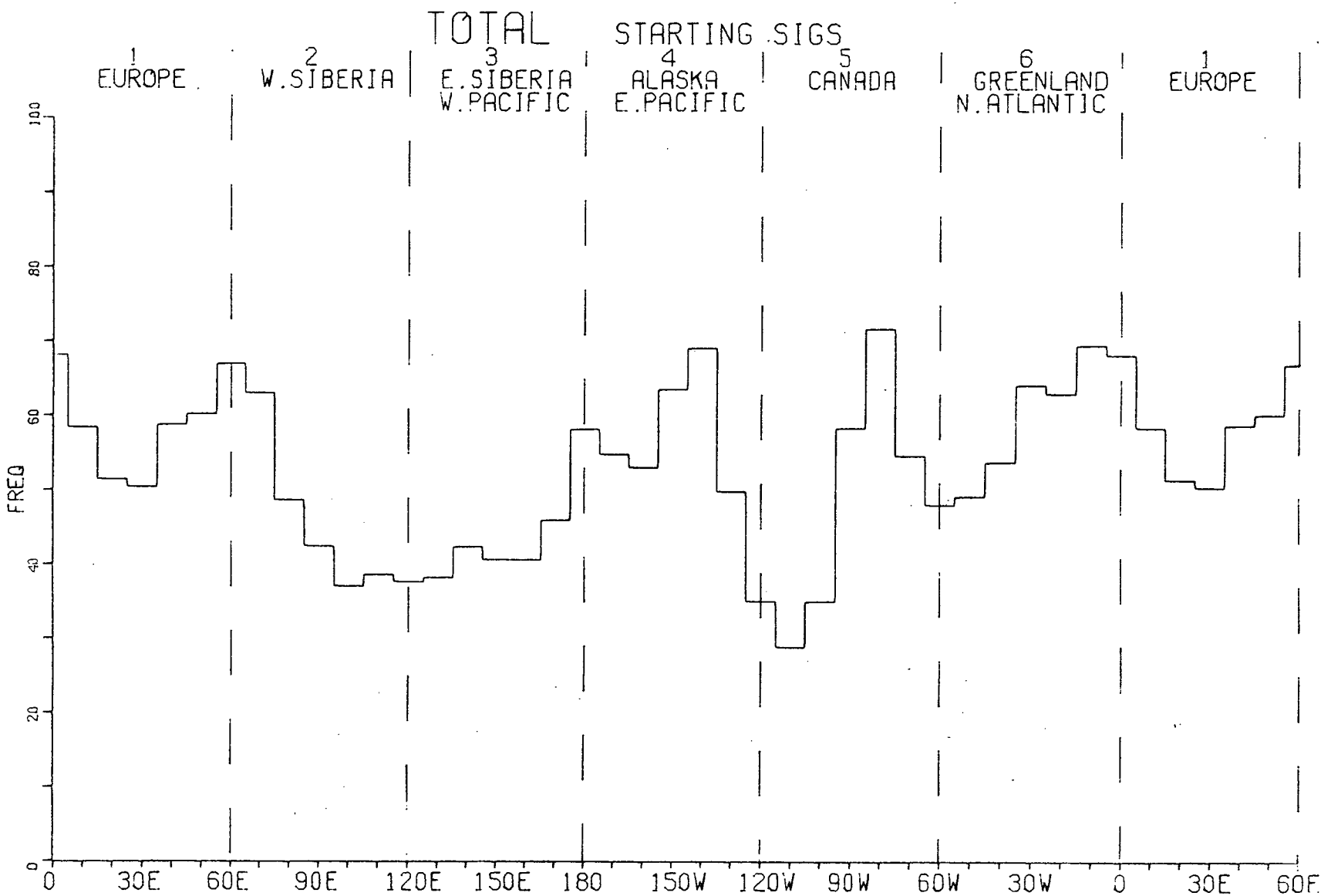

Fig. 5.13 Total (i.e. annual) frequency by longitude of initiation of all signature-sequences.

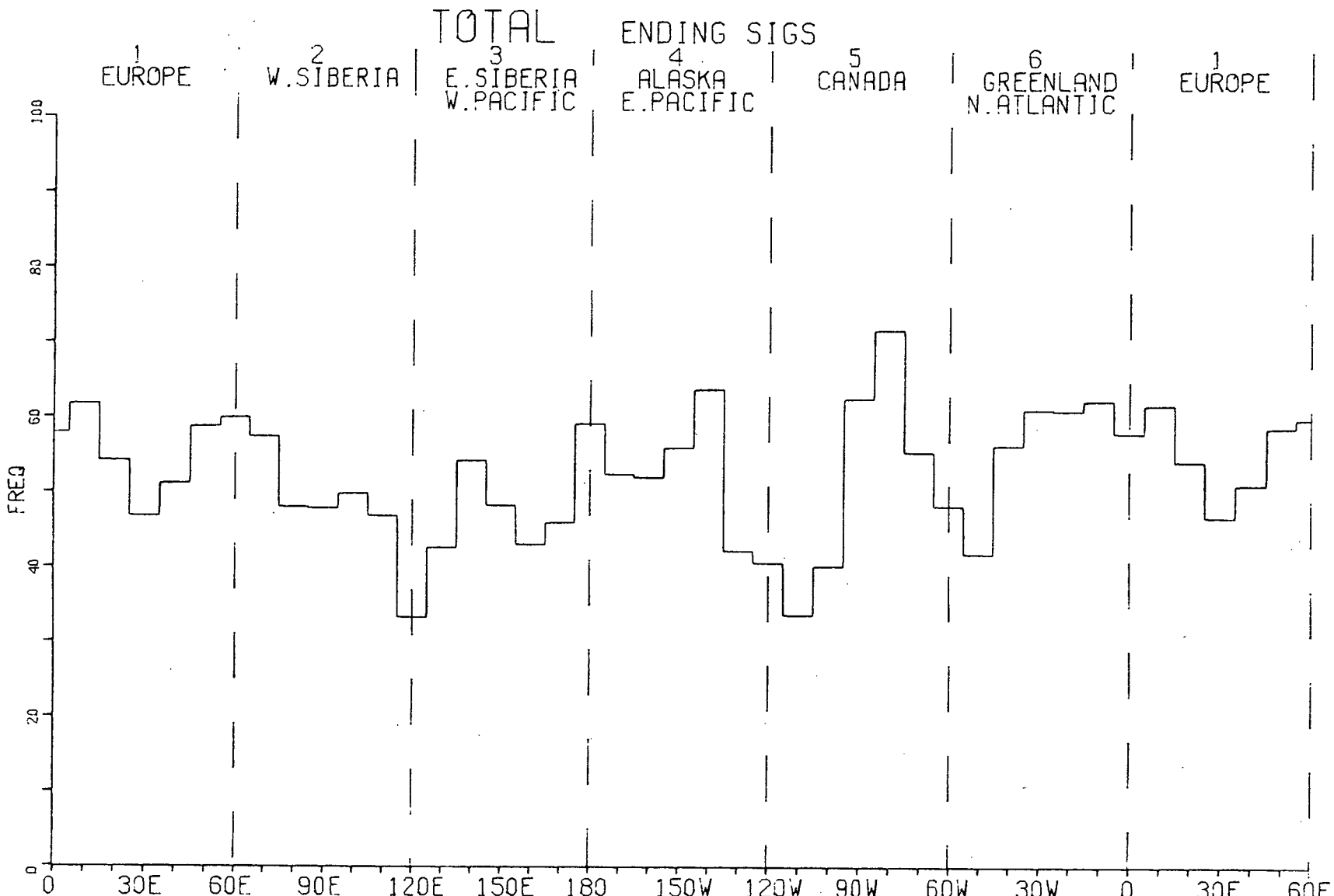

Fig. 5.14 Total (i.e. annual) frequency by longitude of termination of all signature-sequences.

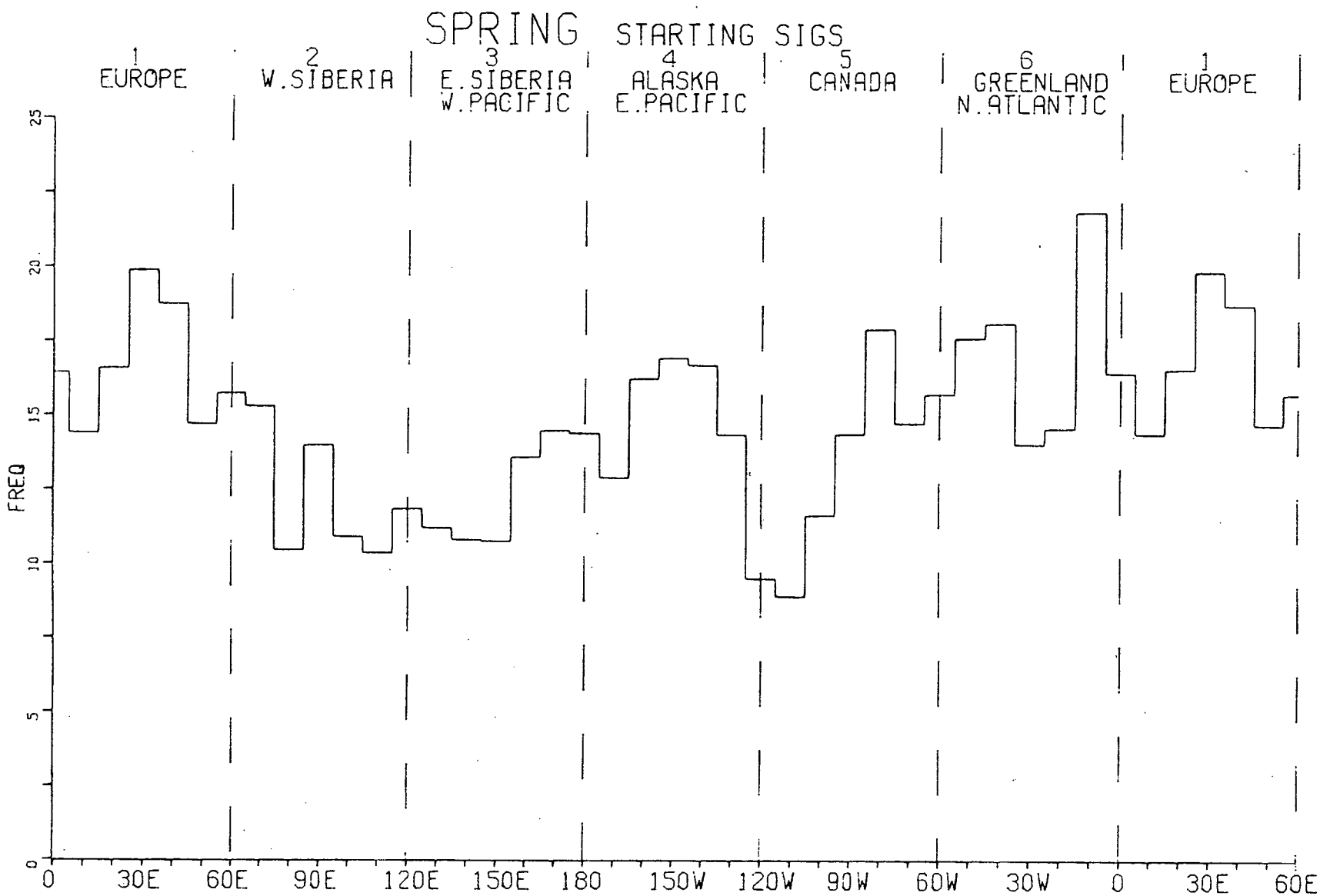

Fig. 5.15 As in Fig. 5.13 for SPRING

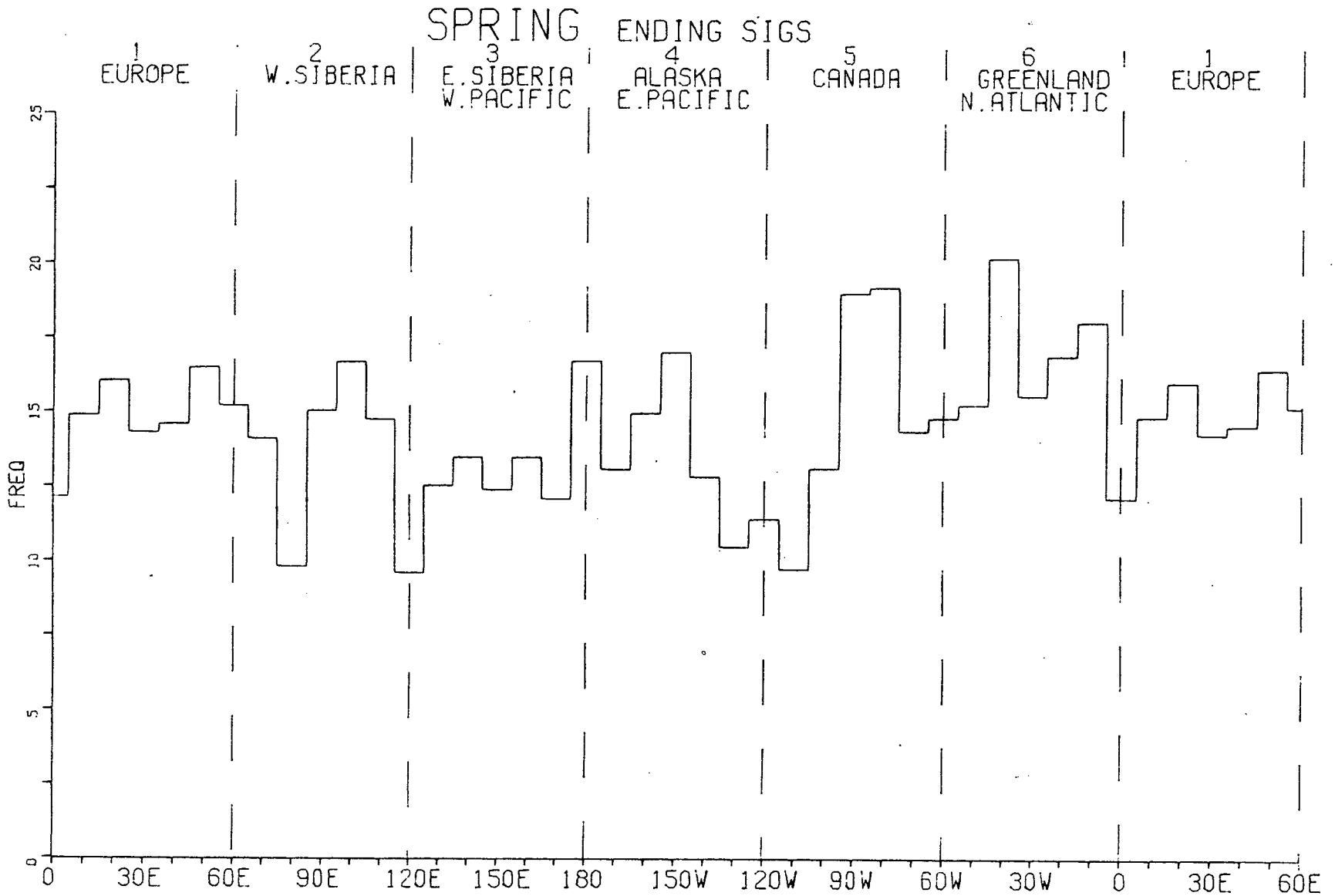

Fig. 5.16 As in Fig. 5.14 for SPRING

and Alaska, there is a distinct suggestion that blocking signatures initiated in the maximum frequency sector 165°W to 135°W, progress or retrogress rather than remain quasi-stationary. Retrogression appears to predominate. It is well known that blocking highs centred in the vicinity of 160°W create a synoptic situation favourable for cold lows originating in the Gulf of Alaska to track southeastward and to punctuate the otherwise idyllic West Coast spring with periods of unsettled weather. Over Central Canada the maximum at 80°W was noted previously (Section 5.2.2) during the discussion of longitudinal signature distributions. The excess of terminations over initiations suggests that not only do blocks develop 'in situ', but that they are also 'imported' and we shall elaborate upon this in the next section. Frequency distributions for Starting and Ending Signatures during SUMMER, FALL and WINTER will be found in Appendix V (Figs. V - 3 to V - 8).

5.3.6 The Baffin Island Paradox

In the familiar 3-wave pattern of the normal 500MB WINTER circulation (Fig. 4.6), we note a primary trough extending from the Canadian Archipelago southward to the St. Lawrence Valley with its axis along the 70°W meridian. Its intensity naturally diminishes with the approach of SUMMER (Fig. 4.7) but its normal seasonal location remains essentially unchanged.

Why, then, do we find for every season a maximum frequency of blocking signatures, not only in the location of the normal trough, but centred near its deep quasi-permanent core? There is certainly no parallel for this paradox in the case of that other primary feature, the Asiatic trough, where the incidence of signatures is much lower (Fig. 5.1).

To what extent are these North-Eastern Canada signatures associated with blocking? There have been several studies of anomalous circulations featuring strong positive mid-troposphere height anomalies over Baffin Island and Davis Strait (e.g., Namias, 1958) but to our knowledge the question has not been addressed explicitly. The differing opinions of Sumner and Woffinden on the question of blocking frequency in that area have already been noted (5.2.1). Treidl et al. (1980a) concluded that except for SPRING, which "showed an interesting flare-up in blocking activity", the counts of occurrences over Canada were low.

In an attempt to resolve the paradox we listed all Blocking Sequences which contained at least one Signature in the area 60°N to 75°N and 60°W to 90°W for the period July 1955 to June 1956. There were 15 cases. We then examined the corresponding daily 500MB analyses with particular care and found that during 12 cases the Sequence was in fact concurrent with an <u>observed</u> blocking episode. On the other hand, Treidl's Catalogue lists only five cases for that area during the same period. The difference in results arises almost entirely from the difference between our respective guidelines for deciding whether a blocking episode has occurred on a series of daily analyses (Appendix IV - 2). His are more restrictive and therefore reject cases which we would include.

The listing of these 12 cases and associated comments are presented in Table 5.4. We are convinced that the blocking process in the generally accepted sense was operating on each occasion. As a typical example, consider the Blocking Signature for PE 69 (December 7-11, 1955 64°N 72°W). The 500MB analysis for December 9 (Fig. 5.17) shows a warm blocking high over Western Hudson Bay and a blocking ridge extending eastward to southern Greenland. This condition persisted through to

TABLE 5.4

Twelve Cases of Blocking Affecting Baffin Island (1955-56)

No.	PE	Lat.	Long.	PE	Lat.	Long.	Max. (dams)	Comments
1	53	78N	62W	53	78N	62W	21	Block over Ellesmere Island, developed from retrogression of high-latitude blocking over Scandinavia. Low normally over Baffin area displaced southward
2	66	65N	80W	66	65N	80W	19	Short term (5-day) Block over Hudson Bay during pentad 66
3	69	64N	72W	69	64N	72W	24	Block over Hudson Bay-Southern Baffin Island - Davis Strait. See Dec. 9, 500MB Analysis, Fig. 5.17
4	71	74N	53W	72	68N	80W	27	Block formed by discontinuous retrogression of a North Atlantic blocking wave
5	2	58N	80W	2	58N	80W	36	Associated with a warm Quebec-Labrador anticyclone
6	2	53N	51W	5	60N	66W	47	Robust Blocking four pentads duration
7	4	64N	88W	6	60N	94W	38	Robust Blocking three pentads duration
8	10	67N	62W	11	67N	29W	31	A progressive case where the Anomaly was initially over Davis Strait (PE10) and crossed Greenland to reinforce Atlantic blocking (PE11)
9	17	67N	98W	17	67N	98W	16	Small persistent blocking anticyclone over Northwest Territories
10	15	69N	41E	22	67N	62W	37	Striking example of steady retrogression March 12 - April 20 of a positive anomaly initiated over the Barents Sea and terminated over Davis Strait
11	32	64N	88W	32	64N	88W	13	Short term (5-day) omega-Block
12	34	71N	91W	36	70N	102W	30	Major blocking episode

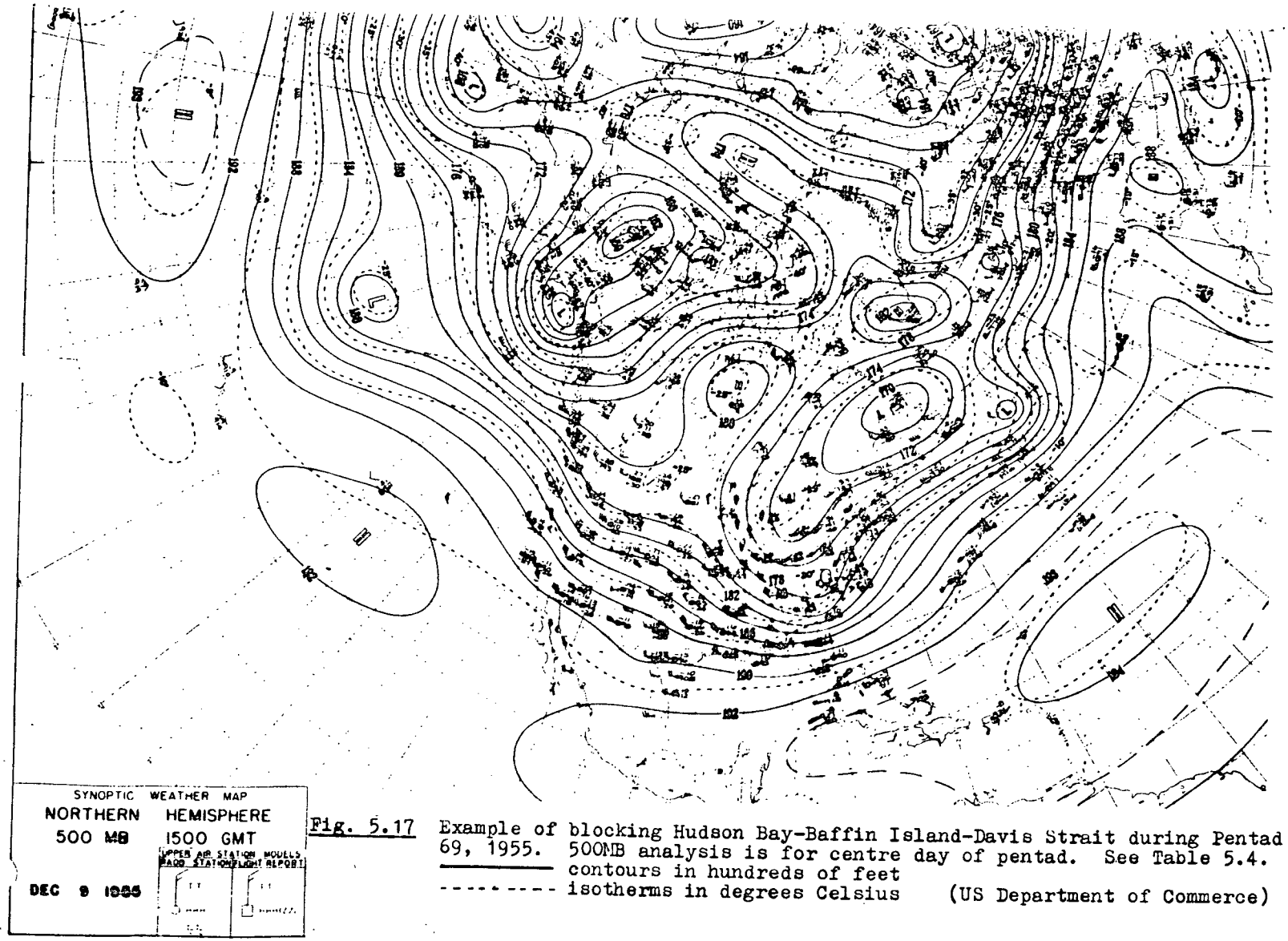

Fig. 5.17 Example of blocking Hudson Bay-Baffin Island-Davis Strait during Pentad 69, 1955. 500MB analysis is for centre day of pentad. See Table 5.4.
——— contours in hundreds of feet
- - - - - isotherms in degrees Celsius (US Department of Commerce)

December 13th. Note how the Baffin Low has bifurcated. The original centre, which was in its normal position on December 4th, has retrograded to Alaska while to the south we find a slow moving anomalous centre of low gph over Labrador. It is true that the Hudson Bay blocking anticyclone lacks the unmistakable robust structure of the major ocean blocks, but the general circulation features over the U.S. and Canada, particularly the split jet over British Columbia, are clear indicators of a significant blocking episode.

Further evidence of the high incidence of winter blocking in the vicinity of the normal 500MB Baffin Low is provided by the distribution of the coefficient of skewness of 5-day average 500MB heights in that area (Fig. 6.9). The inference is that although the most numerous deviations from normal are caused by variations of intensity of the Baffin Low, more or less in its usual position, a sufficient number of large positive anomalies occur to skew the distribution markedly so that the mode is well to the left of the mean. Interpretation of the spatial distribution of the higher moments will be discussed in Chapter 6.

5.3.7 Secular Variation of Blocking Signatures

In view of the range of criteria used by authors for defining blocking, and of the individual judgment required for marginal cases, one is inclined to be somewhat circumspect with regard to studies of interannual variability. Nevertheless, because of the profound impact of recurrent large scale blocking on the climate over vast regions of the globe, the subject has been one of considerable interest, particularly among European climatologists.

Prior to the availability of Northern Hemisphere upper air data, blocking was identified by the application of plausible criteria to analyses of MSL pressure, e.g., Elliot and Smith (1949). If one's interest was focussed on the oceans this gave reasonable results, but in the case of the continents, particularly during the winter season (because of the masking by Arctic air masses) it was difficult and at times impossible to determine if blocking was, in fact, in progress. Nevertheless Elliott and Smith did use the daily analyses of MSL pressure for the months of January and February, 1900 - 1938 to assess the secular variation of blocking over nearly three-quarters of the hemisphere (from 140°E eastward to 40°E). They found that the year-to-year extent of blocking in the three sectors, the Pacific and Atlantic Oceans and the North American continent, were (not surprisingly) in phase and therefore used a combined index for a representation of the extent of blocking in a given year. The result of their study along with a graph of concurrent sun-spot numbers is shown in Fig. 5.18(a). The promising in-phase relationship early in the period becomes out-of-phase later in the record. Lag relationships were also explored and the authors suggested that the phase relationship was probably random. The sample is, of course, too small for statistically sound conclusions.

Brezowsky et al. (1951) examined the secular variation of Atlantic and European blocking from 1881 to 1950 (for all months) using a circulation classification technique, and their curve of overlapping 10 year means shows an interesting quasi-periodicity (Fig. 5.18b). These authors also looked for the possibility of a relationship with solar activity. The result was inconclusive. The sample is still too small not only temporally but, in our opinion, spatially, for meaningful statistical conclusions.

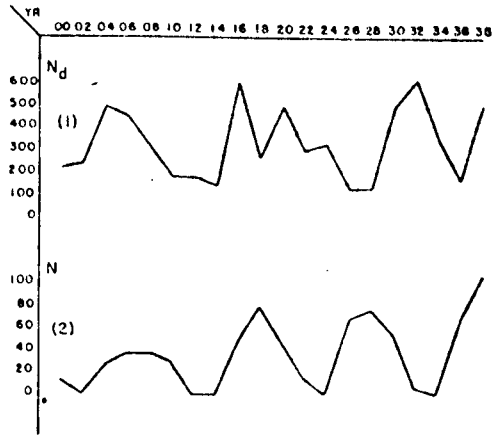

Fig. 5.18(a) Long-period variation in index numbers, N_d, and sunspot numbers, N, for the January-February seasons of the 20 even years: 1900-1938. (Elliott et al., 1949).

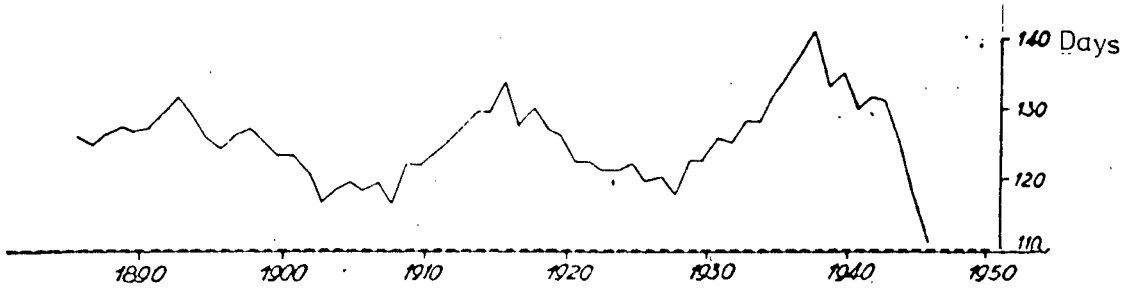

Fig. 5.18(b) Annual frequency of blocking highs, Atlantic and Europe. Overlapping 10-year means. (Brezowsky et al., 1951).

Notwithstanding the expected difficulty (if not impossibility) of interpretation, we thought it would be useful to examine the annual variation of blocking sequences for the Northern Hemisphere which originated south of 74°N from 1946 to 1978. Fig. 5.19 presents, in effect, three frequency distributions:

(a) The top curve is the total duration in pentads per year of all identified sequences.

(b) The middle curve is the corresponding measure for all sequences containing two or more signatures.

(c) The lower curve is for all sequences containing three or more signatures.

For the years 1946 and 1947, it should be noted that upper air data over Siberia and northern China was virtually non-existent. Hence the accuracy of 500MB analyses over these areas falls well short of the standard for the remainder of the hemisphere. Interpretation of Fig. 5.19 should therefore begin with 1948.

The histograms reveal a number of interesting features:

(a) The single signature-sequences (those associated with blocks of relatively short duration) are relatively uniform from year to year. (Compare unstippled areas.)

(b) The sequences containing two or more signatures (usually related to blocks with average or above average persistence) appear to provide the major component of inter-annual variation.

(c) There is a suggestion of a complex quasi-periodicity with a time scale of the order of a decade. Of particular note is the 15-year fluctuation with crests at 1953 and 1968. Again, the sample is too small for interpretations of statistical significance.

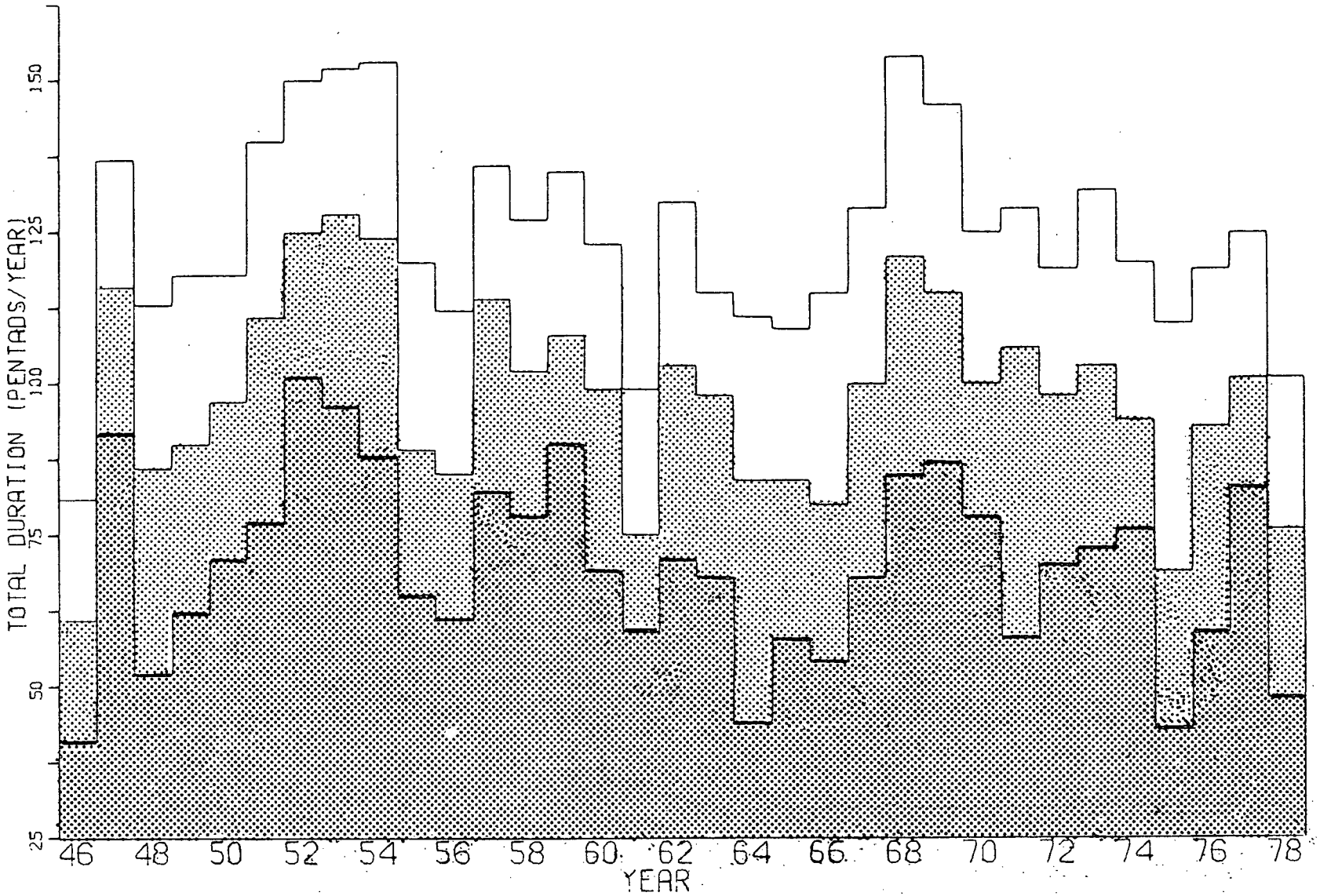

Fig. 5.19 Duration in Pentads per year. Top curve for all Sequences. Middle curve for sequences ⩾ 2 Signatures. Lower curve for Sequences ⩾ 3 Signatures. (One-signature unstippled. Two-signature and ⩾ 3-signature frequencies differentiated by stippling).

(d) The frequency of blocking sequences was well above normal from 1951 to 1954, inclusive. This seems to be related to a statement by Namias (1958) when discussing the so-called 'normal' 700MB charts which were available at that time: "There are suggestions that the eight-year period 1948-1955 may have been abnormal in the sense that pressures were too high relative to a longer period average over the Baffinland-Davis Strait-Greenland area". (The "longer period" referred to one which began in the 1930's with the construction of 700MB contours from MSL analyses using a statistical-differential analysis technique.)

Namias' astute observation is in agreement with Lamb (1972) who also noted the higher average pressure and incidence of blocking anticyclones over Greenland in the 1950's. Now there is a strong teleconnection between positive anomalies centred in the Davis Strait area between 60°N and 70°N and concurrent positive anomalies around the hemisphere centred north of 50°N (Namias, 1958; O'Connor, 1969). Hence it is reasonable to conclude that above normal pressure in that area, 1948 to 1955, is indeed related to the blocking frequency maximum 1951 to 1954.

We thought it would be of interest to compare the secular variation of blocking 1945 to 1977 as reported by Treidl et al. and reproduced in Fig. 5.20(b), with our result for blocking signature sequences, Fig. 5.20 (a). These curves should be compared in a relative sense for reasons already discussed. In Fig. 5.20(b), much above normal blocking in the 1950's, with a strong peak 1953-1954, is reasonably consistent with Fig. 5.20(a). So, too, is the generally below normal blocking in the 1960's terminated by an abrupt reversal to above normal 1968-1969. The subsequent decline in the early 1970's is much more marked in (b) than in (a). Both curves are consistent with an abrupt recovery in 1976,

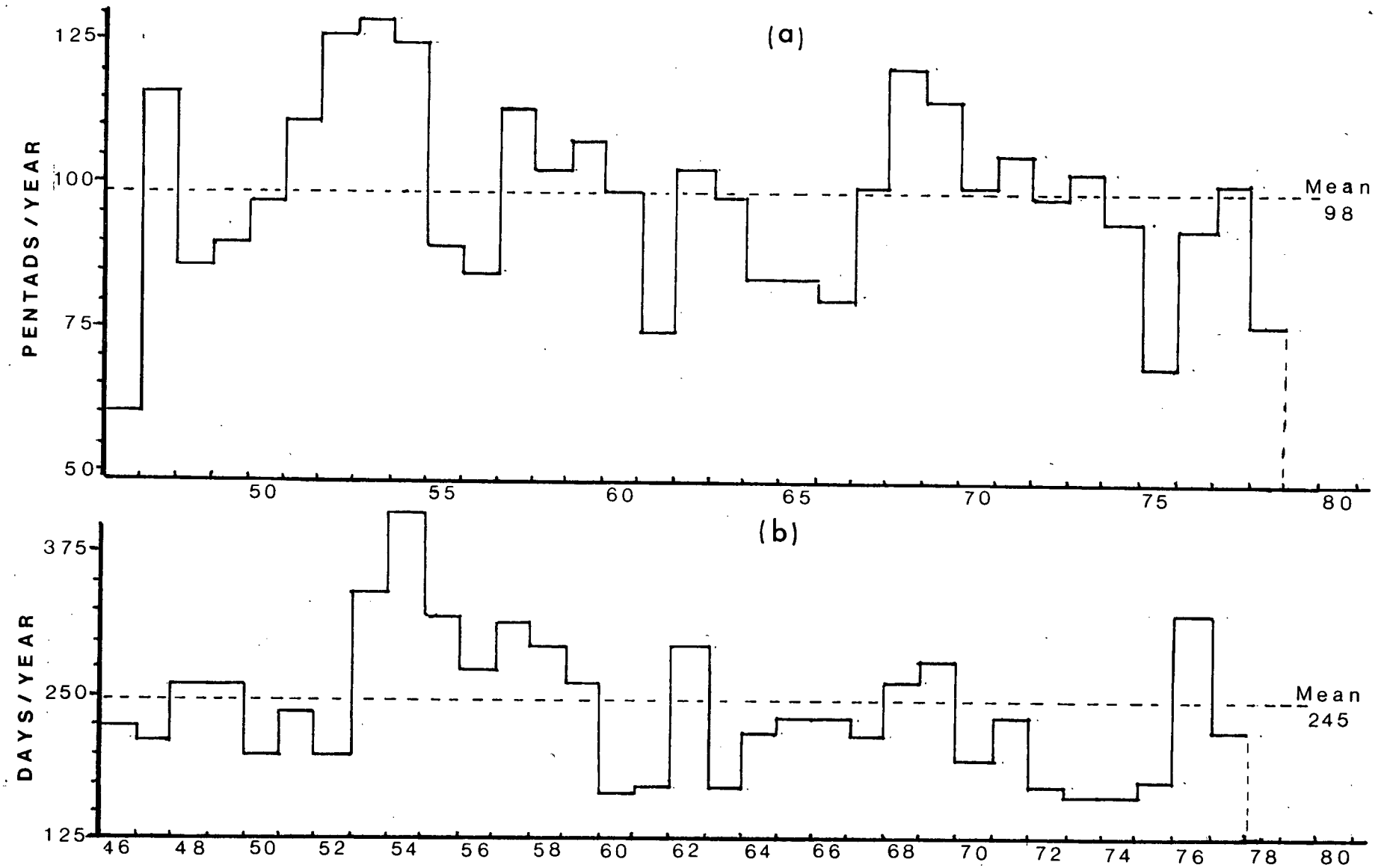

Fig. 5.20 (a) Duration (Pentads/year) of all sequences ⩾ 2 signatures (SEQ_n's).
(b) Duration (Days/year) of blocking, reported by Treidl et al (1980).

but agreement is not good in 1977, or from 1946 to 1952, inclusive. The differences are no doubt mainly attributable to the respective guidelines and methodologies discussed in Chapter 4.

5.4 Summary

In this Chapter we have applied an objective technique to 33 years of 5-day averages of 500MB height for the preparation of the geographical distribution of blocking signature frequency in the Northern Hemisphere. The results are consistent with published investigations of frequency of actual blocking over the oceans, but they also reveal a large area, centred near Baffin Island (or, more precisely, the Foxe Basin) which is subject to a much higher frequency of blocking than these investigations would indicate. The paradox was rationalized.

We found a high incidence near the Pole in Spring and Summer in agreement with Perry (1979) and Treidl et al. (1980a). There was also a high frequency of blocking signatures in a wide sector centred about 60°N, confirming the result of Baur (1958).

Interseasonal comparisons of blocking frequency (highest in spring and summer, lowest in fall and winter) confirm previous studies.

Criteria for identifying a blocking signature-sequence were used to prepare a Catalogue listing their attributes (Time and Location of Initiation, Termination, Component Signatures and Intensity). A test of these sequences showed a strong relationship with actual blocking events, with a 96% success ratio for sequences $\geq$ 2 pentads duration and 62% for those of only one pentad duration.

A comparison between the initial and final locations of the sequence signatures revealed progressive and retrogressive tendencies dependent on the region of origin and the time of year.

The interannual variation of blocking was placed on record but it was not possible to draw statistical conclusions due to the size of the sample (33 years) relative to the time scale (order of 1 decade) of the fluctuations of interest. It is likely that these fluctuations are part of the natural variability of the prevailing climate regime (time scale order of 1 century).

CHAPTER 6

6. CONNECTIONS BETWEEN BLOCKING AND THE STATISTICAL MOMENTS OF THE 5-DAY MEAN HEIGHT FIELDS IN THE LOWER TROPOSPHERE

6.1 Rationale

Nearly all the investigations into the statistics of blocking are founded on the enumeration of episodes either subjectively from examination of sequences of synoptic analyses or (as in our case) by the application of objective analysis to a related parameter (e.g., the blocking signature). Common to both these methods is the principle that a blocking episode will feature some characteristic extremum in the mid-troposphere such as the centre of the anticyclone or the centre of the associated positive anomaly. Unfortunately, in restricting the data to an investigation of extrema, one pays the price of a severe reduction in sample size.

Consider, for example, a proposal to investigate the frequency distribution (spatial and temporal) of all significant positive and negative anomalies on 5-day average 500MB charts over the Northern Hemisphere during the past 33 years. This would be a more general study than the subject of this thesis. On a designated 5-day mean 500MB chart there are 1,977 data points or nearly 2,000 discrete values of gph. On the other hand, an examination of the Master Catalogue of positive and negative anomalies (Fig. 4.2) discloses that there are about 20 anomaly centres per pentad. The data sample, therefore, has been reduced by <u>two</u> orders of magnitude. Moreover, if we confine our attention (as this study does) to large positive anomalies north of a latitude threshold, we find there is still further reduction. Indeed the Blocking Signature Catalogue (Fig. 4.8) reveals an average of two per pentad. Thus, in terms

of sample size, there is an effective reduction of three orders of magnitude from the original set of data.

It is clear, therefore, that for meaningful areal distributions of extreme values a very long record of data is required. Fortunately, the 33-year period did produce reasonably well defined spatial distributions of blocking signatures (Figs. 5.2 to 5.5, inclusive) but it is obvious from the frequency isopleth labels that the number of occurrences per 381 km grid is very low.

Consequently, it seemed appropriate to return to the vastly greater original data set to determine whether it would provide additional information on the nature of low frequency atmospheric variability and, in particular, of the blocking process.

6.2 Purpose and Objectives

So far we have confined this investigation to the 500MB level. However, it is clear from previous discussions of the vertical characteristics of blocking anticyclones that additional information from lower troposphere pressure levels is needed to better define the thermal structure. This is particularly important in winter over the continents. We decided, therefore, to compute seasonal normals and standard deviations of 1000MB 5-day mean height and of 1000MB-500MB thickness. We shall examine Northern Hemisphere fields of Standard Deviation at these levels for evidence of the influence of blocking on the variability of the atmosphere.

A second theme of this Chapter is that in view of the highly anomalous spatial and temporal characteristics of blocking, their total impact may in some way cause the distribution of long term 500MB 5-day

mean height to depart significantly from Gaussian in certain regions. The non-dimensional coefficients of the 3rd and 4th statistical moments, skewness and kurtosis, provide a measure of such departures. Our objective, therefore, will be to investigate hemispheric fields of these parameters at the 500MB level.

We shall not necessarily confine attention exclusively to 'continuum' data. If the evidence so warrants, we shall investigate areas of significant skewness and kurtosis by using the Master Catalogue (Fig. 4.2) to prepare positive and negative anomaly frequency distributions. This may assist with the interpretation of non-Gaussian distributions of low-frequency fluctuations and highlight the role of blocking.

6.3 Preparation of the Working Data Base

6.3.1 Conversion from sea level pressure to 1000MB gph

We acquired from NCAR a 33-year set (1946-1978) of analyses of the daily sea level pressure for the Northern Hemisphere on magnetic tape. This was then converted into contiguous 5-day means in the manner described in Section 4.3.2. Subsequently, these were transformed into values of geopotential height of the concurrent 5-day mean 1000MB surface. A first approximation is

$$Z_{10} \approx \frac{3(p - 1000)}{4} \text{ dams}$$

Where p = MSL pressure

Z_{10} = gph of 1000MB surface

Thus isobars drawn at 4MB intervals on a MSL pressure analysis can be converted to 1000MB contours by relabelling with a 3 dam interval. However, this approximation (6 dams per 8MB) assumes a uniform surface

temperature ($\approx 0^{o}C$), and the conversion factor should range from 5.5 dams (very cold arctic air) to 7.1 dams (warm tropical air) per 8MBs of pressure.

We therefore chose the method used by the British Meteorological Office, described by Moffitt and Ratcliffe (1972). The principle is that empirical relationships between 1000MB and 500MB thickness and surface temperature can be used to provide an approximation for the latter. The algorithm is presented in Appendix VI - 1 and 2, inclusive.

6.3.2 (1000MB - 500MB) Thickness

Five-day averages of the 500MB gph for the 33 year period over the Northern Hemisphere had already been computed (Section 4.3.2). Subtraction of the 1000MB gph from the 500MB gph immediately yielded the fields of (1000MB - 500MB) thickness.

6.3.3 Seasonal Stratification

In this Chapter, our continuum statistics will be calculated by Season and the resulting spatial distribution will be displayed geographically. The nomenclature will follow Chapter 4.

WINTER $WN = (PE_1 \text{ to } PE_{12}) + (PE_{68} \text{ to } PE_{73})$

SPRING $SP = (PE_{13} \text{ to } PE_{31})$

SUMMER $SU = (PE_{32} \text{ to } PE_{49})$

FALL $FA = (PE_{50} \text{ to } PE_{67})$

6.4 Statistical Moments Part I

6.4.1 Normals and Standard Deviation

All statistical moments must be calculated from a baseline which is the mean of the variate. When the period of record reaches a duration (e.g., 30 years) for which the mean may be conventionally accepted as representing the climatological average we shall refer to it as the Normal (Appendix I). The details for computing the Normals and Standard Deviations will be found in Appendix VI - 3.

Normals and Standard Deviation fields for 1000MB and 500MB surfaces and for (1000MB - 500MB) thickness have been prepared for each season and are available from the author. Those relevant to the discussion will be displayed as figures within chapters.

6.4.2 Accuracy of Normal and Variance Fields

If a population (33 years of record of daily gph) is divided into equal sub-sets (5-day means) then the average of the population equals the average of the sub-sets. Consequently our Normal Charts of 5-day mean gph are also Normals for daily mean gph. (The same does not hold true, of course, for the variance and higher moments.) The Normal Charts of the 1000MB and 500MB fields for the Winter Figures 6.1 and 6.2, and Summer Figures 6.3 and 6.4, are in very good agreement with corresponding fields calculated by Blackmon (1976) and Blackmon et al. (1977). We were unable to find normal charts of gph for the Spring and Fall seasons in the literature and it could well be that this is the first time they have been computed. Such charts have been prepared by calendar month, and our 500MB gph and 1000MB - 500MB thickness for Spring and Fall are consistent with corresponding fields calculated by Moffitt and

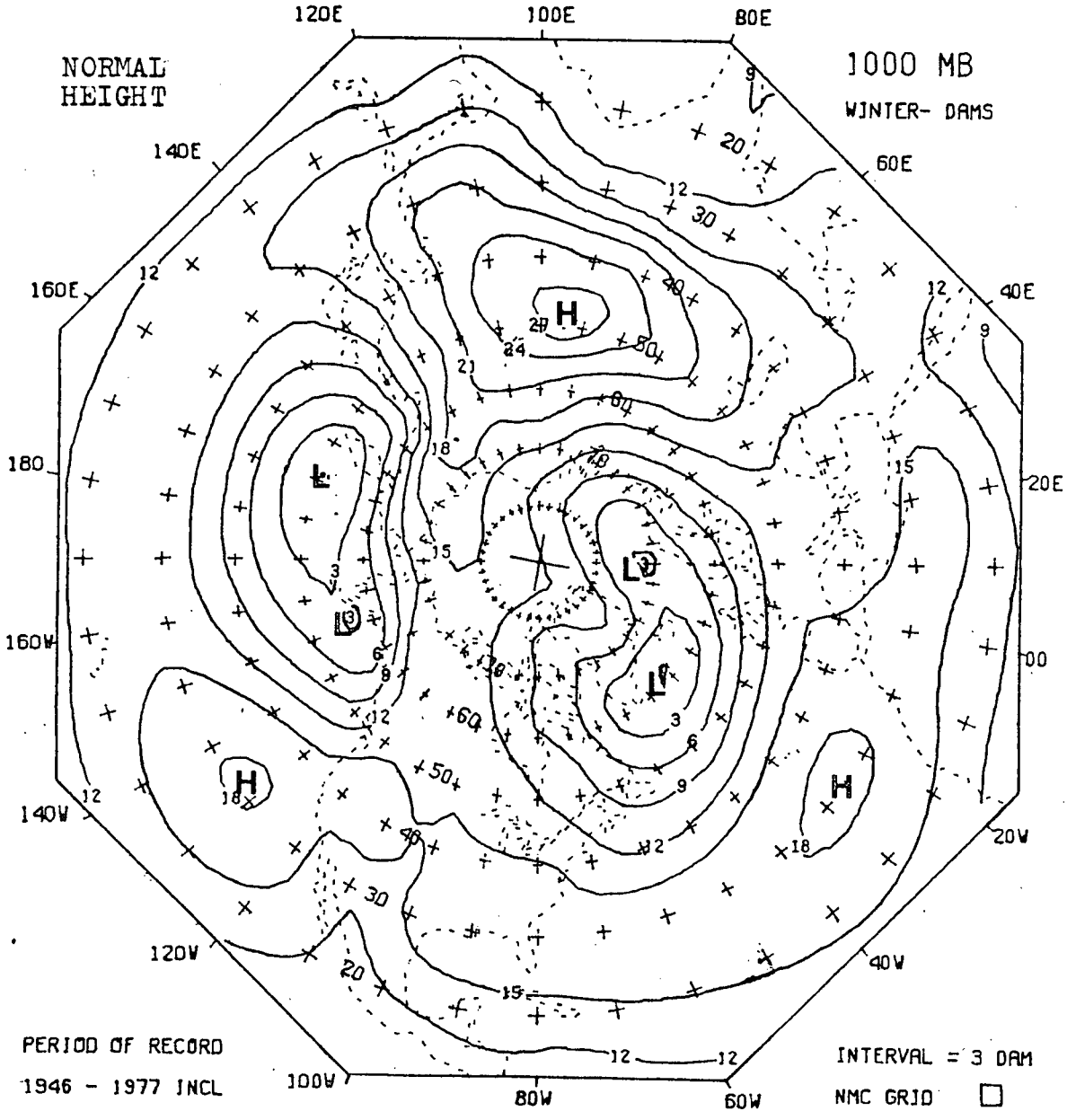

Fig. 6.1 Normal height of the 1000MB surface for WINTER (December 1 to February 28). Contours labelled in decametres (dams). Interval = 3 dams.

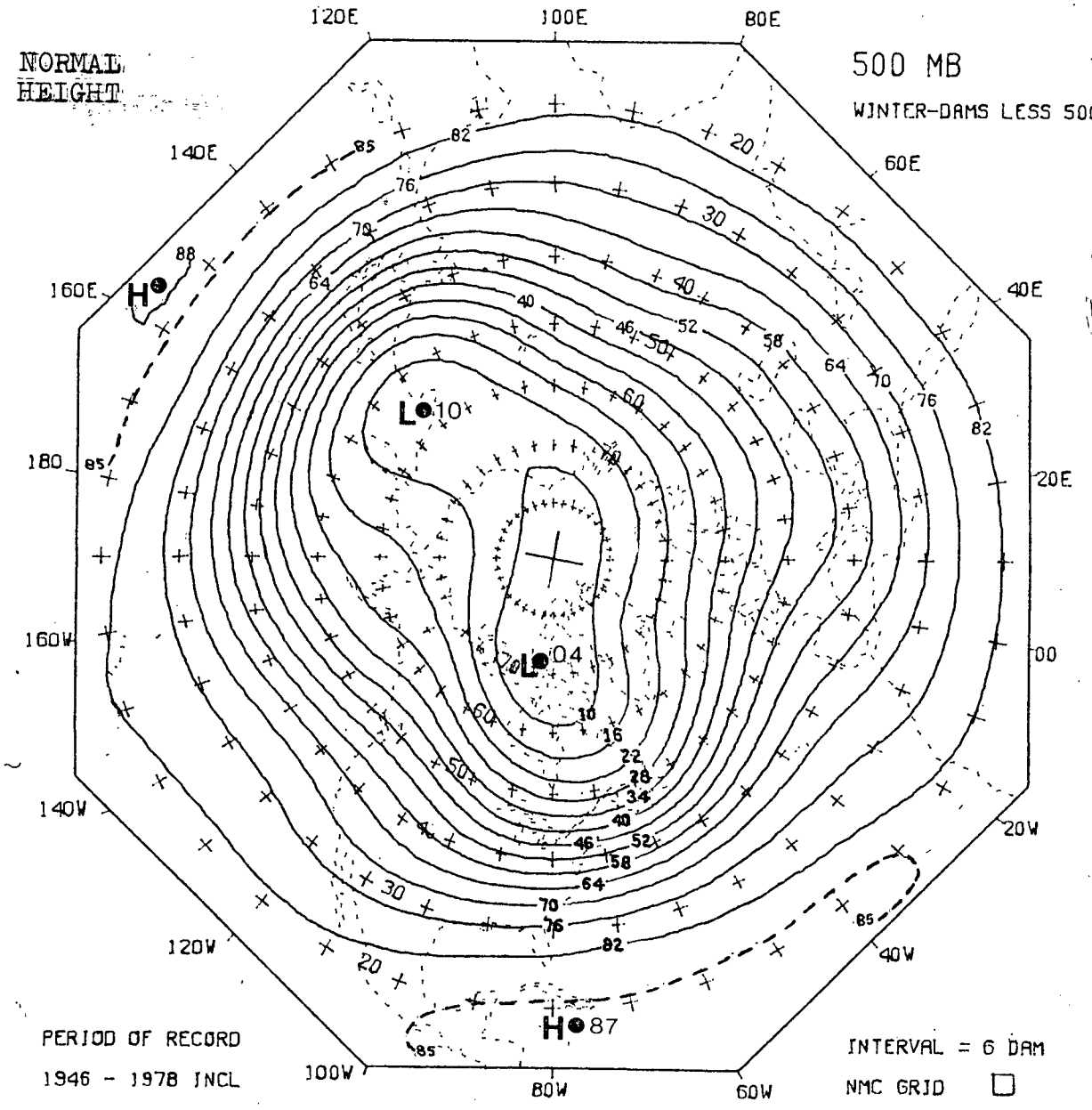

Fig. 6.2 Normal height of the 500MB surface for WINTER (December 1 to February 28). Contours labelled in decametres less 500. Interval = 6 dams.

---------- 585 dams contour

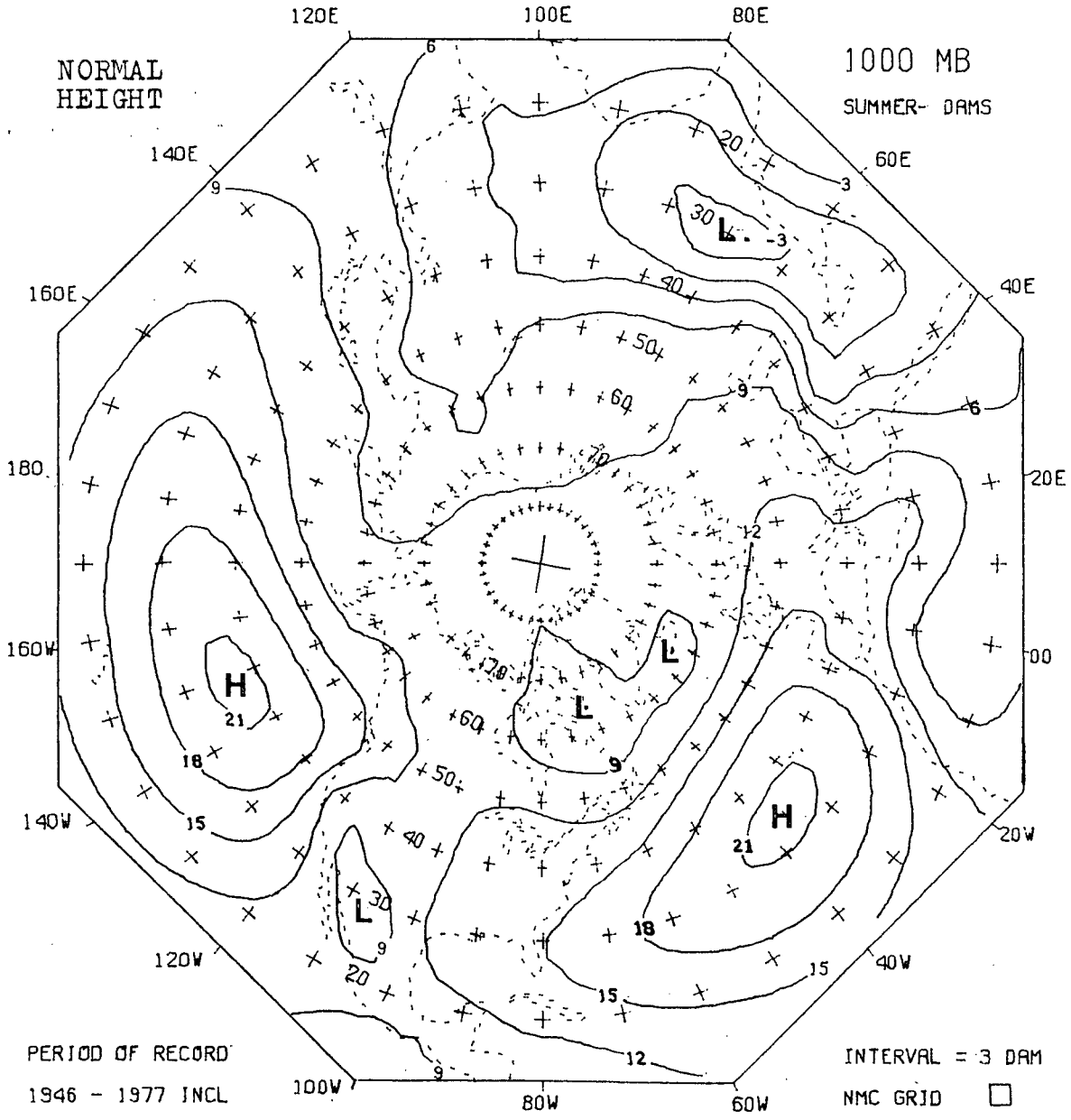

Fig. 6.3 As in Fig. 6.1 except for SUMMER

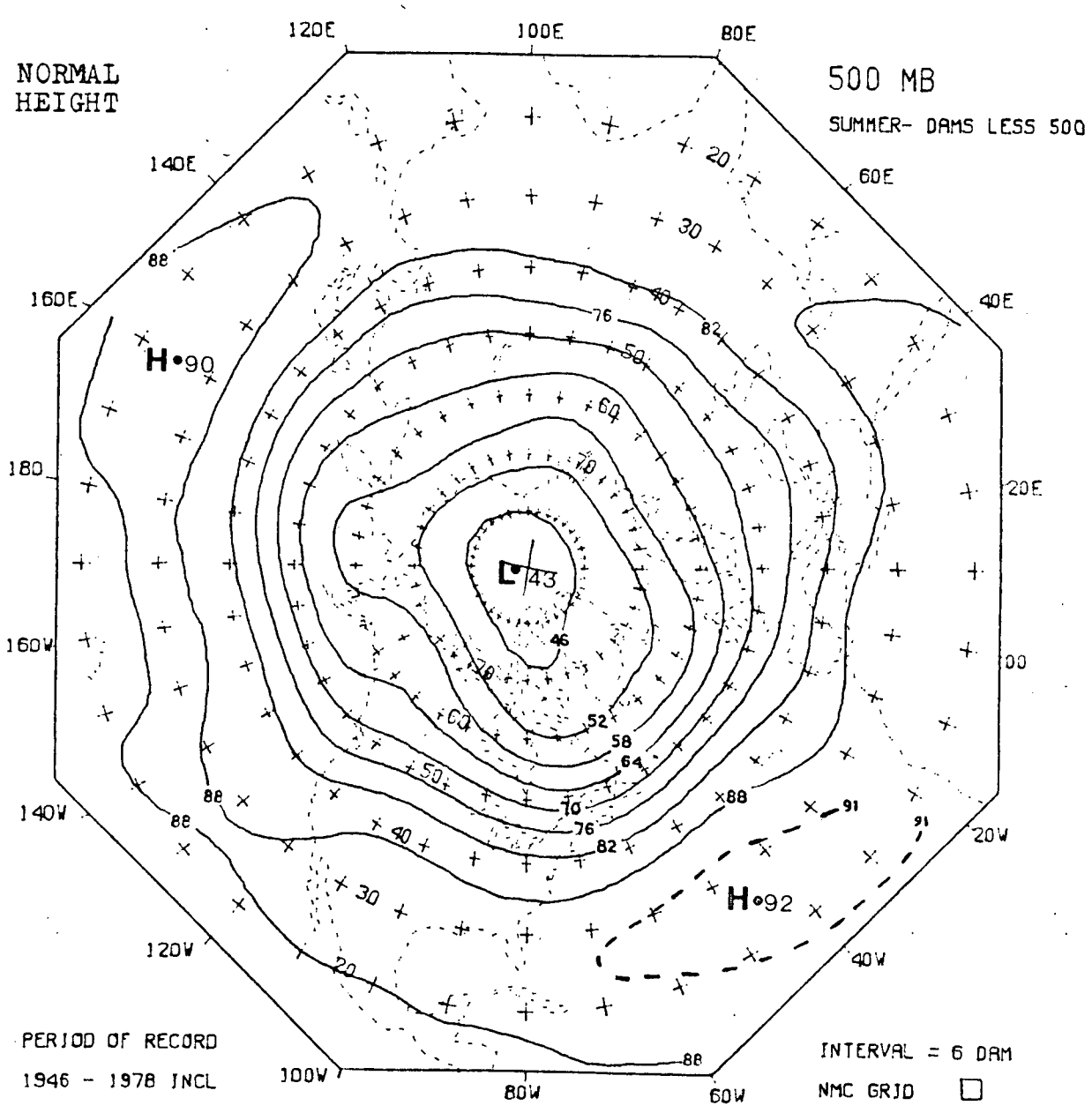

Fig. 6.4 As in Fig. 6.2 except for SUMMER

Ratcliffe (1972) for the mid-season months of April and October, respectively. Similar checks with other atlases, e.g., Lahey et al. (1958) and Crutcher et al. (1970) reinforce confidence in our baseline Normal fields.

In the case of Standard Deviation, we are not aware of any other source where such fields have been computed for 5-day average gph. We note that our 500MB Standard Deviation field for Winter (Fig. 6.5) corresponds closely with the low pass field of Blackmon (1976). It was also encouraging to note that our 1000MB Standard Deviation field for Winter (Fig. 6.6) was in good agreement with the low pass filtered Standard Deviation field of sea level pressure in Fig. 2(a) of the paper by Blackmon et al. (1977). Finally, our results appeared to be consistent with Standard Deviation fields computed by Moffitt and Ratcliffe (1972) after making allowance for the data base difference.

6.4.3 Interpretation of Standard Deviation Fields

In Chapter 5 (Fig. 5.7 WINTER), we noted preferred longitudes for blocking signatures centred, in the mean, over the E Pacific (160°W), E Atlantic (30°W), Ural Mountains (60°E) and Baffin Island (70°W). These four locations correspond closely to the four Winter centres of maximum Standard Deviation at 500MB (Fig. 6.5) suggesting that large positive anomalies associated with blocking highs or ridges provide a significant contribution to the variation of gph North of latitude 50°.

For all seasons there is a close correspondence between the geographic variability of the 1000MB and 500MB gph fields over the oceans, but they differ significantly over the continents, particularly in WINTER (Figs. 6.5 and 6.6). Consider, for example, North America and

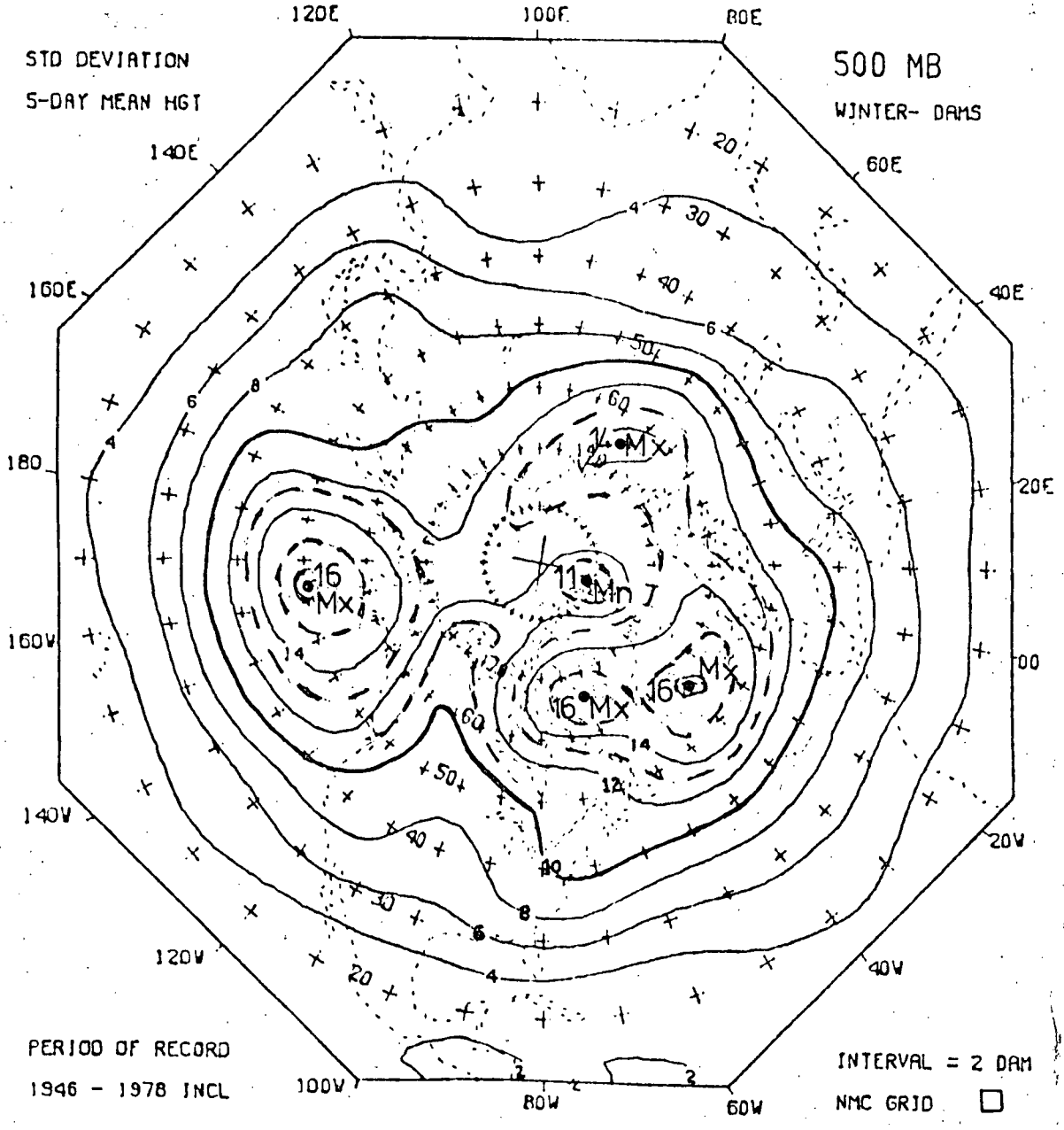

Fig. 6.5 Standard deviation of 5-day average 500MB height for WINTER (December 1 to February 28).

——— Contours (Interval = 2 dams)
- - - - - Intermediate (1 dam interval) contours
▬▬▬ 10 dam contour

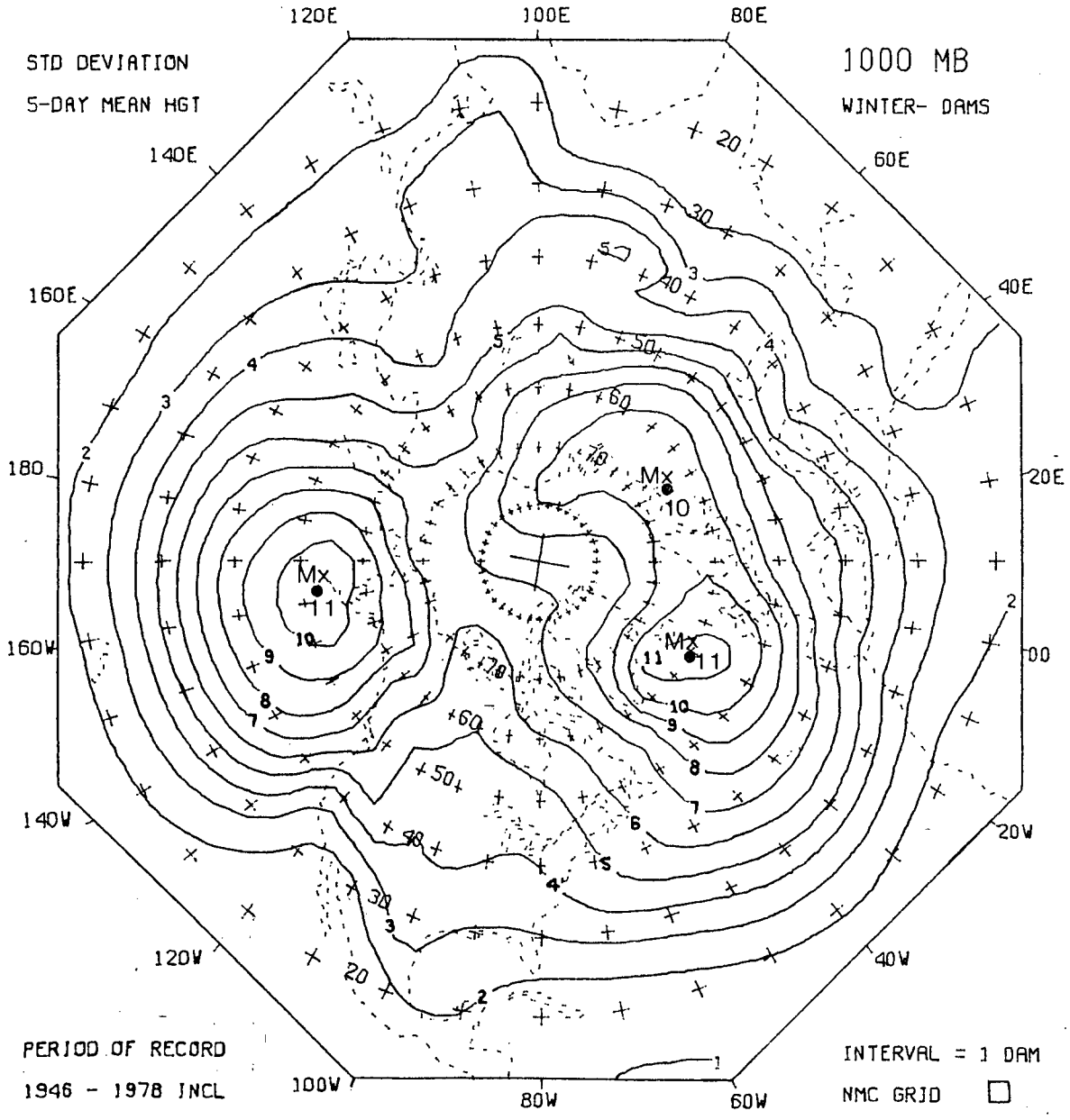

Fig. 6.6 Standard deviation of 5-day average 1000MB height for WINTER (December 1 to February 28). Contour interval = 1 dam.

the North Atlantic. At 1000MB an axis of minimum variance extends from the Canadian prairies to the Northwest Territories and there is a well defined maximum centre over the North Atlantic (60°N 20°W). These features are found in approximately the same locations at 500MB but, at that level, there is a second area of maximum variance over Northeastern Canada centred on Baffin Island with an intensity almost equal to the Atlantic centre (16 dams). This relative difference in the variance pattern between the 1000MB and 500MB levels is related to the thickness field (Fig. 6.7) which also shows a maximum of variability over Northeastern Canada. Sawyer (1970) showed that there is a very high correlation between 500MB gph and 1000MB - 500MB thickness for fluctuations north of 50°N and with a period of ≥ 15 days. In Northeastern Canada the correlation exceeds 0.90. What this implies is that not only is there a frequent occurrence of large fluctuations of 500MB gph and thickness in Northeastern Canada (because of the high Standard Deviations for both) but that they occur in tandem. Large amplitude fluctuations are caused by warm ridges (including blocking highs) and cold troughs (including cold lows). This area, centred on Baffin Island, must therefore not only be the seat of frequent large positive anomalies as we have already shown, but also of large negative anomalies. Now, as stated in Chapter 1, Section 1.2, the areal frequency distributions of negative anomalies (though not the subject of this thesis) were prepared and, indeed, the WINTER distribution of anomalies ≤ -20 dams shows a strong concentration over Baffin Island and Northern Hudson Bay. This sheds more light on the Baffin Island Paradox (Section 5.3.6). That area, in spite of being located precisely under the Normal 500MB trough, is the seat of numerous fluctuations with periods ≥ 10 days. When the 'in situ' anomaly is moderately to strongly positive the pre-existing trough is usually split by a

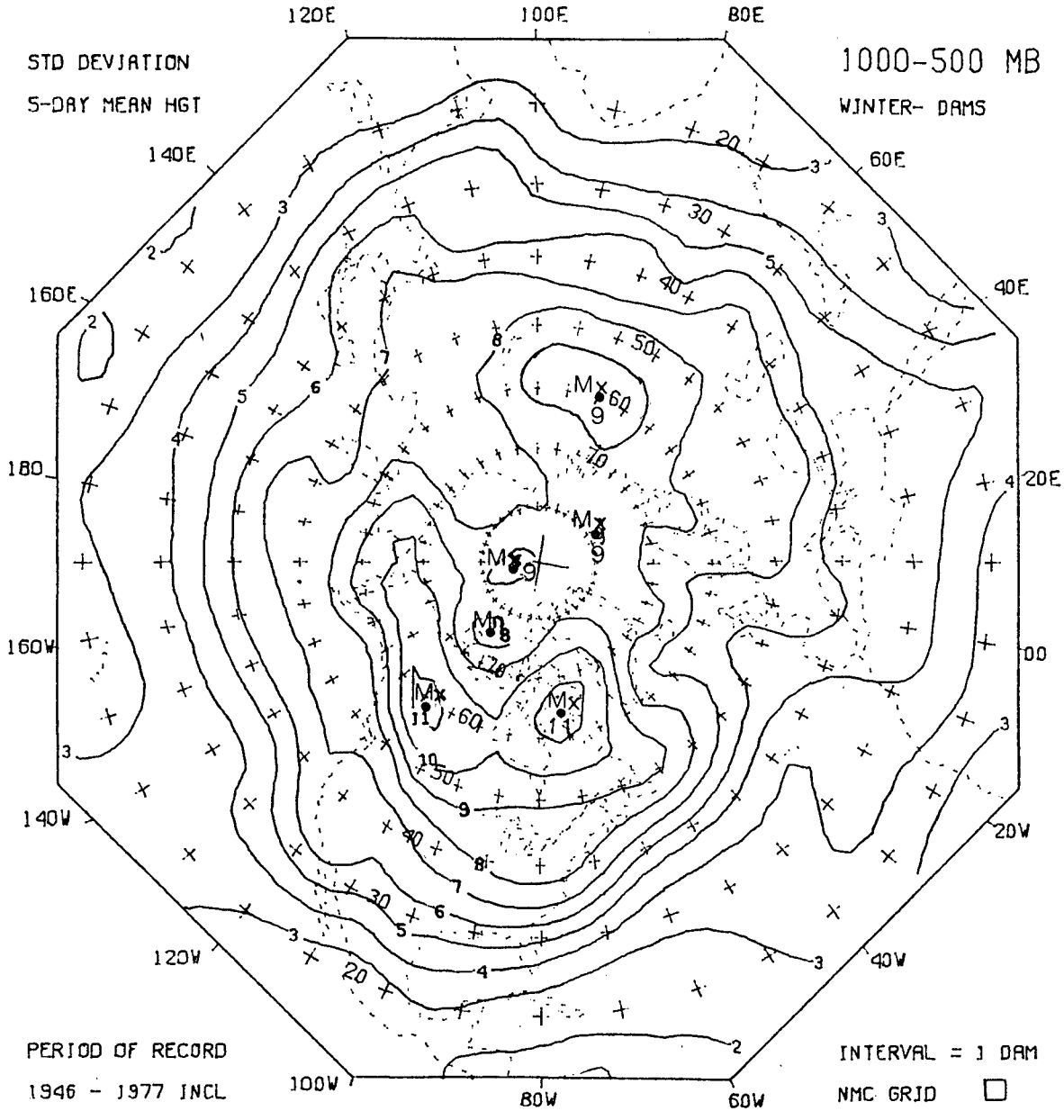

Fig. 6.7 Standard deviation of 5-day average 1000MB - 500MB thickness for WINTER. Contour interval = 1 dam.

blocking ridge (or high) as described in Section 5.3.6. On the other hand, when the 'in situ' anomaly is large negative, there is, usually near the normal location, an intense expanded cyclonic vortex dominating a vast area from Hudson Bay to Greenland. These large positive and negative fluctuations in Northeastern Canada were also found to occur in the other three seasons. (In the case of blocking signatures see the striking annual pattern depicted in Fig. 5.1.)

We could not find a counterpart to the behaviour of the Northeastern Canadian trough in other parts of the hemisphere. The East Asian trough does show the 500MB and thickness fields fluctuating in tandem in WINTER, but the respective patterns of maximum variance reside at a lower latitude (30°N to 50°N) and are less intense. By SUMMER the reversal of the continent-ocean temperature regime is complete and the East Asian baroclinic trough has essentially disappeared.

Over the Oceans, well-defined areas of maximum Standard Deviation at 1000MB and 500MB are in near coincidence for all seasons, but it is interesting to note that these areas are not the residence of corresponding relative maxima of <u>thickness</u> variance. The correlation between 500MB gph and 1000MB - 500MB thickness is still high (greater than 0.8 according to Sawyer) but in WINTER, for example (Figs. 6.5 and 6.7), the 500MB Standard Deviation of 16 dams at the maximum (centred at 57°N 28°W) is greater than the thickness Standard Deviation by a factor of two. An examination of the distribution of the 3rd and 4th moments of these respective variates may throw additional light on the difference in behaviour of the longer period fluctuations over continent and ocean.

6.5 Statistical Moments Part II

For reasons already given we decided to examine the extent to which the temporal distribution of the 5-day average gph and thickness over the 33 years of record, and at each of the 1977 grid points, departed from Gaussian. We followed the methodology of White (1980) and calculated fields of the 3rd and 4th moments about the mean or, more specifically, the non-dimensional coefficients of skewness and kurtosis, respectively.

6.5.1 Skewness

Skewness is the measure of the departure of a frequency distribution from symmetry. It is zero for a Gaussian distribution, usually "positive" if the mode lies to the left of the mean so that the frequencies fall off sharply to the left and usually "negative" if the mode lies to the right of the mean (Fig. 6.8). Skewed distributions of atmospheric variables are not uncommon particularly in the case of discrete events such as amount of rainfall.

Skewness is measured in an absolute sense by the third moment about the mean

$$\mu_3 = \sum_{i=1}^{N} \frac{(z_i - \bar{z})^3}{N}$$

and the relative asymmetry, which takes account of the size of the Standard Deviation (= σ), is given by the non-dimensional coefficient

$$CS = \frac{\mu_3}{\sigma^3}$$

There are other measures of skewness but this has general acceptance in the meteorological literature.

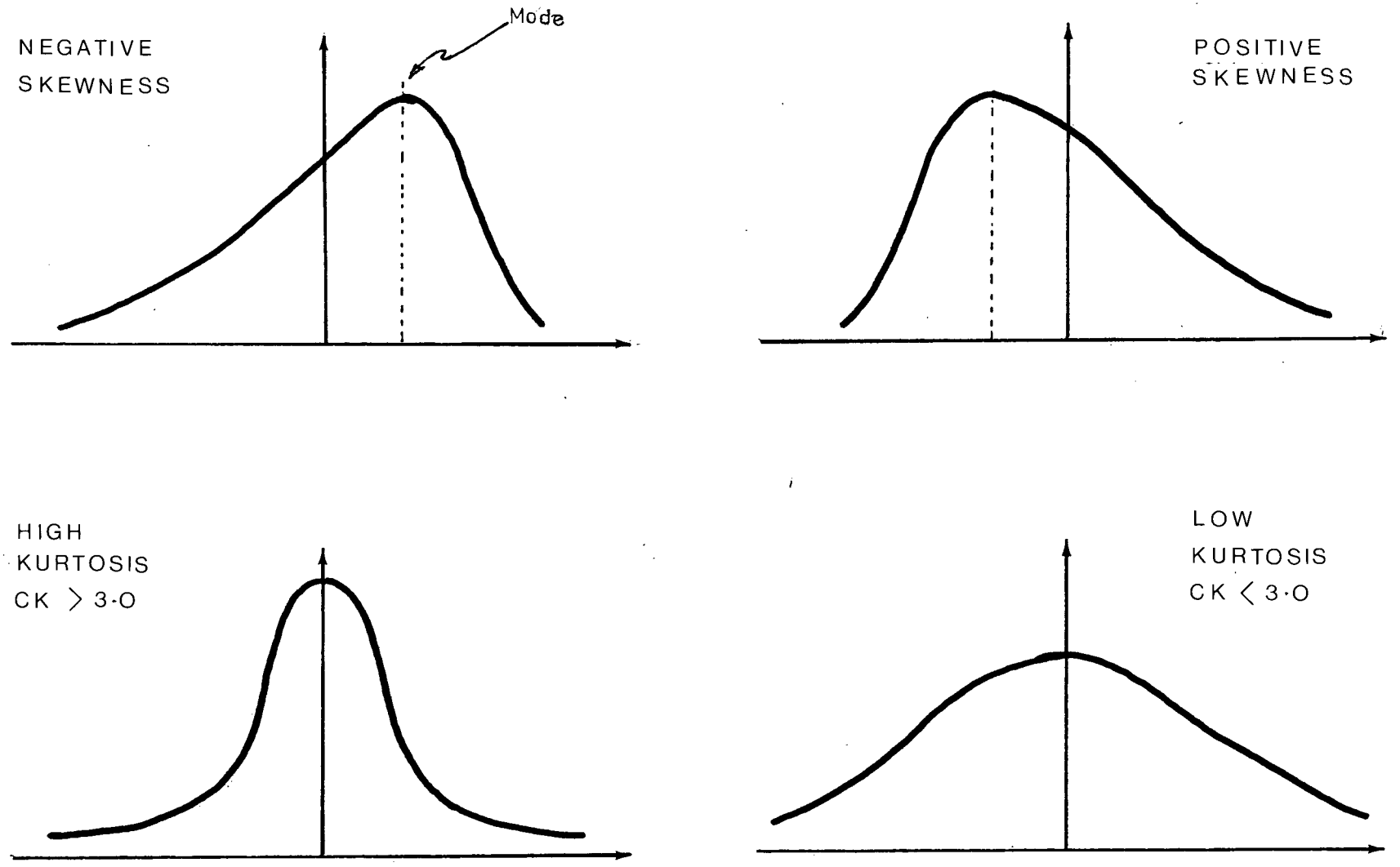

Fig. 6.8 Schematics: Skewness and Kurtosis

The standard error of skewness is given by

$$S.E. \simeq (6/n)^{\frac{1}{2}}$$

Where n = number of statistically independent observations (Brooks and Carruthers, 1953).

One of the problems in the statistical treatment of parameters of the atmospheric continuum is that consecutive observations at conventional time intervals (hourly, daily, etc.) are not independent. However, the longer the time interval the less the dependence. To explore the relationship, Madden (1976) estimated characteristic intervals for effectively independent sample values for Northern Hemisphere sea level pressure. He found that for January the intervals ranged from two days over the Southern U.S.A. to eight days over the Eastern North Atlantic. For July they ranged from less than two days west of the Great Lakes to greater than five days in the mid-oceans. These results would apply to our 1000MB data and in agreement with White (1980) there is no apparent reason why they would differ significantly at 500MB.

By season, for a given grid-point we had 18 x 33 ≃ 600 observations averaged over contiguous 5-day intervals. As an ensemble they are probably considerably less interdependent than daily values. In view of Madden's results it is reasonable to infer that our sample contained the equivalent of about 500 independent observations per season, so that the standard error of skewness was

$$S.E. = \left(\frac{6}{500}\right)^{\frac{1}{2}} = \pm 0.11$$

Turning now to Table 6.1, we concluded that if the calculated Skewness Coefficient (CS) was outside the range ±0.22, it would be significantly different from Gaussian at the 95% level of confidence.

The CS computation is outlined in Appendix VI - 4. Values of the skewness coefficients were computed by season for the 500MB and 1000MB levels and 1000MB - 500MB thickness. These charts are available from the author. We shall discuss the interpretation of those of immediate interest in section 6.6.

6.5.2 Kurtosis

A distribution may be symmetrical and at the same time significantly non-Gaussian. On the one hand it might be sharply peaked at the centre because of an excess frequency of small deviations, and on the other it might be blunted because of a preponderance of large positive and negative deviations. The fourth moment is an absolute measure of this feature

$$\mu_4 = \sum_{i=1}^{N} \frac{(z_i - \bar{z})^4}{N}$$

and kurtosis is the term given to the relative measure, the non-dimensional coefficient

$$CK = \frac{\mu_4}{\sigma^4}$$

For a Gaussian distribution	CK = 3
For a Peaked (Leptokurtic) distribution	CK > 3
For a Blunted (Platykurtic) distribution	CK < 3

These are shown schematically in Fig. 6.8.

TABLE 6.1

Range of coefficients of skewness and kurtosis outside of which the distribution is significantly different (at the 95% confidence level) from a Gaussian distribution, as a function of N, the number of independent events (adapted from Brooks and Carruthers, 1953 and White, 1980)

N	Skewness	Kurtosis
100	±.49	2.27 to 4.06
150	±.40	2.38 to 3.88
200	±.35	2.45 to 3.76
500	±.22	2.62 to 3.48
1000	±.16	2.72 to 3.33
2500	±.10	2.82 to 3.20

A possible cause of platykurtosis could be that the population contains (perhaps as sub-sets) two atmospheric distributions with different means. Brooks and Carruthers (1953) give a number of examples. In extreme cases the distribution may become bimodal with two maxima, one on either side of the mean.

From Table 6.1 we concluded that if the Coefficient of Kurtosis was outside the range 2.6 to 3.5 it would be significantly different from Gaussian at the 95% level.

Calculation of the CK fields is detailed in Appendix VI - 5. Charts showing the spatial distribution of significant kurtosis for 1000MB and 500MB, by season, are available from the author. Interpretation will follow in Section 6.6.

6.5.3 Comparison of CS and CK Fields with Other Results

The Skewness and Kurtosis fields were consistent with those published by Moffitt and Ratcliffe (1972) and White (1980). These authors used daily data rather than 5-day averages, and Moffitt and Ratcliffe calculated monthly instead of seasonal statistics. However, as was the case with Standard Deviation, the lower frequency fluctuations appear to dominate the third and fourth moments. Thus patterns of isopleths were similar with regard to gradient as well as shape.

6.5.4 Site-specific Frequency Distributions

To assist with the interpretation of the Skewness and Kurtosis fields we shall present frequency distributions for sites representative of regions of interest. These distributions will be prepared in two different ways. One histogram will show frequency vs 500MB 5-day average height (the 'continuum'). The other will show frequency vs 500MB 5-day average height anomaly (the 'extremum').

The 'continuum' histograms were obtained from White (1980) and Moffitt and Ratcliffe (1972). They are for point locations chosen for their proximity to the centre of the area of interest.

The 'extremum' histograms were prepared from our Master Catalogue. For the grid-point centred upon the region of interest and the surrounding eight points, we manually recorded all anomaly centres

> +5, +10, +15, ... dams

and < -5, -10, -15, ... dams

This provided a sample of sufficient size to be statistically significant.

Both types of histogram will be used to illustrate the interpretation of CS and CK fields in the next Section.

6.6 Interpretation of Distribution of Skewness and Kurtosis in the Northern Hemisphere

6.6.1 Skewness

6.6.1.1 WINTER - POSITIVE

In WINTER (Fig. 6.9) positive skewness is characteristic of the high latitudes. There are three dominant areas centred respectively over the Bering Sea, the NE Canadian Archipelago and the NE Atlantic Ocean between Iceland and Scandinavia. We shall examine the two first-named areas in further detail.

(a) Bering Sea

The large positive skewness of the 'continuum' distribution at 55°N 175°E is clearly indicated by comparison of the histogram in Fig. 6.10(b) with the superimposed normal curve for the same mean and

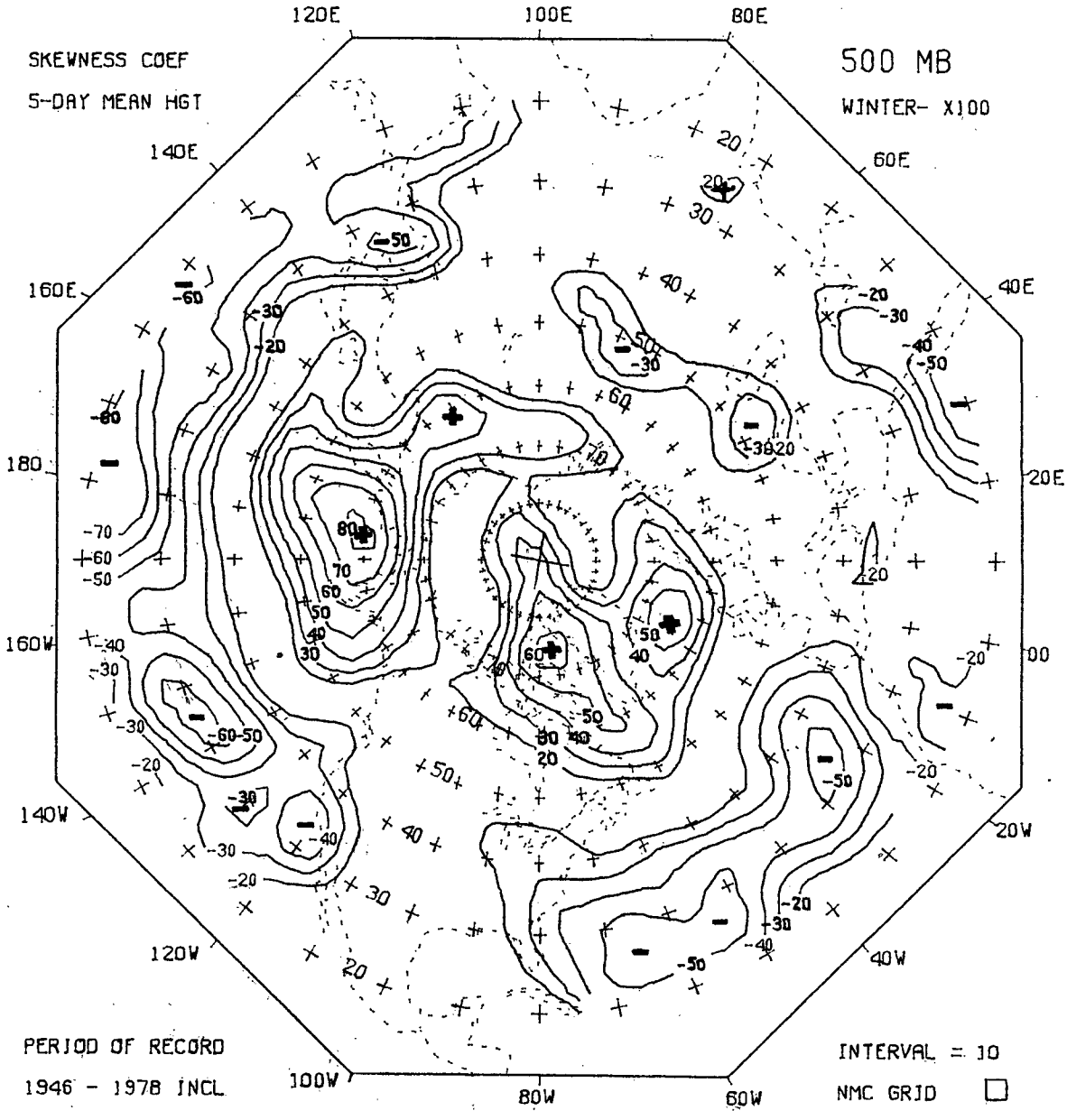

Fig. 6.9 Skewness of 5-day average 500MB height for WINTER (December 1 to February 28). Contours labelled CS x 100. Interval = 10. Areas below level of significance (Table 6.1) not contoured.

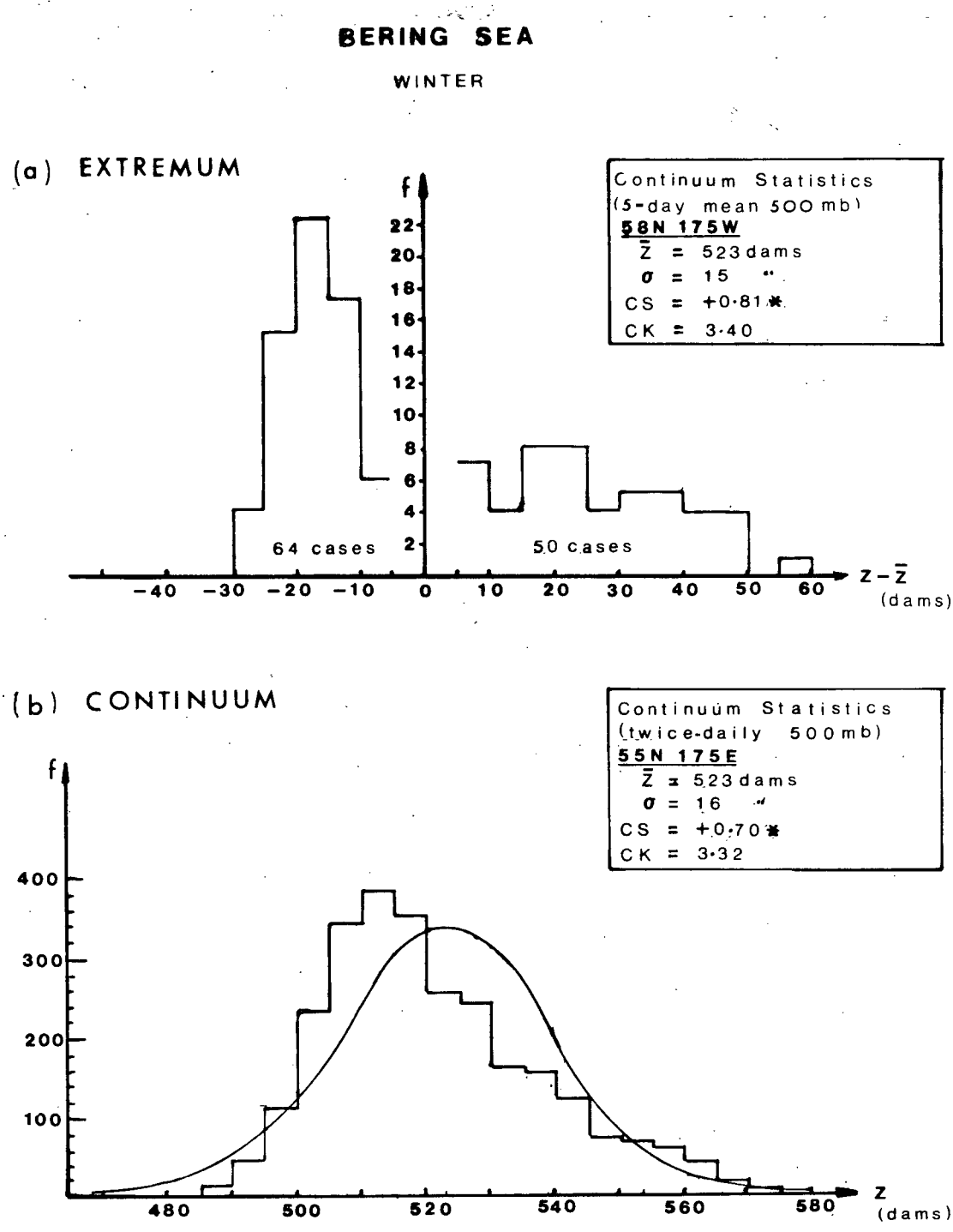

Fig. 6.10(a) Frequency of 500MB Extremum occurring within 9-point grid centred on 58N 175W (Knox).

(b) Frequency of 500MB height at 55N 175E for Winter. Curve shows Gaussian distribution with same mean and variance. (Adapted from White, 1980).

* indicates significant at 95% level.

variance. The upper panel, Fig. 6.10(a), shows the striking difference between the distribution of positive and negative anomalies in the region centred on 58°N 175°W. The two panels are consistent with what is observed from mid-tropospheric analyses for the Bering Sea in Winter (O'Connor, 1964). At the 500MB level the large number of fluctuations clustered about a mode of 510-515 dams result from deep cyclones that usually have their genesis in the normal East Asian Coastal trough. However, although a cyclonic regime predominates, the distribution on the right hand side of Fig. 6.10(a) tells us that the Bering Sea not infrequently becomes the site of large positive anomalies. The majority of these are blocking signatures (Fig. 5.2).

We may reasonably conclude that the positively skewed distribution is partly attributable to the frequency of blocking episodes.

(b) The Northeast Canadian Archipelago

To illustrate the continuum distribution for the Northeast Canadian Archipelago we used a histogram for 80°N 100°W (Fig. 6.11(b)). That location is about 750 km NW of the centre of maximum CS. Nevertheless, it is within the area of interest and does confirm the strong positive skewness characteristic of the region. The upper panel Fig. 6.11(a) for an area centred on 71°N 69°W shows an anomaly frequency distribution somewhat similar to that for the Bering Sea.

As previously noted, this area is the residence of the normal winter 500MB low. The gph fluctuates about the mean value of 506 dams as the Baffin Low gyrates about its normal position and increases or decreases in intensity. On occasion, however (as described in Section 5.3.6), the region is subject to a regime of a very different type. The

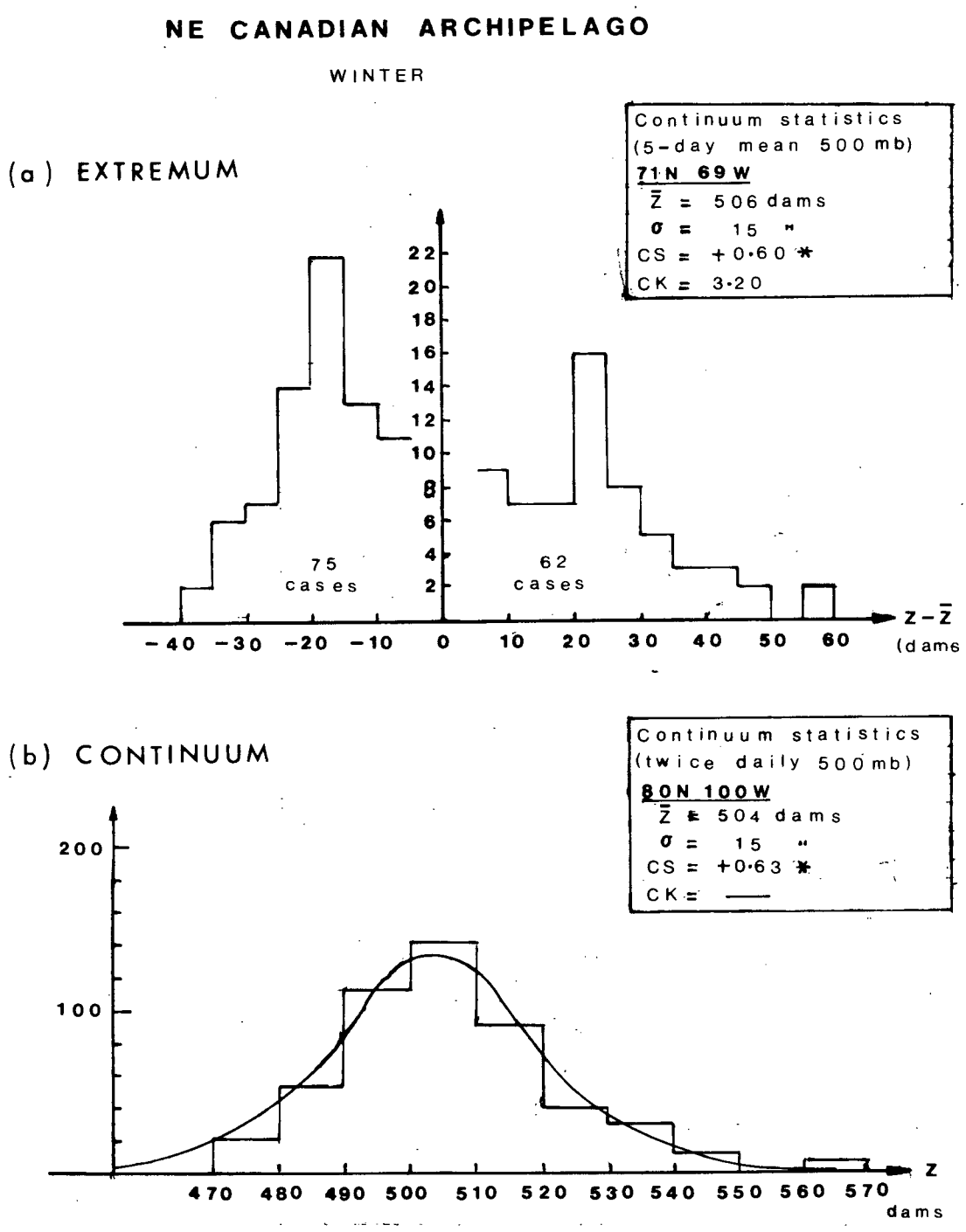

Fig. 6.11(a) As in Fig. 6.10(a) except for 71N 69W (Knox).

(b) Frequency of 500MB height at 80N 100W for January. (Adapted from Moffitt and Ratcliffe, 1972)

* = significant at 95% level.

associated positive anomaly is well above the winter blocking signature threshold (16 dams) as indicated by Fig. 6.11(a). Clearly, these are episodes which contribute to the striking blocking signature maximum of Fig. 5.2. Again we conclude, as in the case of the Bering Sea, that the positive skewness characteristic of the distribution of 500MB height over the Northeast Canadian Archipelago is attributable in part to the nature and frequency of blocking episodes.

6.6.1.2 WINTER - NEGATIVE

Returning to Fig. 6.9, we note vast regions of negative skewness over the oceans between 20°N and 40°N. In this latitude zone, the southern half of which is the normal residence of the sub-tropical anti-cyclone, the 500MB height fluctuates about a high mean value. However, slow-moving persistent cold troughs and lows do penetrate from time to time and the consequent large negative anomalies of 5-day average heights cause the distribution to tail to the left. These lower latitude cold lows often are generated by the blocking process itself, especially if it is initiated by an upstream split jet (Fig. 3.3(a)).

6.6.1.3 SPRING, SUMMER, FALL

In SPRING and FALL, not shown, the patterns of positive skewness are similar to WINTER, although there is noticeable weakening over the Northeast Atlantic. In SUMMER, however (Fig. 6.12), positive skewness has weakened everywhere except for the emergence of a maximum to the southeast of Greenland. Indeed, over the Northeast Canadian Archipelago the pattern characteristic of the other seasons has disappeared entirely. At first sight this is surprising because in SUMMER, Blocking Signature frequencies remain high (Fig. 5.4). Note, however, that the Signature

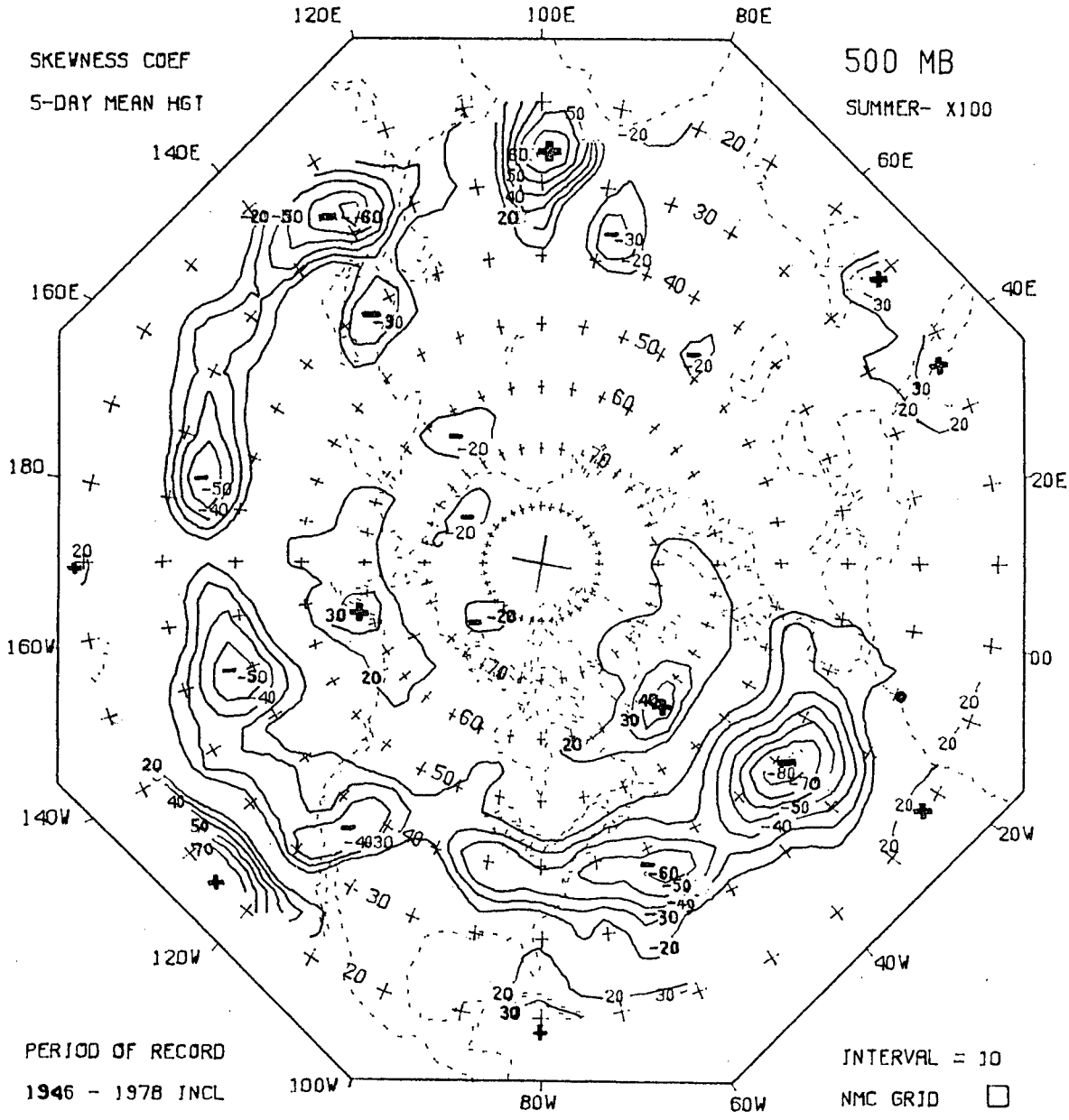

Fig. 6.12 As in Fig. 6.9 except for SUMMER

frequency centre is located about 10 degrees longitude west of its WINTER position. Meanwhile, by SUMMER, the Baffin trough has moved about 10 degrees east (Fig. 6.4). We infer that the reversal of the ocean-continent thermal regime has played a significant role in changing the character of regime alternation over the Canadian Archipelago and also over the Bering Sea. We suggest that dynamic processes which seem to result in a relationship between blocking in high latitudes and positively skewed distributions in Winter, Spring and Fall are strongly modified in Summer. Further investigation will be reserved for future research.

Negative skewness in SUMMER remains large in sub-tropical latitudes but there is a distinct northward shift in pattern. This is consistent with the seasonal northward migration of the sub-tropical anticyclone and the mid-latitude westerlies.

Around the 20°N parallel, regions of positive skewness become discernible. Moreover, there is a remarkably well defined area centred near 25°N 100°E, which is approximately the location of the normal upper troposphere anticylone centre associated with the Asiatic Summer monsoon. The positive skewness in all these regions is probably attributable to anomalous events in the Intertropical Convergence Zone. Though not directly connected with the subject of this thesis, it should warrant further investigation.

6.6.2 Kurtosis

In WINTER (Fig. 6.13) significantly high kurtosis (i.e., ≥ 3.5) occurs over the Arctic regions immediately to the north of Canada and also over wide swaths of the sub-tropical oceans. On the other hand, significantly low kurtosis (i.e., < 2.6) extends from the mid- to east

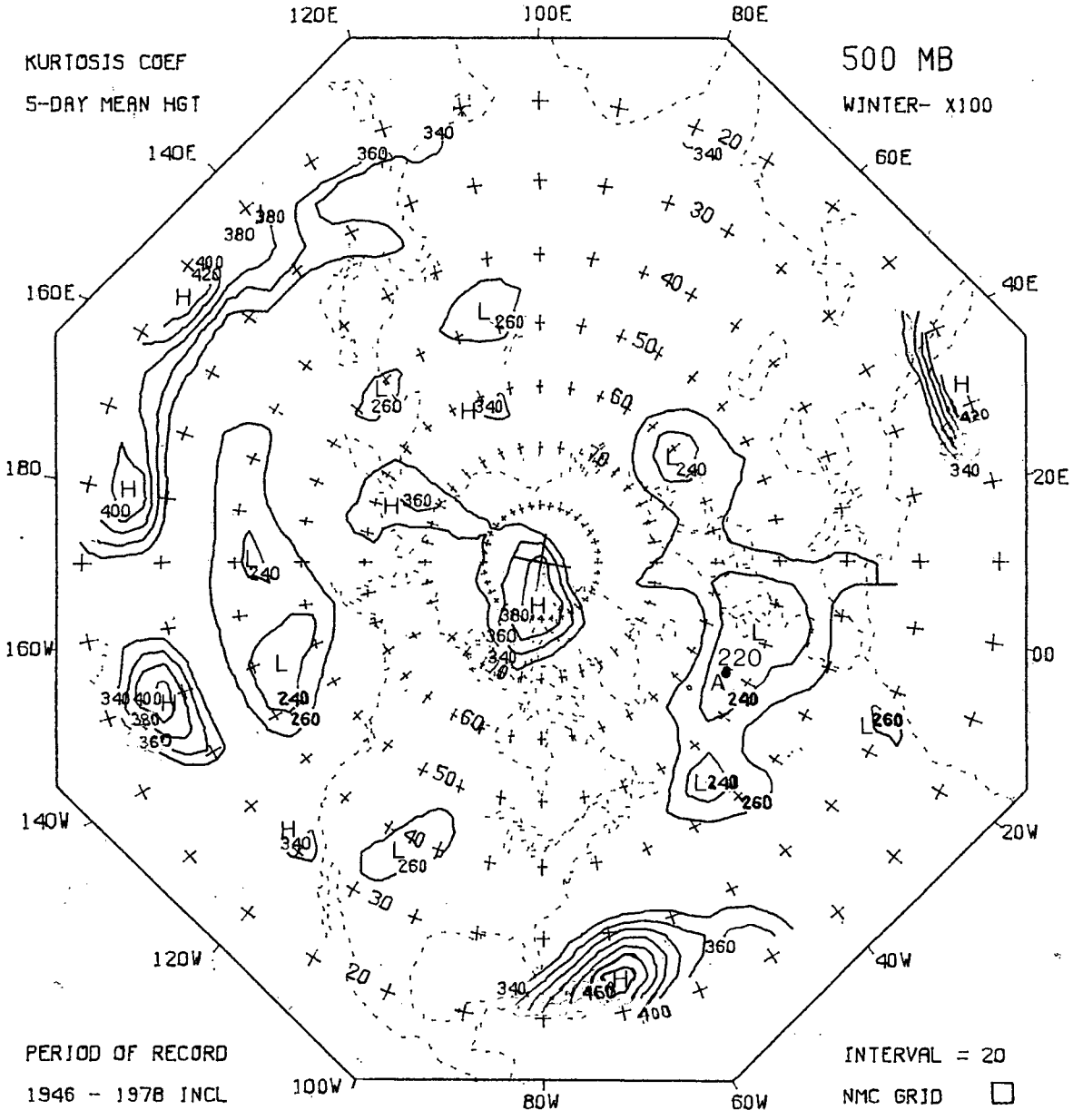

Fig 6.13 Kurtosis of 5-day average 500MB height for WINTER (December 1 to February 28). Contours labelled CK x 100. Interval = 20. Areas below level of significance (Table 6.1) not contoured.

Pacific Ocean along the 40°N to 50°N latitude zone, and also from the central Atlantic Ocean to Scandinavia and Northern Russia.

To further examine the nature of these low kurtosis distributions we present histograms for two locations near 'A' over the Eastern Atlantic. Fig. 6.14(b), for 52.5^{o}N 25°W, clearly shows a platykurtic distribution for continuum data. The distribution for frequency extrema (Fig. 6.14(a)) is for an area centred at 57°N 22°W. It reinforces the inference that over area 'A' the atmospheric regimes can be classified into two-sub-sets each with a different mean of 500MB gph. The interpretation in terms of blocking will be reserved for the next section. The Eastern Atlantic - Scandinavia low kurtosis persists throughout SPRING, SUMMER and FALL (not shown). Over the Pacific Ocean, however, each season shows a noticeable weakening from the winter pattern.

6.6.3 Further Discussion

We shall confine this discussion to the WINTER distributions of skewness and kurtosis to avoid complications introduced by the ocean-continent temperature reversal.

As indicated earlier the low kurtosis over the eastern halves of the mid-latitude oceans indicates that the 500MB height population consists of two sub-sets which have frequency distributions with different means. Is it possible that the distributions arise from two types of regime, one of which includes the ensemble of nascent or maturing blocking systems? We have noted from a large number of case studies that the birth and growth of the blocking wave appears to take place in regions of low kurtosis. The wave crest amplifies rapidly northward (often without appreciable change of phase) and culminates in a strong blocking anticyclone in the higher latitudes.

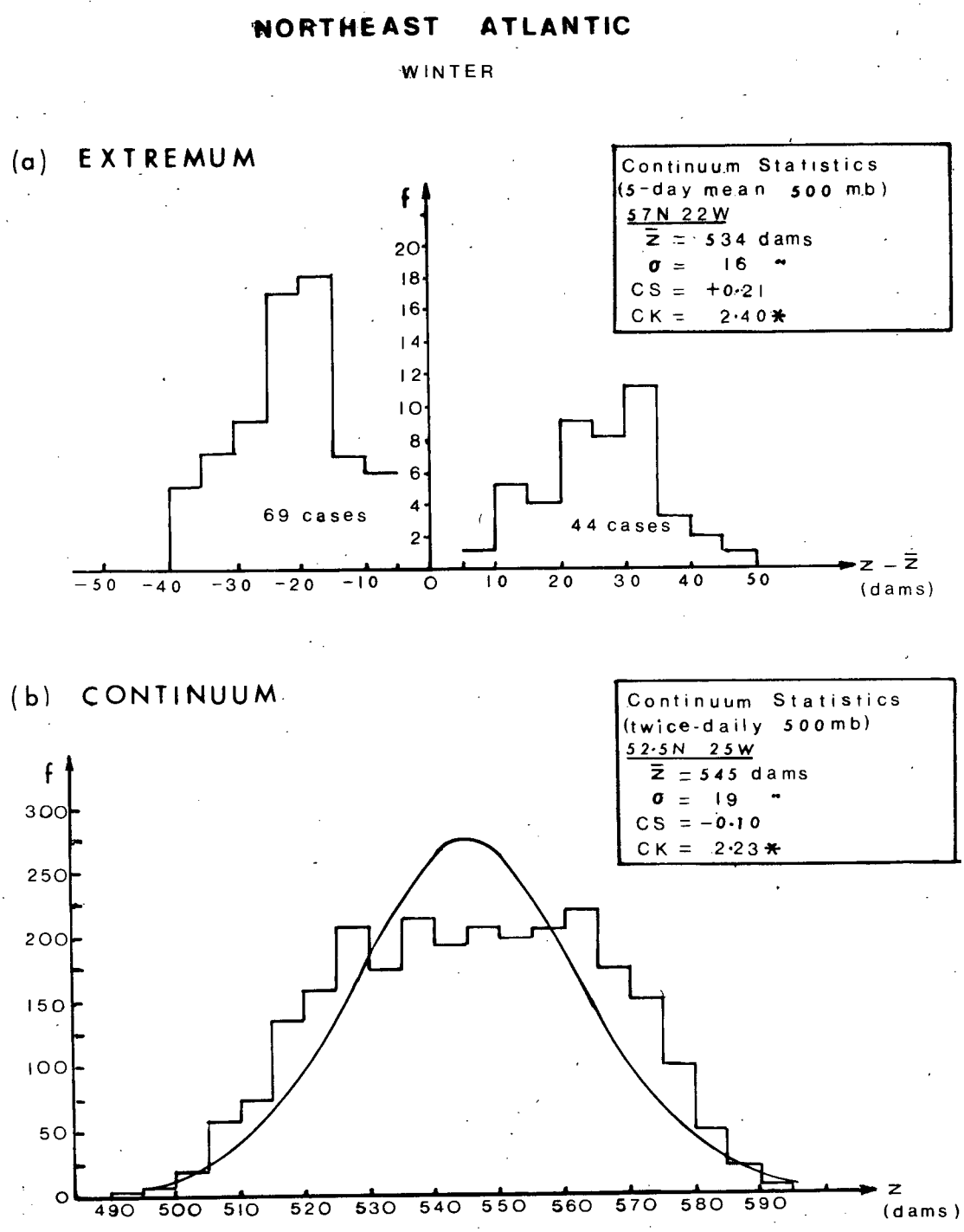

Fig. 6.14(a) As in Fig. 6.10(a) except for 57N 22W (Knox).

(b) As in Fig. 6.10(b) except for 52.5N 25W for Winter (adapted from White, 1980).

In the case of the Northeast Atlantic, if the blocking is retrograde, the blocking wave often moves into the Canadian Archipelago and the resulting positive anomaly of 500MB height is a factor in creating the large positive skewness observed in Winter distributions for that area. If it is quasi-stationary it will persist over the Iceland-Scandinavia region. The strong positively skewed distribution over this area (Fig. 6.9) may be attributed to the relative frequency of these events. If progressive, the blocking wave will proceed across the northern Eurasian continent. The distribution of positive Coefficient of Skewness between 60°N and 70°N extending into northeastern Siberia is suggestive of the influence of this category.

Turning now to the western hemisphere, the Bering Sea appears to be the graveyard, or the crossroads, for blocking anticyclones from three directions. We have already mentioned how northward amplification from the central and eastern Pacific Ocean brings warm blocking anticyclones into that region. From the discussion of Signature Sequences in Chapter 5, there is evidence that the Bering Sea also received blocks retrograding from Alaska, or less frequently, progressing from Siberia.

What seems to emerge from this analysis is the impression that blocking systems evolve in a manner somewhat analogous to unstable baroclinic cyclones. The initiation of both processes begins well south of the termination. The final stage of the typical baroclinic cycle is the cold cyclonic vortex in the high latitude with, of course, higher gph to the south. The final stage of the typical blocking cycle is the reverse, a warm high latitude anticyclone and, frequently, low gph to the south. Moreover, the dimensions of blocking waves in the mid-troposphere are larger than synoptic scale baroclinic waves. It would appear then that blocking may be initiated by the realization of baroclinic instability

in the long-wave part of the spectrum (Fig. 2.9). This view has already been given some theoretical justification by a number of authors quoted in Chapter 2. The subsequent response to the amplifying wave in terms of large scale vorticity redistribution results in the characteristic quasi-barotropic structure of the blocking system components.

It would appear, then, that the blocking phenomenon is really a manifestation of long-wave amplification, and that a climatological-diagnostic study would hardly be complete without a treatment in that context. This we propose to do in the next chapter.

CHAPTER 7

7. HARMONIC ANALYSIS OF THE 500MB HEIGHT DURING BLOCKING EPISODES IN WINTER

7.1 Rationale

So far in this dissertation we have perceived blocking configurations as spatially isolated anomalies of the large scale mass distribution in the troposphere. Their features were described in 'configuration space' (i.e., as they appear on conventional synoptic analyses) using for reference the NMC I,J grid. This afforded the most convenient method of identification for heuristic diagnostics and also for obtaining the statistical results presented in Chapters 5 and 6.

Sometimes, however, additional insights into attributes of physical systems (e.g., the 500MB height field) may be obtained by specification in terms of functions related to characteristic responses of the atmosphere (e.g., oscillations). Some aspects of the large scale responses of the atmosphere to thermal and mechanical forcing were reviewed in Chapter 2. These are customarily described as the planetary and synoptic scale waves, the resultant of which provides the main features of the tropospheric motion systems. Moreover, whatever the generic causes, blocking seems ultimately to be a manifestation of such large scale interaction. We therefore decided to investigate blocking in 'wave number space'. To do so it was necessary to specify the 500MB height field $Z(\lambda,\theta,t)$ in terms of sinusoidal functions.[1] The technique, harmonic

---

[1] In this Chapter θ designates latitude and ϕ is reserved for phase angle of the zonal harmonic.

analysis, is well-known and the application to our specific problem will be outlined in Section 7.3.3.

7.2 Objectives

7.2.1 Our first objective was to determine whether the spatial harmonics of blocking episodes were distinctive to the region in which they occurred. For example, were the spectral attributes of Northeast Pacific - Alaska blocks characteristically different, on average, from those which reside in the North Atlantic - Greenland area? If so, was there a connection between these attributes and those of the normal 500MB height distribution for the winter season? A similar investigation, which was conducted concurrently, has been reported by Austin (1980) and we shall compare results in Section 7.4.1.

7.2.2 The second objective was to pursue our investigations of the 'Baffin Island Paradox' by an interpretation of the spectral statistics arising out of the results of 7.2.1, above. We also applied harmonic analysis to typical cases of retrogressive and progressive blocking in the Baffin area. The extent to which blocking waves crossing this region originated upstream or downstream was also determined. A count was made of progressive vs retrogressive blocking signatures during the past 33 winters.

7.2.3 The third objective was to examine the spectral circumstances associated with interruptions to persistent regimes of large amplitude waves. These are regimes, sometimes of several weeks duration, during part of which one or more major blocking episodes will be in progress. The interruption is characterized by a sudden increase in the zonal

westerlies, a condition which, at any given latitude, is relatively transitory (∿ a few days).

7.2.4 Our fourth and final objective was to illustrate how zonal harmonics from 20°N to the Pole could be related to salient features of a complete major blocking system, including the frequently occurring cyclonic structure south of the blocking anticyclone.

7.3 Methodology and Techniques

7.3.1 Data Base

We confined our investigation primarily to the data of seven winters, namely:

December 1, 1946 - February 28, 1947	90 days
December 1, 1949 - February 28, 1950	90 days
December 1, 1955 - February 29, 1956	91 days
December 1, 1962 - February 28, 1963	90 days
December 1, 1968 - February 28, 1969	90 days
December 1, 1976 - February 28, 1977	90 days
December 1, 1978 - February 28, 1979	90 days

The occurrence of major blocking episodes during these winters and their profound impact on the short term climate has been well documented in the literature (for example, Namias (1975) and the Monthly Weather Review issues referenced in the bibliography).

Although our definition of the WINTER season is December, January and February, we added November and March to the data base of each winter except 1978-79 for which March was not available. Data for these flanking

months would be necessary to determine the complete life history of those blocks which happened to be already in progress on December 1st or those which had not terminated by the end of February.

For the purpose of frequency analyses documented in Chapters 4, 5 and 6, we found that the 5-day average of 500MB height was a practical temporal resolution. On the other hand, a pilot study of the harmonic analysis of 1977-78 daily data revealed that there were a significant number of occasions when the genesis and dissolution of long-wave components occurred quite rapidly (one to three days). We therefore chose to use daily data for the harmonic analyses of this chapter.

The 1200Z 500MB geopotential height for each day of the seven winters (and flanking months) at each point of the NMC grid was extracted from the 33-year record described in Section 4.3.1. These heights were then interpolated to each 5-degree intersection of Latitude and Longitude.

A typical major blocking system may extend from the sub-tropics to the Arctic. Therefore, it was decided to compute the above values of $Z(\lambda,\theta,t)$ for every 5° parallel of Latitude from 25°N to 85°N. These arrays constitute our working data. It is from them that subsequent derived data were computed, using techniques to be described in the following sections.

7.3.2 Selection of Representative Latitudes for Analyses and Display of Results

For the investigations into the change of $Z(\lambda,\theta,t)$ (and harmonics) with time, it was clearly necessary to select representative latitudes (or zones). The choice of the northern latitudes was based on Fig. 5.2 which shows the areal frequency distribution of blocking signatures during the WINTER. The preference for the 50°N to 70°N zone is unmistak-

able. Consequently, we decided that $Z(\lambda,t)$ at 60°N or, alternatively, averaged between 50°N and 70°N would be the data most likely to indicate the blocking anticyclone evolution and its zonal component of motion. Moreover, from examination of a large number of total blocking system episodes (e.g., Figs. 2.3 and 2.4) it appeared that the associated flanking cold lows are usually centred between 30°N and 50°N. Therefore, we selected $Z(\lambda,t)$ around 40°N, or mean values for 30°N to 50°N, to approximate salient features of the southern structure.

Since earlier pilot studies had shown that only the lower wave numbers (1 to 6) would be of consequence, we felt that the spatial smoothing of Z by latitude zone would be advantageous since it would suppress higher wave number 'noise'. As it turned out the difference for all practical purposes was not appreciable. Some results will be displayed based on data from cross-zonal averaging while others will use discrete latitudes, and the plots will be identified accordingly.

7.3.3 The Hovmöller Diagram

To obtain a visual perspective of the day-to-day evolution of hemispheric 500MB height, we used a simple but effective diagram named after the Swedish meteorologist Hovmöller (1949). It depicts the variation of $Z(\lambda,\theta_n,t)$ by longitude (abscissa) and time (ordinate) around a specified parallel of latitude θ_n (or latitude zone).

Figure 7.1 is an example, computed from data for the period December 1, 1962 to March 31, 1963. Note that in order to complete patterns which happened to be truncated by the Greenwich meridian ($\lambda = 0$), the right hand boundary was extended to $\lambda = 30^{o}$E. Isopleths of 500MB height $Z(\lambda,t)$ are drawn at an interval of 10 dams and, for brevity, labeled with values of $(Z - 500)$. Areas of high geopotential are shaded.

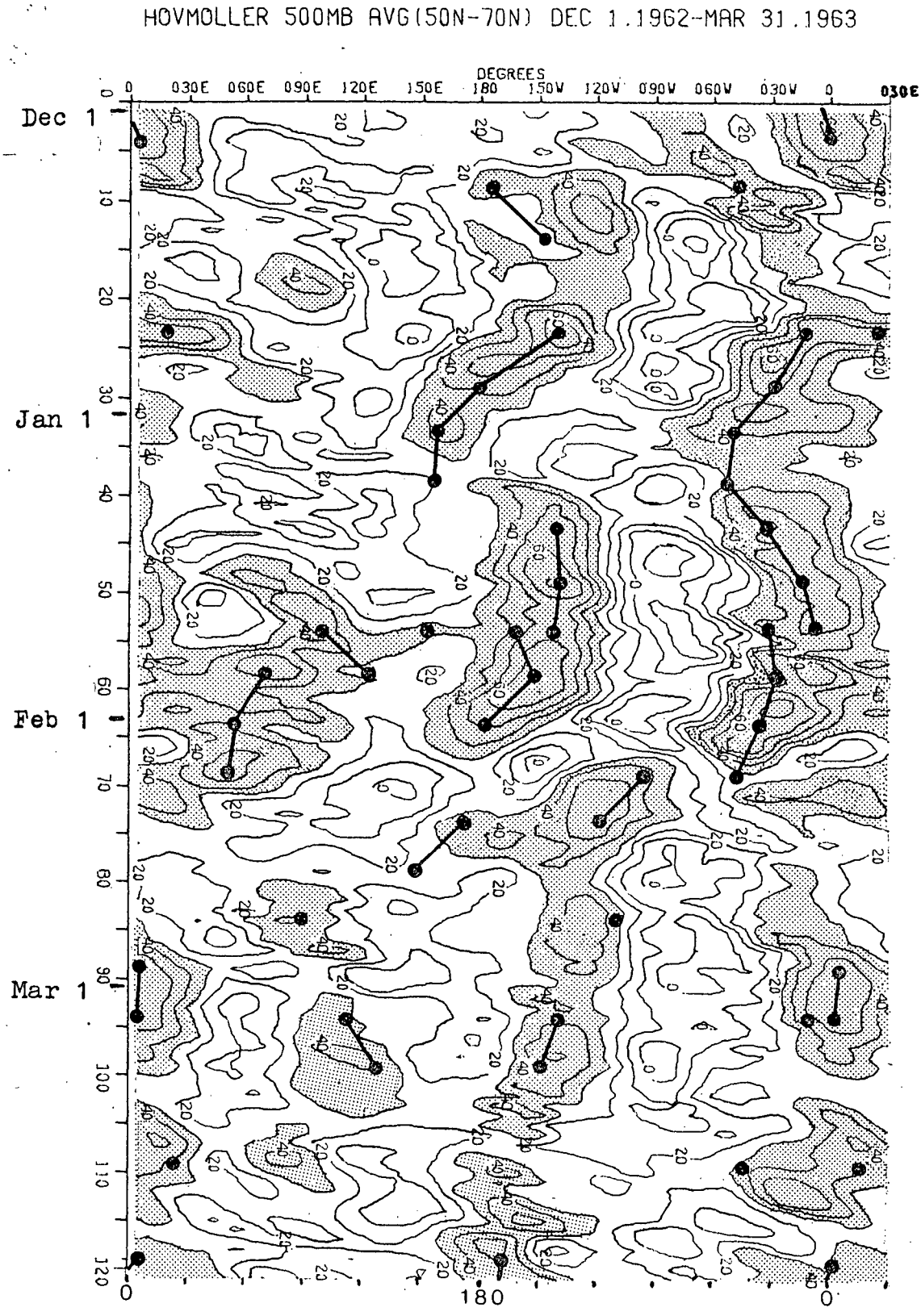

Fig. 7.1 Hovmöller Diagram of 500MB height profile averaged across the zone 50°N - 70°N. Ridges are shaded. Positions (λ,t) of Blocking Signatures marked • . Isopleths labelled Z - 500. Contour Interval = 10 dams.

The large amplitude long-wave patterns oscillating about their mean winter position are clearly evident. Westward (retrograde) motion, indicated by the downward tilt to the left of the isopleth axes, is not uncommon, particularly in the 50°N to 70°N zone where planetary vorticity advection may be the determining factor.

The smaller amplitude transient troughs and ridges, usually associated with synoptic scale waves, are particularly evident in the 30°N to 50°N zone (Fig. 7.2), a region of maximum baroclinic activity during the winter season. Their eastward progress, reflected by the downward tilt to the right of the axes, is also apparent.

Blocking signatures, marked ●, have been superimposed on Fig. 7.1. The close correspondence between their motion and the long wave 'ridge' axes would appear to confirm the choice of the 50°N to 70°N zone for harmonic analysis of blocking episodes.

Hovmöller diagrams of 500MB height have been prepared for each of the selected winters; those for 1978-79 will be found in Appendix VII, Fig.-1 and-2. For convenient calculation of speed (W to E) of troughs and ridges, Table VII-1 has been provided.

Notwithstanding the usefulness and convenience of the Hovmöller diagram as a compact source of information for diagnostic purposes, it should be used with some reservation. It is, after all, a one-dimensional profile of two-dimensional patterns and cannot therefore indicate the N-S components of structure or motion. For case study diagnostics it should if possible be complemented by sources of data which provide this information such as daily or 5-day mean 500MB Analyses.

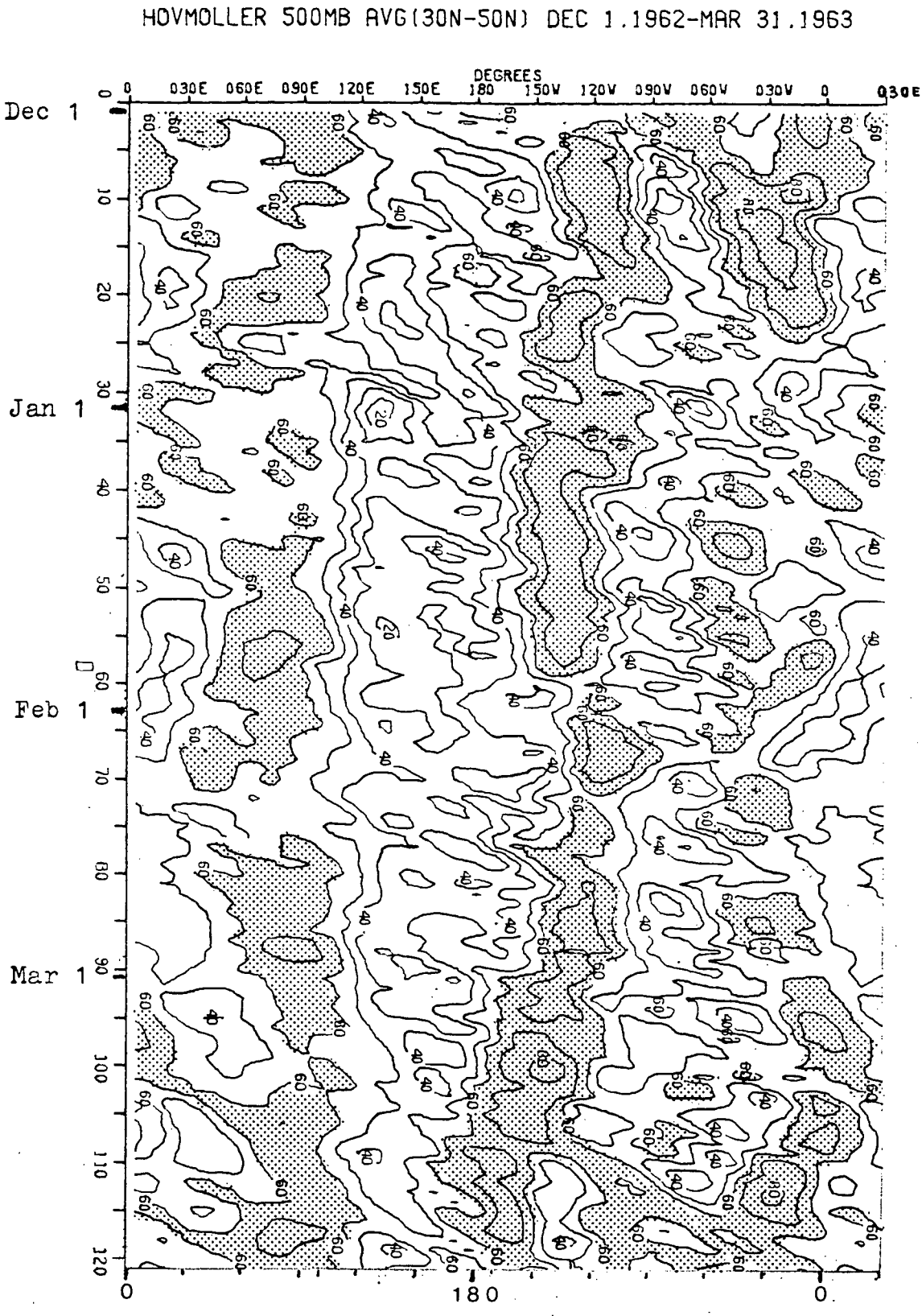

Fig. 7.2 Same as Fig. 7.1 except for 30°N - 50°N and without blocking signature locations.

7.3.4 Zonal Harmonic Analysis of the 500MB Height Field

(a) One-dimension

We shall summarize here, following Boville and Kwizak (1959) the discrete Fourier series method for calculating the first six harmonics of the instantaneous distribution of 500MB height around a specific latitude (or zone).

Let $Z(\lambda_i)$ = 500MB height at longitude λ_i and divide the latitude into 72 equal intervals so that $\lambda_i = 0, 5^o, 10^o$, etc.

$$\text{Then } Z(\lambda_i) = a_o + \sum_{n=1}^{6} (a_n \cos n\lambda_i + b_n \sin n\lambda_i) + R$$

$$\text{Where } a_o = \frac{1}{72} \sum_{i=1}^{72} Z(\lambda_i) = \text{mean of } Z(\lambda_i) = \overline{Z}$$

$$a_n = \frac{1}{36} \sum_{i=1}^{72} Z(\lambda_i) \cos n\lambda_i$$

$$b_n = \frac{1}{36} \sum_{i=1}^{72} Z(\lambda_i) \sin n\lambda_i$$

$$R = \text{Residual} = \sum_{n=7}^{35} (a_n \cos n\lambda_i + b_n \sin n\lambda_i)$$

We used the reformulation:

$$Z(\lambda_i) = A_o + \sum_{1}^{6} A_n \cos (n\lambda_i - \phi_n) + R$$

Where A_n = Amplitude = $\sqrt{a_n^2 + b_n^2}$

and ϕ_n = Phase angle = $\tan^{-1} b_n/a_n$

$$\text{The Variance} = \sigma^2 = \frac{\sum_{i=1}^{72} [Z(\lambda_i) - \bar{Z}]^2}{72}$$

For brevity, the harmonics (A_n, ϕ_n) will be designated as W_n.

Now σ^2 is proportional to the eddy (i.e., wave) kinetic energy of the circulation and it can be shown that

$$2\sigma^2 = \sum_{n=1}^{\infty} A_n^2 \qquad \text{(Godson, 1959)}$$

The percentage of the total variance contributed by W_n will be designated S_n and therefore

$$S_n = \frac{A_n^2}{2\sigma^2} (100)$$

Values of A_o, σ, A_n, ϕ_n and S_n were determined for each day at every five degree latitude and also for values of $Z(\lambda,t)$ averaged across the two zones (30^oN - 50^oN) and (50^oN - 70^oN), respectively.

The results for latitudes 60^oN and 40^oN for the period December 28, 1962 to February 17, 1963 show that the first six components contribute <u>on average</u> about 95% of the total variance for the zone 50^oN to 70^oN and about 85% for the zone 30^oN to 50^oN. These results are entirely consistent with Eliasen (1958) and Barrett (1958).

(b) Two dimensions

(i) Day-Specific Harmonics

Since values of A_n and ϕ_n were available for every 5 degrees of latitude from 25^oN to 85^oN it was a straightforward matter of interpolation to prepare, for a selected calendar day the two-dimensional representation of W_n. Analyses showing the spatial distribution of A_n were constructed for December 23, 1978 and January 4, 1979 and the results will be discussed in Section 7.4.

(ii) Normal Harmonics

One of our objectives was to compare the phase of harmonics during blocking episodes with those for the normal WINTER distribution of 500MB height. Therefore, analyses were completed for the first four normal harmonics. (Wave 2 is displayed in Fig. 7.3.) These normals will be used for baseline reference purposes during the presentation of results in Section 7.4. (Note that the contour interval for the Normal Charts is 1 dam, whereas for day-specific Charts, when amplitudes are much larger, the interval has been increased to 3 dams.) The complete set of Normal Charts W_1 to W_4 will be found in Appendix VII, Figs. VII - 3 to VII - 6, inclusive.

7.3.5 Temporal Variations of the Zonal Harmonics at Selected Latitudes

(a) Zonal Profile of $A_n(\lambda,t)$

Hovmöller diagrams of the first four harmonics for the two latitude zones were constructed for each of the seven winters. An example is provided by Fig. 7.4 showing the temporal variation of the profile of

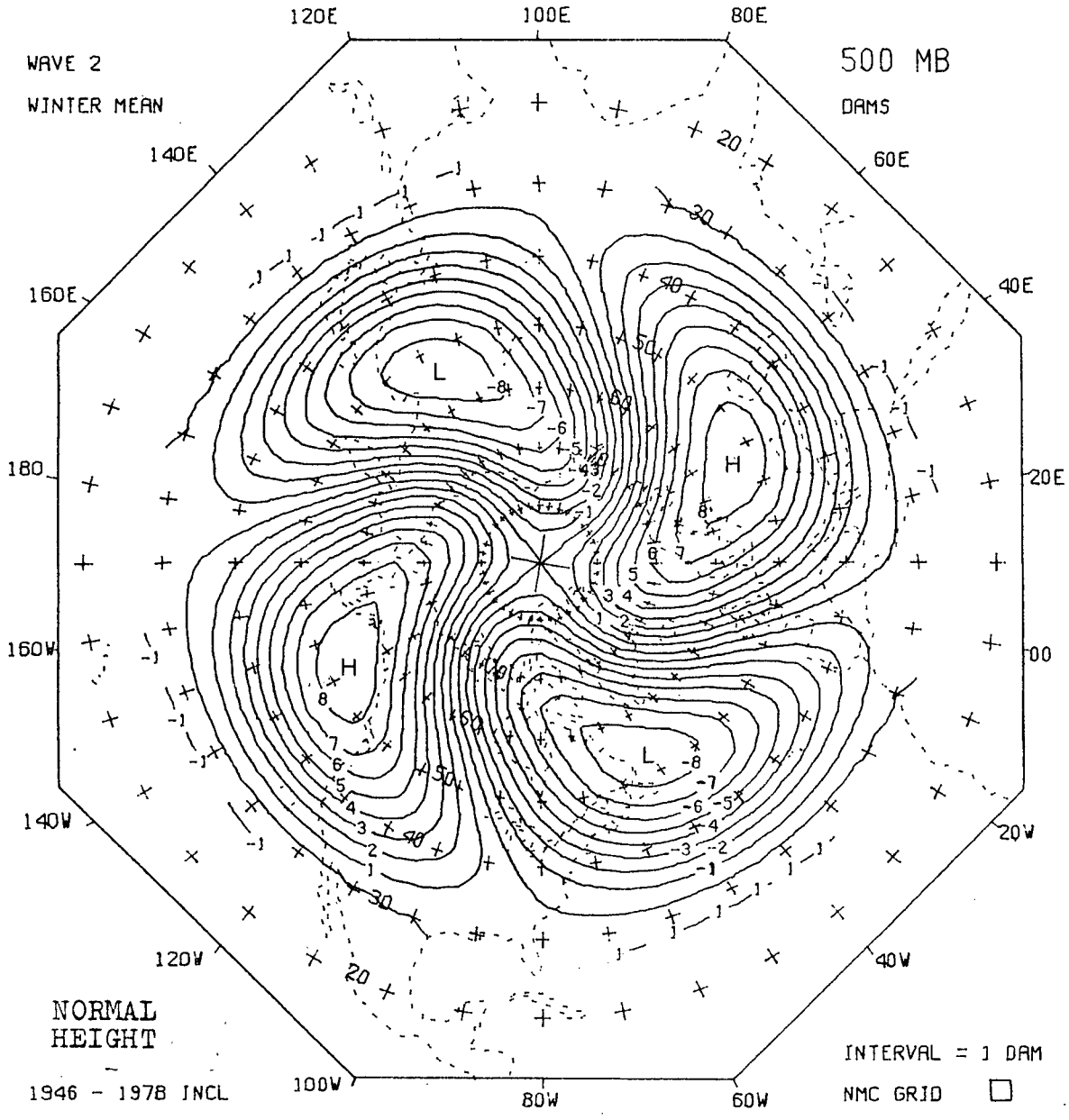

Fig. 7.3 Second harmonic (W2) of the normal 500MB height field for WINTER (December 1 to February 28). Contours labelled in decametres. Interval = 1 dam.

WAVE 2 500MB AVG(50N-70N) DEC 1.1962-MAR 31.1963

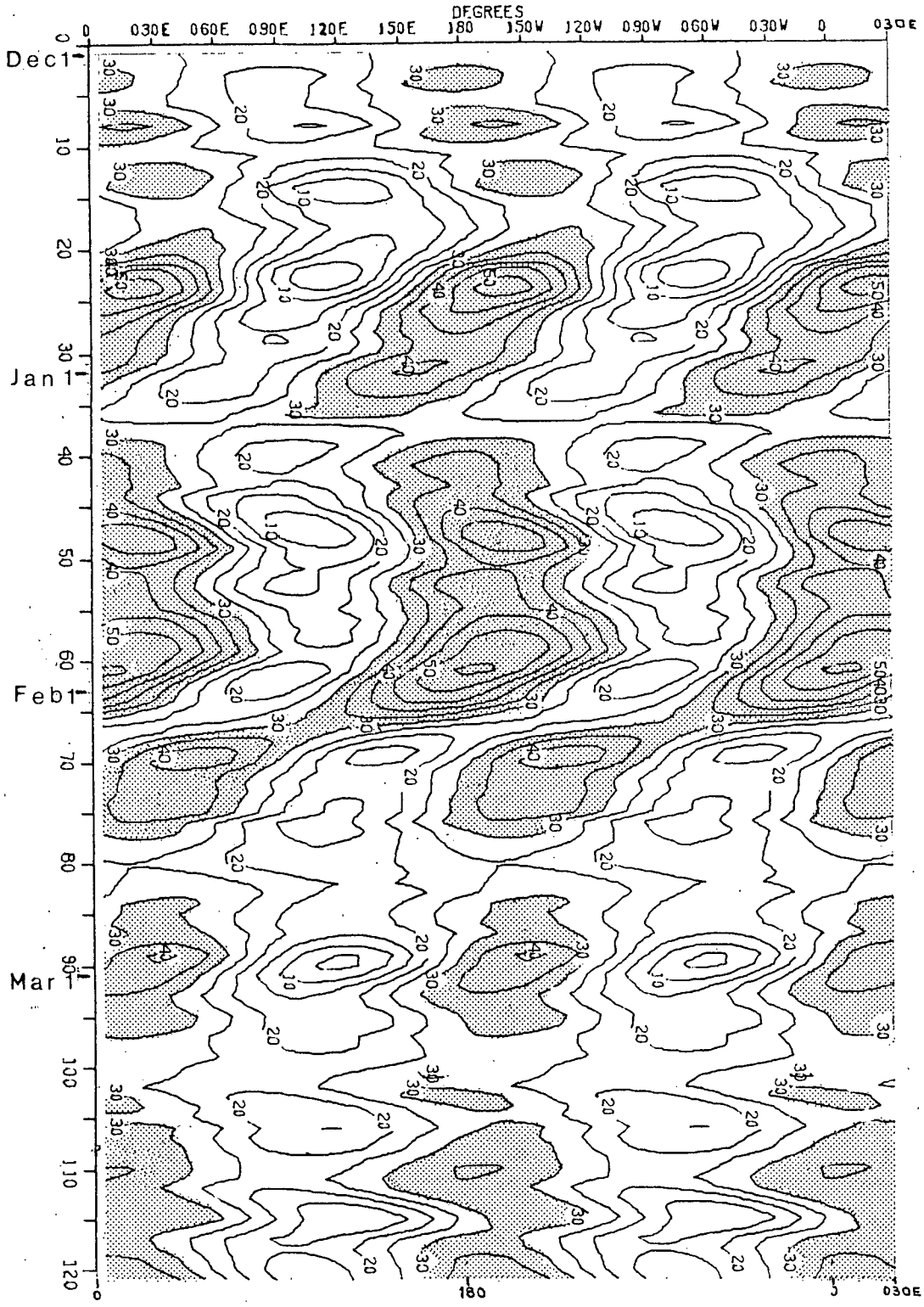

Fig. 7.4 Time-Longitude (Hovmöller) diagram of Second Harmonic of 500 MB height profile averaged across the zone 50 N - 70 N. Contour Interval = 5 dams.

the second harmonic, W_2, around the zone 50^oN to 70^oN for the winter of 1962-63.

(b) Variation of Amplitude and Phase

To focus exclusively on the change of amplitude and phase of the long-wave components we followed Haney (1961) and plotted A_n and ϕ_n against time for selected latitudes and wave numbers of interest. Fig. 7.5 shows the variation with time of the amplitude A_2 and phase ϕ_2 of the second harmonic W_2 around latitude 60^oN for 1962-63.

7.3.6 Computation and Presentation of Zonal Indices of U, V and U/V

The evolution of the expanding circumpolar vortex was briefly discussed in Section 2.6 and it was noted that the blocking phenomenon is frequently associated with a southward shift of a zonal wind maximum into the sub-tropics.

We therefore measured the following variables at selected latitudes (or latitude zones) and plotted them against time:

$$U_t = \frac{1}{2\pi} \int_0^{2\pi} u_t d\lambda = [u_t]$$

For this study t = calendar day

λ = longitude (at increments of 5 degrees)

[] = symbol for "average taken around a parallel (or zonal band) of latitude"

u_t = W - E algebraic component of geostrophic wind measured every 5° longitude

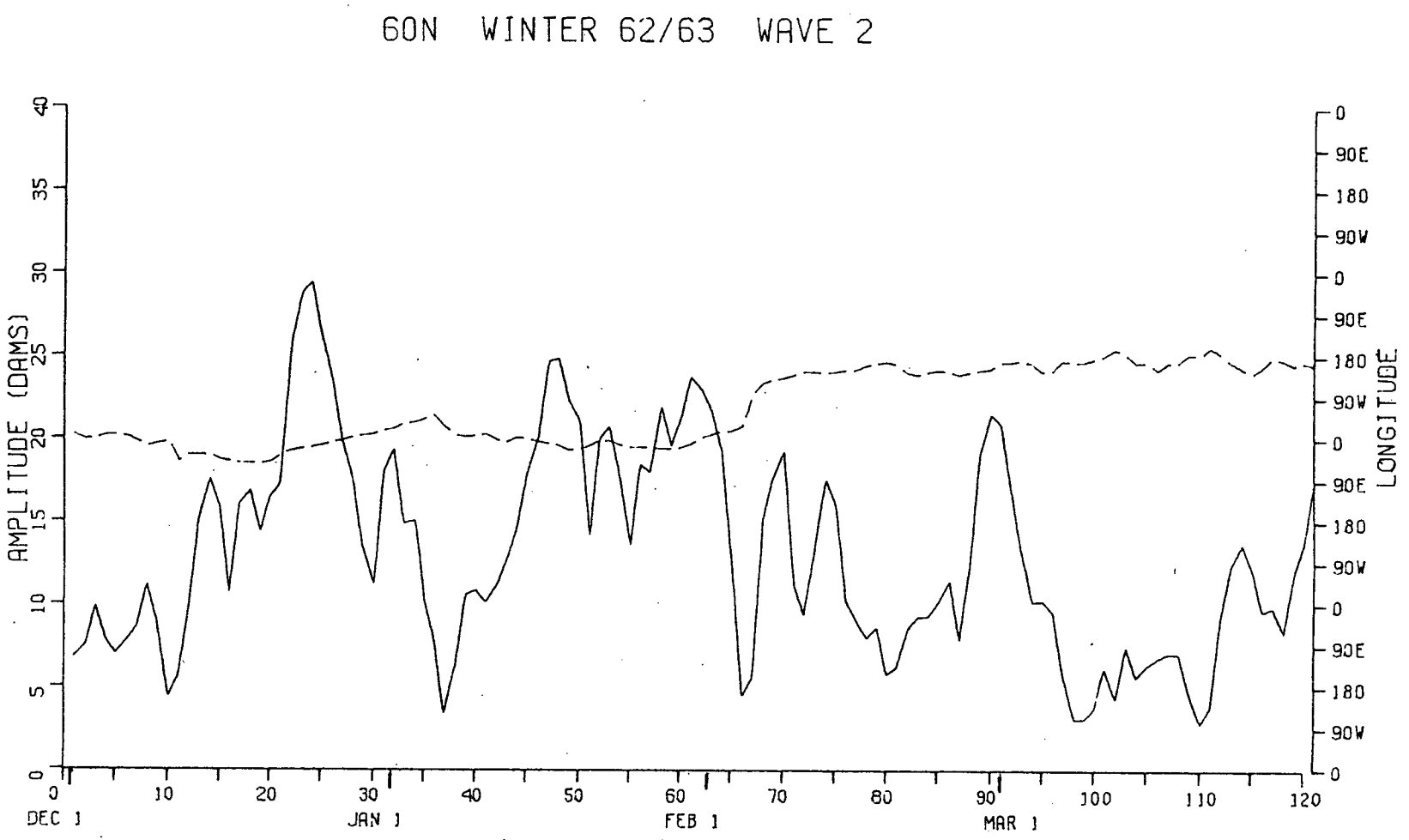

Fig. 7.5 Amplitude and phase angle of wave number 2 at 60°N as a function of time.

——————— amplitude in dams
- - - - - - - phase angle in degrees longitude

$$V_t = \frac{1}{2\pi} \int_0^{2\pi} |v_t| d\lambda = [|v_t|]$$

$|v_t|$ = absolute value of the N - S component measured every 5° longitude

$$R_t = U_t/V_t$$

U_t is the zonal average of u_t

V_t is the zonal average of $|v_t|$

and R_t may be interpreted as an indicator of the degree of predominance of zonal over meridional around a specific latitude.

The variation of U_t for the 1962-63 winter for 50^oN to 70^oN and 30^oN to 50^oN, respectively, is shown in Fig. 7.6. It is evident that the U_t maxima for the northern zone tend to coincide with U_t minima for the southern zone and vice versa. This observation is consistent with the statistical result of a strong correlation between U_t maxima at 60^oN and U_t minima at 40^oN (Panofsky and Brier, 1968). That study also found a significant lag correlation indicating that zonal maxima at 60^oN precede those at 40^oN, a result that fits the concept of a winter-time process of quasi-cyclical circumpolar vortex expansion.

The variation of R_t will be discussed in Section 7.4.

7.3.7 Concluding Remarks

We now have the information base and analytical techniques required to proceed with the four objectives outlined in Section 7.2. The results will be presented in the next Section.

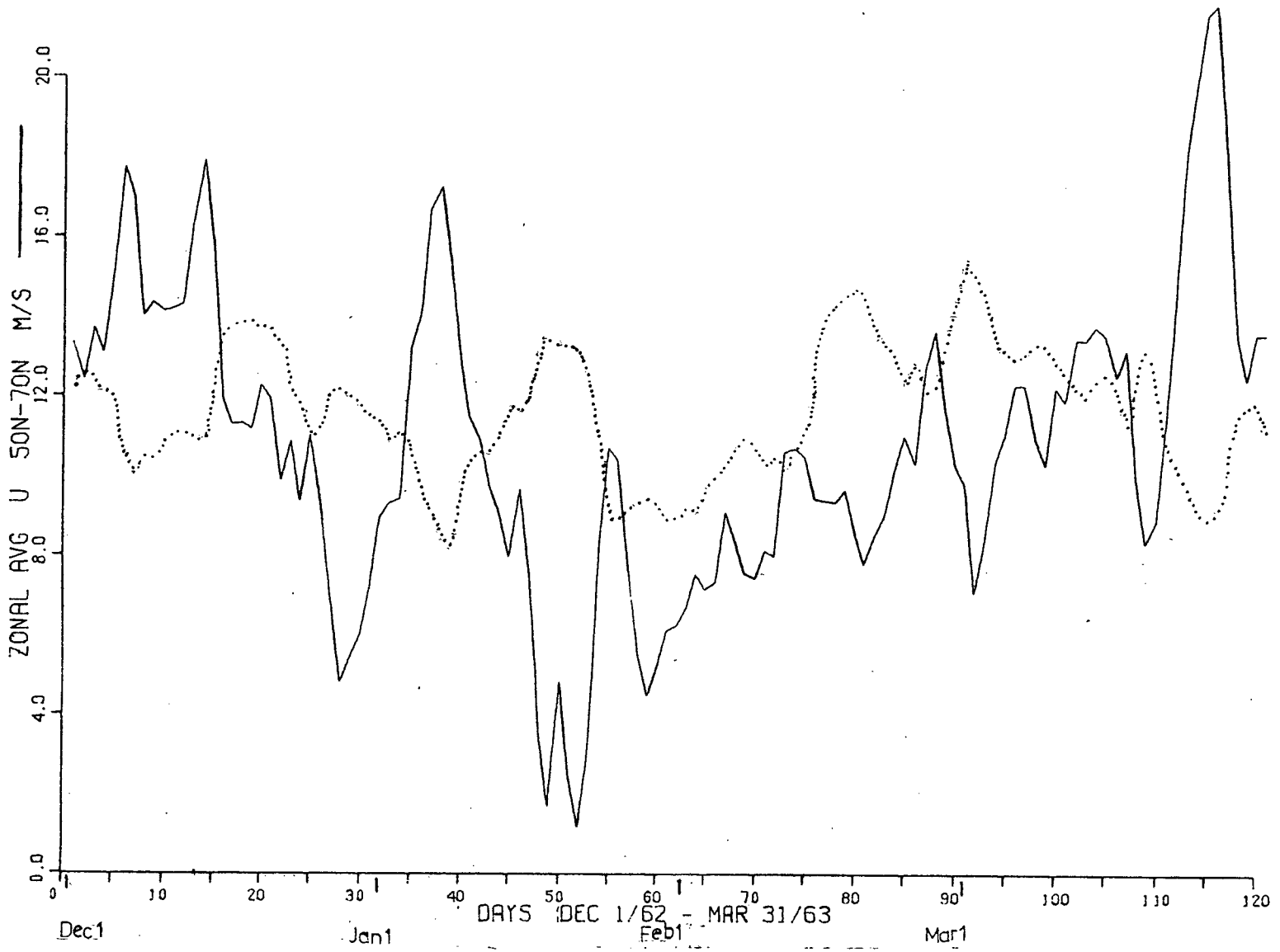

Fig. 7.6 Comparison between U_t 50°N - 70°N ———

and U_t 30°N - 50°N .....

7.4 Presentation of Results

7.4.1 Spectral Attributes of Blocking by Region of Occurrence

Our first objective was to determine how the spatial harmonics of blocking were related to the region in which the episodes occurred. A sample of cases was selected from each of the following regions:

Location Category		No. of Cases	No. of Days
Eastern Pacific - Alaska	(180W - 120W)	5	42
Baffin - Hudson Bay	(100W - 60W)	4	26
Northeast Atlantic - Greenland	(60W - 0)	6	42
Western Europe	(0 - 60E)	5	39
Double Blocking (Atlantic-Pacific)		5	43

The cases were selected from the Blocking Signature Sequence Catalogue and confirmed by the daily Synoptic Analyses or the Monthly Weather Review. A case (except for Double Blocking) could only qualify provided there was no significant concurrent blocking elsewhere in the Northern Hemisphere. This usually had the effect of reducing the duration of eligible cases to five to eight days.

Some winters (e.g., 1962-63, 1978-79) featured pronounced regimes of concurrent major blocking, usually over NE Pacific - Alaska and NE Atlantic - Western Europe. These "Double Blocking" episodes were always associated with extremes of weather, often with serious social and economic consequences. We therefore created a "Double Blocking" category and selected a sample of cases in the manner described above.

We also decided it would be useful to compare the mean harmonics for the categories in the above tabulation (for which it would be reasonable to assume the circulation at 60°N would have a strong meridional

component V) with those for situations of predominantly zonal flow. We therefore created a "Zonal" category and eligible cases were selected with reference to plots of U and R as described in Section 7.3.6. We looked for coincident maxima in U and R ensuring strong zonal flow and relatively weak meridional flow V. A sample of 12 cases each of two - three day duration was selected. (At 60°N predominantly zonal regimes are transitory.)

In order to compare the phases of category harmonics with those for the "normal" 500MB height distribution, the latter were extracted from the plots of the zonal harmonics for normal wave components 1 to 4. These are shown in Fig. 7.7[1] and a few comments would seem appropriate. It is noted, for example, that at 60°N constructive ridge interference is greatest between

W1 and W2 over Western Europe (20°E)

W3 and W4 over NE Atlantic (20°W)

and at 50°N between

W2 and W3 over NE Pacific (140°W).

Moreover, the trough line of W1 crosses the NE Pacific intersecting 60°N at 160°W. Therefore, if W1, on any given occasion, is near normal phase, it will interfere destructively with any tendency for ridging over the NE Pacific Ocean.

The parameters σ, A_n, ϕ_n and S_n at 60°N were abstracted for each day of each case. (All blocks were centred between 50°N and 70°N.) They were then averaged by category and the results are presented in Table 7.1 along with corresponding data for the normals.

---

[1] Figure 7.7 is consistent with the results of Graham (1955) and Eliasen (1958) who presented normal harmonics for January.

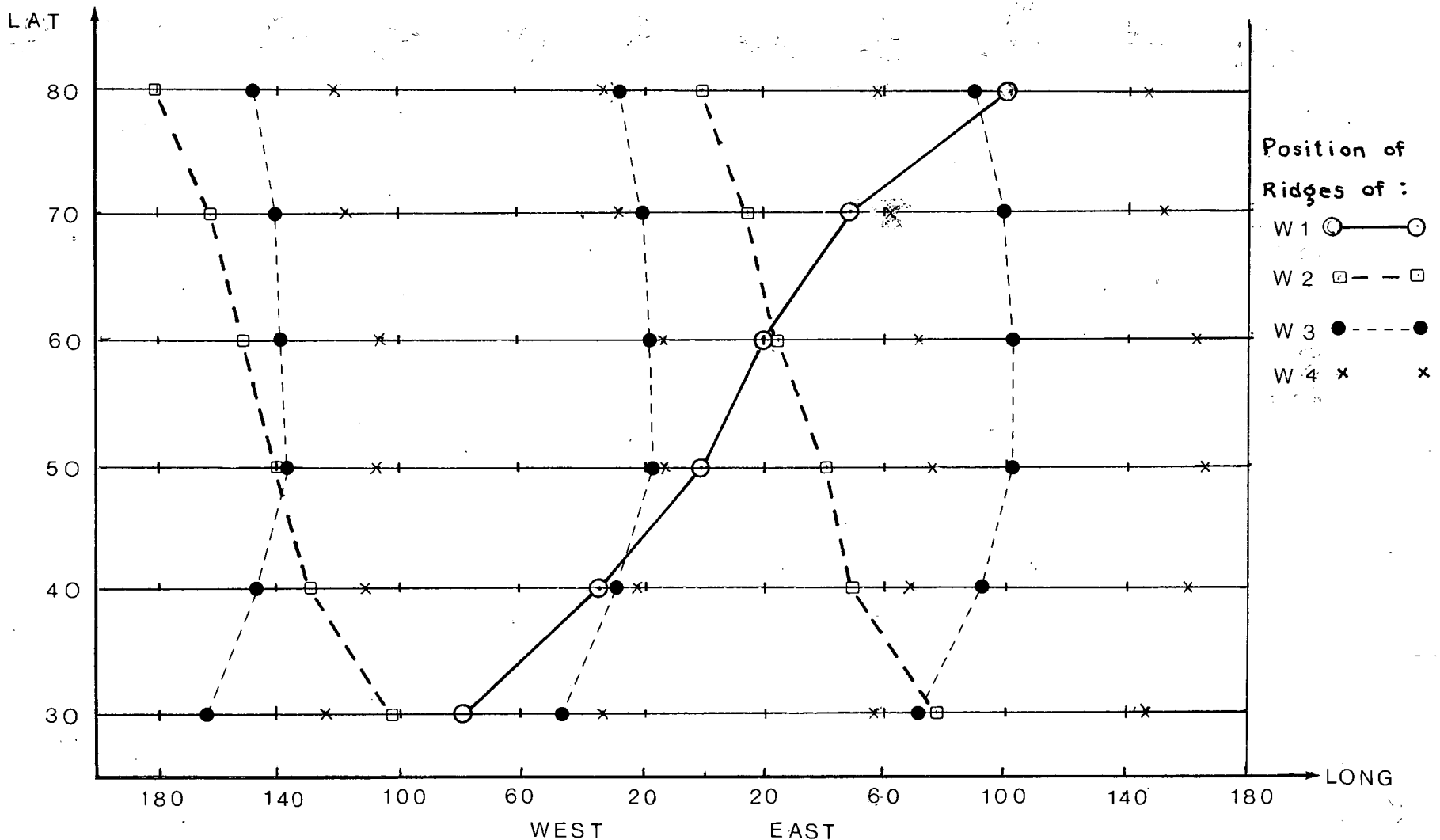

Fig. 7.7 Phase of Harmonics 1 to 4 for Normal 500MB height - WINTER - (December, January and February).

TABLE 7.1

Mean Spectral Attributes of WINTER Blocking Episodes 60°N 500MB

CATEGORY	σ	A_1	ϕ_1	S_1	A_2	$\phi_2/2$	S_2	A_3	$\phi_3/3$	S_3	A_4	$\phi_4/4$	S_4	A_5	ϕ	S_5	A_6	ϕ	S_6
	m	m	degs	%	m	degs	%	m	degs	%	m	deg	%	m	deg	%	m	deg	%
NORMAL (Winter)	75	50	+20	22	81	-155 + 25	59	43	-140 - 20 +100	17	15	- 17	2	-	-	-	-	-	-
ZONAL	92	62	-	23 (±15)	57	-	19	50	-	15	47	-	13	45	-	12	32	-	6
PACIFIC BLOCKING	147	78	-72	14	121	-141	34	102	-139	24	83	-179	16	51	-	6	29	-	2
BAFFIN BLOCKING	129	117	-89	41	77	- 24	18	71	- 22	15	58	- 89	10	48	-	7	36	-	4
NE ATLANTIC BLOCKING	169	162	- 1 (±35)	46 (±21)	96	- 8	16	99	- 12	17	86	- 9	13	53	-	5	41	-	3
W EUROPEAN BLOCKING	171	143	+11	35	132	+ 30	30	100	+ 12	17	76	- 5	10	48	-	4	34	-	2
DOUBLE BLOCKING	202	111	+64	15	206	+ 20	52	137	+ 7	23	70	+ 10	6	40	-	2	29	-	1

Standard Deviation (SD)

As expected, the SD of the hemispheric circulation during the blocking episodes is much larger than 'normal' (usually more than two-fold). It is least (129m) for blocking in the Baffin - Hudson Bay area, a result that is consistent with our remarks in Section 5.3.6, and greatest (202m) for 'Double Blocking.' The Standard Deviation for the Zonal category (92m) was not far removed from the Normal (75m).

Blocking over NE Pacific and Alaska

The primary components were W_2 (34%) and W_3 (24%) which interfere constructively at an average position of 140^oW, close to their normal phase. W_1 at 72^oW is clearly not contributing to the blocking structure and is 90 degrees removed from its normal phase location. W_4 (16%) phased at 179 W reinforces W_2 and W_3, and tends to shift the resultant maximum 500MB height about 10 - 20 degrees further west. This is consistent with the location of our blocking signature maximum, Figs. 5.2 and 5.7.

Blocking over Baffin Island (and Hudson Bay)

We shall reserve detailed comment for Section 7.4.4 and simply note here that the S_n values are similar to those for Atlantic Blocking.

Blocking over the NE Atlantic - Greenland

The primary component is W_1 (S_1 = 46%, ϕ_1 = 1^oW) and the balance is made up of more or less equal contributions from the other three components. Note that W_3 and W_4 are close to their normal phase (20^oW) while W_1 and W_2 are 20 to 30 degrees west of normal.

Blocking over Western Europe

Clearly W_1 and W_2 are the dominant components, interfering constructively at 20^oE which is very close to normal phase for both. Also W_3 ($\phi_3/3=12^oE$) contributes significantly.

Double Blocking (E Pacific - Alaska; NE Atlantic - W Europe)

Because of the geometry of the prescribed configuration it is not surprising that W_2 (S_2 = 52%) is the dominant component. It is interesting to note that the average phases ($20^oE, 160^oW$) are almost precisely the normal W_2 phase positions at 60^oN. W_3 (S_3 = 23%, $\phi_3/3=7^oE, 127^oE, 113^oW$) provides significant reinforcement but contributions from W_1 (S_1 = 15%, $\phi_1 = 64^oE$) and W_4 (S_4 = 6%) are inconsequential.

Zonal

Unlike the blocking categories there are no predominant components. The variance is shared across the spectrum and W_5 and W_6 account for 18%. Also, because wave components moved rapidly, ϕ_n values have no meaning and were omitted.

Summary

The average circumpolar harmonics at 60^oN for blocking occurring in the 50^oN - 70^oN zone show that the amplitudes of the primary components are more than double their normal value. The contributions to the mean blocking structures from the wave component ridges may be relatively assessed as follows:

	W_1	W_2	W_3	W_4
NE Pacific - Alaska	Small	Large	Large	Moderate
Baffin - Hudson Bay	Large	Small	Small	Moderate
NE Atlantic - Greenland	Large	Small	Small	Small
W Europe	Large	Large	Moderate	Small
Double	Nil	Very Large	Moderate	Small

The position relative to normal of the dominant wave component ridges will depend on the blocking location category and, of course, on the history of motion. Clearly the large W_1 component of the Baffin Island blocks will be well removed from its normal longitude. On the other hand, NE Pacific, N Atlantic and W Europe blocks are frequently a result of highly amplified wave components which are interfering constructively near their normal positions.

These results are reasonably consistent with those of Austin (1980). The methodology differed in that rather than drawing conclusions from individual cases we obtained our results from averages of categories. We also chose to separate W Europe blocks from those over the North Atlantic and found significant spectral differences.

As far as we are aware, blocking over the North-Eastern Canadian Archipelago (including Baffin Island) has never been explicitly examined by harmonic analysis. We shall report on further results in Section 7.4.3.

7.4.2 Interruptions of Major Blocking Episodes

During the course of this investigation we were struck by the nature of the interruptions to the otherwise persistent hemispheric regimes of large amplitude waves. Invariably these regimes were associated

with major blocking episodes, sometimes of several weeks duration (e.g., January 9 to February 4, 1963). The interruption is characterized by rapid decrease of amplitude and the concurrent establishment, for a few days, of strong zonal flow. Each of the 14 'zonal' cases summarized in the previous Section (Table 7.2) occurred during the peaks of interruptive episodes.

The winter of 1962-63 provided a set of remarkable examples. The two dominant harmonics of the persistent regimes were clearly W_2 and W_3, but on three occasions W_3 collapsed, W_2 lost significant power and the ensuring strong zonal flow was marked by low amplitude harmonics with power more evenly distributed over the spectrum.

The interruptions are consistently revealed by: Fig. 7.8, showing the time-longitude variation of W_3; by Fig. 7.9, showing the corresponding plot of Amplitude vs time; and by Fig. 7.10, showing the change with time of R = U/V. The interruptions are identified by O_1 (December 8, 1962), O_2 (January 7, 1963), O_3 (February 7-12, 1963), O_4 (March 15, 1963) and O_5 (March 27, 1963). The most striking of these five occasions were O_2, O_3 and O_4, because in each case they were flanked by long-wave regimes of unusual amplitude and persistence.

The change of Standard Deviation and the redistribution of power among the harmonics during the transition O_2 is illustrated in the following table:

TABLE 7.2

Date	σ(m)	S_1(%)	S_2	S_3	S_4	S_5	S_6	R = U/V
30 Dec. 1962	137	4	34	33	17	9	1	0.6
7 Jan. 1963	76	3	10	1	31	13	35	2.1
9 Jan. 1963	144	10	27	44	10	0	7	1.3
14 Jan. 1963	193	6	29	53	0	3	7	0.6

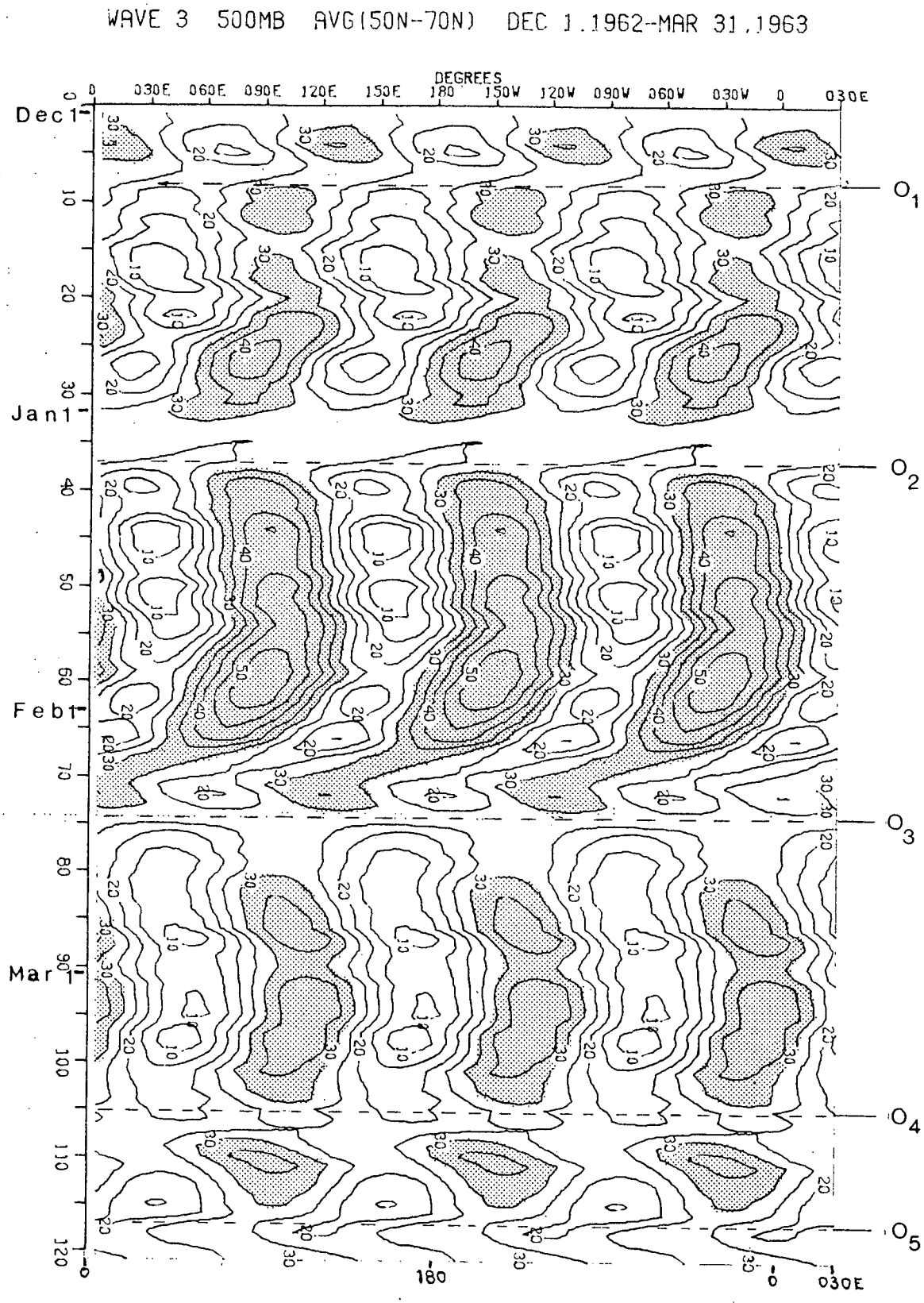

Fig. 7.8 As in Fig. 7.4 except for Third Harmonic. Minima of amplitude at O_1, O_2, O_3, O_4, O_5.

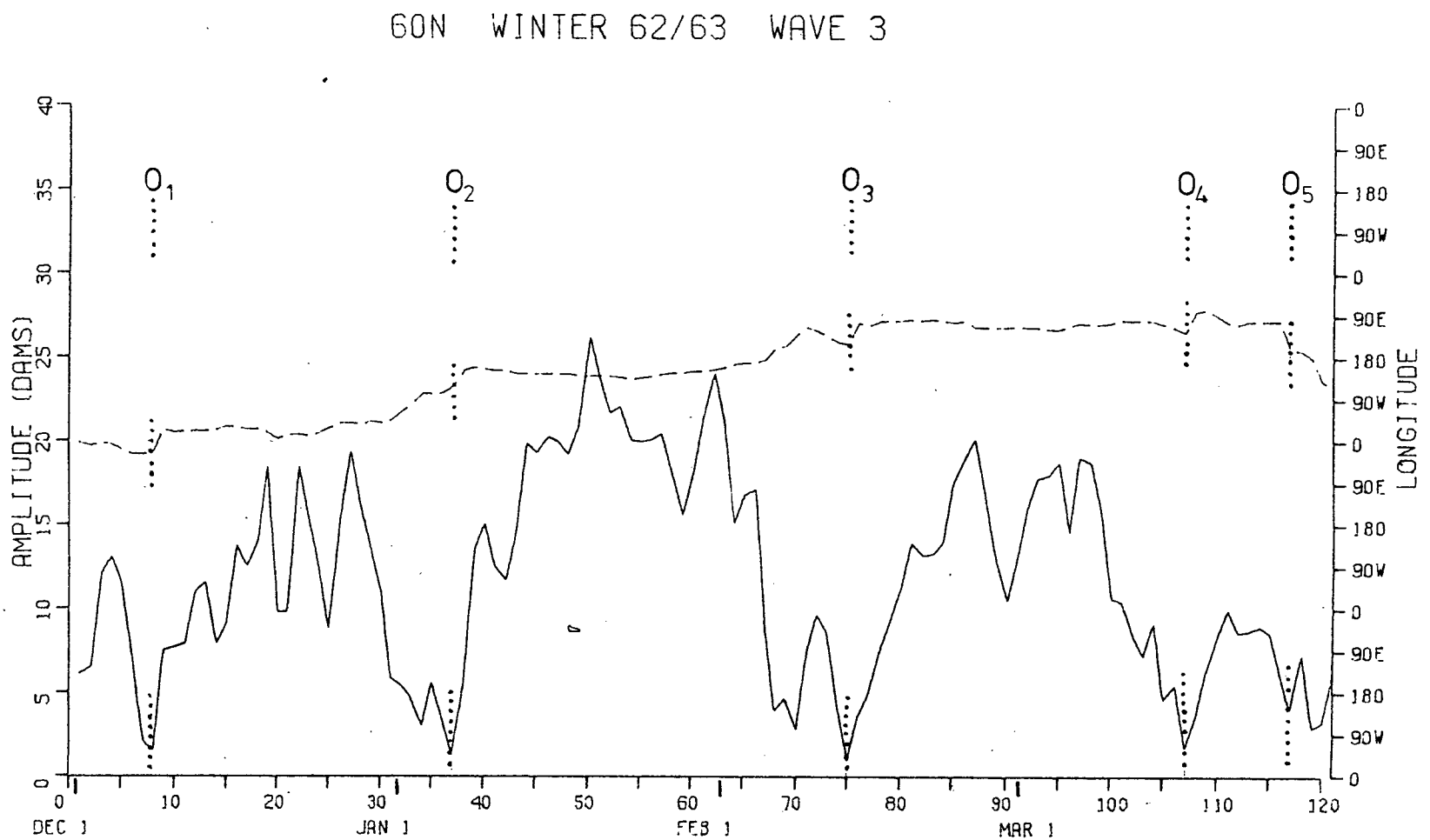

Fig. 7.9 As in Fig. 7.5 except for wave number 3.

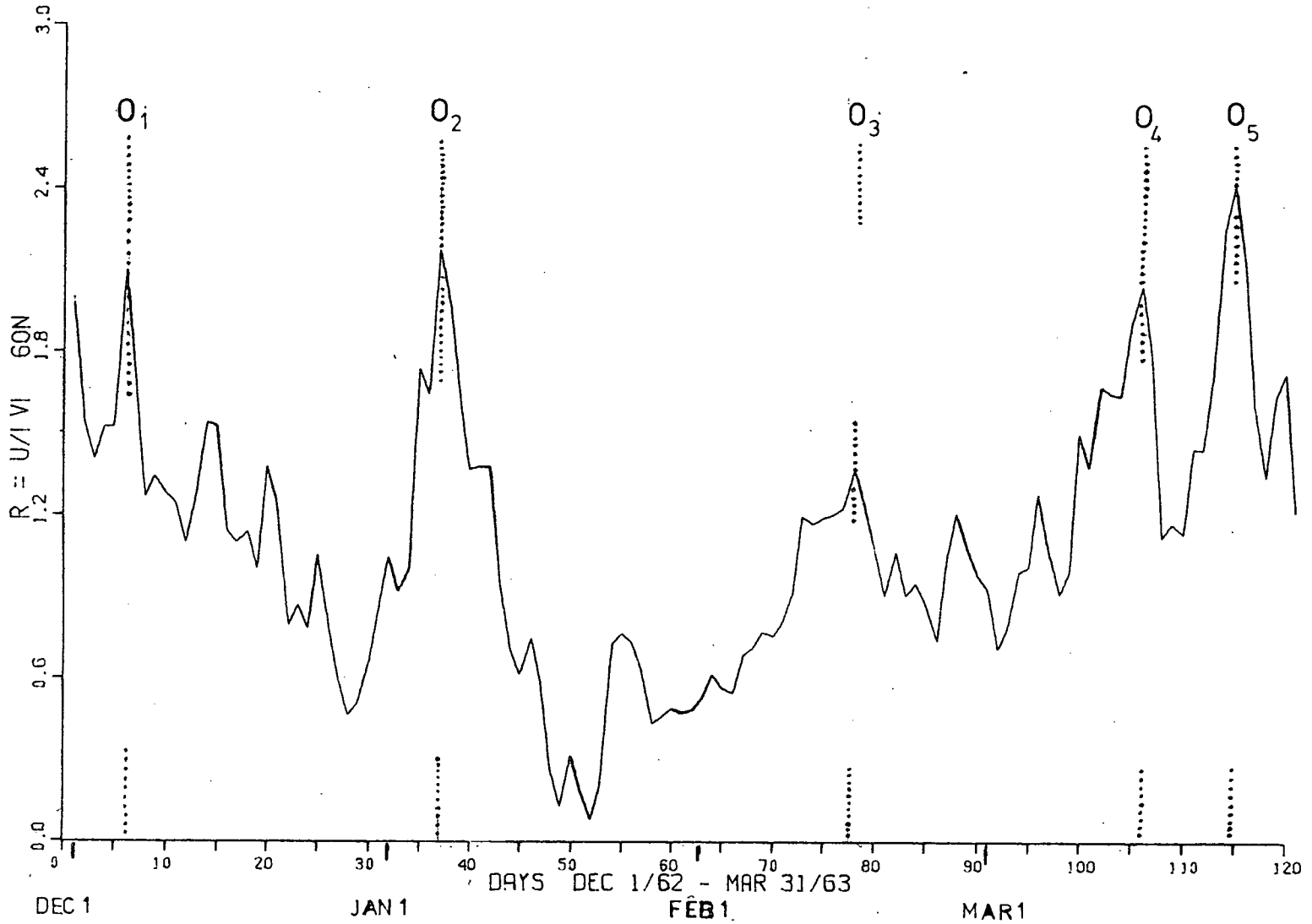

Fig. 7.10 Change with time of the ratio R of zonal (U) to meridional (V) components at 60°N, December 1, 1962 to March 31, 1963.

The inception of strong zonal flow implies enhanced baroclinicity and therefore an increase in available potential energy. Moreover, because the N-S thermal gradient $-\frac{1}{\theta}\frac{\partial\theta}{\partial y}$ is increasing, so too is the range of wave lengths over which instability may occur (Fig. 2.9). The ensuing realization of baroclinic instability in the form of deepening extra-tropical cyclones results in the conversion of available potential energy into eddy kinetic energy. Table 7.2 shows that, at one stage of the zonal flow of January 7, 1963, 35% of the eddy (or wave) energy was accounted for by the W_6 component. This is a wave length which, at 60°N, is representative of the scale of baroclinic systems which are the mature stage of "free" or "transient" unstable waves that originated in lower latitudes. Table 7.2 also shows that the energy transfer to the longer wave components W_2 and W_3 representing the "forced" oscillations, was swift ($\leq$ 2 days) and ushered in a protracted double (and later triple) blocking regime from January 9 to February 4. This is clearly shown on the Hovmöller Diagram of Fig. 7.1 (50°N to 70°N), and the full-latitude extent of the long-wave pattern is confirmed by Fig. 7.2 (30°N to 50°N).

The extraordinary rate at which these massive energy transfers occur is not being accurately replicated by numerical models. Hence the onset of these persistent long-wave regimes and their subsequent evolution poses a difficult problem for medium range forecasting (Baumhefner and Downey, 1978; Somerville, 1980).

7.4.3 Baffin Island Blocking

In Section 7.4.1 it was noted from Table 7.1 that the Amplitude Spectrum of Baffin blocking was nearly the same as for Atlantic blocking. The mean Phase Spectrum was, of course, shifted westward. If the samples

examined are representative, the implication is that the Baffin Block may be a later stage of a retrograding Atlantic Block. Is retrogression of Baffin blocks a predominant characteristic or are they as likely to be quasi-stationary or progressive?

To answer this question we conducted a census, from the Blocking Signature Sequence Catalogue, of all Sequences whose trajectories lay across the Canadian Archipelago, an area we defined with boundaries 60°N, 80°N and 50°W, 100°W. There were 61 Sequences and a total of 115 signatures for the 33 winters. The movement from one signature to the following was assessed as 'retrograde' or 'progressive.' If the sequence was only 1 pentad in duration, the motion was categorized 'indeterminate.'

The count for the 33 winters was

Retrogression	63
Progression	27
Indeterminate	25
Total	115

Clearly the most likely motion during a Baffin blocking episode is retrogression but at least 25% of the time there can be progression.

What is the spectral history of a typical retrograding Baffin blocking episode? The sequence December 21, 1978 to January 6, 1979 is one such example. To provide a perspective of the synoptic evolution, Fig. 7.11 displays a panel of 5-day mean 700MB charts, Taubensee (1979) and Wagner (1979).

The significant spectral attributes are listed in Table 7.3. A retrograde North Atlantic blocking wave is clearly evident through

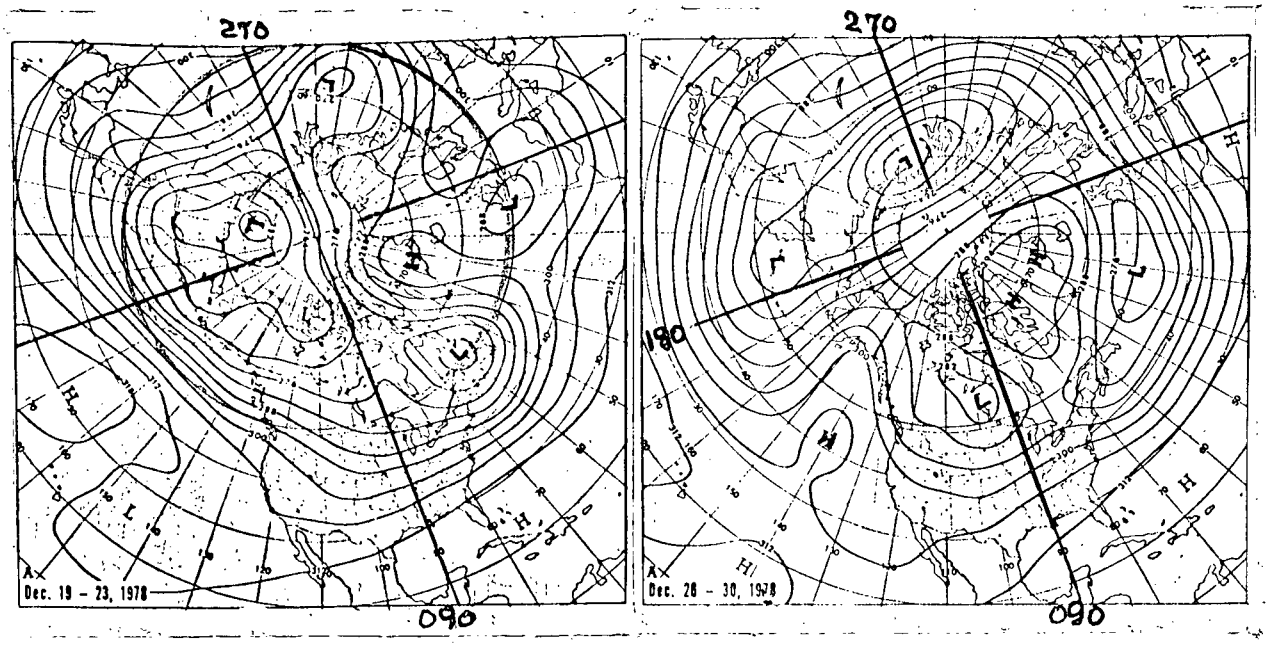

(a) (b)

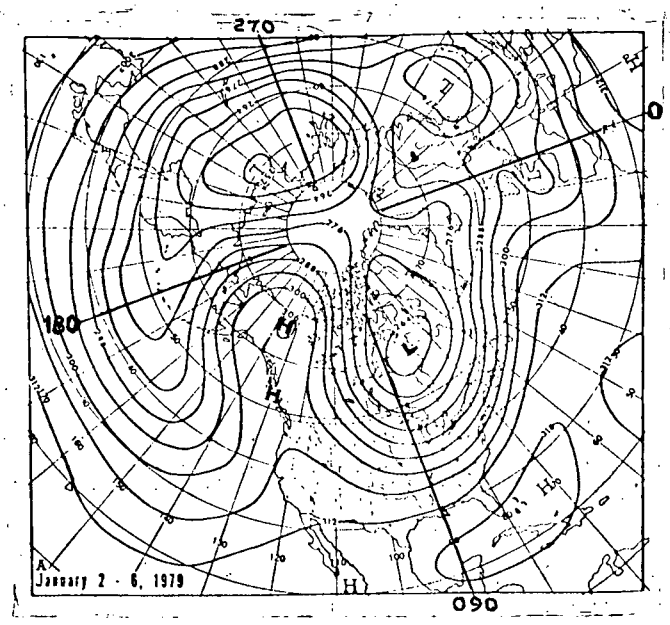

(c)

Fig. 7.11 Sequence of 5-day mean 700MB charts:
(a) 19-23 Dec 1978 N. Atlantic - Greenland Block
(b) 26-30 Dec 1978 Baffin I. Block established
(c) 2-6 Jan 1979 Alaska - West Coast Block
(Taubensee, 1979, Wagner, 1979).

TABLE 7.3

Harmonics at 60°N associated with retrograde blocking from the N. Atlantic to NE Canada and subsequent blocking Gulf of Alaska

Location	Date 1978-79	σ	ϕ_1	S_1	$\phi_2/2$	S_2	$\phi_3/3$	S_3
Atlantic	Dec. 21	167	+ 1	47	—	0	- 19	31
	22	183	- 7	55	3	10	- 21	19
	23	179	-12	53	- 3	14	- 19	19
	24	152	-22	88	—	2	—	2
	25	125	-28	84	—	3	—	2
	26	107	-34	65	22	16	—	4
Baffin	27	106	-54	47	8	15	- 45	25
	28	117	-75	43	—	4	- 35	27
	29	136	-83	45	—	0	- 29	39
	30	171	-90	52	—	2	- 28	34
	31	203	-88	60	—	3	- 24	22
	Jan. 1	196	-92	65	—	1	- 21	17
	2	150	-85	58	—	3	- 12	20
Alaska	3	169	-69	25	-152	28	-142	17
	4	189	-81	17	-152	44	-153	18
	5	218	-82	15	-155	50	-149	12
	6	234	-92	13	-157	69	—	2

December 26, 1978, with the main power contributed by W1 which peaks at 88% on December 24.

The process continues into a slowly retrograding Baffin block December 27 to January 1 following which there is a transfer of power to W2 (nearly 70% by January 6) and the W2 ridge is phased over the NE Pacific ($\simeq 155^{o}$W). This component combines with the residual W1 (now quasi-stationary at 90°W) to form the strongly amplified blocking ridge from Alaska south-eastward along the West Coast of North America (Fig. 7.11(c)). Meanwhile the Baffin trough has been restored to its normal longitude.

The general characteristics of this sequence have been observed synoptically many times (e.g., Namias, 1975) but we are not aware of reference in the literature to day-to-day harmonic analyses. (The zonal harmonic graphics for December 23, 1978 and January 4, 1979 will be presented in Section 7.4.4.)

There is a marked variation in Baffin blocking frequency even during the winters when hemisphere frequency of blocking is high. For example, during the winters of 1946-47, 1955-56, 1968-69 and 1978-79, we counted a total of 9 + 8 + 13 + 8 = 38 signatures or 9.5 per winter, whereas for the winters of 1949-50, 1962-63, 1976-77 we counted 2 + 0 + 6 = 8 signatures or 2.7 per winter. The predominance of W1 during the high frequency winters, particularly at 70°N, is quickly noted from a comparison of amplitude-time plots, e.g., Fig. 7.12 (1949-50) vs Fig. 7.13 (1978-79). Of the winters examined, those with low frequency Baffin Blocking seem to have large amplitude ridges which are the result of constructive interference between W2 and W3 over the Pacific and W1 and W2 over the NE Atlantic. These ridges oscillate slowly about their

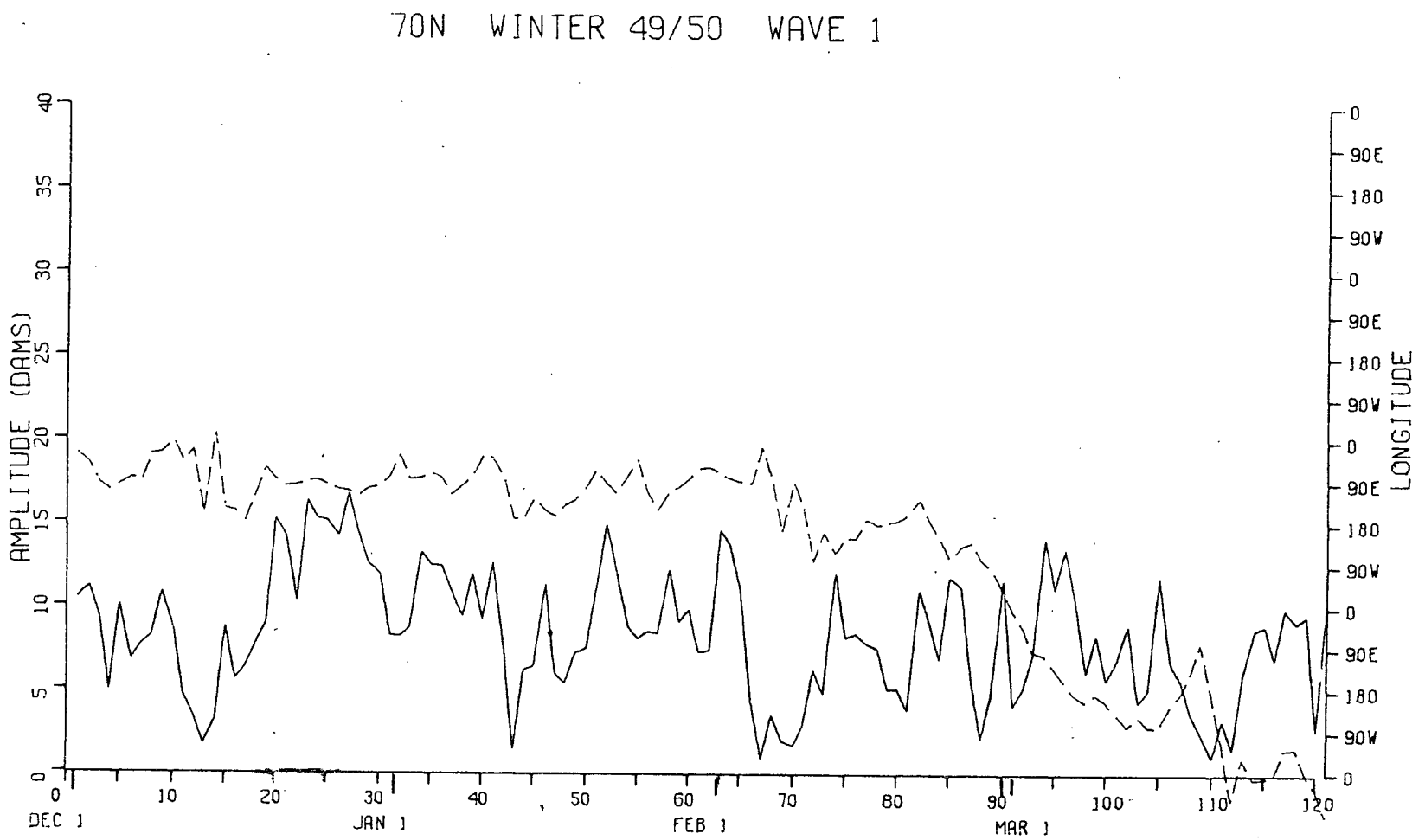

Fig. 7.12 Amplitude and phase angle of wave number 1 at 70°N as a function of time. December 1, 1949 to March 31, 1950.

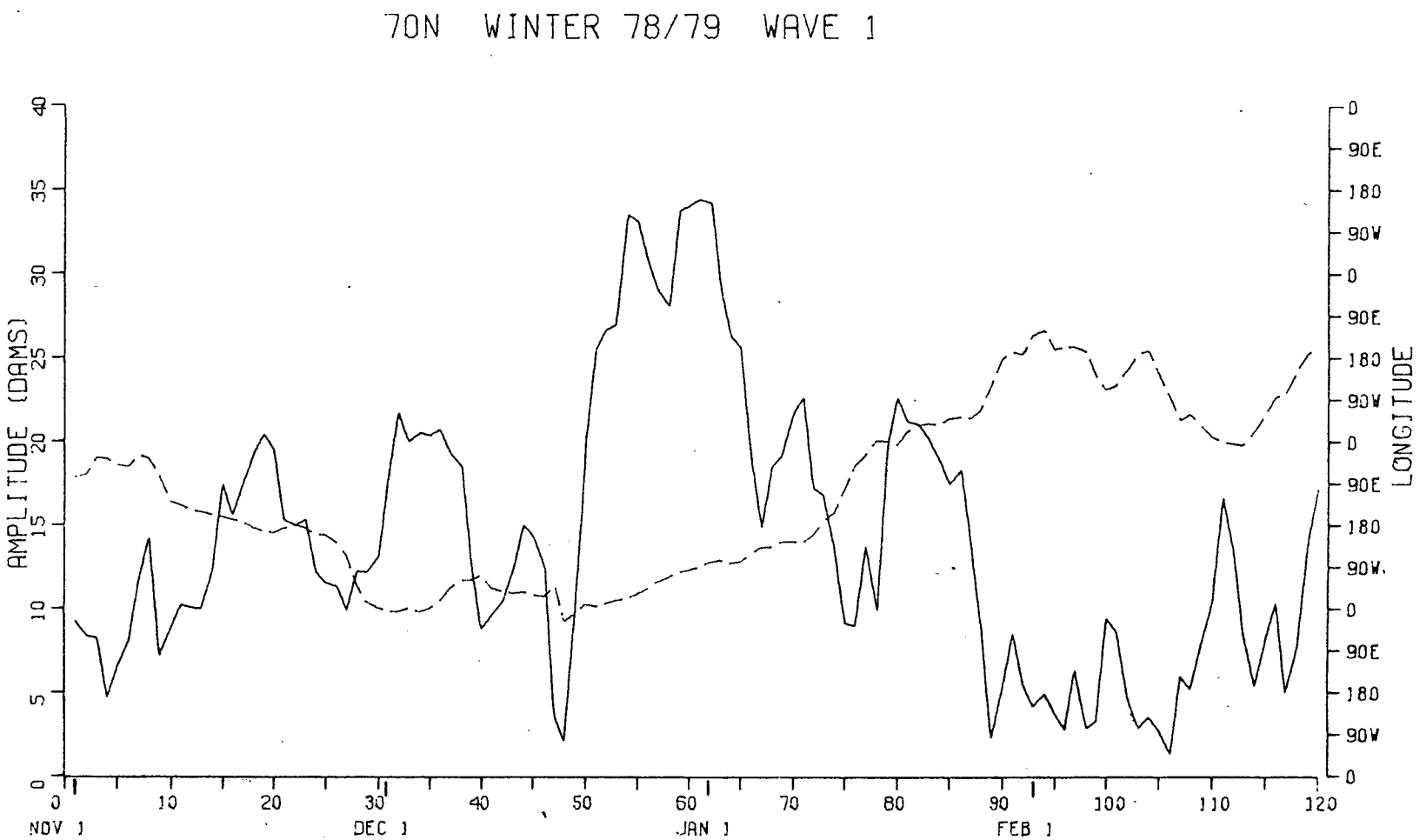

Fig 7.13 As in Fig. 7.12 except for November 1, 1978 to February 28, 1979.

mean winter location (e.g., Fig. 7.1). Those winters with high frequency Baffin Blocking, e.g., 1978-79, Fig. VII - 1, feature a repeating pattern of retrograding blocking waves initiated over the N Atlantic, subsequently crossing northern Canada and usually weakening or terminating west of Hudson Bay. A subsequent amplification of the long-wave pattern over the NE Pacific and Alaska is associated with a readjustment of the hemispheric wave mode and, ultimately, the primary power resides in the W2 and W3 components. There were two such cycles observed from December 1, 1978 to February 28, 1979 and a third in March (not shown). Baffin blocking may then be perceived as an intermediate stage of such a cycle.

Summary

Blocking over the eastern Canadian Archipelago is frequently the result of a retrograding blocking wave from the North Atlantic. It has a similar amplitude signature and W1 usually contributes at least 50% of the variance, but, at 60°N the W1 ridge is displaced 90 degrees or more west of its normal location. Examination of Hovmöller diagrams of $Z(\lambda,t)$ at 60°N and superimposed blocking locations suggests that Baffin Blocks, though frequent, are not as persistent or robust as oceanic episodes.

7.4.4 Zonal Harmonics of Blocking Systems

- Two case studies -

So far this Chapter has focussed on a one-dimensional harmonic analysis of 500MB height for the 50°N - 70°N zone, and related the temporal variation of the wave components to blocking episodes. This zone was chosen because the main target of interest was the blocking anti-

cyclone. However, if we wish to investigate the evolution of entire blocking systems (and this would include the flanking cold lows or troughs such as portrayed in the sequence of Fig. 1.2) then it would be necessary to analyze the spatial and temporal variation of the harmonics in the 30°N - 50°N zone. Such analyses will be part of our research subsequent to this dissertation.

However, discrete one-dimensional analyses, even though over representative zones, do not provide an integrated visual perception of the harmonics of a blocking system. To achieve this requires a two-dimensional zonal harmonic analysis. The purpose of this section, therefore, will be to present and discuss the results of this kind of analysis applied to instantaneous (i.e., 1200Z) 500MB height fields during two geographically disparate blocking episodes. These situations were December 23, 1978 - a N Atlantic-Greenland block and January 4, 1979 - a NE Pacific-Alaska block.

These dates are contained in the sequence which was presented in the previous section (Table 7.3 and Fig. 7.11) to illustrate an example of retrograde Baffin Island blocking. Here we shall emphasize the spatial characteristics of the zonal harmonics on the two dates, but we shall also comment on temporal aspects of the transition period particularly as they apply to the southern structure of the blocking systems.

(a) Atlantic - Greenland Block, December 23, 1978

The first three zonal harmonics of the 500MB height field on December 23, 1978 are displayed in Figs. 7.14 to 7.16, respectively. The corresponding digital data are presented in Table 7.4 as well as those for components 4, 5 and 6:

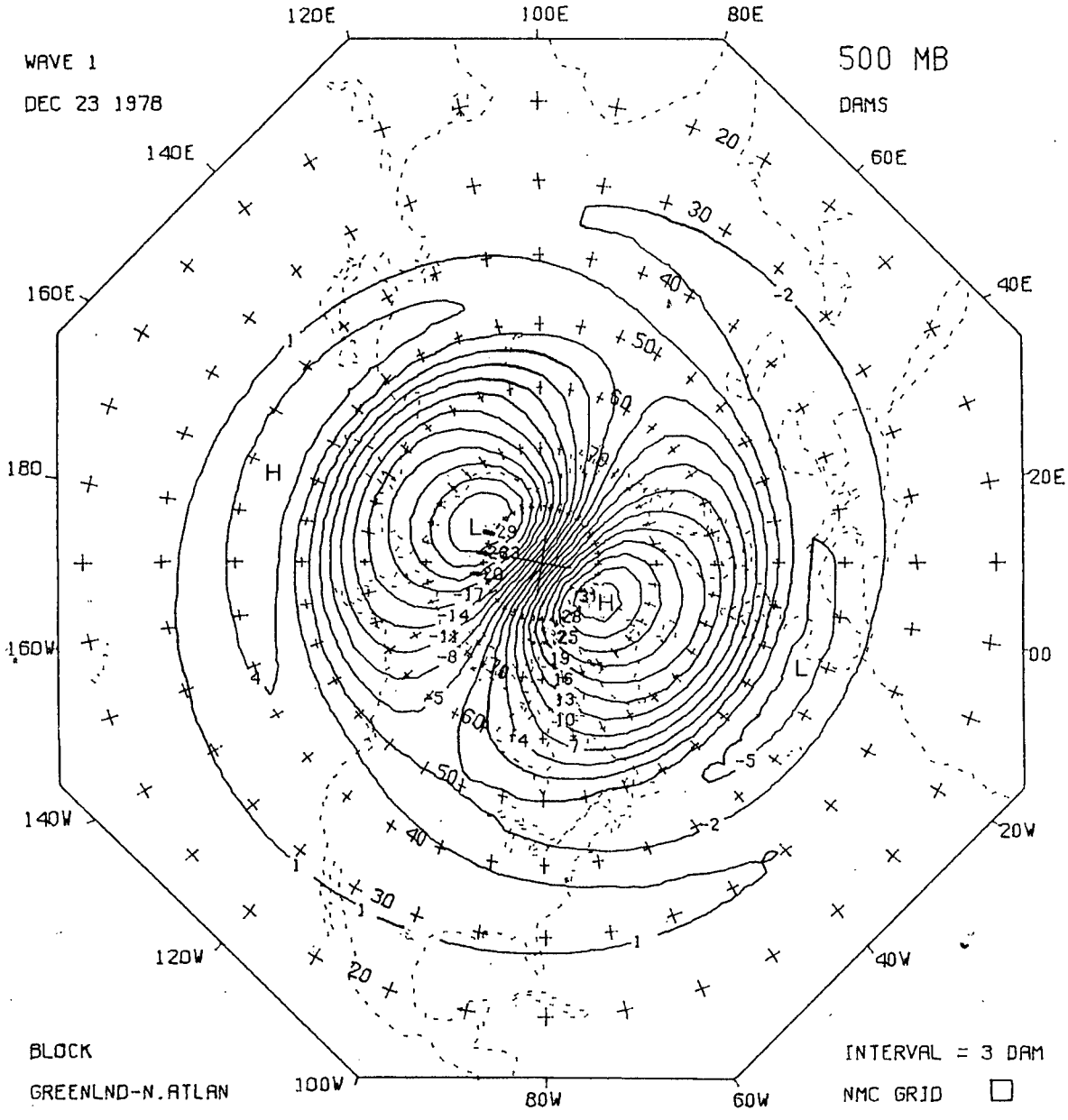

Fig. 7.14 First harmonic (W1) of the 500MB height field on December 23, 1978 during a major episode of blocking over the North Atlantic and Greenland. Contours in dams. Interval = 3 dams.

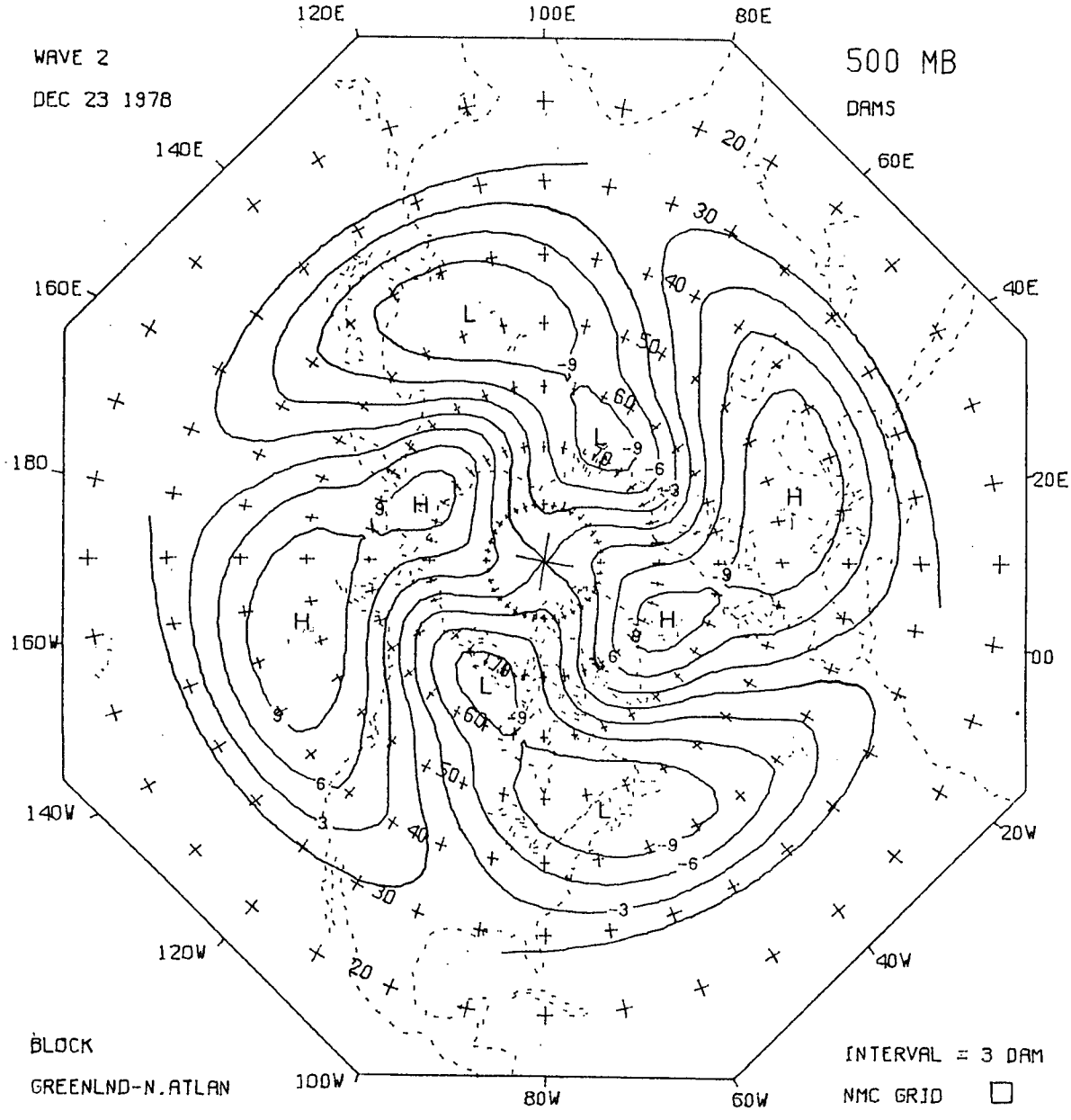

Fig. 7.15 As in Fig. 7.14 except for second harmonic(W2)

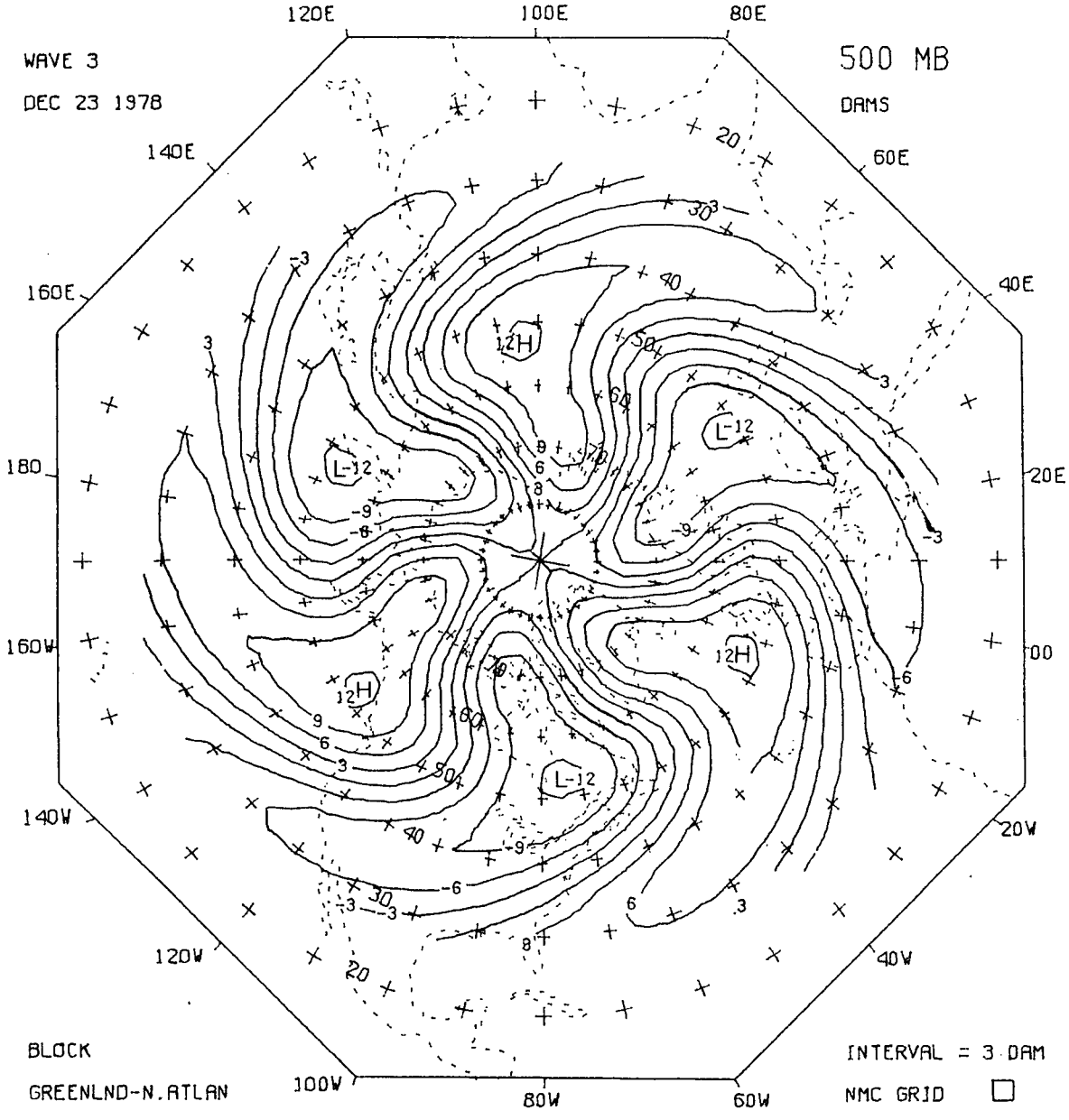

Fig. 7.16 As in Fig. 7.14 except for third harmonic (W3).

TABLE 7.4

North Atlantic Block Zonal Harmonics 500MB December 23, 1978

			WAVE 1			WAVE 2			WAVE 3			WAVE 4			WAVE 5			WAVE 6		
LAT	AVG	SD	A	φ	S	A	φ	S	A	φ	S	A	φ	S	A	φ	S	A	φ	S
	m	m	m		%	m		%	m		%	m		%	m		%	m		%
85	5108	156	220	- 30	99	18	27	1	6	-108	0	0	27	0	1	174	0	1	52	0
80	5112	237	332	- 27	98	38	16	1	34	-126	1	2	- 90	0	6	- 7	0	2	- 54	0
75	5130	239	321	- 21	90	69	-20	4	81	-115	6	5	- 96	0	9	- 37	0	5	- 55	0
70	5140	221	270	- 17	75	103	-37	11	115	- 95	14	14	-126	0	19	-130	0	2	64	0
65	5160	196	224	- 14	66	105	-32	14	113	- 83	17	20	168	1	42	-149	2	10	133	0
60	5193	179	185	- 12	53	94	- 5	14	109	- 58	19	65	110	7	51	-160	4	26	-177	1
55	5252	163	106	- 3	21	98	30	18	125	- 42	30	98	107	18	41	-169	3	58	-175	6
50	5346	144	25	85	2	118	44	33	126	- 46	38	68	102	11	19	152	1	66	177	11
45	5470	132	62	159	11	116	55	38	110	- 68	35	31	81	3	24	117	2	44	178	6
40	5586	115	50	-177	9	101	66	39	92	-105	32	12	95	1	27	152	3	37	-167	5
35	5679	96	29	-128	5	62	69	21	88	-144	42	6	114	0	38	150	8	21	-138	2
30	5753	74	18	- 91	3	13	44	2	71	-180	46	16	- 22	3	44	143	18	25	- 54	6
25	5810	59	3	- 66	0	30	-96	13	41	137	23	25	- 24	9	38	135	21	28	- 28	11

The phase and large amplitude of W1 in the higher latitudes are consistent with the results of Section 7.4.1. A profile along the 20°W meridian reveals an asymmetric wave structure cresting at 77°N (33 dams) and troughing at 45°N (-6 dams). The trough is a reflection of the observed low geopotential height over the mid-Atlantic (Fig. 7.11 (a) and (b)), a condition which is typically associated with high latitude blocking. We also note a di-pole configuration across the North Pole from a maximum at 77°N 20°W to a minimum at 77°N 160°E (-30 dams). This minimum is a reflection of the deep low over the Arctic Ocean.

North of 60°N, W1 accounts for between 50 and 100 percent of the hemispheric variance, while in the mid-latitudes (40°N - 50°N) W2 and W3 account for about 70 percent. It is the constructive interference of the latter components that replicates much of the deep low in the Newfoundland area, Figs. 7.11(a) and (b).

(b) Transition December 23, 1978 to January 4, 1979

The first four zonal harmonics of the 500MB height field on January 4, 1979 are displayed in Figs. 7.17 to 7.19, respectively. The corresponding digital data are presented in Table 7.5.

A number of features of the evolution of events in the 50°N to 70°N zone during this transition period were discussed in Section 7.4.3. It is also noted that the W1 di-pole configuration of Fig. 7.14 rotated clockwise about the N Pole. This high latitude retrogression was presumably a result of strong planetary vorticity advection. By January 4, 1979, the W1 maximum was located at 70°N 90°W.

Meanwhile W2, initially weak over Kamchatka, amplified as its maximum progressed slowly eastward to mainland Alaska. Note that it, too,

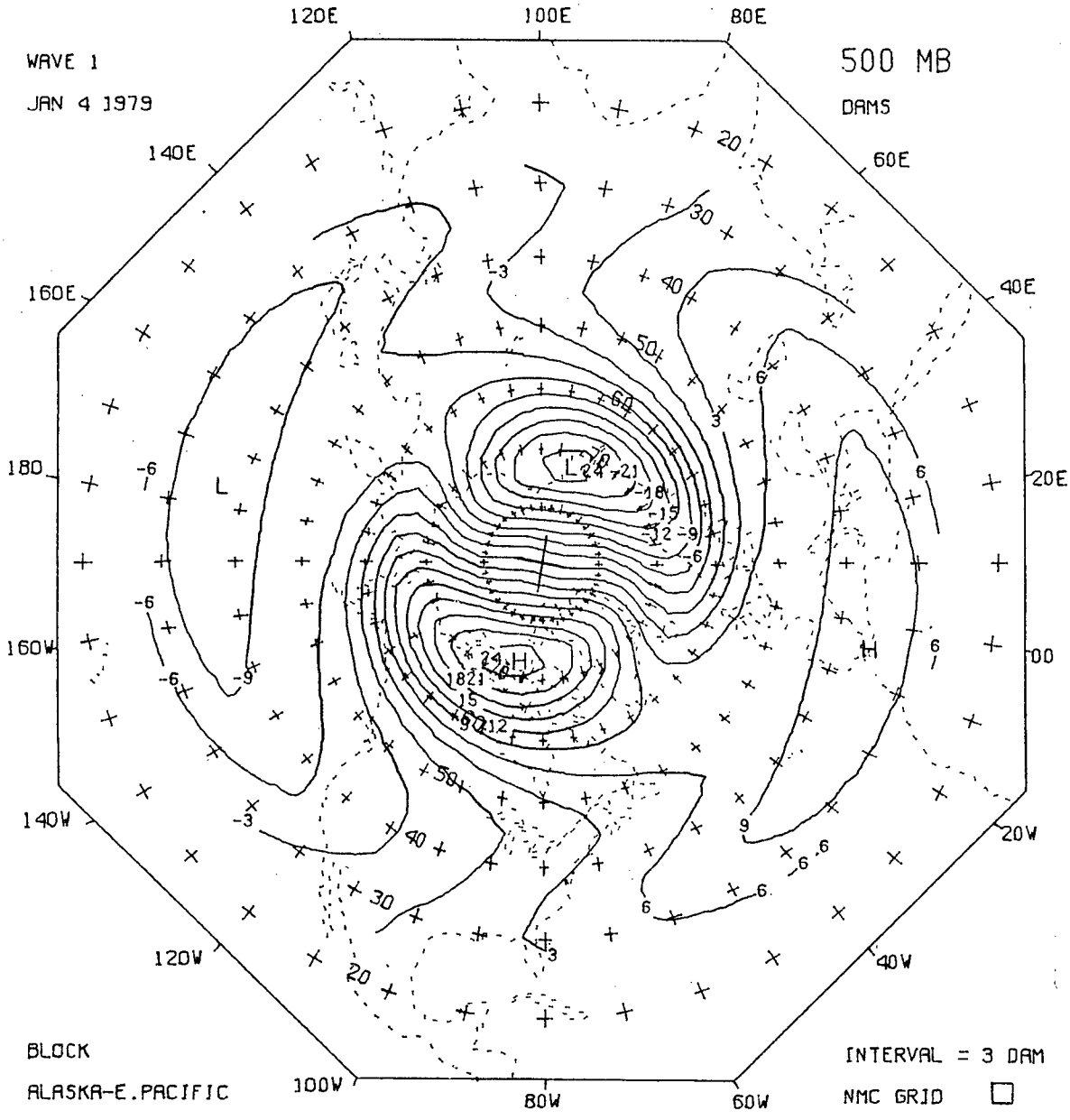

Fig. 7.17 First harmonic (W1) of the 500MB height field on January 4, 1979 during a major episode of blocking Alaska and Southward along West Coast of B.C. Contours in dams. Interval = 3 dams.

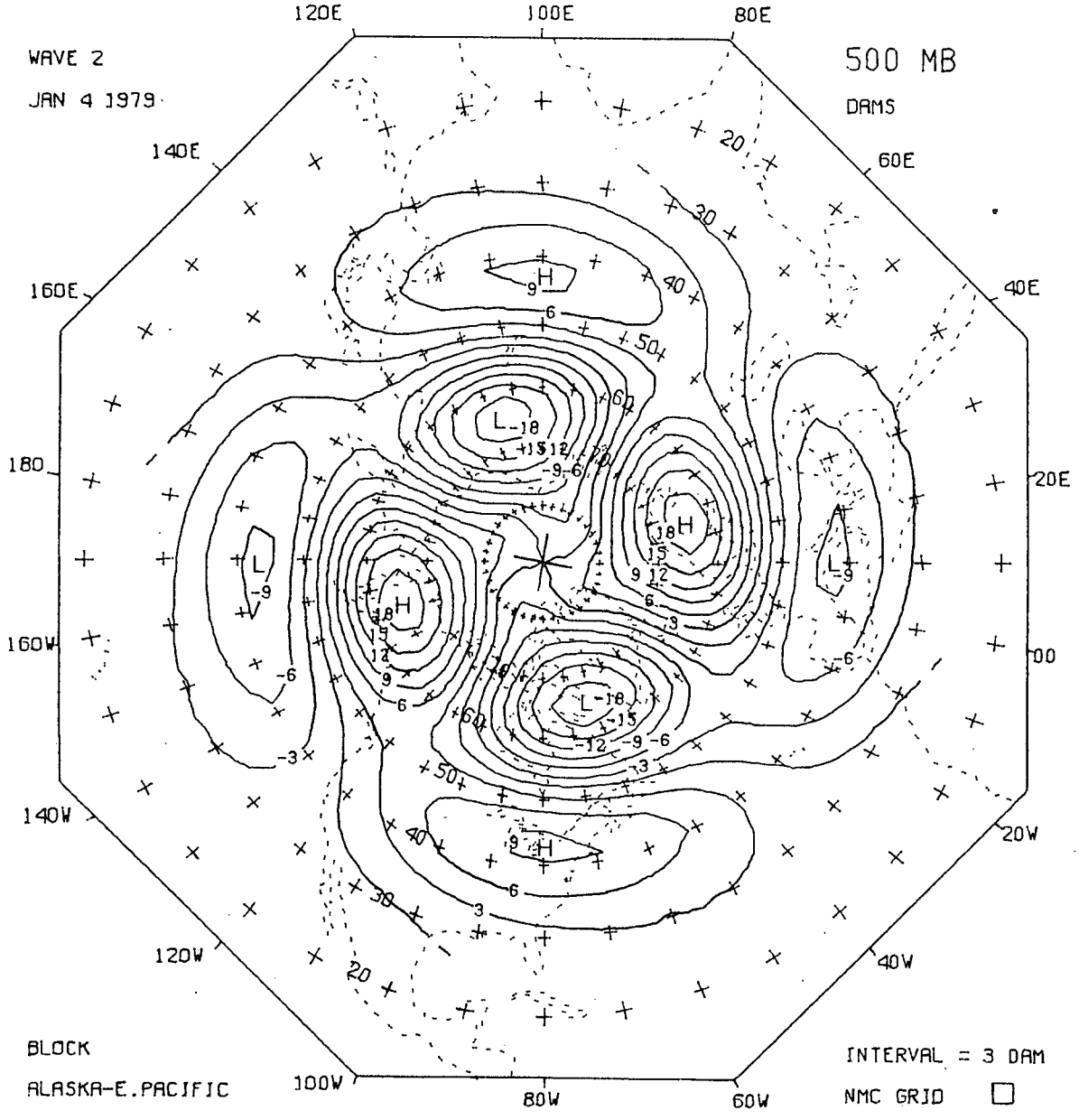

Fig. 7.18 As in Figure 7.17 except for second harmonic (W2)

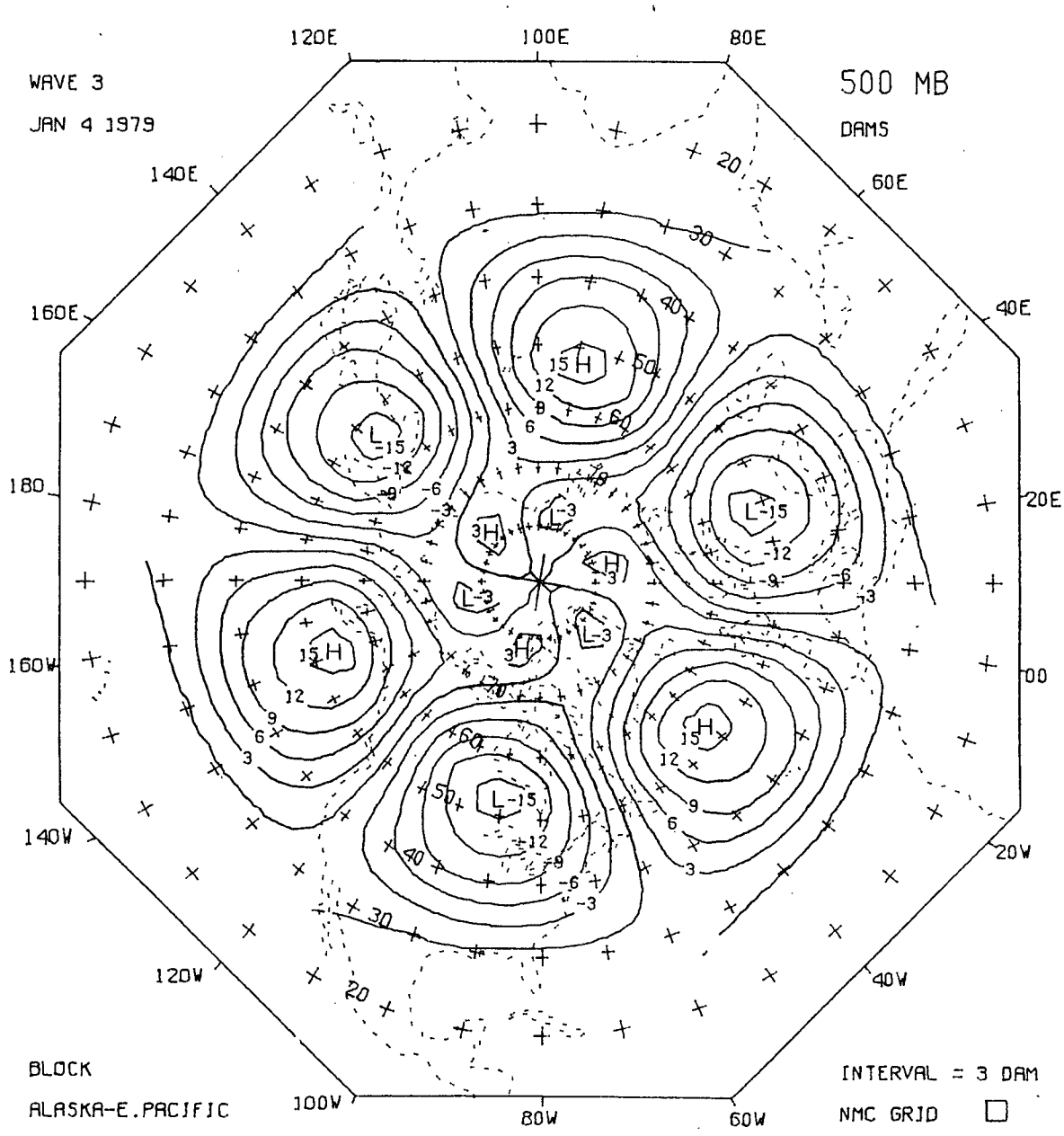

Fig. 7.19 As in Fig. 7.17 except for third harmonic (W3).

TABLE 7.5

Alaska Block Zonal Harmonics 500MB January 4, 1979

			WAVE 1			WAVE 2			WAVE 3			WAVE 4			WAVE 5			WAVE 6		
LAT	AVG	SD	A	φ	S	A	φ	S	A	φ	S	A	φ	S	A	φ	S	A	φ	S
	m	m	m		%	m		%	m		%	m		%	m		%	m		%
85	5184	58	77	- 94	91	21	- 43	7	14	100	3	2	- 79	0	3	- 20	0	1	129	0
80	5140	122	160	- 83	86	46	- 6	7	44	90	6	13	- 71	1	7	- 73	0	0	- 98	0
75	5135	189	245	- 90	84	99	42	14	37	62	2	10	-128	0	6	- 42	0	6	- 49	0
70	5159	220	257	-100	68	168	51	29	28	- 44	1	37	142	1	20	116	0	11	- 27	0
65	5178	210	191	-103	41	206	52	48	65	- 87	5	57	170	4	32	100	1	16	45	0
60	5207	189	110	- 81	17	178	55	44	113	- 97	18	99	-162	14	54	59	4	26	77	1
55	5258	185	82	- 37	10	84	65	10	162	- 95	38	130	-157	25	80	54	9	30	81	1
50	5338	182	80	- 10	10	45	158	3	157	- 92	37	137	-157	28	77	64	9	45	50	3
45	5428	173	83	3	12	90	-165	14	132	- 92	29	109	-148	20	64	84	7	70	23	8
40	5521	160	100	0	20	97	-154	18	102	- 94	20	75	-128	11	42	92	4	82	9	13
35	5626	127	119	- 5	44	60	-144	11	48	- 98	7	51	-106	8	14	144	1	62	0	12
30	5726	86	95	- 12	61	30	-114	6	9	157	1	42	- 62	12	19	-114	3	26	- 7	5
25	5797	62	48	- 15	30	27	- 92	10	22	98	6	39	- 36	20	22	-114	6	9	-141	1

had a bi-cellular structure in the meridional (N - S) plane, and that the eastward motion of the southern cells (centred in the 40°N - 50°N zone) was so much greater relative to the northern (60°N - 70°N) that the maxima and minima were almost in longitudinal opposition by January 4 (Fig. 7.18). Meanwhile Wave 3 amplified almost 'in situ' (140°W - 150°W).

(c) Alaska - NE Pacific Block, January 4, 1979

During the 12-day period to January 4 there has been a major change in the resultant long-wave pattern (Fig. 7.11(c)). At 65°N, W2 has doubled its amplitude (10 to 20 dams) and has become the dominant harmonic (S_2 = 70% by January 6). Constructive interference at 60°N

between W2 ($\phi_2/2 = 153^{o}$W, S_2 = 44%)

and W3 ($\phi_3/3 = 152^{o}$W, S_2 = 18%)

account for the blocking ridge from Alaska southward, paralleling the West Coast of British Columbia. The block occurred in conjunction with an intense low level Arctic air mass which stretched from the Yukon to Colorado and brought record-breaking cold to the mid-west. The frigid outflow to coastal British Columbia froze ponds and rivers and for two weeks a common sight in Vancouver was skating on natural ice!

Note, too, the structure of W1 (Fig. 7.17) and W2 (Fig. 7.18) in the latitude zone 30°N - 40°N across the central Pacific Ocean. Here we find reinforcing minima with W1 playing the dominant role. The constructive interference accounts for the mean E - W oriented trough (Fig. 7.11(c)), a typical concomitant of NE Pacific-Alaska blocking. In the lower latitudes there is a shift of power to higher wave numbers, e.g., S_6 = 13% at 40°N and, moreover, 14% of the total variance is

unaccounted for. At these latitudes, in Winter, additional harmonics (up to W12) must be calculated in order to include the effect of intense baroclinic activity on the variation of 500MB height (Van Mieghem, 1961).

7.5 Summary

We have confirmed that the zonal harmonics of blocking episodes have characteristics related to the region of occurrence. Our results are consistent with those of Austin (1980) who used the particularly apt phrase, "spectral signature", for harmonic distributions peculiar to the blocking category.

It was also noted that regimes of blocking (or, more generally, large amplitude quasi-stationary long waves) can be interrupted swiftly by strong zonal flow featuring a much reduced total wave variance. On such occasions the power, which formerly resided with the low wave number components, is spread more evenly across the spectrum.

Baffin blocking, though a frequent occurrence, is less robust and persistent than blocking over the northern oceans. Its predominant motion is retrograde.

Zonal harmonic analysis of the two-dimensional 500MB circulation of the Northern Hemisphere reveals a wave component structure associated not only with the higher latitude anticyclone but also with the lower latitude cyclonic activity which plays an important role in maintaining the blocking system.

Van Mieghem (1961) stated:

> Average spectral distributions of general circulation parameters should be computed for different world weather types (strong zonal circulation, zonal circulation with strong eccentricity, strong meridional circulation, blocking flow patterns, . . .) and for transition periods between world weather types.

We fully agree and hope that this Chapter contributes in some measure toward such a goal.

CHAPTER 8

RESULTS AND CONCLUSIONS

The objective of this study was to investigate the climatology and certain diagnostics of blocking in the Northern Hemisphere. The data record was January 1, 1946 to February 28, 1979 at the 500MB and 1000MB levels. Data locations were the 1977 grid points of the U.S. National Meteorological Centre octagonal grid. Three different methodologies were employed which required the computation respectively of:

(i) Anomaly Centres of 5-day mean 500MB height (date, location and magnitude)

(ii) Statistical Moments (zero to four) of the frequency distributions of the 5-day mean 500MB, 1000MB, and 1000MB - 500MB thickness at each grid point

(iii) Zonal Harmonics of daily 500MB height for each of seven winters.

The main results and conclusions are as follows.

ANOMALY CENTRES

1. The close relationship between a blocking anticyclone and the associated positive anomaly of 5-day mean 500MB height can be used to advantage for computation of blocking frequency using machine processing methods. Criteria were developed based on season, magnitude of the positive anomaly centre and latitude, which determined with a high degree of probability the existence or otherwise of a blocking anticyclone. Qualifying anomalies were called "blocking signatures." A Catalogue was prepared which identified by date, location and magnitude

every signature that had occurred in the Northern Hemisphere from January 1, 1946 to February 28, 1978.

2. Our geographical distribution by season of blocking signature frequency in the Northern Hemisphere is consistent with published investigations of blocking over the Pacific and Atlantic Oceans and Western Europe. However, our results also reveal an area over the Northeastern Canadian Archipelago (including Baffin Island and Davis Strait) with a much higher frequency of blocking signatures than previous investigations would indicate. The test of an independent sample of blocking signatures by comparison with corresponding daily synoptic analyses confirmed that this was indeed a high frequency blocking region. However, these blocks are usually less robust and persistent (except possibly in the Spring) than occurrences over the oceans.

3. The trajectory of an actual blocking anticyclone is closely related to the corresponding "blocking signature sequence." Displacement criteria were developed to identify these sequences. A Catalogue was prepared listing their attributes including dates of initiation, termination and component signature data.

4. A statistical analysis of within sequence displacements revealed motion tendencies dependent on the region of origin and time of year.

5. There was a marked interannual variation of signature sequences ≥ 2 pentads in duration (i.e., moderate to strong blocking episodes) which suggested a 10 to 15 year cycle. However, it was not possible to draw a statistically valid conclusion due to the size of the sample (33 years) relative to the fluctuation period ($\sim$ one decade).

STATISTICAL MOMENTS

1. The geographical distribution of the statistical moments of the geopotential height continuum were useful in an interpretive sense. Normal and Standard Deviation fields for 5-day mean 1000MB, 500MB and 1000MB - 500MB thickness, revealed the difference in nature of the two maxima of Standard Deviation (WINTER) at 500MB, one over Baffin Island and the other southeast of Greenland. The former derives a larger contribution from variations caused by the incidence of cold lows or warm (mid-troposphere) blocking ridges.

2. Skewness fields (500MB) showed strong, well-defined positive areas in the higher latitudes for WINTER, SPRING and FALL. These identified with some (but not all) areas of blocking signature maxima. Site-specific histograms strongly suggested that the positive skewness was attributable in part to the occasional establishment of blocking regimes in areas of low normal geopotential height.

3. Kurtosis fields (500MB) showed significantly low values in WINTER over the eastern Pacific, the eastern Atlantic and western Europe. These are the regions where ridges begin their northward amplification, sometimes (but not always) terminating in a blocking anticyclone in higher latitudes. Site-specific histograms reinforce the likelihood of the low kurtosis areas indicating bi-modal distributions. Presumably the sub-set with the higher mean would reflect the incidence of ridge amplification.

ZONAL HARMONICS

1. The zonal harmonics (W1 to W6) of the 500MB height profile at 40°N and 60°N, respectively, were computed for each day of seven winters

and their flanking months (i.e., November to March, inclusive). Indices of zonal (U) and meridional (V) components of flow were also computed.

2. It was found that the spatial harmonics of blocking episodes were distinctive to the region in which they occurred. For example, W2 and W3 predominate during blocking over Alaska and the eastern Pacific. In other words, the blocking anticyclone has a spectral signature associated with its regional location. (Our results confirm those of Austin, 1980.)

3. Regimes of blocking may be interrupted swiftly by strong zonal flow featuring a much reduced variance which is more evenly spread across the long-wave spectrum. In a case study (1962-63) the interruptions were strikingly unambiguous, at quasi-periodic intervals (30 to 40 days) and transitory ($\sim$ a few days). The behaviour of the harmonics during the resumption of blocking suggested that 'forced' oscillation components (W2 and W3 in this case) amplify from eddy kinetic energy derived from 'free' oscillation components whose previous amplification derived from major baroclinic development. This example supports a long-standing hypothesis that blocking may be a response to rapid deepening of baroclinic waves.

4. Zonal harmonic analysis of the two-dimensional 500MB circulation of the Northern Hemisphere during typical major blocking episodes reveals wave structures in both higher and lower latitudes with characteristics of motion and growth associated with the total blocking system. This study emphasized the higher latitudes (50°N to 70°N), site of the majority of blocking anticyclone centres when they reach the mature stage. The full zonal analysis of case studies suggest that it

would be profitable to investigate the ensemble characteristics of the lower latitude (30°N to 50°N) harmonics.

5. A recurring theme throughout this study was the Baffin Island Paradox, the intriguing maximum of blocking signatures centred each season in the area of the Normal Baffin trough. The zonal harmonics of 61 episodes of Baffin blocking indicate that the amplitude spectrum was similar to Atlantic blocking (with a westward shift of phase). The majority of Baffin blocks arise from retrograding North Atlantic blocking waves. Their termination is often (but NOT invariably) followed by a re-adjustment of the zonal long-wave pattern featuring the development of an amplified blocking ridge from Alaska southeastward along the West Coast of North America.

The seven winters studied were notable for major blocking episodes. Even so, there was a marked variation in Baffin blocking frequency. This appeared to be related to the predominant characteristic of the winter's blocking regimes. Those with low frequency Baffin blocking featured large amplitude ridges oscillating slowly about their mean winter location. Those with high frequency Baffin blocking featured several occasions of a retrograding amplified long wave train in the higher latitudes out of phase with the lower latitude train. This frequently resulted in the inverted cellular pattern of Fig. 3.4 and a 5 to 10 degree latitude southward displacement of the Baffin Low from its Normal location.

GENERAL

1. The 5-day mean was an effective filter for screening out the higher frequency fluctuations occasioned by mobile synoptic-scale systems

and retaining, without undue attenuation, the majority of the lower frequency phenomena of interest to this study.

2. Another recurring theme was the large proportion ($\simeq$ 80%) of the temporal variation of 500MB height accounted for by the low-frequency fluctuations. This is readily apparent from a comparison between the Standard Deviation field of daily height, Fig. 1.1(b), and of 5-day mean height, Fig. 4.4. In the space domain the long-wave components (1 to 5) accounted for $\geqslant$ 90% of the variance of higher latitude (60°N) circumpolar 500MB gph profiles and $\geqslant$ 80% of lower latitude (40°N).

3. The value of GCM diagnostics was illustrated in Chapter 2 where an example demonstrated the great influence on the general ciculation of large scale mountain systems. The frequency and harmonic analyses of our study reinforce the widely-held hypothesis that the large scale orography of the Northern Hemisphere plays a vital role in the blocking process.

4. Our study has produced a number of spin-offs. The Master Catalogue, an inventory of all positive and negative anomalies of 5-day mean 500MB height in the Northern Hemisphere for the past 33 years, and also the Blocking Signature Sequence Catalogue should be useful sources of information for research in such topics as large scale climatology and medium and long range weather prediction.

5. Finally, we believe that the three avenue approach to our investigation of blocking, namely, Anomaly Frequency, Continuum Statistics and Zonal Harmonics has achieved our objectives and yielded a number of significant results concerning the nature of blocking in the Northern Hemisphere.

REFERENCES

American Meteorological Society (a): Meteorological and Geoastrophysical Abstracts. Rigby, M., Editor.

American Meteorological Society (b), 1974-1979: Weather and Circulation of (Month, Year), Monthly Weather Review, Vol. 102-107 inclusive.

Austin, J.F., 1980: The Blocking of Middle Latitude Westerly Winds by Planetary Waves. Quarterly Journal of the Royal Meteorological Society, 106, 327-350.

Barrett, E.W., 1958: Some Applications of Harmonic Analysis to the Study of the General Circulation. Ph.D. Thesis, Department of Meteorology, University of Chicago, 209 pp.

Baumhefner, D.P. and P. Downey, 1978: Forecast Intercomparisons from Three Numerical Weather Prediction Models. Monthly Weather Review, 106, 1245-1279.

Baur, F., 1958: The Seasonal and Geographic Distribution of Blocking Highs on the Northern Hemisphere to the North of the 50th Parallel in the Period of 1949-1957. Időjárás, 62(2), 73-82.

Berggren, R., B. Bolin and C.-G. Rossby, 1949: An Aerological Study of Zonal Motion, its Perturbation and Break-down. Tellus, 1, 14-37.

Berkofsky, L. and E.A. Bertoni, 1955: Mean Topographic Charts for the Entire Earth. Bulletin of the American Meteorological Society, 36, 350-354.

Blackmon, M.L., 1976: A Climatological Spectral Study of the Geopotential Height of the Northern Hemisphere. Journal of the Atmospheric Sciences, 33, 1607-1623.

Blackmon, M.L., J.M. Wallace, N.-C. Lau and S.L. Mullen, 1977: An Observational Study of the Northern Hemisphere Wintertime Circulation. Journal of the Atmospheric Sciences, 34, 1040-1053.

Bolin, B., 1950: On the Influence of the Earth's Orography on the General Character of the Westerlies. Tellus, 2, 184-195.

Boville, B.W., and M. Kwizak, 1959: Fourier Analysis Applied to Hemispheric Waves of the Atmosphere. CIR-3155 TEC-292, Atmospheric Environment Service, Downsview, Ontario, Canada, 21 pp.

Brezowsky, H., H. Flohn and P. Hess, 1951: Some Remarks on the Climatology of Blocking Action. Tellus, 3, 191-194.

Brooks, C.E.P., and N. Carruthers, 1953: Handbook of Statistical Methods in Meteorology. Her Majesty's Stationery Office, London, England, 412 pp.

Charney, J., 1947: Dynamics of the Long Waves in a Baroclinic Westerly Current. Journal of Meteorology, 4, 135-162.

Crutcher, H.L., and J.M. Meserve, 1970: Selected Level Heights, Temperatures, and Dew-Points for the Northern Hemisphere. NAVAIR 50-1C-52, U.S. Govt. Printing Office, Washington, D.C.

Diehl, L.W., 1977: Dynamics of Baroclinic Waves and Blocking Ridge Development. M.Sc. Thesis, Department of Geography, University of Alberta, 106 pp.

Eady, E.T., 1949: Long Waves and Cyclone Waves. Tellus, 1, 35-52.

Egger, J., 1980: Blocking and Stratospheric Warming. Contrib. Atmos. Phys. (Germany), 53, 172-80.

Eliasen, E., 1958: A Study of the Long Atmospheric Waves on the Basis of Zonal Harmonic Analysis. Tellus, 10, 206-215.

Elliott, R.D., and D.B. Smith, 1949: A Study of the Effects of Large Blocking Highs on the General Circulation in the Northern Hemisphere Westerlies. Journal of Meteorology, 6, 67-85.

Godson, W.L., 1959: The Application of Fourier Analysis to Meteorological Data. CIR-3168 TEC-295, Atmospheric Environment Service, Downsview, Ontario, Canada, 25 pp.

Graham, R.D., 1955: An Empirical Study of Planetary Waves by Means of Harmonic Analysis. Journal of Meteorology, 12, 298-307.

Green, R.A., 1969: The Weather and Circulation of December 1968. Monthly Weather Review, 97, 281-286.

Haltiner, G.J. and F.L. Martin, 1957: Dynamical and Physical Meteorology. McGraw-Hill, 470 pp.

Haltiner, G.J., 1967: The Effect of Sensible Heat Exchange on the Dynamics of Baroclinic Waves. Tellus, 19, 183-198.

Haney, R.L., 1961: Behaviour of the Principal Harmonics of Selected 5-day Mean 500MB Charts. Monthly Weather Review, 89, 391-396.

Hare, F.K., 1968: The Arctic. Quarterly Journal of the Royal Meteorological Society, 94, 439-459.

Haurwitz, B., 1940a: The Motion of Atmospheric Disturbances. Journal of Marine Research, 3, 35-50.

Headquarters, Air Weather Service, 1946-1948: Northern Hemisphere Historical Weather Maps Sea Level and 500 Millibar. Air Weather Service, Washington, D.C.

Holton, J.R., 1979: An Introduction to Dynamic Meteorology. 2nd Ed. Academic Press, New York, 391 pp.

Hovmöller, E., 1949: The Trough-and-Ridge Diagram, Tellus, 1, 62-66.

Jenne, R.L., 1970: The NMC Octagonal Grid, National Centre for Atmospheric Research, Boulder, Colorado.

Jenne, R.L., 1975: Data sets for Meteorological Research, NCAR-TN/IA-111 Atmospheric Technology Division, National Centre for Atmospheric Research, Boulder, Colorado.

Johnson, C.B., 1948: Anticyclogenesis in Eastern Canada during Spring. Bulletin of the American Meteorological Society, 29, 47-55.

Johnson, K., 1978: An Observational Study of Planetary Waves during a Stratospheric Warming. Proceedings of the Twelfth Stanstead Seminar, Dept. of Meteorology, McGill University, Montreal.

Knox, J.L., 1979: Blocking Frequency in the Northern Hemisphere. Unpublished paper presented to the Annual Congress of Canadian Meteorological and Oceanographic Society, May, 1979. (Mimeo, 27 pp).

Knox, J.L., 1981: Master Catalogue of 5-Day Mean 500MB Height Anomaly Centres for the Northern Hemisphere 1946-1978 (to be published).

Labitzke, K., 1978: On the Different Behaviour of the Zonal Harmonic Height Waves 1 and 2 During the Winters 1970/71 and 1971/72. Monthly Weather Review, 106, 1704-1713.

Lahey, J.F., R.A. Bryson, E.W. Wahl, L.H. Horn, and V.D. Henderson, 1958: Atlas of 500MB Wind Characteristics for the Northern Hemisphere. University of Wisconsin Press, Madison, Wisconsin.

Lamb, H.H., 1972: Climate: Present, Past and Future, Vol. 1, Methuen, London, 613 pp.

Lau, N.-C., 1980: Personal Communication.

Madden, R.A., 1976: Estimates of the Natural Variability of Time-averaged Sea-level Pressure. Monthly Weather Review, 104, 942-952.

Mahlman, J.D., 1979: Structure and Interpretation of Blocking Anticyclones as Simulated in a GFDL General Circulation Model. 1979 Stanstead Seminar, Sponsored by McGill University, Montreal, P.Q., Canada.

Moffitt, B.J., and R.A.S. Ratcliffe, 1972: Northern Hemisphere Monthly Mean 500 Millibar and 100-500 Millibar Thickness Charts and some Derived Statistics (1951-1966). Geophysical Memoirs, Vol. 16, Meteorological Office, London, England, 61 pp.

Namias, J., 1950: The Index Cycle and its Role in the General Circulation. Journal of Meteorology, 7, 130-139.

Namias, J., 1958: Synoptic and Climatological Problems Associated with the General Circulation of the Arctic. Transactions American Geophysical Union, 39(1), 45-51.

Namias, J., 1975: Short Period Climatic Variations. Vol. I and II. University of California, San Diego. 648 pp.

Namias, J., 1978: Multiple Causes of the North American Abnormal Winter 1976-77. Monthly Weather Review, 106, 279-295.

Namias, J., and P.F. Clapp, 1944: Studies of the Motion and Development of Long Waves in the Westerlies. Journal of Meteorology, 1, 55-77.

Namias, J., and P.F. Clapp, 1951: Observational Studies of General Circulation Patterns. Compendium of Meteorology, Meteorological Society, 551-567.

O'Connor, J.F, 1964: Hemispheric Distribution of 5-day Mean 700MB Circulation Centres. Monthly Weather Review, 92, 303-315.

O'Connor, J.F., 1966: Catalogue of 5-day Mean 700MB Height Anomaly Centres 1947-1963 and Suggested Applications. Technical Memorandum 37, 63 pp. National Meteorological Centre, Washington, D.C.

O'Connor, J.F., 1969: Hemispheric Teleconnections of Mean Circulation Anomalies at 700 Millibars. ESSA Technical Report WB 10, 103 pp. National Meteorological Centre, Silver Spring, Maryland.

Palmen, E. and K.M. Nagler, 1949: The Formation and Structure of a Large-scale Disturbance in the Westerlies. Journal of Meteorology, 6, 227-242.

Palmen, E. and C.W. Newton, 1969: Atmospheric Circulation Systems - Their Structure and Physical Interpretation. Academic Press, New York, 603 pp.

Panofsky, H.A. and G.W. Brier, 1968: Some Applications of Statistics to Meteorology. The Pennsylvania State University.

Perry, J.D., 1979: Address to Specialist Group on Dynamical Problems, Atmospheric Blocking: Meeting - September 1979. Weather, 35, 148-152.

Petterssen, S., 1956: Weather Analysis and Forecasting, Vol. I, McGraw-Hill, 428 pp.

Quiroz, R.S., 1979: Tropospheric-Stratospheric Interaction in the Major Warming Event of January-February 1979. Geophysical Research Letters, 6, 645-648.

Rex, D.F., 1950a: Blocking Action in the Middle Troposphere and its Effect upon Regional Climate (I): An Aerological Study of Blocking. Tellus, 2, 196-211.

Rex, D.F., 1950b: Blocking Action in the Middle Troposphere and its Effect upon Regional Climate, II: The climatology of Blocking. Tellus, 2, 275-301.

Rossby, C.-G., 1939: Relations between Variations in the Intensity of the Zonal Circulation and the Displacements of the Semi-permanent Centres of Action. Journal of Marine Research, 2, 38-55.

Rossby, C.-G., 1940: Planetary Flow Patterns in the Atmosphere. Quarterly Journal of the Royal Meteorological Society, 66, Supplement, 68-87.

Sawyer, J.S., 1970: Observational Characteristics of Atmospheric Fluctuations with Time Scale of a Month. Quarterly Journal of the Royal Meteorological Society, 96, 610-625.

Serebreny, S.M., E.J. Weigman and R.G. Hadfield, 1961: Jet Stream Climatology at 500MB North of 50°N. U.S. Navy Weather Research, NWRF 20-00661-045, 138 pp.

Smagorinsky, J., 1972: The General Circulation of the Atmosphere. Meteorological Challenges: A History. Ed. D.P. McIntyre. Information Canada, Ottawa, 338 pp.

Somerville, R.C.J., 1980: Tropical Influences on the Predictability of Ultralong Waves. Journal of the Atmospheric Sciences, 37, 1141-1156.

Sumner, E.J., 1954: A Study of Blocking in the Atlantic-European Sector of the Northern Hemisphere. Quarterly Journal of the Royal Meteorological Society, 80, 402-416.

Sumner, E.J., 1959: Blocking Anticyclones in the Atlantic-European Sector of the Northern Hemisphere. Meteorological Magazine, 88, 300-311.

Taljaard, J.J., H. Van Loon, H.L. Crutcher and R.L. Jenne, 1969: Climate of the Upper Air, Vol. I. Charts of Monthly Mean Pressure, Temperature, Dew Point and Geopotential in the Southern Hemisphere. NAVAIR 50-IC-55. Off. Chief of Naval Ops., Washington, D.C.

Taubensee, R.E., 1979: Weather and Circulation of December 1978. Monthly Weather Review, 107, 354-360.

Treidl, R.A., E.C. Birch and P. Sajecki, 1980a: Blocking in the Northern Hemisphere: A Climatological Study. Submitted to ATMOSPHERE-OCEAN (1980).

Treidl, R.A., E.C. Birch and P. Sajecki, 1980b: A Catalogue of Northern Hemisphere Blocking Situations for the Period 1945-1977. Atmospheric Environment Service, Downsview, Ontario, Canada (to be published).

Tung, K.K., 1977: Stationary Atmospheric Long Waves and the Phenomenon of Blocking and Sudden Warming. Ph.D. Thesis, Harvard University, 222 pp.

U.S. Department of Commerce, 1954-1973: Weather and Circulation of (Month, Year). Monthly Weather Review, Vol. 82-101, inclusive.

U.S. Department of Commerce, 1949-1956: Daily Series Synoptic Weather Maps, Northern Hemisphere Sea Level and 500 Millibar Charts, U.S. Weather Bureau, Washington, D.C.

Van Mieghem, J., 1961: Zonal Harmonic Analysis of the Northern Hemisphere Geostrophic Wind Field. Union Géodisique et Géophysique Internationale, Monographie 8, Paris, 57 pp.

Wagner, A.J., 1979: Weather and Circulation of January 1979. Monthly Weather Review, 107, 499-506.

White, G.H., 1980: Skewness, Kurtosis and Extreme Values of Northern Hemisphere Geopotential Heights. Monthly Weather Review, 108, 387-401.

White, W.B., and N.E. Clark, 1975: On the Development of Blocking Ridge Activity over the Central North Pacific. Journal of Atmospheric Science, 32, 489-502.

Woffinden, C.M., 1960: Blocking Action. Meteorological Magazine, 89, 236-240.

Yeh, T.-C., 1949: On Energy Dispersion in the Atmosphere, Journal of Meteorology, 6, 1-16.

APPENDICES

Arrangement and Purpose

Appendices are numbered according to the Chapter to which they apply. Subsections and Figures number consecutively from the beginning of each Appendix.

The material includes derivations of results presented in the text; procedural details for testing criteria; adjunct sets of diagrams; and other supporting documentation.

The Hovmöller diagrams presented in Appendix VII - 1 (Figs. VII - 1 and 2) are integral to Sections 7.3.3 and 7.4.3 of Chapter 7. The Normal Harmonics for 500MB - Winter, Figs. VII - 3 to 6, inclusive, provide a complete set W1 to W4, of which W2 was presented as an example in Fig. 7.3.

APPENDIX I

I - 1. Conventions adopted in this thesis regarding terms with possible ambiguous meaning and regarding abbreviations.

NORMAL

The average value of a variable, taken over a sufficient period of time that it can be accepted as a mean for climatological purposes. Thus, the Normal distribution of 500MB height for the Winter.

GAUSSIAN

Because of the above use of the word "normal," the alternative, Gaussian, will be used to refer to a distribution which is statistically normal.

HEIGHT (of a constant pressure surface)

Abbreviation for "geopotential height" (gph). The geopotential Φ of unit mass of air at geometric height z is equal to the work required to raise the mass to that height from sea level.

$$\Phi = \int_0^z g dz$$

The "geopotential height" Z is the height of a given level in the atmosphere in units proportional to the geopotential energy of unit mass at that level.

$$Z = \frac{1}{980} \int_0^z g dz = \frac{\Phi}{g}$$

Z and z are interchangeable for most meteorological purposes.

APPENDIX II

II - 1. The Motion of Planetary Waves.

Assume a homogeneous incompressible fluid on a rotating sphere and a uniform non-divergent zonal flow. If the flow is perturbed, the inertial response of the fluid to the varying Coriolis Force will generate a planetary (or Rossby) wave.

The equations of motion are:

$$\frac{du}{dt} - fv = -\frac{\partial \Phi}{\partial x} \qquad \text{(II - 1)}$$

$$\frac{dv}{dt} + fu = -\frac{\partial \Phi}{\partial y} \qquad \text{(II - 2)}$$

where Φ = geopotential.

For horizontal non-divergent motion:

$$\frac{\partial u}{\partial x} + \frac{\partial v}{\partial y} = 0 \qquad \text{(II - 3)}$$

Therefore $\frac{d}{dt}(\zeta + f) = 0$

where ζ = relative vorticity = $\frac{\partial v}{\partial x} - \frac{\partial u}{\partial y}$

and f = planetary vorticity = $2\Omega \sin\phi$

Therefore $\zeta + f$ = constant (II - 4)

i.e., the absolute vorticity is conserved.

If the zonal flow has a mean speed U and the perturbation is (u', v')

$$u = U + u' \qquad v = v'$$

Now, define a stream function ψ such that

$$u' = -\frac{\partial\psi}{\partial y} \qquad\qquad v' = \frac{\partial\psi}{\partial x}$$

Then $\zeta' = \frac{\partial v'}{\partial x} - \frac{\partial u'}{\partial y} = \nabla^2\psi$

and from (II - 4)

$$\left(\frac{\partial}{\partial t} + U\frac{\partial}{\partial x}\right)\nabla^2\psi + \beta\frac{\partial\psi}{\partial x} = 0 \qquad \text{(II - 5)}$$

This wave equation will be satisfied

by $\psi = Ae^{ik(x-ct)}\cos my$

$$\text{if } c = U - \frac{\beta}{k^2 + m^2} \qquad \text{(II - 6)}$$

If $m = 0$ (no wave component along meridians)

$$\text{then } c = U - \frac{\beta}{k^2} = U - \beta\left(\frac{L}{2\pi}\right)^2 \qquad \text{(II - 7)}$$

Thus all planetary waves move west <u>relative to the zonal flow</u> and the longer the wave length the greater the retrogressive speed.

A wave will become stationary <u>relative to the surface</u> if

$$L = 2\pi\sqrt{\frac{U}{\beta}}$$

II - 2. The Response of Large-scale Waves to Advection of Relative and Planetary Vorticity.

To isolate the principle under discussion we assume an incompressible non-divergent barotropic atmosphere, and that the field of geopotential height at 500MB is described by the wave form

$$\Phi = F(t) \sin kx \sin ly$$

where the wave numbers k and l are defined as $k = \frac{2\pi}{L_x}$ $\quad l = \frac{2\pi}{L_y}$

Then, following Holton (1979) it can be shown that

$$\nabla^2\left(\frac{\partial\Phi}{\partial t}\right) \simeq -(k^2 + l^2)\frac{\partial\Phi}{\partial t}$$

But $\quad \frac{\partial}{\partial t}\nabla^2\Phi = -f_o\vec{V}_g \cdot \nabla\left(\frac{1}{f_o}\nabla^2\Phi + f\right)$

Therefore $\quad \frac{\partial\Phi}{\partial t} = K\vec{V}_g \cdot \nabla(\zeta_g + f) \qquad$ (II - 8)

where K is a positive constant

$\zeta_g = \frac{1}{f_o}\nabla^2\Phi$ is the relative vorticity

f is the planetary vorticity

$\frac{\partial\Phi}{\partial t}$ is the local tendency.

In Fig. II - 1 there is depicted at time t a schematic of the Φ-field, of the associated ζ-field, and of the f-field.

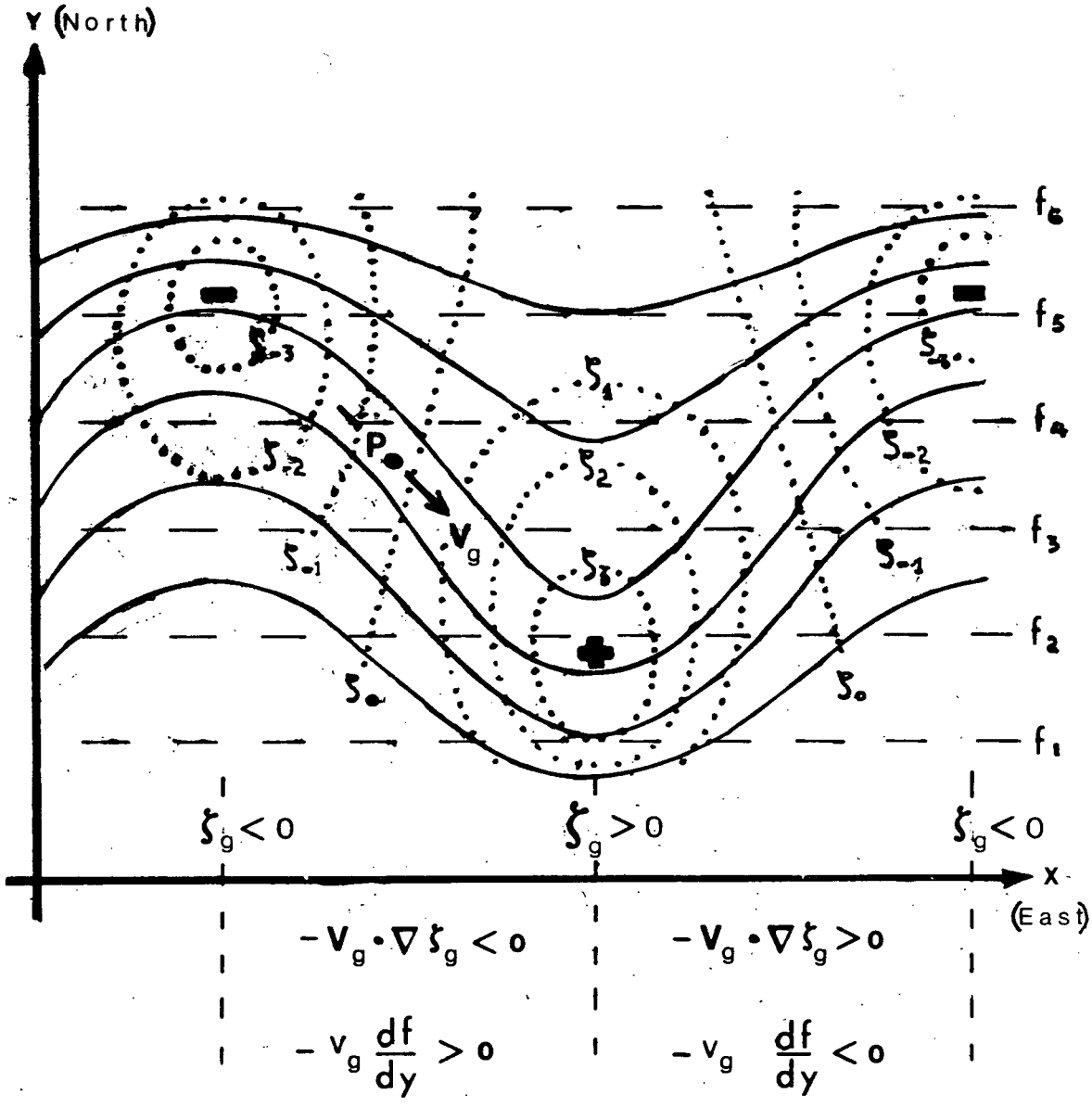

Fig. II-1 Schematic 500MB height and vorticity fields showing regions of planetary and relative vorticity advection.

——— Wave form of Φ

— — — Lines of constant planetary vorticity.

.....Lines of constant relative vorticity.

(Adapted from Holton, 1979.)

East of the ridge line and west of the trough line, e.g., at point P, $\nabla\zeta > 0$ along the flow so that $\vec{V}_g \cdot \nabla\zeta > 0$. Therefore this term contributes to <u>an increase of Φ with time</u>.

Also, at P, $\nabla f = \frac{\partial f}{\partial y}\vec{j}$

where $\vec{j}$ is a unit vector pointing north,

and $\frac{\partial f}{\partial y} > 0$. But the y-component of $\vec{V}_g < 0$ and therefore $\vec{V}_g \cdot \nabla f < 0$.

Hence this term contributes to a <u>decrease of Φ with time</u>. Thus the advection of relative vorticity over P will cause an increase of Φ and tend to make the ridge progressive, while advection of planetary vorticity will tend to make the ridge retrograde.

In the higher latitudes the large-scale pressure systems (warm blocking highs, cold quasi-stationary lows) tend to have relative vorticity isopleths parallel to the stream flow and therefore relative vorticity advection is small, at least near the core. On the other hand, the planetary effect is large and hence they often retrograde.

APPENDIX III

III - 1. Analytic Discussion of the Anomaly Field

Consider the field:

$$Z = -a_2 y + a_3 \sin kx \sin my$$

At a maximum or minimum (e.g., centre of high or low)

$$\frac{\partial Z}{\partial x} = ka_3 \cos kx \sin my = 0$$

and $$\frac{\partial Z}{\partial y} = -a_2 + ma_3 \sin kx \cos my = 0$$

Figure III - 1 shows 2 orthogonal cross-sections xOz and y'O'z' through a maximum.

For any given value of y, if $\frac{\partial Z}{\partial x} = 0$, then

$x = \pi/2k,\ 3\pi/2k,\ .\ .\ .\ (2n+1)\pi/2k,\ .\ .\ .$

Now fix x at one of these values, say, $x = \pi/2k$ and consider the variation of Z in the z'y' plane:

$$\frac{\partial Z}{\partial x} = -a_2 + ma_3 \cos my = 0$$

Therefore $y = \frac{1}{m} \cos^{-1}\left(\frac{1}{m}\frac{a_2}{a_3}\right)$

(i) If $a_2 = 0$, then $y = \pi/2m,\ 2\pi/2m,\ .\ .\ .\ n\pi/2m,\ .\ .\ .$

(ii) If $a_2 = ma_3$, then $y = 0,\ a\pi/m,\ .\ .\ .\ n\pi/m,\ .\ .\ .$

and therefore the number of maxima and minima is reduced by one half.

(iii) If $a_2 > ma_3$, then $\cos^{-1} \frac{1}{m}(\frac{a_2}{a_3})$

is indeterminate and there can be no maxima or minima.

The functions $\bar{Z}$, Z and therefore $Z - \bar{Z}$ may be varied at will by assigning values to a_1, a_2, a_3, k and m. Patterns can be made even more realistic if the linear term $-a_2y$ is replaced by a cubic $-a_4y^3$. This will determine a parabolic N-S profile for the "instantaneous" zonal wind because

$$\frac{\partial Z}{\partial y} = -3a_4y^2$$

To simulate phase shift with latitude the function sin my may be generalized to $\sin[my + \phi(y)]$.

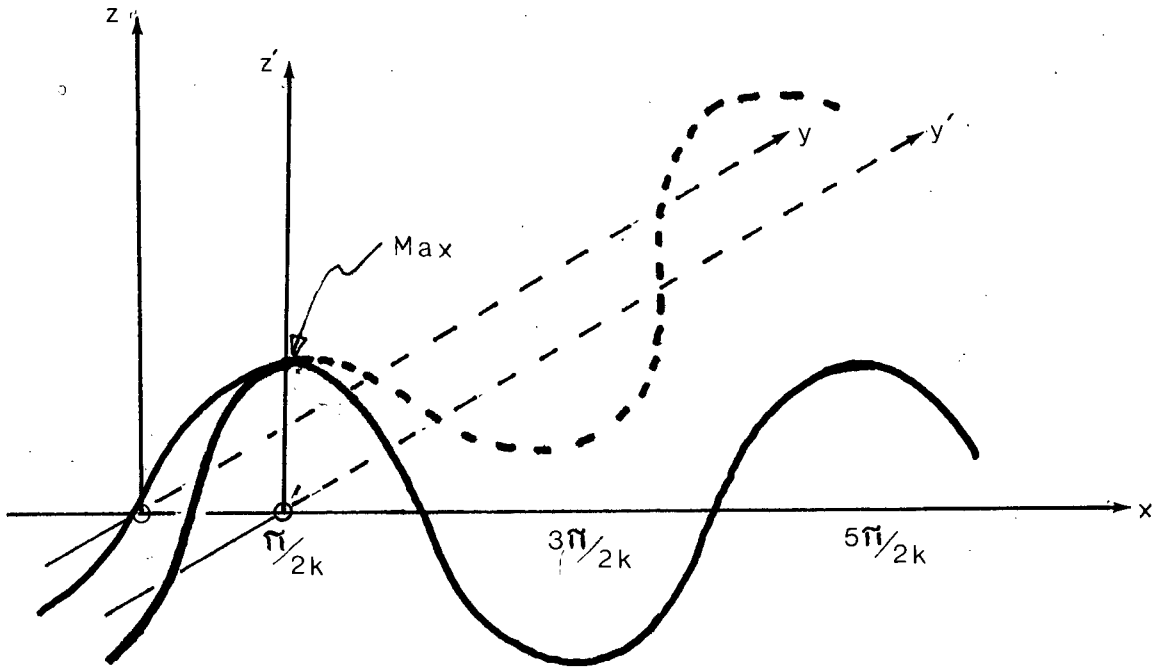

Fig. III-1 Orthogonal cross-sections xOz and y'O'z' through a maximum of Z(x,y).

APPENDIX IV

IV - 1. To Develop a Filter Function Which Illustrates the Effect of the 5-day Average

Let geopotential height profile around a given latitude be $Z(\lambda,t)$

Resolve into harmonics

$$Z_k(\lambda,t) = A_k \cos(k\lambda - \omega_k t)dt$$

where k = wave number

λ = longitude

A_k = amplitude

ω_k = angular frequency (day^{-1})

Assume that wave components move with constant speed which will be $\frac{\omega_k}{k}$, that they maintain constant amplitude A_k, and that the initial phase angle is zero:

Let averaging interval = T days

Then the time mean of $Z_k(\lambda,t)$ is

$$\overline{Z}_k(\lambda,t) = \frac{1}{T}\int_0^T Z_k(\lambda,t)dt = \frac{1}{T}\int_0^T A_k \cos(k\lambda - \omega_k t)dt$$

$$\text{Therefore } \overline{Z}_k = -\frac{A_k}{\omega_k T}\int_0^T \cos(k\lambda - \omega_k t)d(k\lambda - \omega_k t)$$

$$= -\frac{A_k}{\omega_k T}\Big[\sin(k\lambda - \omega_k t)\Big]_0^T$$

$$= -\frac{A_k}{\omega_k T}\Big[\sin(k\lambda - \omega_k T) - \sin k\lambda\Big]$$

$$= -\frac{A_k}{\omega_k T}\left[\sin k\lambda \cos \omega_k T - \cos k\lambda \sin \omega_k T - \sin k\lambda\right]$$

$$= \frac{A_k}{\omega_k T}\left[\sin \omega_k T \cos k\lambda + (1 - \cos \omega_k T)\sin k\lambda\right]$$

Now, let the amplitude of $\bar{z}_k = \bar{A}_k$

Then, $\bar{A}_k = \frac{A_k}{\omega_k T}\left[\sin^2\omega_k T + (1 - \cos \omega_k T)^2\right]^{1/2}$

$$= \frac{\sqrt{2}\, A_k}{\omega_k T}\left(1 - \cos \omega_k T\right)^{1/2}$$

and $\frac{\bar{A}_k{}^2}{A_k{}^2} = \frac{2(1 - \cos \omega_k T)}{\omega_k{}^2 T^2}$

Let μ_k = phase speed (in rads long. day^{-1})

Then $\mu_k = \frac{\omega_k}{k}$

Also, let the averaging interval be 5 days.

Then $R_k = \frac{\bar{A}_k{}^2}{A_k{}^2} = \frac{2(1 - \cos 5k\mu_k)}{(5k\mu_k)^2}$

where R_k is the response function.

<u>Examples</u>

If $k = 1$ and $\mu_k = 0.087^r\text{day}^{-1}$ $\quad R_k = 0.99$

If $k = 4$ and $\mu_k = 0.087^r\text{day}^{-1}$ $\quad R_k = 0.78$

(A phase speed of $.087^r$ day $^{-1}$ is equivalent to 5 degree day^{-1}, a fairly typical long wave speed).

If k = 8 and $\mu_k = 0.174^r$ day^{-1} $R_k = 0.01$

If k = 12 and $\mu_k = 0.174^r$ day^{-1} $R_k = 0.03$

Thus wave components in the 'long-wave' category moving at characteristic speeds (0 to 5 degree longitude day^{-1}) will be passed at between 80% and 100% of the original amplitude. Components with speeds characteristic of mobile baroclinic waves in the mid-latitudes will be almost entirely attenuated.

The filter function is shown in Fig. 4.0.

IV - 2. Guidelines for Identification of a Blocking Episode

A. Necessary and Sufficient (This Study)

1. The 500MB analyses are used exclusively.
2. There must be a disruption in the pre-existing zonal flow by a pattern resembling one of Sumner's six classifications (see 3.2).
3. During the 5-day period of the positive anomaly being tested, an anticyclonic centre must be observed on at least three of the five consecutive daily 500MB analyses.
4. The centre of the anticyclone must be north of 45^oN.

B. Sufficient (Treidl et al, 1980a)

"1. Closed isopleths must be present simultaneously in the surface and 500MB charts, splitting the westerly current aloft into two branches.

2. The latitude belt where the high occurs extends northward from 35°N.

3. The minimum duration of the high must be five days."

IV - 3. Procedure for Determination of Blocking Signature Criteria

A. Select a large sample of positive anomalies from the Catalogue and list year, pentad, position and magnitude in chronological order on a Master Sheet.

B. From an information source (e.g., published charts of daily 500MB height analyses for the Northern Hemisphere, or the Monthly Weather Review) and by applying the guidelines of Section 4.5.1.2, determine if, in fact, a blocking episode was in progress at the time of and in the region of a specific listed anomaly. Enter the particulars on a Master Sheet.

C. Divide the cases into four seasonal sets.

D. Plot:

Anomaly Magnitude (dams)

vs

Anomaly Latitude (degrees)

and mark the point ● if the anomaly was associated with a contemporaneous block and ○ if it was not.

E. Draw a curve separating the ●'s from the ○'s.

F. The results for WINTER and SUMMER are shown in Figs. 4.3(a) and 4.3(b), respectively.

PENTAD CALENDAR

WINTER		SPRING		SUMMER		FALL	
PE	Interval	PE	Interval	PE	Interval	PE	Interval
68	Dec02 - Dec06	13	Mar02 - Mar06	32	Jun05 - Jun09	50	Sep03 - Sep07
69	Dec07 - Dec11	14	Mar07 - Mar11	33	Jun10 - Jun14	51	Sep08 - Sep12
70	Dec12 - Dec16	15	Mar12 - Mar16	34	Jun15 - Jun19	52	Sep13 - Sep17
71	Dec17 - Dec21	16	Mar17 - Mar21	35	Jun20 - Jun24	53	Sep18 - Sep22
72	Dec22 - Dec26	17	Mar22 - Mar26	36	Jun25 - Jun29	54	Sep23 - Sep27
73	Dec27 - Dec31	18	Mar27 - Mar31	37	Jun30 - Jul04	55	Sep28 - Oct02
1	Jan01 - Jan05	19	Apr01 - Apr05	38	Jul05 - Jul09	56	Oct03 - Oct07
2	Jan06 - Jan10	20	Apr06 - Apr10	39	Jul10 - Jul14	57	Oct08 - Oct12
3	Jan11 - Jan15	21	Apr11 - Apr15	40	Jul15 - Jul19	58	Oct13 - Oct17
4	Jan16 - Jan20	22	Apr16 - Apr20	41	Jul20 - Jul24	59	Oct18 - Oct22
5	Jan21 - Jan25	23	Apr21 - Apr25	42	Jul25 - Jul29	60	Oct23 - Oct27
6	Jan26 - Jan30	24	Apr26 - Apr30	43	Jul30 - Aug03	61	Oct28 - Nov01
7	Jan31 - Feb04	25	May01 - May05	44	Aug04 - Aug08	62	Nov02 - Nov06
8	Feb05 - Feb09	26	May06 - May10	45	Aug09 - Aug13	63	Nov07 - Nov11
9	Feb10 - Feb14	27	May11 - May15	46	Aug14 - Aug18	64	Nov12 - Nov16
10	Feb15 - Feb19	28	May16 - May20	47	Aug19 - Aug23	65	Nov17 - Nov21
11	Feb20 - Feb24	29	May21 - May25	48	Aug24 - Aug28	66	Nov22 - Nov26
12	Feb25 - Mar01	30	May26 - May30	49	Aug29 - Sep02	67	Nov27 - Dec01
		31	May31 - Jun04				

Season	Total Pentads
WINTER = PE 68 - PE 12	18
SPRING = PE 13 - PE 31	19
SUMMER = PE 32 - PE 49	18
FALL = PE 50 - PE 67	18
YEAR = PE 1 - PE 73	73

Note: For Leap Year PE 12 contains 6 days.

Fig. IV - 1. The Pentad Calendar

APPENDIX V

V - 1. Smoothing of Areal Frequency Isopleths

Figs. 5.1 to 5.5, inclusive

The positive anomaly centres, from which the blocking signatures were selected, were located by a search program to the nearest grid point I,J. It was obvious from a few trial plots of the frequency isopleths that this procedure introduced an artificial 'clustering' at certain grid-points. That is to say, there was a frequency gradient between adjacent grid points which was unjustified by the spacing of upper air stations.

Therefore the field was slightly smoothed as in Fig. V - 1

$$\overline{F}_C = \frac{1}{8}(4F_C + F_A + F_B + F_D + F_E)$$

Where F_C = Initial Frequency at point C

F_A = Frequency at Point A

F_B = Frequency at Point B

F_D = Frequency at Point D

F_E = Frequency at Point E

V - 2. Nomenclature

Master Catalogue	The Catalogue identifying all positive and negative Anomaly Centres of 500MB 5-day average height fields. (Fig. 4.2).

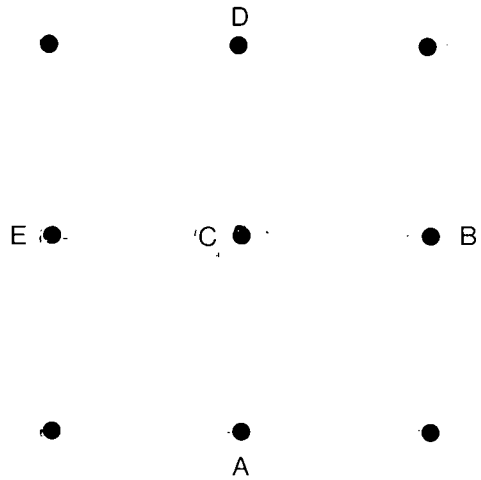

$$\bar{F}_c = \frac{1}{8}\left(4F_c + F_a + F_b + F_d + F_e\right)$$

Fig. V-1 Smoothing function used in the construction of frequency fields Fig. 5.1 to 5.5 inclusive.

Blocking Signature Catalogue	The Catalogue identifying all positive Anomaly Centres in the MASTER Catalogue which satisfied Criterion (3). (Fig. 4.8)
Blocking Signature Sequence Catalogue	The Catalogue which sorts the Signatures into Sequences using Criterion (4). (Fig. 5.11)
SIG	Any positive anomaly listed in the Blocking Signature Catalogue
SEQ	Any Sequence listed in the Blocking Signature Sequence Catalogue
SEQ_1	Sequence consisting of <u>only</u> 1 SIG
SEQ_n	Sequence consisting of <u>more than</u> 1 SIG
K.BLK	A blocking episode identified from daily analyses by KNOX guidelines, APPENDIX IV - 2
T.BLK	A blocking episode identified from daily analyses by TREIDL guidelines, APPENDIX IV - 2
PREDICTAND	Identification of blocking episode (by unspecified source) by date, location and duration of actual block from daily analyses.
PREDICTOR	Identification of SIG and SEQ from Catalogue and relevant data

V - 3. Test of Blocking Signatures and Sequences

1. This is a test of Blocking Signatures and Sequences to determine:

   (a) The success ratio for SIG components of SEQ's. How often are they related to a 5-day period of a blocking episode?

(b) The success ratio for SEQ's with respect to blocking episodes.

2. The independent data periods are June - November 1955, March - June 1956 and January, February and December 1952.

3. Let us designate the data related to the actual blocking episode as the PREDICTANDS and the data related to the SIGS and SIG. SEQ's as the PREDICTORS.

   Then the source of the PREDICTANDS was the Northern Hemisphere 500MB Daily Analyses and the source of the PREDICTORS was the Blocking Signature Sequence Catalogue.

4. The period chosen provides independent data because it was not used to determine the threshold Criterion (3).

5. Go to the Blocking Signature Sequence Catalogue and, for that period,

   List each SEQ on a Master Sheet by

   (a) PE number of each component SIG

   (b) Starting date and location

   (c) Ending date and location

   (d) Maximum amplitude reached (dams)

6. For each SEQ examine corresponding 500MB daily height analyses and determine whether or not a related blocking anticyclone existed during each SIG pentad.

   Use guidelines in Appendix IV - 1, KNOX

   Enter (under K.BLK) Yes ● No ○

7. Consult an independent Catalogue of blocking in the Northern Hemisphere (we used Treidl et al., 1980b) and proceed as in 6.

   Enter (under T.BLK) Yes ● No ○

8. Enter comments concerning breaks in continuity of blocking episode during a SEQ, degree of confidence in block identification, occurrence north or south of 75°N.
9. Count all SIG's which occurred in period corresponding to SEQ_1, SEQ_n and SEQ. Let number = N_1, N_n and N.
10. Success ratio SIG's = $\frac{K.BLKS}{N}$
11. Proceed as in 10. for SEQ's.
12. For results see Table III of the main text.

V - 4. Retrograde Atlantic Blocking as Revealed by a Blocking Signature Sequence

Fig. V - 2 illustrates how a blocking signature sequence identified the wave of blocking which retrogressed from Scandinavia to Baffin Island December 16-31, 1976. The motion of individual daily 500MB anticyclone centres (shown as 12-hour displacement vectors) was erratic. Nevertheless, the vectors appear to be grouped in three areas, the first over Northern Scandinavia (December 16-20), the second over Greenland-Iceland (December 19-28) and the third over Baffin Island-Davis Strait (December 29-31). The adjustment in the mass field, December 19-20, was a striking example of "discontinuous retrogression." Note how the seat of blocking activity was transferred rapidly upstream from the Gulf of Finland to the East coast of Greenland. The vector clusters are reflected by Signatures A, B and C, respectively, and the retrograding blocking wave is associated with the westward signature motion. The Hovmöller (time-longitude) diagram for 500MB gph, 50-70°N (not shown), clearly confirms the retrograde motion.

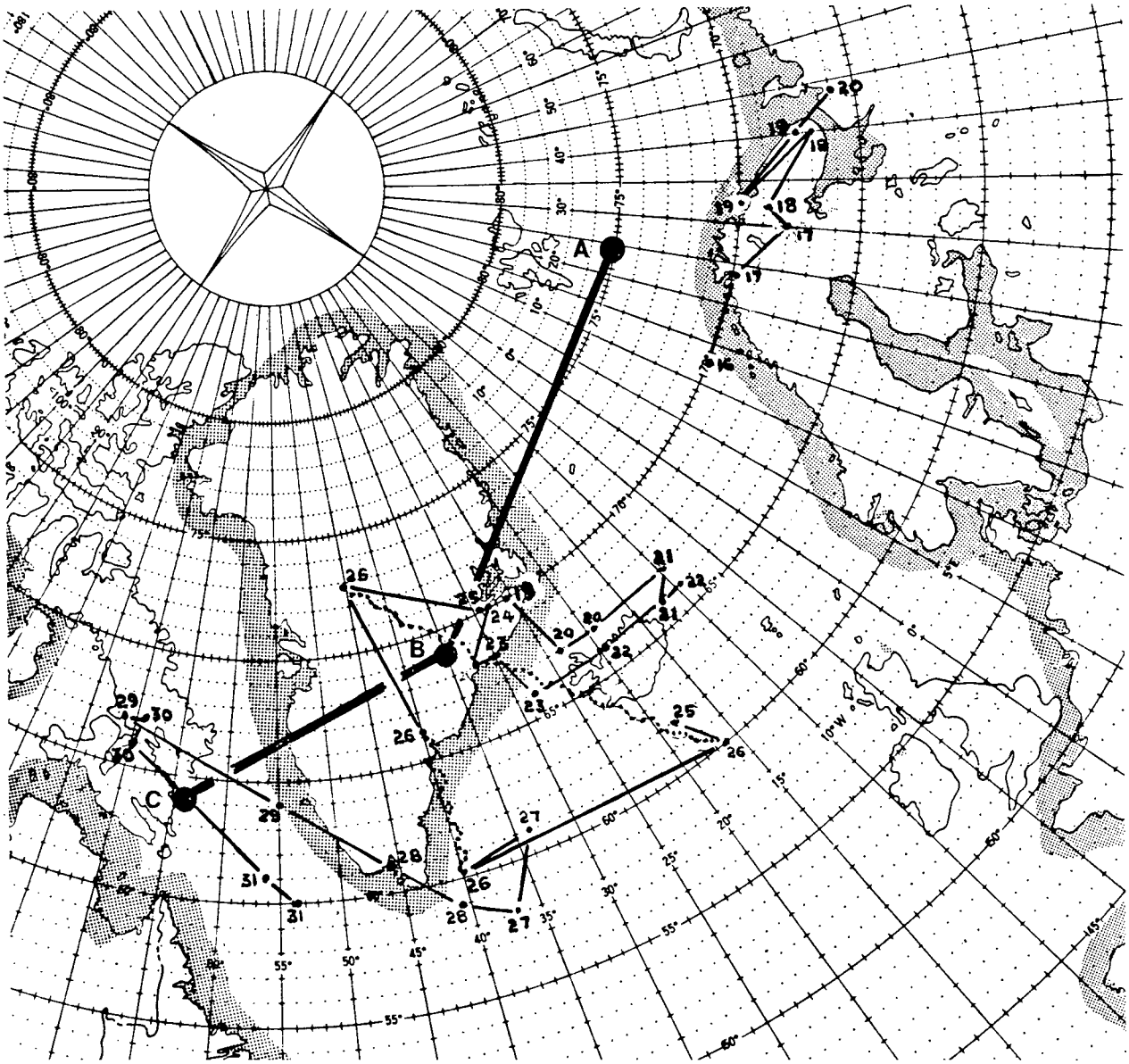

Fig. V-2 Identification of a retrograding North Atlantic Block by a Blocking Signature Sequence.

Period was 1200Z Dec. 16 to 1200Z Dec. 31, 1976.

•———• 12 - hour displacement of 500MB anticyclone centre. (Canadian Meteorological Centre).

•·····• Simultaneous centre-pair along ridge line.

●———● 5 - day displacement of positive anomaly centres (blocking signatures) for:

A	Pentad 71	December 17 - 21
B	Pentad 72	December 22 - 26
C	Pentad 73	December 27 - 31

Note discontinuous retrogression which occurred December 19th and 20th.

V - 5. Frequency Distributions for Starting and Ending Signatures during SUMMER, FALL and WINTER

The following series of Figures (V - 3 to V - 8) taken together with Figs. 5.13 to 5.16 of the main text provide a complete set by season, and by year, of Frequency Distributions for Starting and Ending Signatures. (See Chapter 5.)

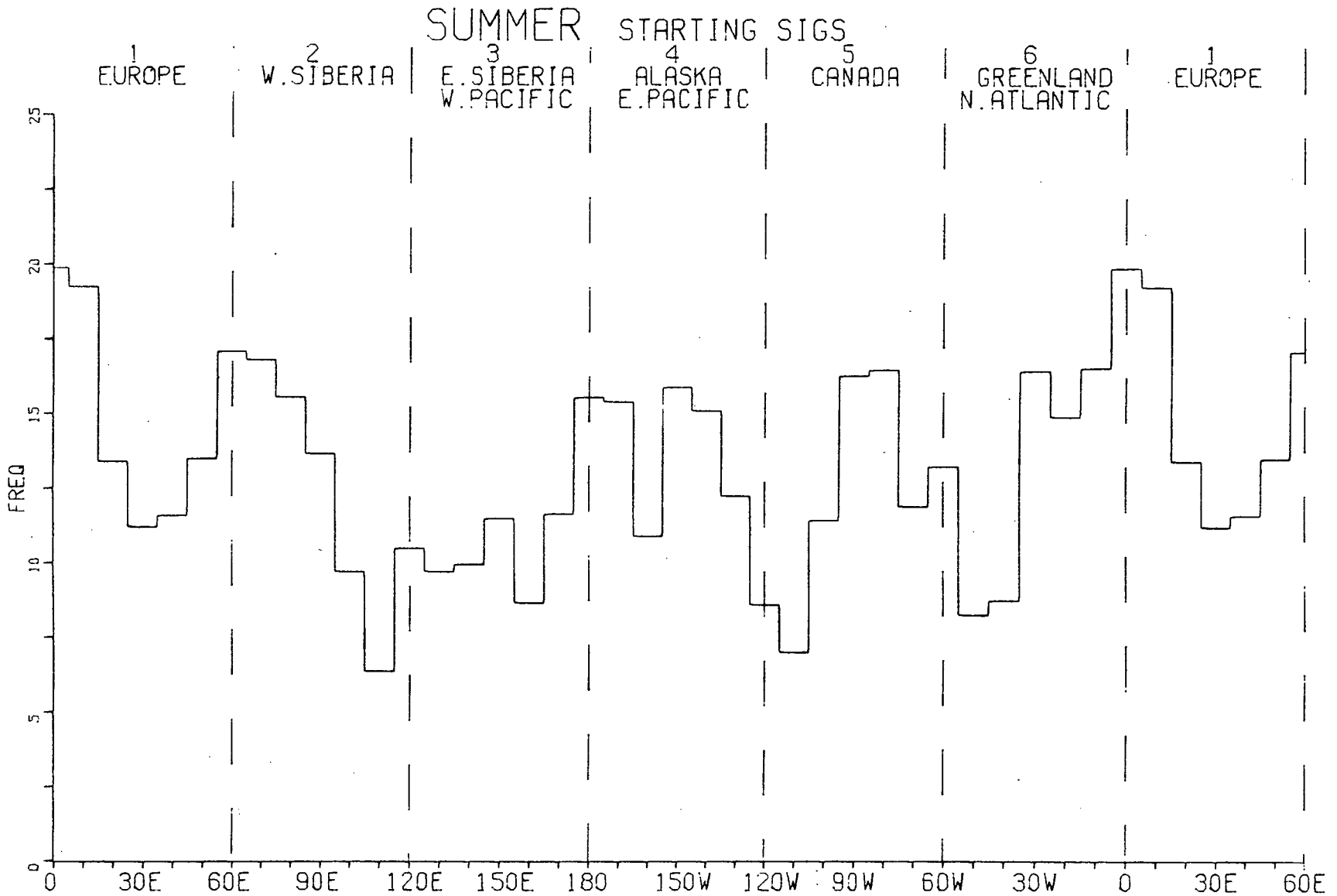

Fig. V-3 As in Fig. 5.13 except for SUMMER

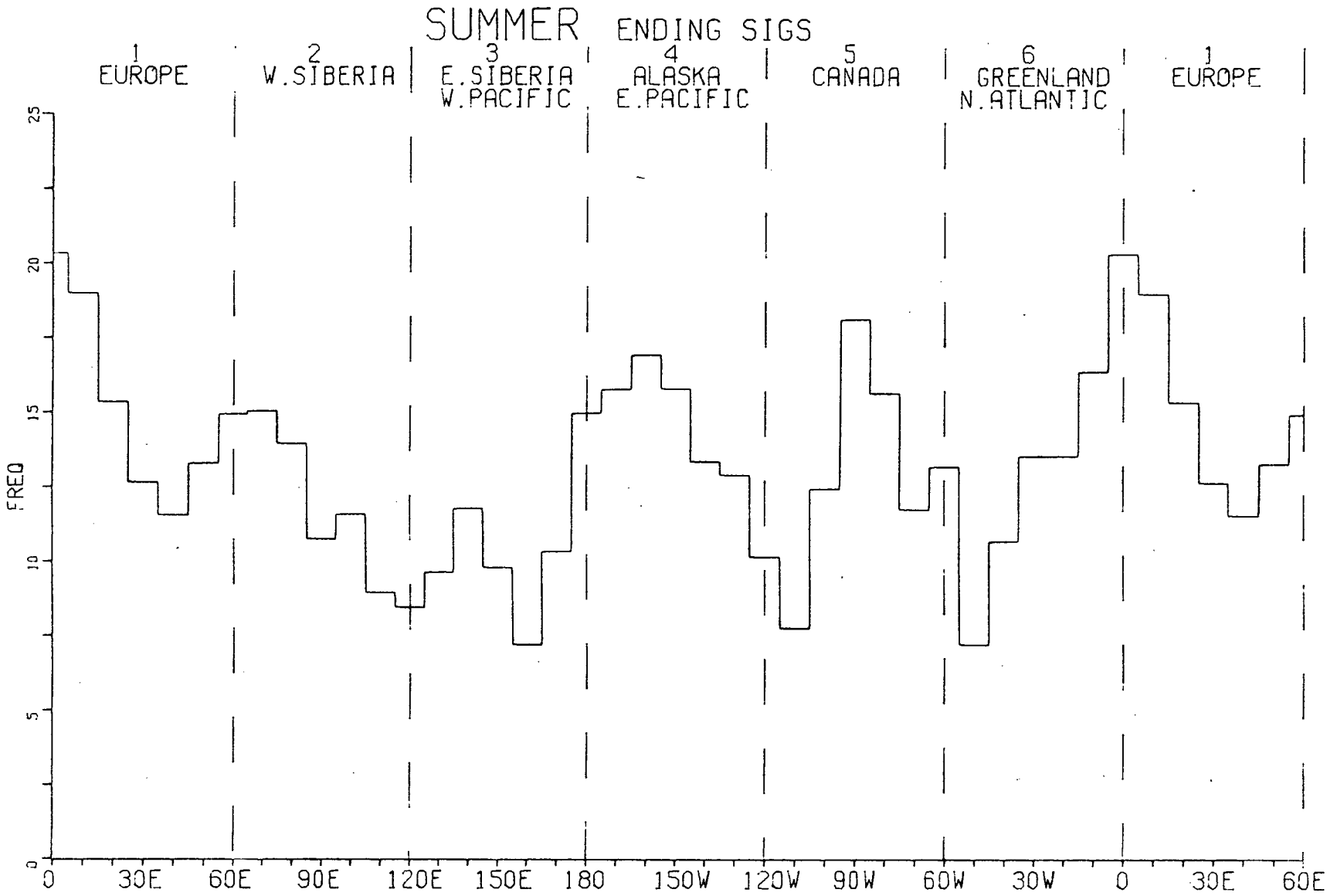

Fig. V-4 As in Fig. 5.14 except for SUMMER

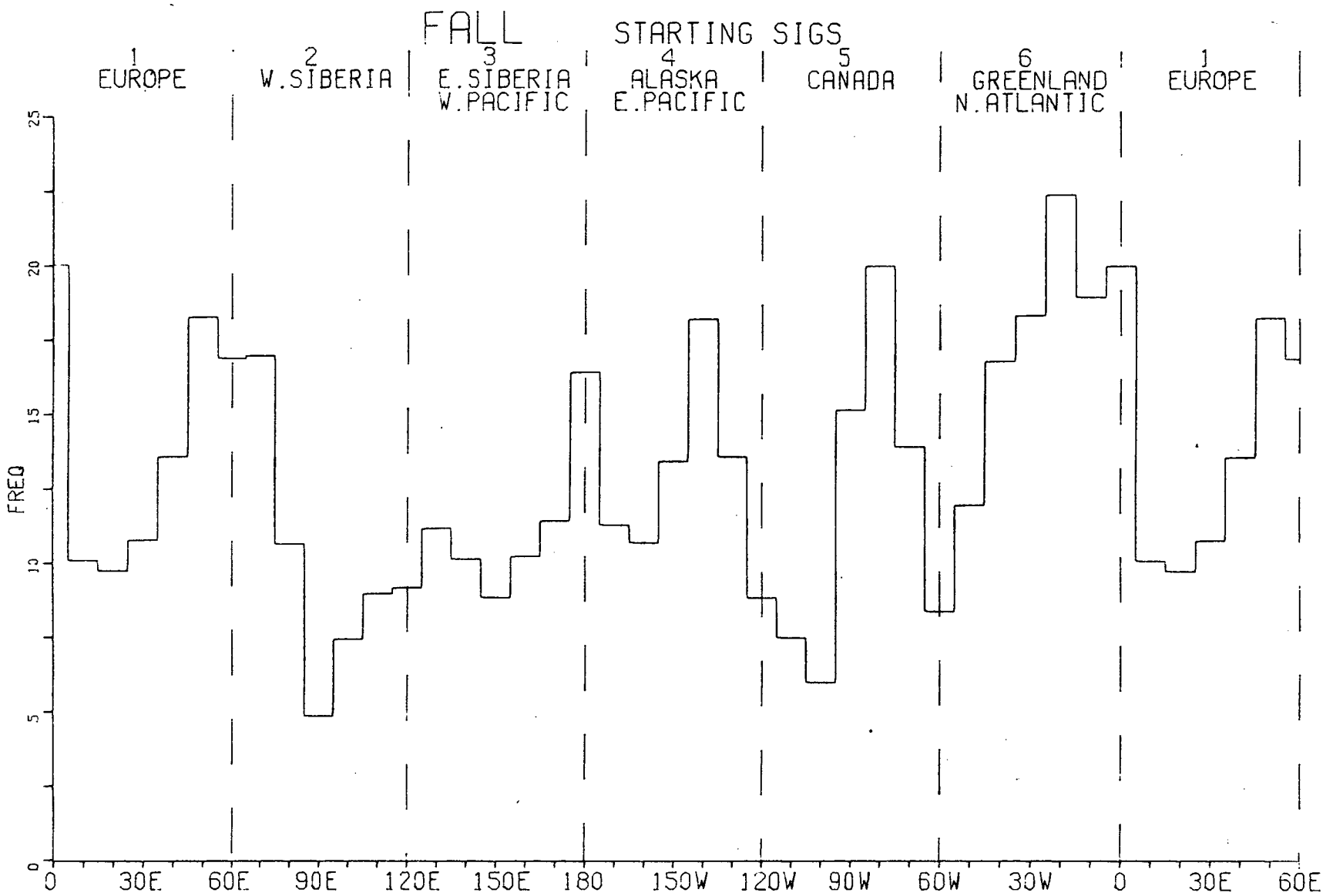

Fig. V-5 As in Fig. 5.13 except for FALL

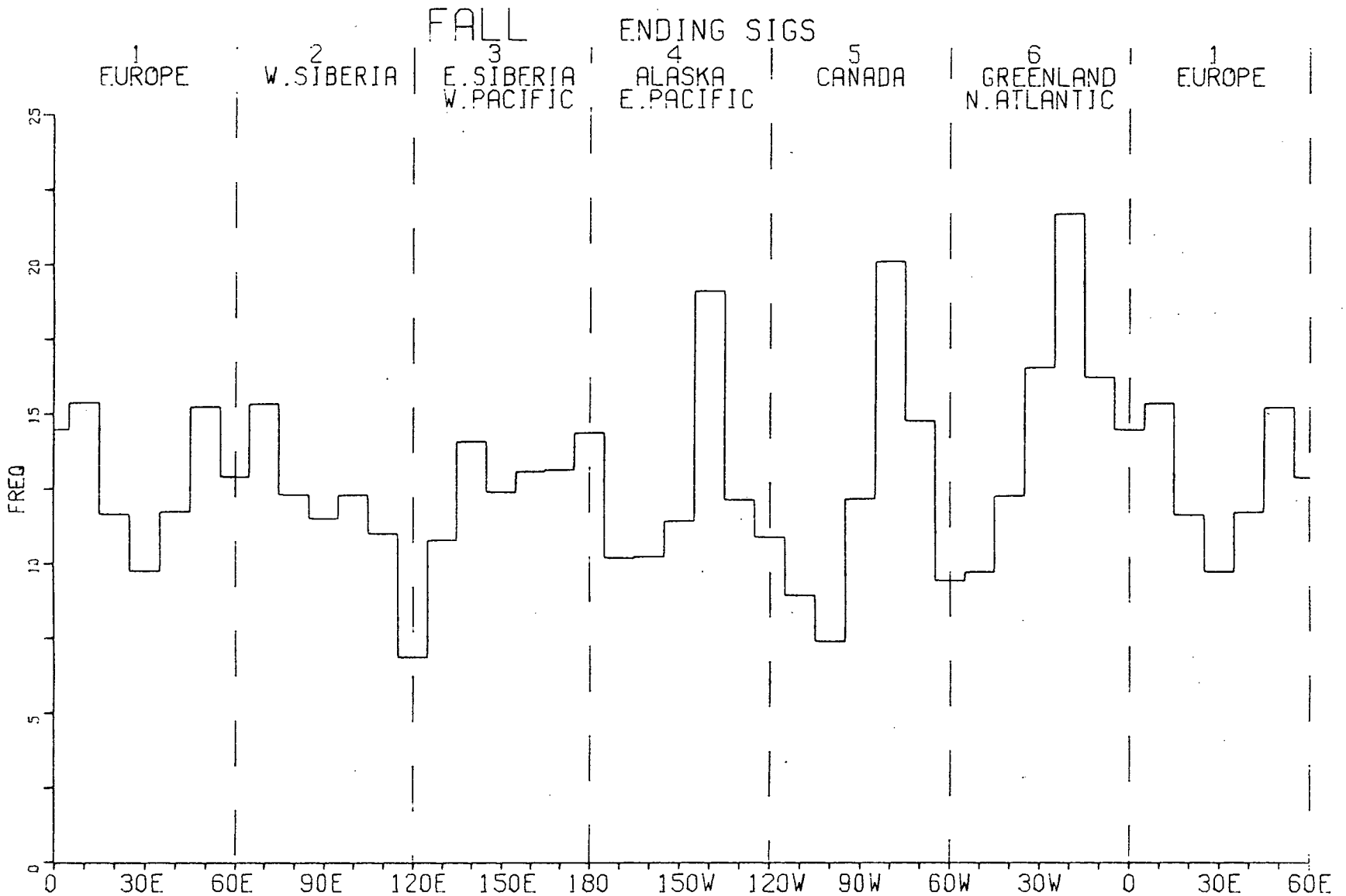

Fig. V-6 As in Fig. 5.14 except for FALL

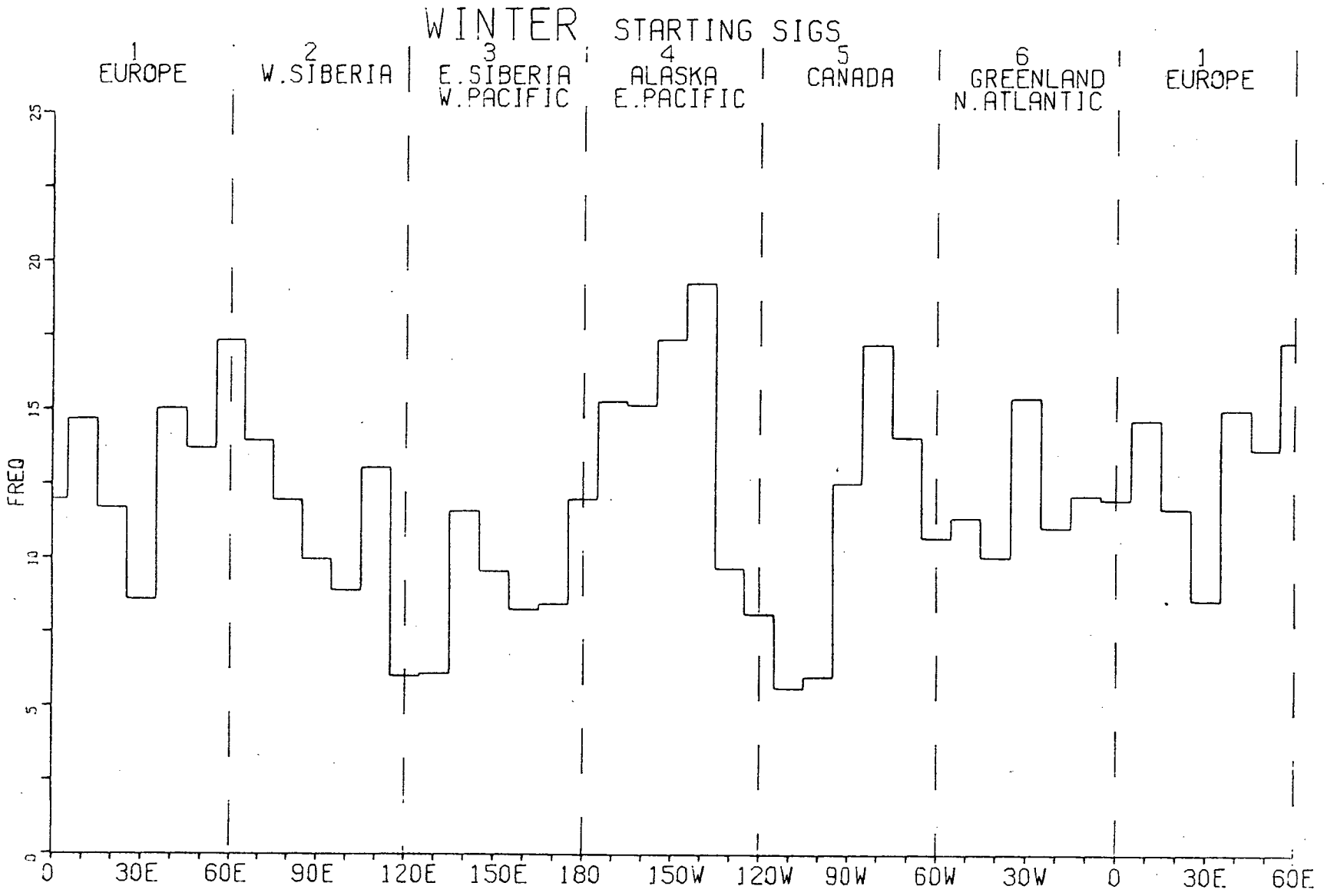

Fig. V-7 As in Fig. 5.13 except for WINTER

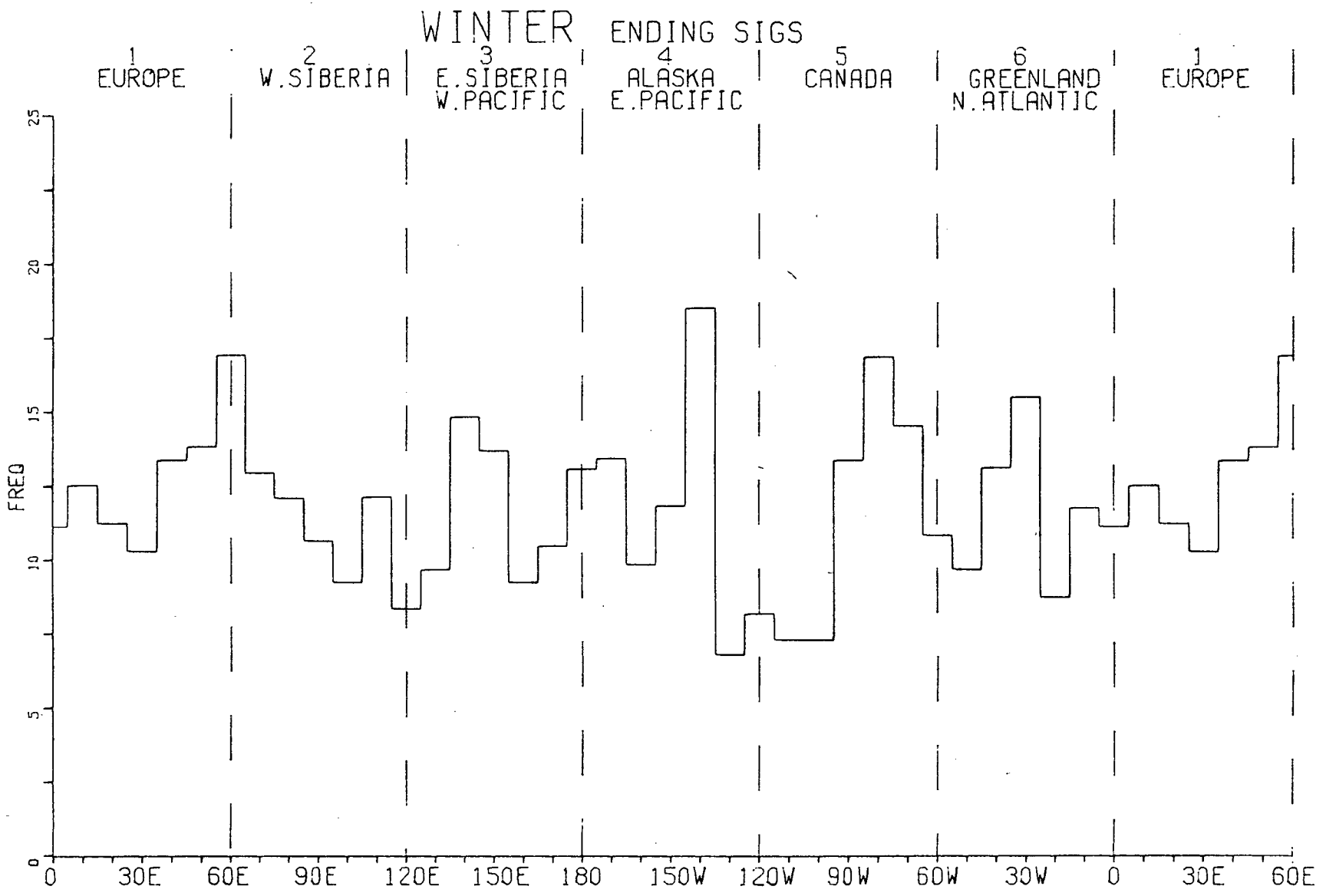

Fig. V-8 As in Fig. 5.14 except for WINTER

V - 6. Program for Computing and Plotting Histograms of Blocking Signature Frequency per 10° Longitude. Reference: Chapter 5, Section 5.2.2.

On the next page is listed the computer algorithm for preparing longitudinal histograms of Blocking Signature Frequency from data read from the I,J grid. This program has a general application and is designed to correct a bias which occurs when counting grid points into the 10° poleward converging sectors. It eliminates the requirement for repeated (and expensive) coordinate system transformations on large Hemispheric data sets.

```
C*****************************************************
C* PROCESS DATA GRIDS FROM UNIT 8 TO GENERATE        *
C* HISTOGRAMS BY LONGITUDE BAND.                     *
C*****************************************************
      INTEGER*2 IDATA(1980),LEN
      REAL ABSC(43),MID(36)
      READ(5,101) NDIV
C*************************************
C* SET UP ABSCISSA VECTOR USED BY PLT *
C*************************************
      DO 1 I=1,43
 1     ABSC(I)=I*0.2-0.1
      ABSC(43)=8.4
C
      RADDEG=57.2958
      ZK2=973.71202
      DO 70 L=1,5
C*************************************
C* READ IN A GRID IN NMC FORMAT, AND  *
C* PLOT THE HISTOGRAM FOR THAT GRID.  *
C*************************************
       DO 5 I=1,36
 5      MID(I)=0.0
       CALL READ(IDATA,LEN,0,LNUM,8,&99)
       K=LEN/2-1977
       INT=1
       N1=15
       N2=33
C*************************************
C* STEP THROUGH THE DATA POINTS,      *
C* TALLYING VALUES INTO THE CORRECT   *
C* LONGITUDE ZONE.                    *
C*************************************
       DO 65 J=1,51
        DO 60 I=N1,N2
         K=K+1
         VAL=IDATA(K)/(100.0*FLOAT(NDIV)**2)
         IF(VAL.EQ.0.0) GOTO 60
C*******************************
C* DIVIDE EACH GRID BLOCK INTO  *
C* 'NDIV' BY 'NDIV' SUBUNITS    *
C* TO ACCURATELY ASSIGN PORTION *
C* OF DATA VALUE TO LONG. BAND. *
C*******************************
         DO 50 II=1,NDIV
          DO 50 JJ=1,NDIV
           X=I+II/FLOAT(NDIV)-24.55
           Y=J+JJ/FLOAT(NDIV)-26.55
           R2=X**2+Y**2
C*****************************
C* COMPUTE LATITUDE OF (X,Y) *
C*****************************
           RLA=RADDEG*ARSIN((ZK2-R2)/(ZK2+R2))
C*****************************
C* IF LAT>75N, IGNORE POINT  *
C* OTHERWISE, COMPUTE LONG.  *
C*****************************
           IF(RLA.GT.75) GOTO 50
           IF(X.EQ.0.0) GOTO 10
            ELON=RADDEG*ATAN(ABS(Y/X))

           GOTO 15
10         ELON=90.0
15         IF(Y.LT.0.0) GOTO 25
           IF(X.LT.0.0) GOTO 20
           GOTO 40
20         ELON=180.0-ELON
           GOTO 40
25         IF(X.LT.0.0) GOTO 30
           ELON=360.0-ELON
           GOTO 40
30         ELON=180.0+ELON
40         RLO=15.0+ELON
           IF(RLO.GE.360.0) RLO=RLO-360.0
C*****************************
C* TALLY VALUE INTO THE      *
C* APPROPRIATE LONG. BAND.   *
C*****************************
           LB=RLO/10.0+1
           MID(LB)=MID(LB)+VAL
50       CONTINUE
60     CONTINUE
       IF((J.EQ.15).OR.(J.EQ.37)) INT=INT-1
       N1=N1-INT
       N2=N2+INT
65    CONTINUE
      WRITE(6,100)(MID(I),I=1,36)
C*************************************
C* CALL PLT TO PLOT THE HISTOGRAM.    *
C*************************************
      CALL PLT(MID,L,ABSC)
70   CONTINUE
99   CALL PLOTND
     STOP
100  FORMAT(' ',18F6.1,/,' ',18F6.1)
101  FORMAT(I4)
     END
```

APPENDIX VI

VI - 1. Conversion of the Thickness of the 1000MB - 500MB Layer into its Mean Temperature

It can be shown from the hydrostatic equation and the equation of state that for dry air the thickness of a layer is proportional to its mean temperature ($\overline{T}$). In the real atmosphere the presence of water vapour decreases the density and therefore increases the thickness which now becomes proportional to the 'mean virtual temperature' ($\overline{T}_v$). This is the mean temperature of a layer of dry air with the same density as the moist air layer. Now $\overline{T}_v > \overline{T}$, but reference to Table 72 of List (1966) will show that the difference is quite small (0.02^o to 0.50^oC) for the range of mean temperatures of the 1000MB - 500MB layer usually encountered in the mid- and high latitudes. Consequently it will be sufficiently accurate for our purposes to assume $\overline{T}_v = \overline{T}$.

It follows that contours of constant thickness can readily be converted to isotherms of constant $\overline{T}$. Hence the 1000MB - 500MB thickness field is, in effect, a field of mean temperature for the lower half of the troposphere.

The conversion is readily derived from the hypsometric equation:

$$Z_2 - Z_1 = \frac{R_d}{g}\int_{p_2}^{p_1} T_v \frac{dp}{p}$$

Where Z_2 = gph at level 2

Z_1 = gph at level 1

R_d = gas constant for dry air = $287JK^{-1}kg^{-1}$

T_v = virtual temperature at pressure p

g = acceleration of gravity

As explained above this may be written:

$$Z_2 - Z_1 \approx \frac{R_d}{g} \bar{T} \int_{p_2}^{p_1} \frac{dp}{p} = \frac{R_d}{g} \bar{T} \ln \left(\frac{p_1}{p_2}\right)$$

If p_1 = 1000MB and p_2 = 500MB

then $Z_{500} - Z_{1000} = 20.27\bar{T}$

Thus for any value of $(Z_{500} - Z_{1000})$ in metres

$$\bar{T} = \left(\frac{Z_{500} - Z_{1000}}{20.27}\right)$$

Even more convenient relationships can be derived which will make possible the direct relabelling of conventional 1000MB - 500MB thickness contours drawn at 6 dam intervals in terms of isotherms of ^{o}C (or K) with integral values at 3° intervals.

We have:

(a) $0.5\ (Z_{500} - Z_{1000})$ dams - 4.0 dams = $\bar{T}$ degrees K

e.g., $Z_{500} - Z_{1000}$ = 546 dams

Therefore $\bar{T} = (0.5)(546) - 5.0 = 269K$

and successive contours can be labelled as isotherms at 3° intervals.

(b) In the (1000MB - 500MB) normal charts (available from the author) the contours are labelled in dams less 500.

The following relationship obtains:

$$0.5(Z_{500} - Z_{1000} - 500) - 27 = \overline{T} \text{ degrees C}$$

$$\text{e.g., } 0.5(546 - 500) - 27 = -4^{o}C$$

Again, since 6 dams corresponds to $3^{o}C$ (or 3K) the thickness contours may quickly be relabelled as 3° interval isotherms. The conversion table is as follows:

TABLE VI - 1

Thickness (dams) 1000 - 500MB	$\overline{T}(^{o}C)$	$\overline{T}(K)$
492	-31	242
498	-28	245
504	-25	248
510	-22	251
516	-19	254
522	-16	257
528	-13	260
534	-10	263
540	- 7	266
546	- 4	269
552	- 1	272
558	+ 2	275
564	+ 5	278
570	+ 8	281
576	+11	284

VI - 2. Transformation of the MSL Pressure into Geopotential Height of the 1000MB Surface

The transformation algorithm is generated as follows:

Let height of 500MB surface $= {}^{K}Z_{2,i}(I,J)$

Let height of 1000MB surface $= {}^{K}Z_{1,i}(I,J)$

Let MSL pressure $= {}^{K}p_{i}(I,J)$

Where K = year

i = pentad number

(I,J) = NMC coordinate

2 = 500MB index

1 = 1000MB index

For the time being we shall abbreviate these variables to Z_2, Z_1 and p.

Z_1 is the unknown but so closely related to p that:

$$Z_1 \approx \frac{3(p - 1000)}{4} \text{ dams}$$

is a reasonable first approximation.

Z_1 is also temperature dependent, significantly so for substantial deviations of p from 1000MB.

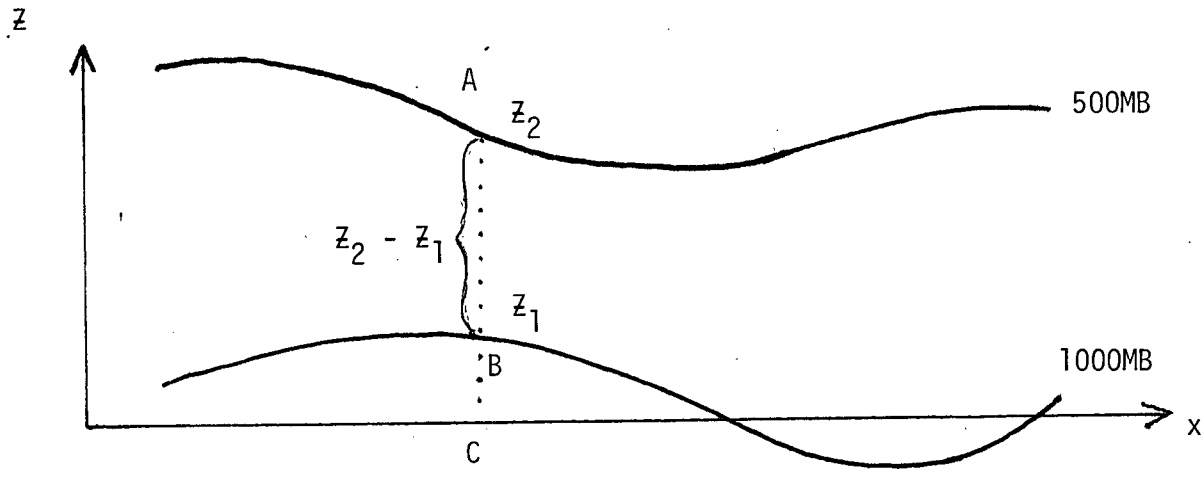

This is a West to East cross-section schematic showing topography of 500MB and 1000MB surfaces.

Consider the air column AB. Its vertical extent $Z_2 - Z_1$ (called thickness) is proportional to the mean temperature of AB = T_M. In fact:

$$Z_2 - Z_1 \simeq 2.027\ T_M$$

What we want, however, is not T_M but τ_m, the mean temperature of the air column BC. Clearly, there must be a strong positive correlation between T_M and τ_m. The following empirical relationships (Moffitt and Ratcliffe, 1972) gave good results when tested over a wide range of thicknesses for MSL pressure deviations from 1000MB, of up to 30MB.

(i) If $Z_2 - Z_1 \leqslant 478.00$ dams,

$$\tau_m = (0.93 \times 478 - 223)\ \text{K}.$$

(ii) If 541.50 dams $\geqslant Z_2 - Z_1 > 478.00$ dams,

$$\tau_m = [0.93 \times (Z_2 - Z_1) - 223]\ \text{K}$$

(iii) If $Z_2 - Z_1 > 541.50$ dams.

$$\tau_m = [0.52 \times (Z_2 - Z_1) - 1]\ K$$

To compute Z_1 at this stage, the first approximation is:

$$^{K}Z_{1,i}(I,J) \simeq \frac{3(^{K}p_i(I,J) - 1000)}{4}$$

These values of Z_1 are used in (i), (ii) or (iii), whichever applies. This will provide the field of τ_m.

The second and final approximation for the 1000MB height is:

$$Z_1 = \frac{(p - 1000)\tau_m}{342}$$

The field of $^{K}Z_{1,i}(I,J)$ provides the 1000MB height data set.

VI - 3. <u>Computation of Normal and Standard Deviation Fields</u>

The Normal geopotential height at (I,J) for the i th pentad is:

$$(\bar{Z})_{(I,J)} = \frac{1}{N}\left(\sum_{K=1}^{N} {}^{K}Z_i\right)_{(I,J)}$$

Where N = period of record and Z_1 represents the <u>5-day average</u> of gph for pentad i.

The Normals for the respective seasons are:

$$(\bar{Z}_{WN})_{(I,J)} = \frac{1}{18}\left[\sum_{i=1}^{12} (\bar{Z}_i)_{(I,J)} + \sum_{i=68}^{73} (\bar{Z}_i)_{(I,J)}\right]$$

$$(\bar{Z}_{SP})_{(I,J)} = \frac{1}{19}\left[\sum_{i=13}^{31} (\bar{Z}_i)_{(I,J)}\right]$$

and so on.

For the Seasonal Standard Deviations at (I,J) we used:

$$(\sigma_{WN})_{(I,J)} = \sqrt{\frac{\sum_{K=1}^{N}\left[\sum_{i=1}^{12}\left(K_{Z_1} - \bar{Z}_{WN}\right)^2_{(I,J)} + \sum_{i=68}^{73}\left(K_{Z_i} - \bar{Z}_{WN}\right)^2_{(I,J)}\right]}{18N}}$$

etc., etc.

VI - 4. Computation of Coefficient of Skewness

Specifically for WINTER at (I,J):

$$CS_{WN} = \frac{\sum_{K=1}^{N}\left[\sum_{i=1}^{12}\left(K_{Z_i} - \bar{Z}_{WN}\right)^3_{(I,J)} + \sum_{i=68}^{73}\left(K_{Z_i} - \bar{Z}_{WN}\right)^3_{(I,J)}\right]}{18N\left(\sigma_{WN}\right)^3_{(I,J)}}$$

A program was written to calculate values of CS_{WN}, CS_{SP}, CS_{SU} and CS_{FL} for each grid-point for the 1000MB, 500MB and thickness data and the results were printed out in a geographical format. Subsequently a 'plot contour' routine yielded spatial distributions of areas of significant skewness, either positive or negative.

VI - 5. Computation of Coefficient of Kurtosis

Specifically for WINTER at (I,J):

$$CK_{WN} = \frac{\sum_{K=1}^{N}\left[\sum_{i=1}^{12}\left(K_{Z_i} - \bar{Z}_{WN}\right)^4_{(I,J)} + \sum_{i=68}^{73}\left(K_{Z_i} - \bar{Z}_{WN}\right)^4_{(I,J)}\right]}{18N\left(\sigma_{WN}\right)^4_{(I,J)}}$$

A procedure similar to that for calculating fields of skewness was followed.

APPENDIX VII

VII - 1. Hovmöller Diagrams and Computation of Zonal Speed of troughs and ridges

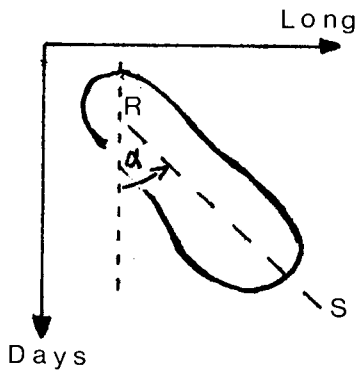

For rapid computation of zonal speed of troughs or ridges, let the contour axis RS make an angle α with the merid-λ through R. Then the zonal speed c in degrees of longitude per day (for the relative axis scales of the diagrams used in this thesis) is

$$c = 5 \tan \alpha$$

The following tabulation is provided for convenience of the user.

TABLE VII - 1

Angle of Contour Axis with Meridian α (degs.)	Zonal Speed of trough or ridge		
	Angular Speed (Degs. Long. per Day)	Linear Speed ($kmhr^{-1}$)	
		$40^{o}N$	$60^{o}N$
80	28	101	66
70	14	49	32
60	9	31	20
50	6	21	14
40	4	15	10
30	3	10	7
20	2	6	4
10	1	3	2

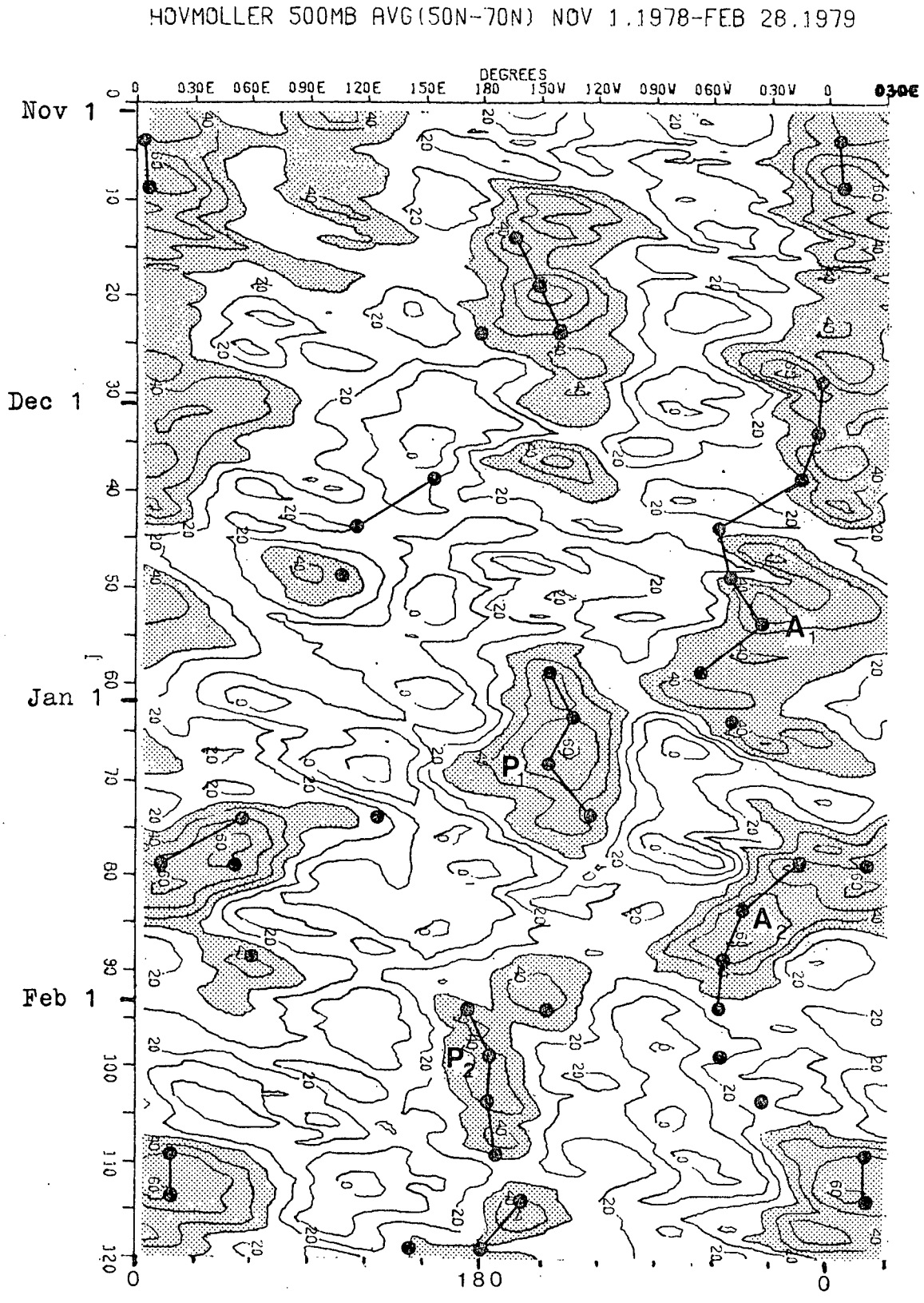

Fig VII-1 Same as Fig. 7.1 except for November 1, 1978 to February 28, 1979. Note episodes of Atlantic Blocking A followed by Pacific-Alaska Blocking P. (See Section 7.4.3).

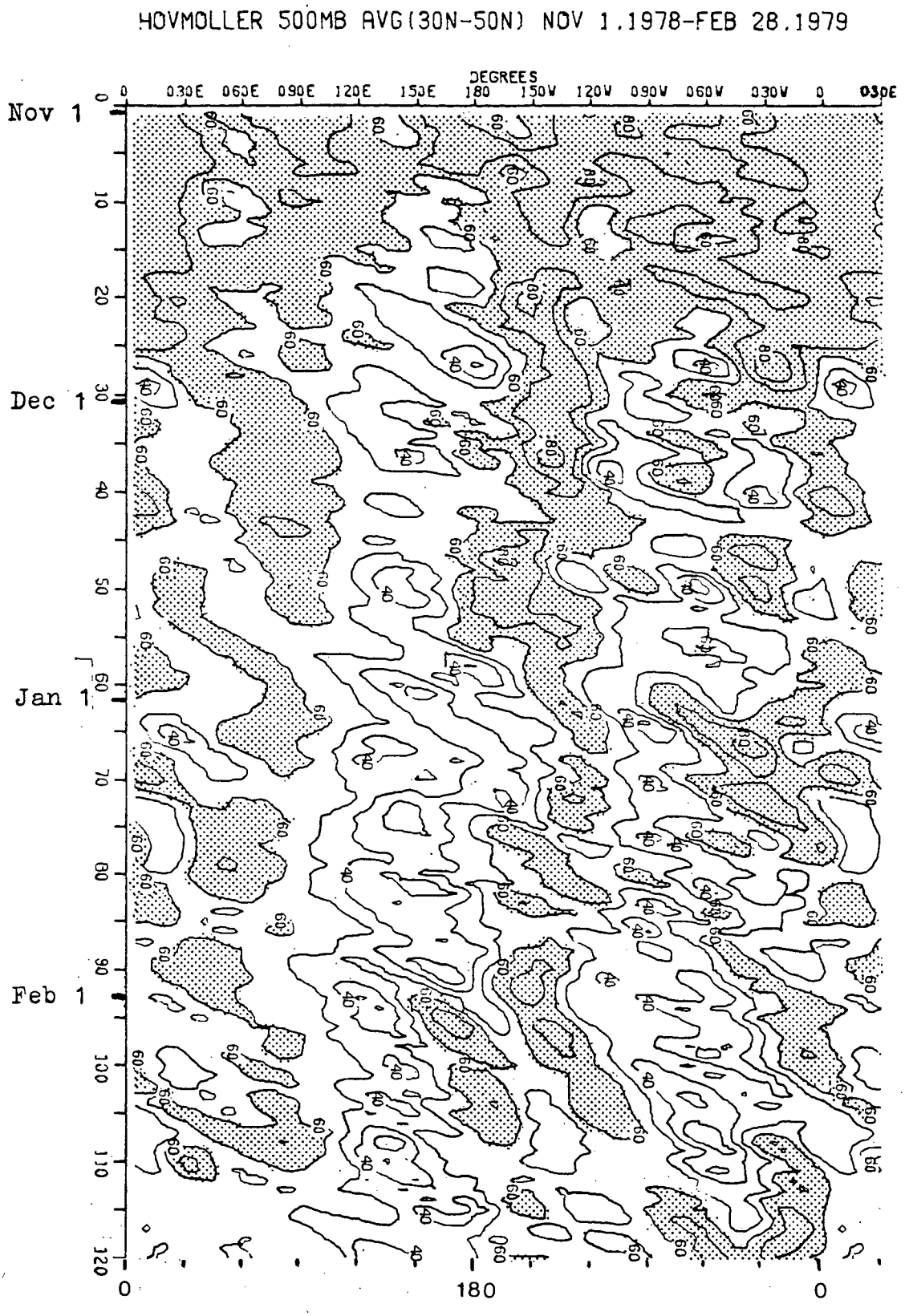

Fig. VII-2 Hovmoller Diagram for 30°N - 50°N November 1, 1978 to December 28, 1979. (See Section 7.4.3).

VII - 2. Zonal Harmonics for the Normal 500MB Height Field - WINTER

The following figures, VII - 3 to VII - 6, inclusive, show the Zonal Harmonics in the Northern Hemisphere for Waves 1 to 4, respectively. (See Section 7.3.4(b) of the Text.)

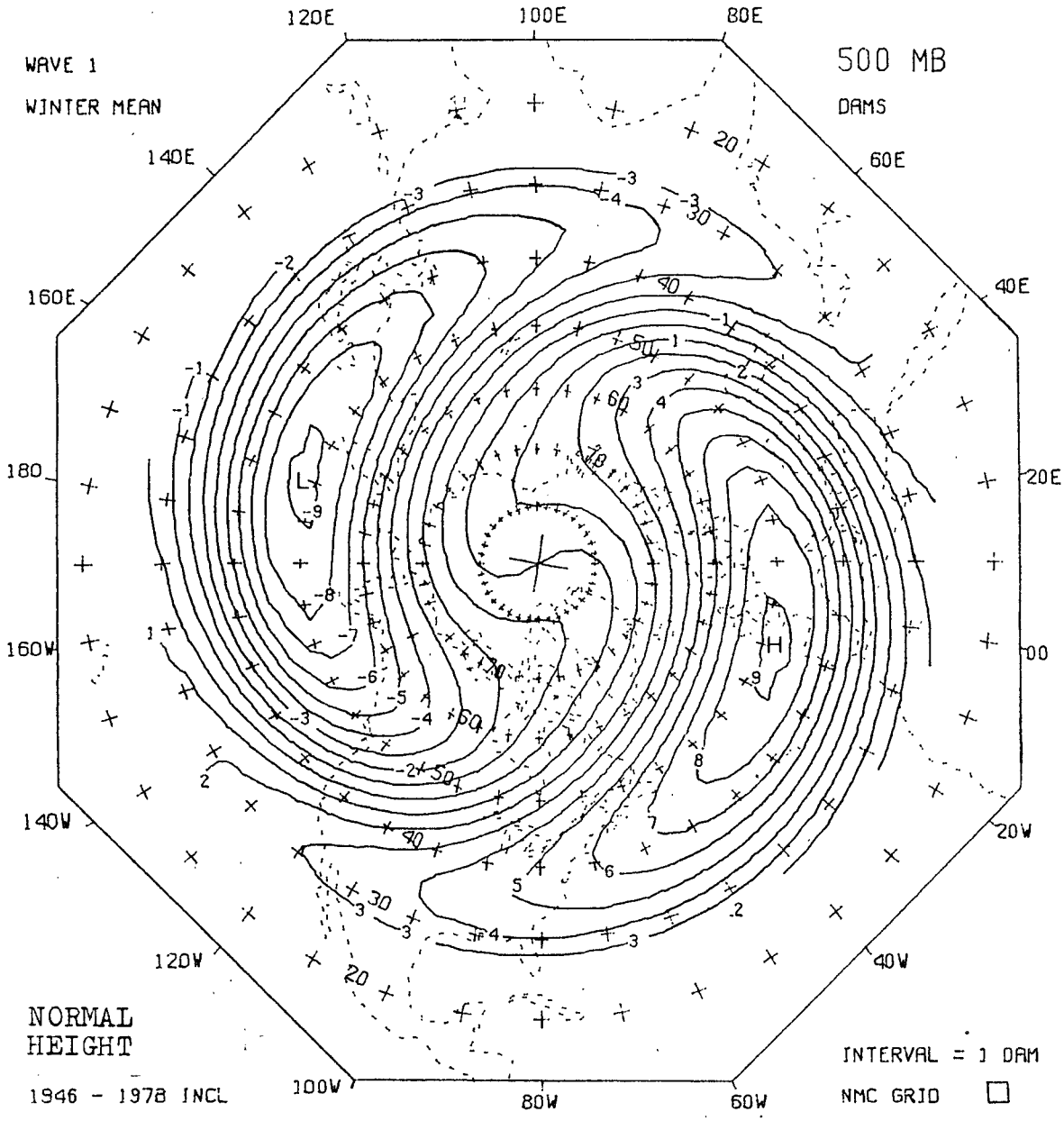

Fig. VII-3. First harmonic (W1) of the normal 500MB height field for WINTER (December 1 to February 28). Contours labelled in decametres. Interval = 1 dam.

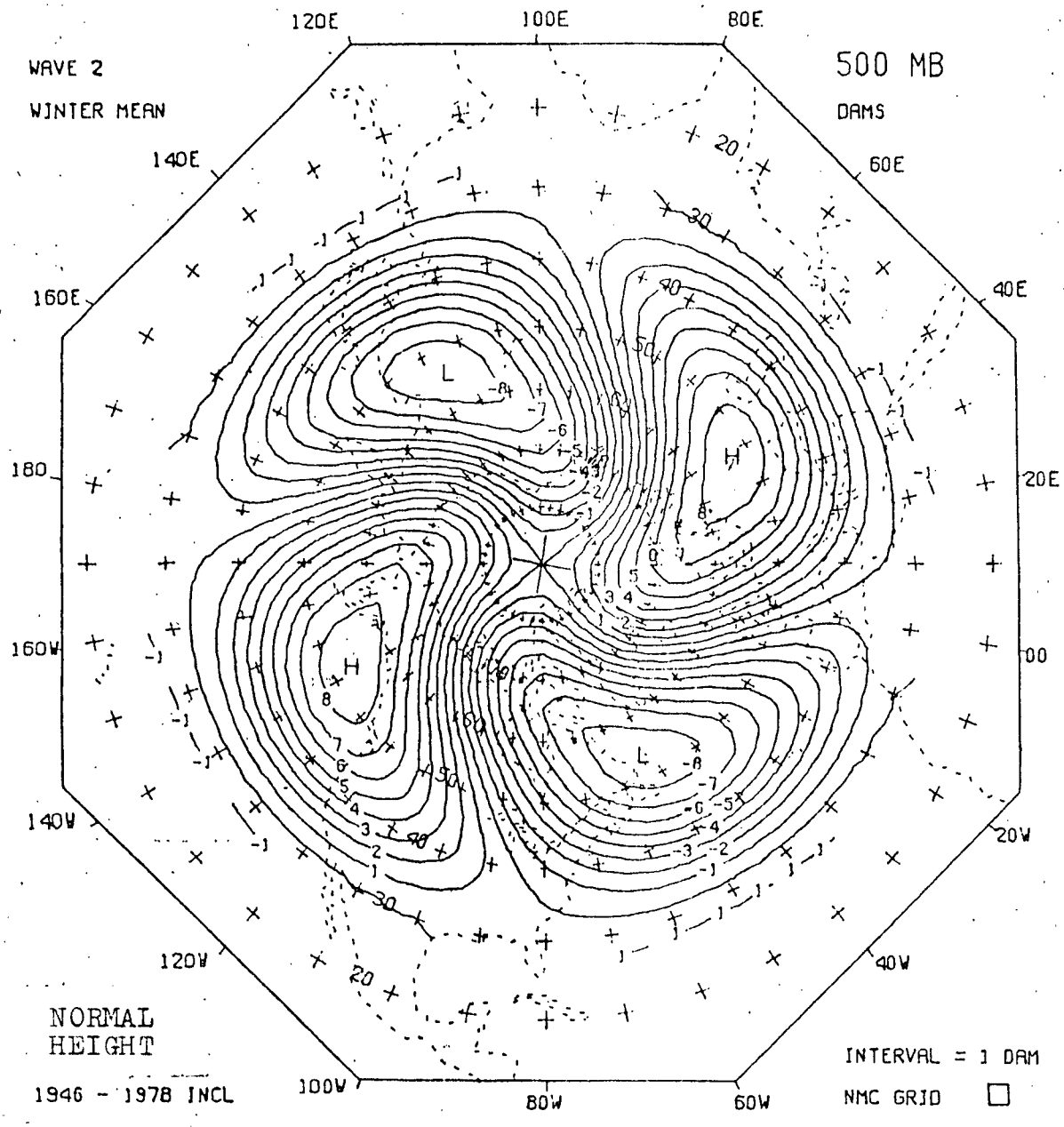

Fig. VII-4 As in Figure VII-3 , except for second harmonic (W2).

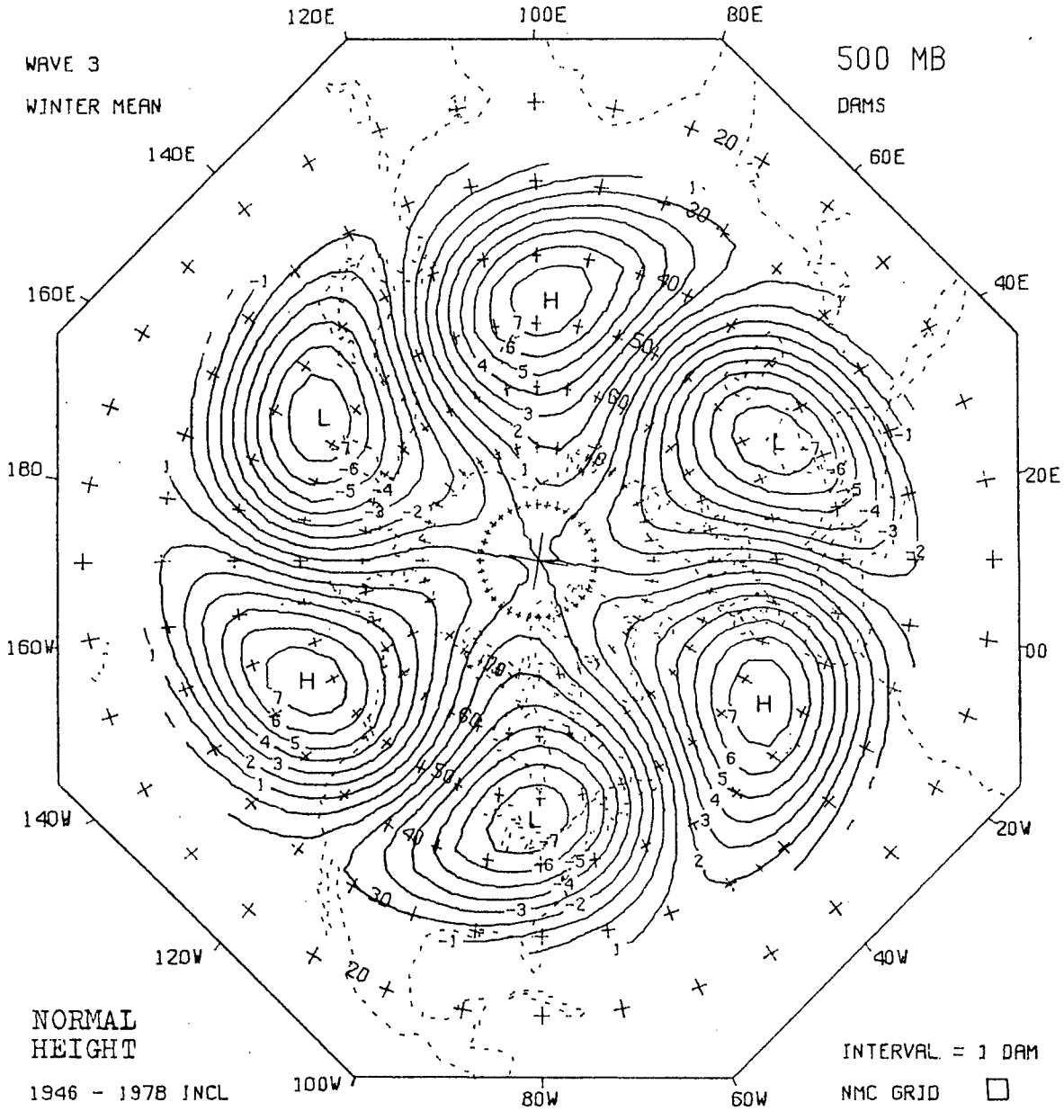

Fig. VII-5 As in Fig. VII-3, except for third harmonic (W3).

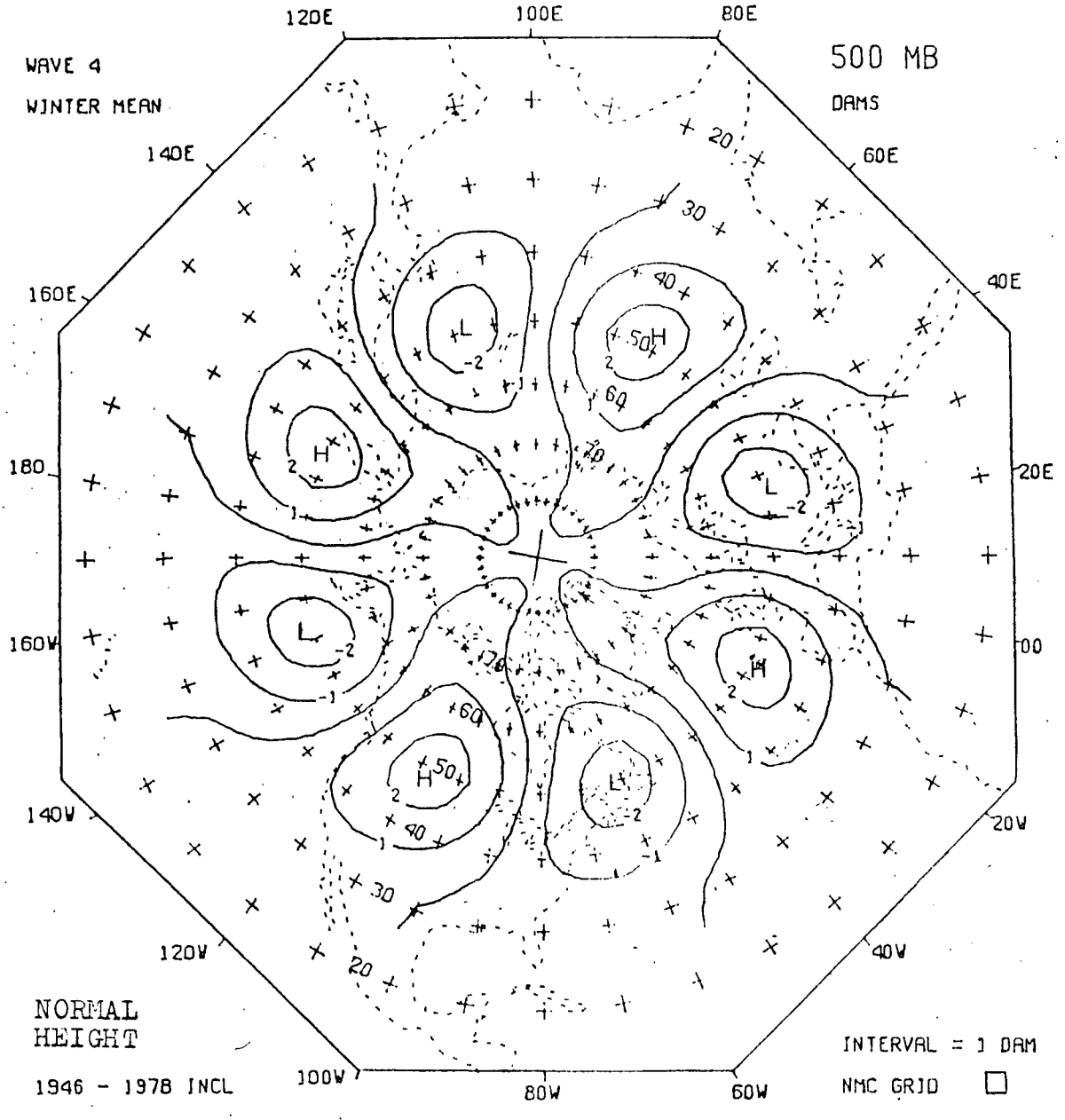

Fig. VII-6 As in Fig. VII-3, except for fourth harmonic (W4).